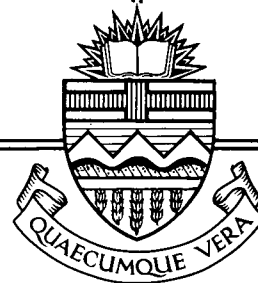


Handwritten signature

Structural Engineering Report 143



**SHRINKAGE AND FLEXURAL
TESTS OF
TWO FULL-SCALE
COMPOSITE TRUSSES**

by
**ANITA BRATTLAND
D. J. LAURIE KENNEDY**

DECEMBER, 1986

RECENT STRUCTURAL ENGINEERING REPORTS

Department of Civil Engineering

University of Alberta

112. *Ultimate Strength of Timber Beam Columns* by T.M. Olatunji and J. Longworth, November 1983.
113. *Lateral Coal Pressures in a Mass Flow Silo* by A.B.B. Smith and S.H. Simmonds, November 1983.
114. *Experimental Study of Steel Plate Shear Walls* by P.A. Timler and G.L. Kulak, November 1983.
115. *End Connection Effects on the Strength of Concrete Filled HSS Columns* by S.J. Kennedy and J.G. MacGregor, April 1984.
116. *Reinforced Concrete Column Design Program* by C-K. Leung and S.H. Simmonds, April 1984.
117. *Deflections of Two-way Slabs under Construction Loading* by C. Graham and A. Scanlon, August 1984.
118. *Effective Lengths of Laterally Unsupported Steel Beams* by C.D. Schmitke and D.J.L. Kennedy, October 1984.
119. *Flexural and Shear Behaviour of Large Diameter Steel Tubes* by R.W. Bailey and G.L. Kulak, November 1984.
120. *Concrete Masonry Prism Response due to Loads Parallel and Perpendicular to Bed Joints* by R. Lee, J. Longworth and J. Warwaruk.
121. *Standardized Flexible End Plate Connections for Steel Beams* by G.J. Kriviak and D.J.L. Kennedy, December 1984.
122. *The Effects of Restrained Shrinkage on Concrete Slabs* by K.S.S. Tam and A. Scanlon, December 1984.
123. *Prestressed Concrete Beams with Large Rectangular Web Openings* by T. do M.J. Alves and A. Scanlon, December 1984.
124. *Tests on Eccentrically Loaded Fillet Welds* by G.L. Kulak and P.A. Timler, December 1984.
125. *Analysis of Field Measured Deflections Scotia Place Office Tower* by A. Scanlon and E. Ho, December 1984.
126. *Ultimate Behaviour of Continuous Deep Reinforced Concrete Beams* by D.R. Ricketts and J.G. MacGregor, January 1985.

127. *The Interaction of Masonry Veneer and Steel Studs in Curtain Wall Construction* by W.M. McGinley, J. Warwaruk, J. Longworth and M. Hatzinikolas, May 1985.
128. *Evaluation of Existing Bridge Structure by Nondestructive Test Methods* by L. Mikhailovsky and A. Scanlon, May 1985.
129. *Finite Element Modelling of Buried Structures* by D.K. Playdon and S.H. Simmonds, October 1985.
130. *Behaviour and Ultimate Strength of Transversely Loaded Continuous Steel Plates* by K.P. Ratzlaff and D.J.L. Kennedy, November 1985.
131. *Inelastic Lateral Buckling of Steel Beam-Columns* by P.E. Cuk, M.A. Bradford and N.S. Trahair, December 1985.
132. *Design Strengths of Steel Beam-Columns* by N.S. Trahair, December 1985.
133. *Behaviour of Fillet Welds as a Function of the Angle of Loading* by G.S. Miazga and D.J.L. Kennedy, March 1986.
134. *Inelastic Seismic Response of Precast Concrete Large Panel Coupled Shear Wall Systems* by M.R. Kianoush and A. S , March 1986.
135. *Finite Element Prediction of Bin Loads* by A.H. Askari and A.E. Elwi, June 1986.
136. *Shear Behavior of Large Diameter Fabricated Steel Cylinders* by J. Mok and A.E. Elwi, June 1986.
137. *Local Buckling Rules for Structural Steel Members* by S. Bild and G.L. Kulak, May 1986.
138. *Finite Element Prediction of Reinforced Concrete Behavior* by S. Balakrishnan and D.W. Murray, July 1986.
139. *Behavior and Strength of Masonry Wall/Slab Joints* by T.M. Olatunji and J. Warwaruk, July 1986.
140. *Bayesian Analysis of In-Situ Test Data for Estimating the Compressive Strength of Concrete in Existing Structures* by G.J. Kriviak and A. Scanlon, July 1986.
141. *Shear-Moment Transfer in Slab-Column Connections* by S.D.B. Alexander and S.H. Simmonds, July 1986.
142. *Minimum Thickness Requirements for Deflection Control of Two-Way Slab Systems* by D.P. Thompson and A. Scanlon, November 1986.
143. *Shrinkage and Flexural Tests of Two Full-Scale Composite Trusses* by A. Brattland and D.J.L. Kennedy, December 1986.

Flu:

Structural Engineering Report 143

SHRINKAGE AND FLEXURAL TESTS
OF TWO FULL-SCALE COMPOSITE TRUSSES

by

Anita Brattland

and

D.J. Laurie Kennedy

Department of Civil Engineering
University of Alberta
Edmonton, Alberta

December 1986

Abstract

Composite trusses supporting concrete slabs on wide rib profile steel deck have proven to be an economical system for long span floors. A preferred truss configuration that is simple to fabricate consists of hollow structural section top and bottom chords with double angle web members welded on either side. The shrinkage and flexural behaviour of two such (essentially identical) composite trusses with a span of 11.5 metres was studied.

Shrinkage measurements to determine the effects of slab shrinkage on truss deflection and member stresses were recorded over periods of 65 and 85 days. A method was developed to compute shrinkage deflections, based on equilibrium of the shrinkage-induced forces at midspan, that gives excellent agreement with test results. The method assumes a linear strain distribution through the depth, and uses the free shrinkage strain of the concrete and the stress-strain characteristics of the concrete in tension.

The flexural tests show that ductile behaviour up to failure can be obtained without failure of the web members, provided that the design is based on the ultimate tensile strength of the bottom chord, and the web members and shear connection are designed for the concomitant forces. The maximum moments attained were about 1.2 times the unfactored ultimate moment predicted by S16.1. The maximum strain in the bottom chord of both trusses was significantly higher than the yield strain but did not reach the ultimate strain

due to premature shear connection failure. The failure mode of the first composite truss suggests that additional rules for establishing the length of stud shear connectors for use in slabs on ribbed deck should be provided in S16.1. A design procedure for double angle web members was developed, based on the test results.

Acknowledgements

This report is based on an M.Sc. thesis of the same title submitted by Anita Brattland to the Faculty of Graduate Studies and Research at the University of Alberta in the winter of 1986-87. Dr. D.J. Laurie Kennedy supervised the preparation of the thesis.

Financial support for this research was provided by the Canadian Steel Construction Council and supplemented with funds granted to Dr. Kennedy by the Natural Sciences and Engineering Research Council of Canada and the Central Research Fund of the University of Alberta. The shear studs for the test specimens were supplied and installed by the Calgary office of the Nelson Stud Welding Division, TRW Canada Ltd. at no cost. Personal funding of the student author from the Natural Sciences and Engineering Research Council of Canada and from the Alberta Region of the Canadian Institute of Steel Construction is gratefully acknowledged.

Special thanks are extended to E.Y.L. Chien and M.I. Gilmor of the Canadian Institute of Steel Construction for their interest and helpful comments.

Table of Contents

Chapter	Page
1. INTRODUCTION	1
1.1 General	1
1.2 Objectives	2
1.3 Scope	3
2. LITERATURE REVIEW	5
2.1 General History of Composite Steel-Concrete Construction	5
2.2 Flexural Capacity and Stiffness	7
2.2.1 Composite Beams	7
2.2.2 Composite Open-Web Steel Joists	13
2.2.3 Composite Trusses	18
2.3 Shear Connection	19
2.3.1 Strength of Studs in Solid Slabs	21
2.3.2 Strength of Studs in Slabs on Ribbed Deck	23
2.4 Effective Slab Width	26
2.5 Longitudinal Shear	29
2.6 Shrinkage Behaviour	35
2.6.1 Shrinkage Models	36
2.6.2 Deflection of Composite Flexural Members	38
3. COMPOSITE TRUSS DESIGN	42
3.1 General Design Procedures	42
3.1.1 Moment Capacity	42
3.1.2 Steel Top Chord	45
3.1.3 Web Members and Connections	45
3.1.4 Shear Connectors	46

3.1.5	Serviceability	47
3.2	Test Specimen Design	48
3.2.1	Description	48
3.2.2	Unique Features	51
3.2.2.1	Bottom Chord	51
3.2.2.2	Triangulation	52
3.2.2.3	Web Members	54
3.2.2.4	Welded Connections	57
3.2.2.5	Shear Connection	58
3.2.2.6	Longitudinal Shear	59
3.2.2.7	Bearing Detail	59
4.	EXPERIMENTAL PROGRAM	60
4.1	General	60
4.2	Test Specimens	61
4.2.1	Fabrication	61
4.2.2	Assembly of Composite Trusses	62
4.3	Shrinkage Tests	65
4.3.1	Test Set Up	65
4.3.2	Instrumentation	69
4.3.3	Testing Procedure	72
4.4	Flexural Tests	74
4.4.1	Test Set Up	74
4.4.1.1	Load Apparatus and Reactions	76
4.4.1.2	Safety and Stability	81
4.4.1.3	Calibration of Instrumentation ..	82
4.4.2	Instrumentation	82
4.4.2.1	Loads and Reactions	83

	4.4.2.2 Displacements	83
	4.4.2.3 Steel Strains	85
	4.4.2.4 Concrete Strains	88
	4.4.3 Testing Procedure	89
5.	GEOMETRIC PROPERTIES	91
5.1	Steel Sections	91
5.1.1	Dimensions	91
5.1.2	Section Properties	91
5.2	Steel Trusses	97
5.2.1	Dimensions	97
5.2.2	Moments of Inertia	97
5.3	Composite Trusses	97
5.3.1	Dimensions	97
5.3.2	Moments of Inertia	99
6.	MATERIAL PROPERTIES AND BEHAVIOUR	100
6.1	Steel	100
6.1.1	General	100
6.1.2	Ancillary Tests	100
6.1.2.1	Tension Coupons	100
6.1.2.2	Stub Columns	104
6.1.2.3	Tension Test on Bottom Chord HSS	105
6.1.3	Test Results	107
6.1.3.1	Tension Coupons	107
6.1.3.2	Stub Columns	112
6.1.3.3	Tension Test on Bottom Chord HSS	115
6.1.3.4	Summary of Results	119

6.2	Concrete	122
6.2.1	General	122
6.2.2	Ancillary Tests	124
6.2.3	Properties of Concrete in Compression ..	124
6.2.4	Properties of Concrete in Tension	126
6.3	Nelson Studs	128
6.3.1	Push-out Tests	128
6.3.2	Test Results	130
7.	SHRINKAGE TEST RESULTS	133
7.1	Deflections	133
7.2	Shrinkage Control Specimens	136
7.3	Slab Shrinkage	142
7.3.1	Average Overall Shrinkage	142
7.3.2	Local Slab Strains	146
7.3.3	Shrinkage Cracks	148
7.4	Steel Strains	149
7.4.1	Average Chord Strains	153
7.4.2	Local Steel Chord Strains	153
7.4.3	Web Member Strains	154
7.5	Variation of Strain Through Truss Depth	155
8.	ANALYSIS OF SHRINKAGE TESTS	159
8.1	Effective Moment of Inertia of Steel Trusses .	159
8.2	Distribution of Shrinkage Strains	160
8.2.1	Concrete Slab Strains	160
8.2.2	Steel Top Chord Strains	165
8.2.3	Steel Bottom Chord Strains	165
8.3	Shrinkage Forces in Members	167

8.4	Calculation of Deflection due to Shrinkage ...	175
8.4.1	Curvatures	177
8.4.2	Restrained Shrinkage Method	177
8.4.3	Unrestrained Shrinkage Method	180
8.4.4	Equilibrium Method	183
8.4.5	Summary	187
9.	FLEXURAL TEST RESULTS	191
9.1	Deflections and Overall Behaviour	191
9.2	Bottom Chord Strains	207
9.3	Top Chord Strains	209
9.4	Concrete Strains	209
9.5	Variation of Strain Through Truss Depth	214
9.6	Separation of Compression Angle Web Members ..	219
9.7	Interface Slip Between Slab and Top Chord	221
9.8	Failure Modes	223
10.	ANALYSIS OF FLEXURAL TESTS	227
10.1	Effective Moment of Inertia of Composite Trusses	227
10.2	Moment-Deflection Response	229
10.3	Strain-Force-Moment Relationships	235
10.4	Top Chord Behaviour	240
10.5	Web Member Behaviour	240
11.	SUMMARY, CONCLUSIONS, AND RECOMMENDATIONS	245
11.1	Summary	245
11.2	Conclusions and Recommendations	247
11.3	Areas of Further Research	253
	REFERENCES	255

List of Tables

Table	Page
4.1	Web member substitutions at fabrication63
4.2	Comparison of calculated and measured weights of test specimens66
4.3	Movement at reactions and load points80
4.4	Load cell specifications84
5.1	Measured dimensions of HSS sections92
5.2	Measured dimensions of angle sections93
5.3	Cross sectional properties of steel sections95
5.4	Mass variation of sections from specified values96
5.5	Steel truss measurements98
5.6	Slab dimensions98
6.1	Chemical composition of steel sections101
6.2	Mechanical properties of 300W web members108
6.3	Mechanical properties of 350W top chord109
6.4	Mechanical properties of 350W bottom chord113
6.5	HSS stub column test results116
6.6	Summary of test results for bottom chord120
6.7	Summary of mechanical properties of steel sections121
6.8	Concrete mix design123
6.9	Concrete properties in compression - truss 1125
6.10	Concrete properties in compression - truss 2125
8.1	Shrinkage deflection parameter values for truss 1179
8.2	Shrinkage deflection parameter values for truss 2179

Table	Page
8.3 Midspan shrinkage deflection calculations	188

List of Figures

Figure	Page
3.1	Moment resistance of a composite truss43
3.2	Half-elevation of steel truss50
3.3	Joint designations and loading diagram50
4.1	Concrete slab on truss 167
4.2	Composite truss 267
4.3	Location of strain gauges measuring shrinkage strains on truss 171
4.4	Location of strain gauges measuring shrinkage strains on truss 271
4.5	Location of slab instrumentation measuring concrete strains on composite truss 173
4.6	Location of slab instrumentation measuring concrete strains on composite truss 273
4.7	Load, shear force, and bending moment diagrams75
4.8	Schematic diagram of reaction assembly77
4.9	Reaction assembly - truss 277
4.10	Schematic diagram of loading assembly78
4.11	Jack assembly - truss 278
4.12	Location of strain gauges on composite truss 187
4.13	Location of strain gauges on composite truss 287
6.1	Identification and location of tension coupons103
6.2	HSS 127.0x76.2x4.78 tension test specimen106
6.3	Stress-strain curve for angle member BC from tension coupon110
6.4	Stress-strain curve for HSS 76.2x76.2x6.35 from tension coupon111

Figure	Page
6.5 Stress-strain curves for HSS 127.0x76.2x4.78 from tension coupons	114
6.6 Stress-strain curve for HSS 76.2x76.2x6.35 from stub column tests	117
6.7 Stress-strain curve for HSS 127.0x76.2x4.78 from stub column tests	117
6.8 Stress-strain curve for HSS 127.0x76.2x4.78 from full-scale tension specimen	118
6.9 Typical stress-strain curve for concrete in compression - truss 1	127
6.10 Typical stress-strain curve for concrete in compression - truss 2	127
6.11 Push-out test specimen	129
6.12 Load-slip curve for push-out test - truss 2	132
7.1 Shrinkage deflection of composite truss 1	134
7.2 Temperature variation during shrinkage interval for truss 1	135
7.3 Relative humidity variation during shrinkage interval for truss 1	135
7.4 Shrinkage deflection of composite truss 2	137
7.5 Temperature variation during shrinkage interval for truss 2	138
7.6 Relative humidity variation during shrinkage interval for truss 2	138
7.7 Unrestrained shrinkage strain - truss 1	140
7.8 Unrestrained shrinkage strain - truss 2	141
7.9 Slab shrinkage - truss 1	143
7.10 Slab shrinkage - truss 2	144
7.11 Shrinkage cracks in concrete slab - truss 2	150
7.12 Top chord strain due to shrinkage - truss 1	151

Figure	Page
7.13 Bottom chord strain due to shrinkage - truss 1	151
7.14 Top chord strain due to shrinkage - truss 2	152
7.15 Bottom chord strain due to shrinkage - truss 2	152
7.16 Strain variation with depth due to shrinkage - truss 1	157
7.17 Strain variation with depth due to shrinkage - truss 2	158
8.1 Distribution of strains on slab surface due to shrinkage	161
8.2 Longitudinal shrinkage strain of slab surface	164
8.3 Distribution of strains along top chord due to shrinkage	166
8.4 Distribution of strains along bottom chord due to shrinkage	166
8.5 Shrinkage forces	168
8.6 Free body diagrams for shrinkage forces	170
8.7 Shrinkage strains in top and bottom chords	172
8.8 Shrinkage strain distribution at midspan	174
9.1 Load deflection diagrams - composite truss 1	192
9.2 Deformed truss at 0.99 of maximum load - truss 1	195
9.3 Deformed slab at maximum load - truss 1	195
9.4 Separation of concrete from deck at maximum load - truss 1	196
9.5 Yield lines in compression diagonal BC at maximum load - truss 1	196
9.6 Distortion of truss components beyond maximum load - truss 1	198

Figure	Page
9.7 Truss 1 at midspan deflection of 500 mm	198
9.8 Buckled top chord and slab separation at failure - truss 1	199
9.9 Concrete tensile cone failures around studs - truss 1	199
9.10 Load-deflection diagrams - composite truss 2	200
9.11 Composite truss 2 at load of 100 kN per jack	202
9.12 Separation of concrete from deck at north end of truss 2	202
9.13 Transverse crack at north end of slab - truss 2	204
9.14 Local failure of top chord of truss 2	204
9.15 Reinforcement of top chord of truss 2 at maximum load	205
9.16 North end of truss 2 at failure	205
9.17 Deformed slab at failure - truss 2	206
9.18 Truss 2 at failure	206
9.19 Bottom chord strains at midspan - composite truss 1	208
9.20 Bottom chord strains at midspan - composite truss 2	208
9.21 Top chord strains at midspan - composite truss 1	210
9.22 Top chord strains at midspan - composite truss 2	210
9.23 Strains on top of concrete slab at midspan - truss 1	211
9.24 Strains on top of concrete slab at midspan - truss 2	211
9.25 Midspan concrete surface strains across the slab - truss 1	213

Figure	Page
9.26 North end concrete surface strains across the slab - truss 1	213
9.27 Midspan concrete surface strains across the slab - truss 2	215
9.28 North end concrete surface strains across the slab - truss 2	215
9.29 Concrete surface strains across the slab at 0.195L - truss 2	216
9.30 Concrete surface strains across the slab at 0.317L - truss 2	216
9.31 Strain variation with depth - truss 1	217
9.32 Strain variation with depth - truss 2	218
9.33 Separation of angle web members at mid-height - truss 1	220
9.34 Separation of angle web members at mid-height - truss 2	220
9.35 Interface slip - truss 1	222
9.36 Interface slip - truss 2	222
10.1 Moment-deflection response of composite truss 1	230
10.2 Moment-deflection response of composite truss 2	231
10.3 A comparison of moment-deflection diagrams	234
10.4 Calculated strain variation with depth - truss 1	237
10.5 Calculated strain variation with depth - truss 2	238
10.6 Eccentricities of axial load in member QR - truss 1	242
10.7 Eccentricities of axial load in member QR - truss 2	242

List of Symbols

- a = depth of equivalent rectangular compressive stress block in concrete slab, mm; distance from mid-depth of cover slab to mid-depth of top chord, mm
- A_{bc} = area of steel bottom chord, mm^2
- A_c = effective area of concrete, mm^2
- A_s = area of steel section, mm^2
- A_{sc} = cross sectional area of stud shear connector, mm^2
- A_{tc} = area of steel top chord, mm^2
- b = width of bottom chord section, mm; distance from mid-depth of bottom chord to mid-depth of top chord, mm
- b_e = design effective width of concrete slab, mm
- c = distance from extreme compression fibre of concrete slab to neutral axis of composite flexural member, mm
- C_r = factored compressive resistance of effective area of concrete slab, N
- C_{tc} = compressive force in top chord due to shrinkage, N
- d = depth of bottom chord section, mm; stud diameter, mm

- D = out-to-out depth of steel truss, mm
- e = lever arm between the compressive resistance C_r and tensile resistance T_r , mm
- E = modulus of elasticity of steel, MPa
- E_c = modulus of elasticity of concrete in compression, MPa
- $E_c(t_0)$ = modulus of elasticity of concrete in compression at time t_0 , MPa
- E'_c = tensile modulus of elasticity of concrete, MPa
- $E^*_c(t)$ = age-adjusted modulus of elasticity of concrete in compression at time t , MPa
- f'_c = specified compressive strength of concrete at 28 days, MPa
- F_y = specified minimum yield strength of steel, MPa
- h_d = height of ribbed steel deck, mm
- H = height of stud shear connector, mm
- I = moment of inertia, mm^4
- I_e = effective moment of inertia, mm^4
- I_s = moment of inertia of steel cross section, mm^4
- I_t = transformed moment of inertia of composite flexural member, mm^4

- k = a constant, indicating a linear relationship
- L = span length, mm
- M = bending moment, kNm
- M_r = factored moment resistance, kNm
- M_{rc} = factored moment resistance of composite truss, Nmm
- M_u = ultimate moment, kNm
- M_y = yield moment based on nominal properties, kNm
- M_{ym} = yield moment based on measured properties, kNm
- N = number of stud shear connectors in deck flute
- p = fraction of full shear connection
- P = concentrated load, kN
- q_r = factored resistance of a stud shear connector, N
- $Q_{u(r)}$ = ultimate strength of a stud shear connector in rib of slab on deck, N
- $Q_{u(s)}$ = ultimate strength of a stud shear connector in solid slab, N
- t = top chord flange thickness, mm; time from casting of concrete, days
- t_o = time, after moist curing, at which shrinkage is assumed to begin, days

- t_c = thickness of concrete cover slab, mm
- T_{bc} = tensile force in bottom chord due to shrinkage, N
- T_s = tensile force in slab due to shrinkage, N
- T_r = factored tensile resistance of bottom chord, N
- V_h = total horizontal shear to be transferred at the interface between the steel top chord of the truss and the slab, N
- w_d = average width of deck flute, mm
- y_c = distance from elastic neutral axis to line of action of shrinkage force, mm
- Δ = midspan deflection, mm
- Δ_{sh} = midspan shrinkage deflection, mm
- Δ_y = midspan deflection at yield moment M_y , mm
- Δ_{ym} = midspan deflection at yield moment M_{ym} , mm
- ϵ_{bc} = strain in bottom chord due to shrinkage, $\mu\epsilon$
- ϵ_c = concrete strain, $\mu\epsilon$
- ϵ_f = free (unrestrained) shrinkage strain of concrete, $\mu\epsilon$; strain at failure, $\mu\epsilon$
- ϵ_r = restrained shrinkage strain of concrete, $\mu\epsilon$

- ϵ_s = tensile strain in concrete slab due to shrinkage, $\mu\epsilon$
- ϵ_{sh} = shrinkage strain, $\mu\epsilon$
- ϵ_{st} = steel strain, $\mu\epsilon$; strain at which strain hardening begins, $\mu\epsilon$
- ϵ_{tc} = strain in top chord due to shrinkage, $\mu\epsilon$
- ϵ_u = strain at ultimate strength, $\mu\epsilon$
- ϵ_y = strain at yield strength, $\mu\epsilon$
- ϕ = resistance factor for steel = 0.90
- ϕ_c = resistance factor for concrete in compression = 0.60
- ϕ_{sc} = resistance factor for shear connectors = 0.80
- $\phi(t, t_0)$ = creep coefficient of concrete for the time interval considered
- $\chi(t, t_0)$ = aging coefficient of concrete in compression for the time interval considered
- ρ = radius of curvature of deformed truss at midspan, mm
- ρ_{av} = average radius of curvature of deformed truss, mm

1. INTRODUCTION

1.1 General

By providing interaction between the concrete slab and the steel supporting members of a floor system to take advantage of the performance of concrete in compression and steel in tension, an economical composite system with increased strength and stiffness is achieved. The development of composite flexural members has progressed from solid concrete slabs acting compositely with rolled steel beams and then with open-web steel joists and trusses to concrete slabs supported on ribbed steel deck acting compositely with steel members. Limit states design procedures have resulted in substantial steel weight savings for these members.

Composite trusses with deck-slab systems that incorporate wide rib profile steel deck enable longer spans and larger spacings to be used for design, and provide flexibility in office layout and use. Although more labour is required per tonne of steel for fabrication, total erected steel costs (as compared to the use of composite beams) are reduced due to the saving in steel. Unshored construction with the steel deck as a working platform is fast and permits other trades to follow closely behind. The open web system provides great flexibility for placement of mechanical and electrical services and reduces the ceiling to floor distance. Composite trusses are very stiff so that

deflections and vibrations under service conditions are small. To reduce design costs and increase the economy of fabrication, a sufficient number of repetitive trusses should be used.

The design of composite trusses is currently based on the requirements in CSA Standard CAN3-S16.1-M84, Steel Structures for Buildings (Limit States Design) (CSA, 1984a) for composite open-web steel joists. These requirements are based on a considerable amount of test data on composite open-web steel joists. However, only limited data are available from tests on long span joists and trusses. Additional testing of a practical array of composite trusses is required to ensure that a proven set of design procedures is available to designers. The overall behaviour of 2 such composite trusses is examined in this thesis.

1.2 Objectives

The objectives of this experimental study of composite trusses are:

1. to determine the effects of slab shrinkage on truss deflection and member stresses,
2. to determine truss stiffness prior to and after composite action is achieved based on measured deflections under dead and applied loads,
3. to examine the load-deflection response, load-carrying capacity, and failure mode of composite trusses loaded to failure, including observations of the distribution

- of strains across the slab width, the effect of interface slip on shear transfer at the steel-concrete interface, and indications of longitudinal shear failure in the concrete slab, and
4. to assess the adequacy of the current design provisions in CSA Standard S16.1 for establishing the strength and stiffness of these members.

1.3 Scope

Two 11.5 m span composite trusses were designed, constructed, instrumented, and tested. The truss configuration chosen was simple to fabricate, consisting of hollow structural section top and bottom chords and double angle web members with square-cut ends welded to the sides of the chords. The concrete slab on each specimen was cast on wide rib profile steel deck with ribs oriented perpendicular to the axis of the composite truss. Welded stud shear connectors provided composite action. The test specimens were monitored for several months to study the effects of slab shrinkage and then tested to failure under 4 concentrated applied loads. Shrinkage and flexural test data were analyzed and conclusions were drawn regarding composite truss behaviour under these conditions. The adequacy of current design requirements was assessed.

Because of the extent of the work involved in these shrinkage and flexural studies, a planned investigation of the dynamic behaviour of composite trusses was not

completed, although measurements were taken.

2. LITERATURE REVIEW

This literature review of the design and behaviour of composite flexural members is dealt with in 6 sections. Section 2.1 reviews the development of this type of composite construction from the early 1920's to the present. Sections 2.2 to 2.6 discuss specific aspects of composite behaviour in flexural members, including moment capacity, stiffness, shear connector strength, effective width, longitudinal shear, and shrinkage, all of which are of concern in the present study on composite trusses. In these sections, attention has been focussed mostly on papers published within the last 20 years. Fatigue considerations, of importance in bridge construction, as well as partial shear connection, use of lightweight concrete, and continuous flexural members are not discussed.

2.1 General History of Composite Steel-Concrete Construction

The presence of interaction between steel and concrete in floor systems was not recognized until the early 1920's when tests in Britain and Canada on steel beams encased in concrete showed that bond between the two materials resulted in increased member strength (Cook, 1977; Sabnis, 1979). Prior to this, concrete used in this application had been considered to act only as fireproofing for the steel beams. At the same time, tests were completed in the U.S.A. on rolled steel beams with prongs cut from their top flanges and bent to protrude into the concrete slab (Viest, 1960).

In 1929, Caughey and Scott (as described by Knowles, 1973) extended the fledgling composite design theory to include concrete slabs supported directly on steel beams, recognizing that some type of mechanical shear connection was required to ensure the interaction of the two materials. Many types of shear connectors were developed and investigated, including spiral rods and short lengths of rolled steel sections (especially channels), before the welded stud shear connector became popular in the 1950's. In Canada, composite beam design (concrete-encased steel beams) was included in the first edition of the National Building Code (NRCC, 1942). The behaviour was considered to be linearly elastic. In 1944, composite construction was included in the specifications for bridge design by AASHTO, the American Association of State Highway Officials (Cook, 1977), and in 1946, provisions for composite construction in buildings formed part of the AISC code (AISC, 1948). Following the publication of these documents, composite construction came into more general use and an increasing amount of research was directed towards improving the understanding of its behaviour.

In the 1960's, composite beam design moved towards ultimate strength design methods for both the flexural member and the shear connectors. Researchers studied the effective width of and longitudinal shear in composite slabs, the effect of partial shear connection and interfacial slip on strength and stiffness, the effect of

using light-weight rather than normal-weight concrete on shear connector strength, as well as the behaviour of continuous composite floors. The development of embossments in cold formed sheet steel decks, which had previously been used as slab elements with concrete fill, allowed these decks to be designed to act compositely with the concrete, and led to the composite design of beams and then open-web steel joists with metal deck. This innovation initiated further research on the influence of deck flutes on the strength of shear connectors and led to the design of new deck profiles in the early 1970's. Today, steel beams or trusses supporting steel deck-slabs and interconnected by welded stud shear connectors are the most common type of composite flexural member.

2.2 Flexural Capacity and Stiffness

2.2.1 Composite Beams

In the early 1960's, the design of composite beams for buildings was still based on allowable stress methods as described in a set of design recommendations by the Joint ASCE-ACI Committee on Composite Construction(1960). However, tests on composite beams showed that they could carry increased loads beyond the point of first yield and sustained large deflections prior to failure. Several researchers in Great Britain and the United States were involved in the development of ultimate strength predictions

and design procedures:

1. Chapman(1964) recognized that, for composite beams provided with enough shear connectors to reach the maximum moment of the section, ultimate capacity could be predicted from the fully plastic moment if the plastic neutral axis of the section was located within the slab thickness. He also observed that the shear connectors must be capable of resisting a shear force equal to the maximum horizontal force in the beam at failure but that due to their flexibility, a uniform spacing along the length gave satisfactory behaviour under most loading conditions.
2. Barnard and Johnson(1965) developed a computer program to predict theoretically the ultimate behaviour of composite beams from measured material stress-strain characteristics, assuming that the strain distribution through each section was linear (that is, no slip occurred across the interface) and that the concrete had no tensile strength. Moment-curvature diagrams produced by this method were compared to test results from 6 beam tests and found to be in close correspondence with the actual curves. Further "theoretical tests" led to the development of a design theory to calculate the ultimate strength of a composite beam. To simplify design, an idealized elasto-plastic stress-strain curve was assumed for the steel, and the concrete stress-strain curve was assumed to be linear up to the stress associated with

first yield in the steel. Three design cases were considered: the neutral axis located in the slab so that the steel section was fully plastic at maximum moment, the neutral axis located in the slab with the steel not fully plastic at maximum moment, and the neutral axis located in the steel beam at maximum moment.

3. Slutter and Driscoll(1965) tested 9 shear stud push-out specimens and 12 composite beams in their investigation of ultimate strength behaviour. Their simple design procedure is the basis for the present design provisions for composite beams. They determined that the amount of shear connection provided between points of zero and maximum moment must have adequate strength to satisfy horizontal equilibrium up to the ultimate load on the beam. However, given that the shear connectors have adequate strength, slip at the interface will not reduce the beam's capacity or significantly affect the load-deflection behaviour. The ultimate strength of a beam whose flexural strength is not limited by failure of the shear connectors can be calculated from a simplified plastic stress distribution over the section, using a rectangular concrete stress block with a uniform stress of $0.85f'_c$ and a uniformly distributed stress of F_y (tension or compression, depending on the location of the plastic neutral axis) across the steel section. This calculation results in the maximum possible flexural strength of the section, if the assumption that strain

hardening can be neglected is correct. Slutter and Driscoll also found good agreement between test results and calculations of the flexural strength of beams without adequate shear connection to develop the maximum ultimate strength (that is, beams with partial shear connection).

4. Yam and Chapman(1968) systematically varied a number of parameters in a theoretical analysis of the ultimate strength of composite beams, which took into account the inelastic behaviour of the steel, concrete, and shear connectors, and generally confirmed the new ultimate strength design provisions in the British Standard Code of Practice CP117:Part 1, "Composite Construction in Structural Steel and Concrete, Simply-Supported Beams in Building", published in 1965.
5. Reddy and Hendry(1970) derived formulas and a computer program to calculate the ultimate strength of a composite beam, neglecting the effects of slip but taking into account strain hardening, and found good agreement between their results and those of tests described in the literature.

In spite of these developments, ultimate strength design procedures for composite beams in buildings were not adopted in the Canadian design code until 1974 (CSA, 1974). In the United States, ultimate strength design procedures were proposed in 1983 (AISC, 1983).

Atkinson initiated the use of composite steel beams supporting concrete slabs on corrugated steel decking (Atkinson and Cran, 1972). Early observations showed that both member strength and stiffness were affected when the deck corrugations were placed transverse to the beam.

The first study of the behaviour of a 6.4 m span composite beam supporting a concrete slab on 73 mm steel deck with transverse ribs, interconnected with headed stud shear connectors, was carried out in 1961 by Robinson(1967). Although he concluded that the system was effective, the specimen tested did not reach its ultimate flexural strength, and Robinson pointed to the geometry of the deck profile as the major factor influencing the type of failure and the loss of full composite interaction between the slab and beam. In a systematic test program of 15 composite beams and 39 push-out specimens with 12 different deck configurations, Robinson(1967) determined that for deep narrow ribs with a height-to-width ratio greater than 1, failure by cracking of the concrete ribs occurred prematurely in the elastic range of composite behaviour. A rib height-to-width ratio less than 1 allowed a load greater than that of first yielding to be attained prior to rib cracking. Composite behaviour did not appear to be affected by the diameter and spacing of the shear connectors. In another beam test, Robinson(1969) showed that the ultimate flexural strength calculated using Slutter and Driscoll's method for partial shear connection had good agreement with

test results.

Fisher(1970) evaluated test results of composite beams with deck-slabs from several sources, and observed that those with rib heights up to 38 mm did not experience a significant decrease in ultimate flexural strength or in stiffness at working loads due to the presence of the ribs. For rib heights up to 76 mm, he stated that the ultimate flexural strength of a composite beam with full shear connection could be developed if the average width-to-height ratio of the ribs was greater than about 1.75. For smaller average width-to-height ratios, the rib geometry decreased the strength of the shear connectors, resulting in a decrease in the flexural capacity of the beam.

Robinson and Wallace(1973), after testing 12 push-out specimens and 9 simple span composite beams with slabs on 38 mm deck, identified rib height and width, slab width, number of connectors per rib, stud diameter, and embedment length of studs in the cover slab as variables affecting the strength of shear connectors in concrete ribs. They confirmed that, with full shear connection, the ultimate flexural strength of a composite beam with a slab on 38 mm deep ribbed deck could be attained.

After a comprehensive test program involving 17 composite beams with deck-slabs and an evaluation of the results of 58 other beam tests reported in the literature, Grant, Fisher, and Slutter(1977) concluded that rib geometry and stud embedment length above the rib had the largest

effect on the horizontal shear capacity of a composite beam with a deck-slab whose ribs run transverse to the beam length, and that rib slope and steel yield strength were not important variables. They observed that, for beams with shear connection about equal to that required for full composite action, the reduction in flexural capacity due to loss of interaction was not proportional to the reduction in the degree of shear connection. Grant et al. concluded, based on earlier test results, that the calculated stiffness of a composite beam with a solid slab could be reduced by up to 15% due to the flexibility of the shear connectors. They observed that composite beams with deck-slabs behaved in a similar manner, and further loss of stiffness could be expected if the beams had only partial shear connection. To estimate the effect of partial shear connection on deflection at working loads, Grant et al. developed an equation for the effective moment of inertia of a composite beam with or without deck:

$$[2.1] \quad I_e = I_s + p^{0.5} (I_t - I_s)$$

which showed good agreement with test results, although there was considerable scatter.

2.2.2 Composite Open-Web Steel Joists

Initial testing in the mid-1960's to study the possible composite behaviour of open-web steel joists supporting

concrete slabs were conducted on proprietary products with relatively short spans and centre-to-centre spacings. Later, it became evident that composite open-web steel joists were especially efficient and economical as flexural elements for long span floors. Design rules for composite beams were applied and then modified as investigators studied the performance of composite open-web steel joist test specimens.

Lembeck (as described by Tide and Galambos, 1970) performed 5 tests on conventional and composite open-web steel joists with 6.1 m spans. Composite interaction of the composite joists resulted from the projection of the web members into the concrete slab above the top chord. Lembeck concluded that composite joists were stronger and stiffer than non-composite joists with the same tension chord and web system, and as well, that the size of the steel top chord of a composite joist could be considerably reduced.

After 4 tests on composite and non-composite open-web steel joists, Wang and Kaley(1967) also reported that member stresses and deflections of composite joists were appreciably lower than those of non-composite members. Their tests were conducted only in the elastic range.

Tide and Galambos(1970) tested five 4.9 m span composite open-web steel joists with both cold formed and hot rolled steel chords. Most of these specimens failed due to the provision of an inadequate number of stud shear connectors for full composite action. Tide and Galambos

observed that the web members of a composite joist carry most of the vertical shear in the member. As well, interface slips measured at shear connector locations were larger near the ends of the span, indicating, as would be expected, that connectors near the reactions carry larger shear forces and that the slip accumulates towards the ends.

Cran(1972) made recommendations for the ultimate strength design of composite open-web steel joists, based on the results of full-scale tests on 3 different joists with spans of 12.2, 15.2, and 6.1 m. All exhibited very ductile behaviour although only the 2 long span joists were tested to failure. In both of these cases, failure was initiated by buckling of a web member, which Cran attributed to secondary stresses due to the large deflections. At failure, the maximum strains in the bottom chords of these members were 2.0 and 7.8 times the yield strain. Based on the observation that top chord compressive strains diminished to zero or even became tensile as load was applied to the test specimens, Cran concluded that the contribution of the top steel chord of a composite open-web steel joist could be neglected for strength calculations. For design purposes, the concrete slab acts as the top chord of the truss. Cran also recommended that the calculated elastic deflection of a composite open-web steel joist be increased by 10% to account for shear deflection, with a further increase of 10 to 20% to account for the effects of interface slip, especially for slabs on ribbed deck.

Atkinson and Cran(1972) summarized design requirements for composite open-web steel joists and commented that elastic and ultimate strength design procedures produce almost the same results.

Azmi(1972) described an ultimate strength design theory for composite open-web steel joists with different degrees of shear connection, developed from tests on six 15.2 and 15.5 m span composite joists from 3 manufacturers. The joists supported 1.5 m wide concrete slabs on metal deck with 38 mm high flutes and a rib spacing of 152 mm, and with varying degrees of shear connection provided by stud shear connectors or puddle welds. The web members on most of the specimens were designed to preclude failure by web buckling. Several of the specimens behaved in a very ductile manner (with midspan deflections at failure of up to 498 mm) and collapsed due to fracture of the bottom chord, while shear connector failure of those specimens with only partial shear connection caused buckling of their top chords. Azmi's design equations were based on equilibrium considerations and dealt with 3 cases: a balanced section where the shear connectors have enough strength to transfer the force in the bottom chord at yield, an over-connected section with a shear connector capacity greater than the yield force in the bottom chord (allowing the top chord to develop an appreciable tensile force), and an under-connected section (with partial shear connection) where the steel top chord develops a compressive force. Azmi recognized that two of

the test specimens failed only when the bottom chord reached its ultimate strength, but recommended the use of the yield stress for design because failure by bottom chord fracture "is not guaranteed".

Fahmy(1975) conducted 2 additional composite open-web steel joist tests to complete the test series begun by Azmi, and developed an inelastic method of analysis (and computer program) for composite open-web steel joists with varying degrees of shear connection that showed good agreement with the test results of the 8 composite joists. The failure strains in the bottom chords of Fahmy's specimens reached 0.9 and 1.6% (much higher than the yield strain) before the puddle weld shear connection failed.

In a summary of Azmi and Fahmy's work, Robinson, Fahmy and Azmi(1978) noted that the ultimate performance of composite open-web steel joists was not influenced by the different characteristics of hot rolled versus cold formed steel chord members. From an analysis of the top chord strains, they determined that, for composite open-web steel joists with only partial shear connection, the transition point between a failure by buckling of the top chord as a result of the large compressive force carried by the chord and a failure of the shear connection occurred at a degree of partial shear connection between 50 and 75%.

2.2.3 Composite Trusses

Only two studies on the behaviour of long span composite trusses are reported in the literature. Of course, open-web steel joists really are trusses, and much of the knowledge from research on their composite behaviour, as discussed in Section 2.2.2, is transferable to the study of composite truss behaviour. Small differences exist because composite trusses are individually designed and analysed for a specific use while open-web steel joists are mass-produced proprietary products that are often fabricated automatically by methods (such as resistance welding) that reflect the preferences of individual producers.

Iyengar and Zils(1973) tested a composite truss assembly, typical of that used in the floor system for the Sears Tower in Chicago, that consisted of two 22.9 m span Warren type trusses spaced at 4.6 m centres with a 7.6 m wide slab on 76 mm ribbed steel deck. Interconnection between the 1016 mm deep steel trusses and the 140 mm lightweight concrete slab was provided by 114 mm long stud shear connectors with a diameter of 19 mm. The system was uniformly loaded to a maximum load of 7.2 kPa, corresponding to 1.4 dead plus 1.7 live load. The load-deflection response was only slightly non-linear and agreed with a theoretical prediction. No slab cracks or truss deformations were observed, but the test was not taken to failure.

A performance test on a 12 m span composite truss designed for an Edmonton office tower was conducted by

Bjorhovde(1981). The 850 mm deep steel truss was comprised of HSS top and bottom chords, double angle diagonals in a Warren configuration and HSS verticals. The test specimen supported a 2.3 m wide normal weight concrete slab with a cover depth of 63 mm over 76 mm wide rib profile steel deck. Stud shear connectors with a diameter of 19 mm and length of 114 mm were uniformly distributed along the truss length. The test specimen was loaded with 3 point loads located over the top chord at the quarter points, and showed essentially elastic response at service load levels. Failure was precipitated by buckling of the first compression diagonal prematurely at a load reported to be 95% of the design load, and after repair, at a load calculated to be 1.07 times the design ultimate load. The failure was attributed to misplacement of a stud in a deck flute.

2.3 Shear Connection

The behaviour of a composite flexural member is dependent on the effectiveness of the shear transfer at the interface between the concrete slab and the steel member. Full interaction between the two components will occur only if the shear connection is rigid, and can prevent both slip between and separation of the components. Because shear connectors in popular use are flexible, the effects of interface slip on strength and stiffness have been a major concern for design.

Until the 1960's, the allowable load for any type of shear connector was determined from tests to preclude any inelastic deformation or slip greater than three-thousandths of an inch. Culver and Coston(1961) observed, based on the results of 3 composite beam tests, that loading the connectors to failure did not affect beam behaviour and therefore the maximum useful strength of connectors was not being taken advantage of in design. Both Chapman(1964) and Slutter and Driscoll(1965) recognized that the ultimate strength provided by the shear connectors must be adequate to resist the maximum horizontal shear force in the shear span at maximum load, in order to maximize the moment resistance of the composite section. If full shear connection was provided, interface slip did not affect the ultimate strength of the member. As well, both concluded from test results that, for members loaded with a uniformly distributed load, a uniform connector spacing along the length did not adversely affect the strength because the flexibility of the connectors allowed redistribution of the longitudinal shear forces.

Because headed stud shear connectors are the most common type of shear connection and were used in the research described here, the following discussion on shear connector strength will be limited to studies of their behaviour.

2.3.1 Strength of Studs in Solid Slabs

Viest(1956) conducted the first tests on the static strength of welded stud shear connectors. Based on results from 12 push-out tests on studs varying in diameter from 13 to 32 mm, he determined that the allowable capacity of a stud was proportional to the square of the diameter for studs with a diameter less than 25 mm and to the diameter for studs greater than 25 mm. For all sizes, capacity was also proportional to $\sqrt{f_c}$. He also suggested that the yield strength of the steel stud, the height of the stud, and the stud spacing would also affect strength.

Chapman(1964) identified two failure modes for the shear connection—failure of the connector by shear or yielding and failure of the concrete by crushing. He observed that confinement of the concrete by slab reinforcement strengthened the shear connection.

From their own test results and a review of other published push-out test and beam test data, Slutter and Driscoll(1965) confirmed that the ultimate strength of stud shear connectors was proportional to the square of the diameter and $\sqrt{f_c}$. They found that the connector strengths obtained from push-out tests were lower than strengths measured from beam tests.

As part of a large study to determine the strength and behaviour of shear connectors embedded in normal and lightweight concrete slabs, Ollgaard, Slutter, and Fisher(1971) tested 48 push-out specimens with 16 and 19 mm

diameter studs. Two failure modes were observed. In the first, the stud sheared off the steel beam and remained embedded in the concrete slab while in the second mode, the stud deformed until a crack formed in the concrete behind the head of the stud. Ollgaard et al. developed the following equation from a multiple regression analysis of the test results to calculate the ultimate strength of a stud shear connector:

$$[2.2] \quad Q_{u(s)} = 0.5 A_{sc} \sqrt{f'_c E_c}$$

with the tensile strength of the connector as an upper bound to the connector strength. These relationships are the ones presently used for shear connector design.

Goble(1968) identified pull-out of a welded stud from a thin steel flange as a third failure mode for stud shear connectors. From 50 push-out tests on studs with diameters of 13, 16, and 19 mm welded to flanges with 3 different thicknesses, he defined a shift in failure mode from shear to pull-out at a stud diameter-to-flange thickness ratio (d/t) of about 2.7. He stated that the failure mode shift was related to material properties, so that for a flange with a strength greater than that of the 250 MPa steel used in his tests, the failure mode shift could be expected to occur at a higher d/t ratio.

2.3.2 Strength of Studs in Slabs on Ribbed Deck

Early tests on composite beams supporting concrete slabs on metal decks with corrugations running perpendicular to the axis of the member indicated that the presence of open cells in the slab could reduce the strength of the shear connectors and the stiffness of the member. Larger interfacial slip due to the flexibility of the cells could result in a partial loss of interaction.

From push-out and beam tests with various deck configurations, Robinson(1967) determined that increasing the height of the concrete ribs had a negative influence on flexural capacity, while increasing the width of the ribs improved the performance of the beam, because there was more concrete cover to prevent the connectors from punching out of the ribs, and because a larger width reduced the tendency of the ribs to rotate. He concluded that the configuration of a cellular deck has a strong influence on shear connector capacity. Robinson observed that variations in stud diameter and spacing did not significantly affect the behaviour of his test beams. However, embedment of the heads of the studs in the solid part of the slab contributed to improved behaviour near failure.

Fisher(1970) evaluated shear connector test results from a number of sources in the literature, and concluded that the reduction in strength of a shear connector in ribbed deck was proportional to the rib width-to-height ratio; ie,

$$[2.3] \quad Q_{u(r)} = k \left[\frac{w_d}{h_d} \right] Q_{u(s)}$$

For decks up to 76 mm deep with a rib width-to-height ratio greater than 1.75, shear connector strength was not reduced below that in a solid slab. Fisher observed that concrete confinement from slab reinforcement clipped to the studs improved the shear capacity. He also noted that smaller diameter studs provided more efficient connection, and recommended against using studs with diameters greater than 19 mm. Fisher recommended that studs should extend a minimum of 38 mm into the solid part of the slab above the rib.

Robinson and Wallace(1973) also observed, in their beam and push-out tests, that the length of embedment of a stud in the solid part of the slab above the rib affected shear connector strength. As well, their tests showed that locating 2 studs in a concrete rib increased the shear connection of that rib by only 50%.

Push-off tests by Iyengar and Zils(1973) showed that the ultimate shear strength per stud is reduced when more than one stud is placed in a concrete rib, and that plug welds provided to fasten the decking to the steel section contributed to shear strength. Iyengar and Zils commented that stud shear connectors performed more effectively when located to the outside of a deck flute (that is, the reaction side) rather than the inside or midspan side. They also observed that an increase in connector strength occurred when the length of the stud projection into the solid part of a deck-slab increased.

In their model to predict the reduction in strength of a stud shear connector embedded in a concrete rib compared to the connector strength in a solid slab, Grant, Slutter, and Fisher(1977) accounted for the increase in shear strength with increased embedment of the stud in the solid portion of the slab (observed by Fisher, Robinson and Wallace, and Iyengar and Zils) and for the reduced stud capacity when more than 1 stud is located in each flute (observed by Robinson and Wallace, and Iyengar and Zils) with the equation

$$[2.4] \quad Q_{u(r)} = \frac{0.85}{\sqrt{N}} \left[\frac{H - h_d}{h_d} \right] \left[\frac{w_d}{h_d} \right] Q_{u(s)} \leq Q_{u(s)}$$

This equation, based on test results from 75 composite beams, represents a significant increase in the understanding of the behaviour of studs in ribbed deck-slabs, compared to Fisher's original equation described by [2.3].

The failure mode in early tests concerned with the shear strength of studs embedded in deck-slabs began with cracks forming at the corners of the concrete ribs at the top of the flutes and progressing until the concrete ribs sheared off there. In the vicinity of each stud, the shear surface passed over the head of the stud. Both Fisher(1970) and Robinson and Wallace(1973) observed that test specimens with wider concrete slabs had higher horizontal shear strengths, and at failure the concrete ribs were not

completely sheared off. For test specimens with wide concrete slabs, shear connection failure modes described by Grant, Fisher, and Slutter(1977) include punching of the stud through the rib (also observed by Robinson and Wallace) and shear cone failure of the concrete around each stud (also observed by Iyengar and Zils). In the case of the shear cone failure mode, lengthening the embedment of the stud in the solid part of the slab increases the connection strength by forcing a larger failure surface.

2.4 Effective Slab Width

The calculation of an effective width for the concrete "flange" of a composite steel-concrete beam or truss is a design tool to simplify the computation of its flexural capacity. The actual distribution of longitudinal compressive stresses in the concrete slab measured transversely across the slab width has a maximum value along the line of the shear connection and decreases with distance from that centreline due to the phenomenon of shear lag. For design, a uniform distribution of the maximum concrete stress across the effective width allows the compressive force in the concrete slab to be calculated easily.

Most design specifications define the effective width of a composite beam with equations that are a function of beam span or slab thickness. Of course, the upper limit to the effective width is the spacing between beams in the floor system. These design equations are based on elastic

behaviour. Tests have shown that the effective width is affected by the type of loading and by the geometry of the floor system, especially the ratio of beam spacing-to-span.

Several investigators have addressed the problem of determining the effective slab width of a simple span composite beam in the elastic range. Mackey and Wong(1961) tested 4 small scale composite beam floor systems with different beam spacings and concluded that effective width decreases as the ratio of beam spacing-to-span increases. They calculated the effective width using three methods—by dividing the area under the transverse strain distribution diagram for each beam by the maximum strain ordinate, from stress triangles after the neutral axis was located by plotting the measured strains through the depth of the member, and from an analytical analysis based on plane stress theory. All three of these calculations showed that the effective width was larger than that predicted by equations in the design specifications. Hagood, Guthrie, and Hoadley(1968) conducted further tests on 3 small scale composite floor systems and, using Mackey and Wong's methods to calculate the effective width from their test results, confirmed that the effective width used for design is conservative for interior beams and reasonable for edge beams. Adekola(1968) developed a method of analysis for determining the effective width that takes into account the variation in the depth of the neutral axis across the width of the slab (due to shear lag), and using a computer

program, produced design aids for effective width (in the form of tables). Adekola found that for beams with a span-to-beam spacing ratio greater than 5, the effective width was constant along the beam length.

To be consistent with design principles for flexure, which are based on ultimate strength, the determination of effective width should be based on ultimate rather than elastic behaviour. However, the use of elastic values for effective width was assumed to be conservative because tests indicated that the effective width increased with increasing load (Brendel, 1964). Heins and Fan(1976) developed two equations to predict the effective widths of interior and exterior composite beams at ultimate loads from a linear regression analysis on test data obtained for composite bridges, using an analytical technique to calculate the stress distribution throughout the composite system. They concluded that the equations in the design specifications overestimate the effective width of interior beams and underestimate the effective width of exterior beams at ultimate loads. This conclusion may not be of great concern, for both Hansell et al.(1978) and Nixon(1982) have observed that the ultimate moment resistance of a composite beam is not sensitive to changes in effective width. Nixon used a non-linear finite element program to confirm that the effective width of an interior beam decreases as the load increases. He found that the same phenomenon occurred for an exterior beam, but at a much slower rate. Nixon showed,

using Heins and Fan's equations, that the maximum reduction in effective width of about 20% for an interior beam corresponds to only a 3 or 4% reduction in bending moment.

The effective width equations in the design specifications are applicable to composite members with solid slabs and with slabs over ribbed steel deck. Fisher(1970) studied test results that confirmed that the full thickness of a slab on deck (cover slab plus rib height) should be used to calculate effective width. As well, his studies of strain measurements on concrete deck-slabs showed that shear lag was not more severe than in a solid concrete slab. Azmi(1972) observed from his tests on composite open-web steel joists with deck-slabs that the full 1.5 m width of the slab (1/10th of the span) was effective in compression.

2.5 Longitudinal Shear

So called "longitudinal shear" failure of the concrete slab in the immediate vicinity of the shear connectors has been recognized as a failure mode for composite flexural members. Concrete seldom fails in shear itself but the term "longitudinal shear" has been used to describe this failure mode. Transverse tensions actually develop due to shear lag. Until recently, design specifications have not included provisions for checking the "longitudinal shear". Early investigators (Chapman, 1964; Slutter and Driscoll, 1965) reported premature failures in some composite test specimens

due to the formation of longitudinal cracks in the concrete slab parallel to the line of shear connection and noted the need for additional transverse reinforcement to prevent such cracking. A complex 3-dimensional stress state exists in the concrete near the shear connectors due to the combined effects of longitudinal bending of the composite beam, transverse negative bending of the slab which spans between adjacent beams, vertical shear, and local force transfer at the shear connectors, so that analyses to improve the understanding of the interaction between the shear connectors and the concrete are difficult. Several researchers have studied the problem of longitudinal shear failure and have suggested design methods to choose adequate transverse reinforcement to prevent premature failure.

From tests on 4 half-scale composite beams with varying amounts of transverse reinforcement, Davies(1969) developed an empirical equation to determine the minimum amount of transverse reinforcement required to achieve the ultimate flexural capacity of a composite beam without prematurely developing a longitudinal shear crack. Davies hypothesized that longitudinal cracking began on the underside of the slab near the base of the shear connectors where he believed the concrete stresses were very high, and progressed upward to the top surface of the slab. He observed that longitudinal cracks in his test specimens developed first under the concentrated applied load at midspan and then spread towards the reactions.

Johnson(1970) studied the test results of more than 60 composite beams tested to failure and proposed an ultimate strength design method to determine the required amount of top and bottom transverse reinforcing steel to ensure adequate longitudinal shear strength for composite beams with negative transverse bending in the slab. He concluded that, although all transverse reinforcement contributes to longitudinal shear strength (regardless of its location through the slab depth), at least half the required steel should be located near the lower surface of the slab where stress concentrations resulting from the shear connectors were assumed to occur. Johnson believed that because transverse bending stresses enhance the shear strength of the slab, the top steel provided need not be greater than that required for longitudinal shear or transverse bending. (This conclusion, that transverse bending stresses suppress longitudinal shear cracking, is supported by results of a theoretical analysis reported by Robinson, Fahmy, and Azmi(1978) in reply to a discussion raised by Johns.)

El-Ghazzi, Robinson, and Elkholy(1976) developed ultimate strength design equations to determine the minimum amount of transverse reinforcement required to reach ultimate capacity and the amount of reinforcement that allows simultaneous failure by longitudinal cracking and shear connection failure for beams with partial shear connection. These equations were developed from a theoretical analysis of the concrete stresses on the

predetermined shear surface surrounding the connectors, which takes into account variations in shear strength in the compressive and tensile zones of the slab (the shear strength is not constant through the slab thickness). El-Ghazzi et al. found that the longitudinal compressive bending stress in the slab, the slab width, and the length of the shear span were important variables for estimating the longitudinal shear capacity of a concrete slab. The design equations show good agreement with Davies' test results and empirical equations.

A premature longitudinal shear failure in the slab of a composite stub girder tested by Buckner, Deville, and McKee(1981) led to the development of a simple design method which compares the maximum shear stresses that must be transferred across the critical shear surface adjacent to the rows of shear connectors to shear friction strength values proposed by Mattock, Li, and Wang(1976) for normal and lightweight concretes along initially cracked or uncracked shear surfaces. Buckner et al. state that the longitudinal shear stress in the concrete can be assumed to vary linearly from the maximum value near the connectors to zero at the edges of the effective slab width.

Johnson and Oehlers(1981) discuss a splitting type of failure that has been observed in the concrete of composite test specimens (especially push-out specimens) at shear stud locations, which they believe is unrelated to the phenomenon of longitudinal shear cracking. This splitting failure has

been observed to occur when several of the following adverse conditions are present—a low ratio of span-to-slab width, the application of point loads that are a high percentage of the total applied load, existence of high longitudinal shear stresses for which transverse reinforcement greater than 1% has been provided, or a narrow arrangement of shear connectors (for example, a single straight line). It is possible that some of the longitudinal cracks observed in test specimens and attributed to shear failure were in fact a result of this splitting phenomenon, especially those which developed under points of concentrated load near midspan. It would be expected that concrete shear stresses would be highest near the reactions, where the rate of change of shear is highest. For example, Tide and Galambos(1970) reported that several composite open-web steel joist test specimens with solid slabs developed longitudinal shear cracks over the shear connector closest to the reaction in each shear span, and that these cracks progressed inward as more load was applied and failure was approached. Interface slip measurements at shear connector locations were larger near the reactions, indicating that the end shear connectors carried higher forces.

All of the experimental and theoretical studies discussed above have concluded that longitudinal shear cracks begin to develop near the bottom surface of a solid slab. The work appears to be based on the assumption that the force transfer between the concrete and the stud shear

connector occurs very close to the base of the stud, so that high concrete stresses exist in that area. The basis for this assumption is unclear. It seems more likely that compressive forces in the concrete slab are transferred to the stud near its head, which should be located above the plastic neutral axis of the member. If this is the case, longitudinal shear cracks would begin near the head of the stud and progress up to the surface of the slab. A model to explain how the compressive force in the slab is transferred to the stud shear connectors is described by Leonhardt and Andrä(1981), and involves the formation of a compressive strut behind each stud, extending from the head of the stud to the concrete-steel interface in front of the next stud. Leonhardt and Andrä discuss the importance of friction at the interface to anchor the strut. For a slab on deck with ribs running transverse to the axis of the member, excellent anchorage would be obtained due to the profile of the steel deck. This suggests, however, that the stud should be placed to the inside or midspan side of the deck flute, contrary to the comments of Iyengar and Zils, as discussed in Section 2.3.2.

It is uncertain whether longitudinal shear cracking is a problem in composite members with concrete slabs over ribbed metal deck. The CISC Handbook of Steel Construction(1984) states that cracking has not been observed in deck-slab systems where the ribs run transverse to the longitudinal axis of the member, and surmise that

this may be due to the extra reinforcement provided by the deck. However, Robinson and Wallace(1973), testing composite beams supporting concrete slabs on 38 mm ribbed steel deck, reported the formation of longitudinal cracks in the shear spans of their test specimens at loads ranging from 0.85 to 0.92 times the ultimate load capacity.

2.6 Shrinkage Behaviour

The volume change of concrete due to drying shrinkage has been the subject of many research studies through the years because it can result in excessive stresses, cracking, and deflection in concrete structural members. Cracking can be controlled by careful curing practices and with the use of shrinkage reinforcement and control joints. However, the prediction of deflections due to shrinkage, which is a necessary part of the design procedure, is somewhat more difficult.

Drying shrinkage is caused by loss of water from capillary pores and adsorbed water from the molecules of the cement paste. Therefore, all factors which influence the water content of the concrete, such as cement content and composition, amount and gradation of aggregate, and presence of admixtures affect the amount of shrinkage that will occur. Environmental conditions, such as air temperature and relative humidity, are important factors and it has been shown that the size and shape of the concrete member (usually expressed in the form of a volume-to-surface area

ratio which reflects the length of the diffusion path) affect both the amount and rate of drying shrinkage. The rate of shrinkage decreases over time, reaching equilibrium after an extended period.

2.6.1 Shrinkage Models

Measurements of the ultimate shrinkage strain of unrestrained plain concrete test specimens show a wide scatter. The most common range of values reported is between 400 and 800 $\mu\epsilon$, but several references (Park and Paulay, 1975; Mindess and Young, 1981) indicate that values between 200 and 1100 $\mu\epsilon$ have been measured. In one study by the U.S. Bureau of Reclamation (as described by CPCA, 1978), unrestrained shrinkage strains of 600 to 790 $\mu\epsilon$ for 100 x 100 x 1000 mm concrete specimens were recorded after a period of 38 months. About 34% of that maximum value occurred within 1 month and about 90% occurred within 11 months.

Because of the large number of variables that affect shrinkage, the complex behaviour of the concrete over time is difficult to predict. However, simplified models have been developed to estimate the value of unrestrained shrinkage strain at any time for design purposes. The two most common methods are those proposed by the ACI Committee 209(1971,1982) and the CEB-FIP(1978). Both are partly empirical and based on data from laboratory tests.

The ACI Committee 209 method, which is also described by Branson and Christiason(1972) and Park and Paulay(1975), begins with an equation to calculate the unrestrained shrinkage strain which occurs over a time interval "t" for "standard conditions". A value for the ultimate unrestrained shrinkage strain at "t" equals infinity must be assumed. A mean value of $800 \mu\epsilon$ is recommended if no other information is available. Correction factors are then applied to account for non-standard conditions. Correction factors are included for different curing conditions, relative humidity, temperature, member thickness or volume-to-surface area ratio, and concrete composition (slump, percentage of fine aggregate, air content, and cement content) but do not cover the complete range of these variables.

The CEB-FIP approach to the prediction of the unrestrained shrinkage strain at time "t" involves multiplying a shrinkage coefficient that depends on relative humidity, concrete composition (slump and cement content), and the effective thickness of the specimen (related to the volume-to-surface area ratio) by a function to account for the rate at which shrinkage develops. Graphs are provided to obtain the parameters required in the equation. As in the ACI method, the shrinkage strain at "t" equals infinity must be assumed in the absence of test data, and a value of $800 \mu\epsilon$ is suggested for moist cured concrete.

The presence of steel reinforcement in a concrete member restrains but does not prevent shrinkage movement.

Typical restrained shrinkage strains range from 200 to 300 $\mu\epsilon$ (CPCA, 1978). Only one model to predict the magnitude of restrained shrinkage strain has been proposed and this model requires the unrestrained shrinkage strain at time "t" as an input. Hobbs(1982) measured the shrinkage strains of 40 x 40 x 250 mm concrete specimens with and without a symmetrically placed reinforcing bar over periods of up to 180 days. The tests show that the magnitude of restrained shrinkage strain is influenced by the amount of reinforcement and by the moduli of elasticity of the steel and concrete. He developed a relationship between restrained and unrestrained shrinkage strain that includes the effects of creep in tension. He used the modulus of elasticity of concrete in compression in his calculations.

Glanville(1930) studied shrinkage stresses (caused by restraint) in symmetrically reinforced 152 x 152 x 914 mm concrete specimens. He recognized that tensile stresses were developed in the concrete due to shrinkage and proposed that shrinkage stresses could be calculated by using an effective value of the modulus of elasticity of the concrete that corresponds to a modular ratio of 10 to 20.

2.6.2 Deflection of Composite Flexural Members

In a composite beam or truss, shear connectors as well as steel reinforcement restrain the shrinkage movement of the concrete slab. This restraint induces tensile stresses in the concrete slab and, as well, compressive stresses in

the top flange or chord and tensile stresses in the bottom flange or chord of the composite beam or truss and causes deflection of the member. Serviceability problems (excessive cracking and deflection) of composite beams in several field applications have pointed out the need to predict the magnitude of shrinkage deflections for design purposes.

Calculation procedures to predict the deflection of composite flexural members were borrowed from studies to predict the deflection of concrete composite members. The methods discussed below are all based on a procedure called the "composite section method" summarized by Branson(1964). First, the concrete slab is assumed to shrink. To enforce compatibility between the slab and its supporting member, a tensile force is applied at the centroid of the slab to extend the slab back to its original length. Then, an equal and opposite force is applied to the transformed composite section, again at the centroid of the slab, satisfying external equilibrium of the horizontal forces. The shrinkage deflection of a simply supported beam is then calculated using an elastic formula, assuming the beam is bent in single curvature by equal end moments with a magnitude equal to the horizontal force times the distance to the elastic neutral axis of the composite member.

Roll(1972) used Branson's "composite section method" to confirm that excessive deflection of the composite beams in a small office building left unoccupied for 16 months after erection were in fact due to shrinkage and creep. He found

excellent correlation between the measured and theoretical values at different loading stages and ages of concrete.

Montgomery, Kulak, and Shwartsburd(1983) analyzed elastic, shrinkage, and creep deflections for composite beams located in a school structure that developed excessive deflection during the construction period. The results of their calculations showed good agreement with the measured values. Montgomery et al. recommended the use of the unrestrained value for shrinkage strain in Branson's "composite section method", calculated by the ACI Committee 209 approach. As well, they recommended the use of an age-adjusted effective modulus of elasticity of the concrete for the calculation of the transformed moment of inertia of the composite beam and for use in the deflection equation. The use of this effective modulus of elasticity accounts for the time dependent development of shrinkage which produces tensile stresses that are reduced by creep, and for the time dependence of concrete properties such as f'_c and E_c . The age-adjusted effective modulus was calculated using a creep coefficient (the ratio of creep strain to elastic strain) evaluated by a procedure suggested by ACI Committee 209 (1971,1982) (also summarized by Park and Paulay, 1975) and an aging coefficient selected from tables developed by Bazant(1972), which are based on the ACI creep functions. It should be noted that the age-adjusted effective modulus of the concrete could also be calculated using a CEB-FIP(1978) creep coefficient and an aging coefficient (based on the

CEB-FIP creep functions) obtained from figures prepared by Dilger(1982) according to the procedure reported by Bazant.

Chien and Ritchie(1984) use the restrained value of shrinkage strain and the modulus of elasticity of the concrete at 28 days in Branson's "composite section method" to estimate shrinkage deflection. They suggest that a value of restrained shrinkage strain in the range of 200 to 350 $\mu\epsilon$ is appropriate for design. Their calculation procedure was verified by measurements of shrinkage and deflection on a beam tested by Robinson (as described by Chien and Ritchie, 1984).

In all these methods, the constant moment applied to the beam places the concrete in compression and the authors use a modulus of elasticity for the concrete in compression (adjusted or not adjusted for creep and age effects). This is implicit when applying the constant moment to the transformed cross section. Shrinkage of the concrete actually places it in tension.

3. COMPOSITE TRUSS DESIGN

3.1 General Design Procedures

The design of composite trusses with deck-slabs is presently based on the requirements for joists and composite beams given in Clauses 16 and 17 of CSA Standard CAN3-S16.1-M84, Steel Structures for Buildings (Limit States Design)(CSA, 1984a). No special provisions for composite trusses, defined here as truss systems designed on an individual basis for a specific job, are given. Because these members are normally unshored during construction, they are designed to resist factored loads occurring during deck and concrete placement, as well as occupancy loads. Construction loading is critical for the design of the steel top chord but for occupancy loading, the truss acts compositely and the concrete slab is considered to act as the top chord.

3.1.1 Moment Capacity

The flexural capacity of a composite truss is taken as the couple formed by the tensile force in the steel bottom chord and the compressive force in the concrete cover slab, as shown in Fig. 3.1. Clause 17.4.2 of S16.1 allows only the case of full shear connection with the neutral axis in the cover slab to be considered.

The factored tensile force in the bottom chord is taken

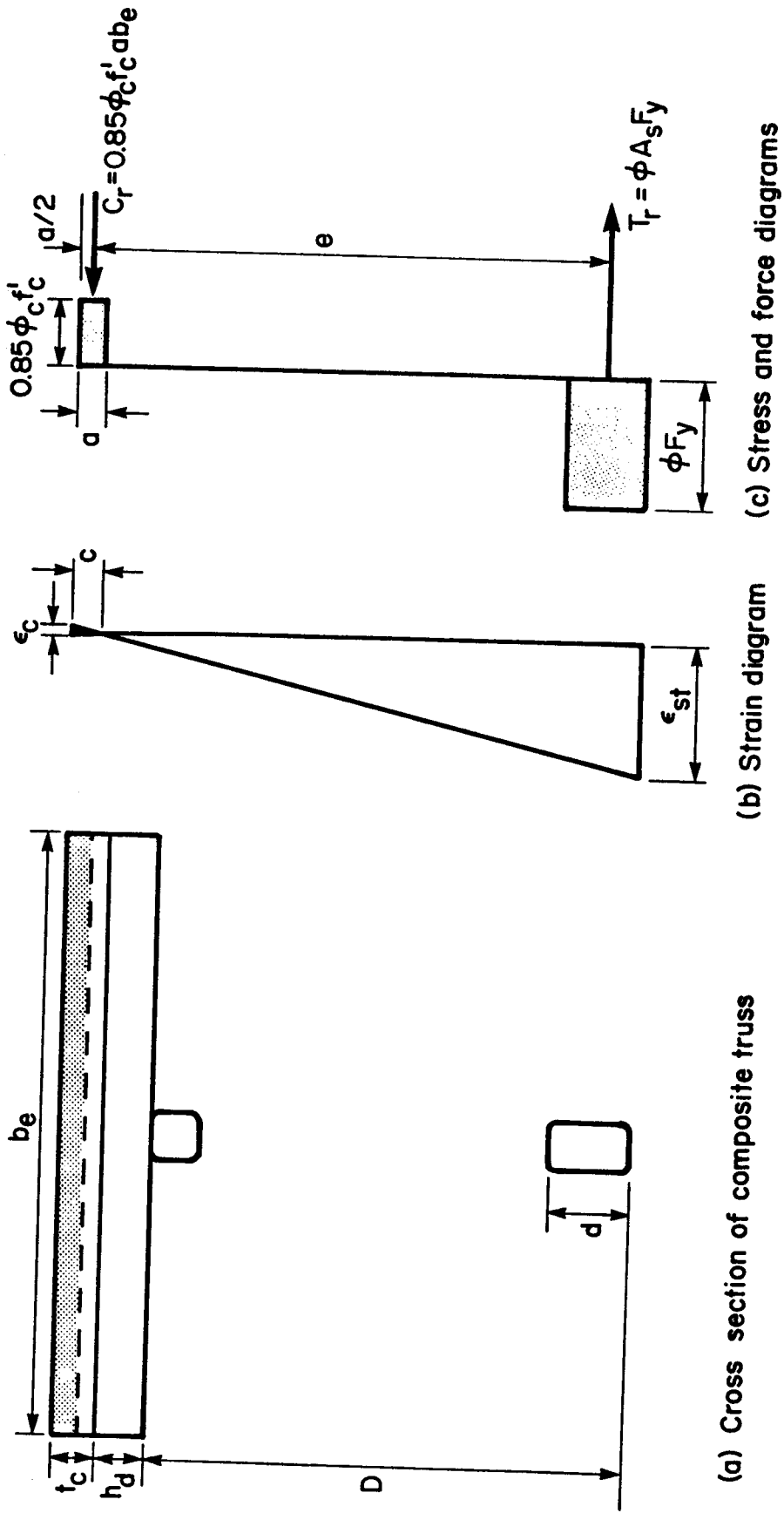


Figure 3.1 Moment resistance of a composite truss

as:

$$[3.1] \quad T_r = \phi A_s F_y$$

The factored compressive resistance of the slab is calculated from an effective concrete area equal to the effective width multiplied by the effective thickness. The effective slab width is based on provisions for composite beams in Clause 17.3.2 of S16.1. By equating the factored compressive resistance of the effective concrete area, calculated from:

$$[3.2] \quad C_r = 0.85 \phi_c f'_c a b_e$$

to the factored tensile resistance of the steel bottom chord, the required effective concrete thickness is:

$$[3.3] \quad a = \frac{\phi A_s F_y}{0.85 \phi_c f'_c b_e}$$

which cannot exceed the thickness of the cover slab. The area of concrete in tension is neglected.

From Fig. 3.1, the factored moment resistance of a composite truss is:

$$[3.4] \quad M_{rc} = \phi A_s F_y e$$

3.1.2 Steel Top Chord

When the truss acts compositely under occupancy loading, the large effective area of the concrete slab acts as the top chord of the composite truss. S16.1 states in Clause 17.4.2 that the area of the steel top chord should be neglected in determining the properties of a composite joist for strength calculations.

However, using unshored construction, the steel truss alone will carry the loads occurring during deck and concrete placement. Therefore, the steel top chord must be designed as a continuous member to resist both the axial forces and bending moments resulting from the factored construction loads applied at or between panel points, as indicated in Clause 16.5.8 of S16.1. Bridging requirements must also be considered.

3.1.3 Web Members and Connections

The web members of a composite truss are proportioned to carry the total vertical shear on the member, according to Clause 17.3.1.2 of S16.1. The effects of joint and connection eccentricities should be considered in the design of compression web members but can usually be neglected for tension web members.

To avoid the development of in-plane joint eccentricities, it is common structural engineering practice to have the centroidal axes of the members meeting at a joint intersect at a common point. When the web members must

be separated so that sufficient welds can be made, the connections may be designed to include the effects of joint eccentricity.

3.1.4 Shear Connectors

In composite truss design, shear connectors are chosen to provide full shear connection so that the horizontal shear force transferred between points of zero and maximum bending moment is

$$[3.5] \quad V_h = \phi A_s F_y$$

S16.1 allows the required shear connectors to be distributed uniformly along the length, with a special provision when concentrated loads are applied. The diameter of shear studs is limited to 2.5 times the thickness of the material to which they are welded in order to prevent a pull-out type of failure or burn-through during welding. Clause 17.3.6 of S16.1 allows the shear resistance of an individual shear stud in a slab over fluted deck to be calculated as

$$[3.6] \quad q_r = 0.5 \phi_{sc} A_{sc} \sqrt{f'_c E_c} \leq 415 \phi_{sc} A_{sc}$$

provided that the average flute width is twice the height of the deck and the stud extends a distance of at least two stud diameters above the top surface of the deck.

3.1.5 Serviceability

During fabrication, a composite truss is normally cambered for the elastic deflection of the truss acting non-compositely under the weight of the fresh concrete, as well as for the deflection of the composite truss due to dead load, shrinkage, and creep. A good estimate of the elastic deflection of the steel truss can be obtained by a computer frame analysis or, alternately, from a manual calculation as suggested in Clause 16.5.14.2 of S16.1. This approximate method of calculation uses a moment of inertia for the steel truss equal to the gross moment of inertia of the chord members about the truss centroid, and the deflection obtained is multiplied by 1.10 to account for the flexibility of the open web.

The live load deflection of a composite truss seldom exceeds the maximum recommended values for floor members, given in Appendix I of S16.1. To estimate the deflection of a composite truss, its moment of inertia is first calculated using a transformed concrete area. To account for the effect of the open web on truss deflection, the transformed moment of inertia is reduced by a value equal to $(1 - 1/1.10) = 0.091$ times the moment of inertia of the steel chords (Chien and Ritchie, 1984; CISC, 1985). This value is then modified to account for interfacial slip, using

$$[3.7] \quad I_e = I_s + 0.85 (p)^{0.25} (I_t - I_s)$$

from Clause 17.3.1.1 of S16.1, with $p = 1.00$ for full shear connection. Further adjustments to this deflection estimate can be made to account for creep and shrinkage effects, as described in Clause 17.3.1.1 of S16.1. Calculation of shrinkage deflections is discussed subsequently in Chapter 8.

Because composite trusses tend to be very stiff, vibration is seldom a problem in design.

3.2 Test Specimen Design

3.2.1 Description

The composite truss configuration chosen for testing is based on Design Example 5.8 of Chien and Ritchie(1984). This design example is for uniformly loaded 11 500 mm span composite trusses spaced at 3000 mm on centres with a 76 mm wide rib profile steel deck and a 65 mm thick cover slab of normal density 20 MPa concrete. Slab reinforcement consists of 152 x 152 MW9.1 x MW9.1 welded wire mesh. The steel truss consists of hollow structural section chords and double angle web members in a Warren configuration with 8 top chord panels. The out-to-out depth of the steel truss is 730 mm. The HSS chords are Class C of grade CSA G40.21-M 350W steel and the grade of the hot rolled web members is 300W. The specified dead and live loads are 13.7 kN/m and 6.0 kN/m respectively, resulting in a factored moment of 431 kNm and a factored shear of 150 kN.

The design of the test specimens followed the requirements given in CSA Standard S16.1-M84 for composite joists, with the incorporation of some unique features as discussed in Section 3.2.2. The concrete slab and HSS chord members were identical with those in Example 5.8 even though the truss was designed for a test loading consisting of four concentrated loads. The slab width of the test trusses was 2350 mm, approximately equal to the calculated effective width of the slab. The top and bottom chords were HSS 76.2x76.2x6.35 and HSS 127.0x76.2x4.78 respectively. A half-elevation of the steel truss, including the web members whose selection is discussed subsequently, is shown in Fig. 3.2. Figure 3.3 shows the letter designations for the joints and the test loading diagram for the composite truss. The factored moment resistance of the composite truss based on S16.1 (using specified material and geometric properties) is 449 kNm, 1.04 times the factored moment of 431 kNm.

No camber was specified for the steel trusses as serviceability was not a consideration in the tests. The estimated elastic deflection of the steel test specimens supporting the weight of the fresh concrete was 19.5 mm. The deflection of the composite truss due to the specified superimposed dead and live loads plus shrinkage and creep (assuming 50% of the live load was sustained) was estimated to be 26 mm, or $L/440$, considerably less than the recommended maximum value for live load deflection of $L/360$ or 32 mm given in S16.1.

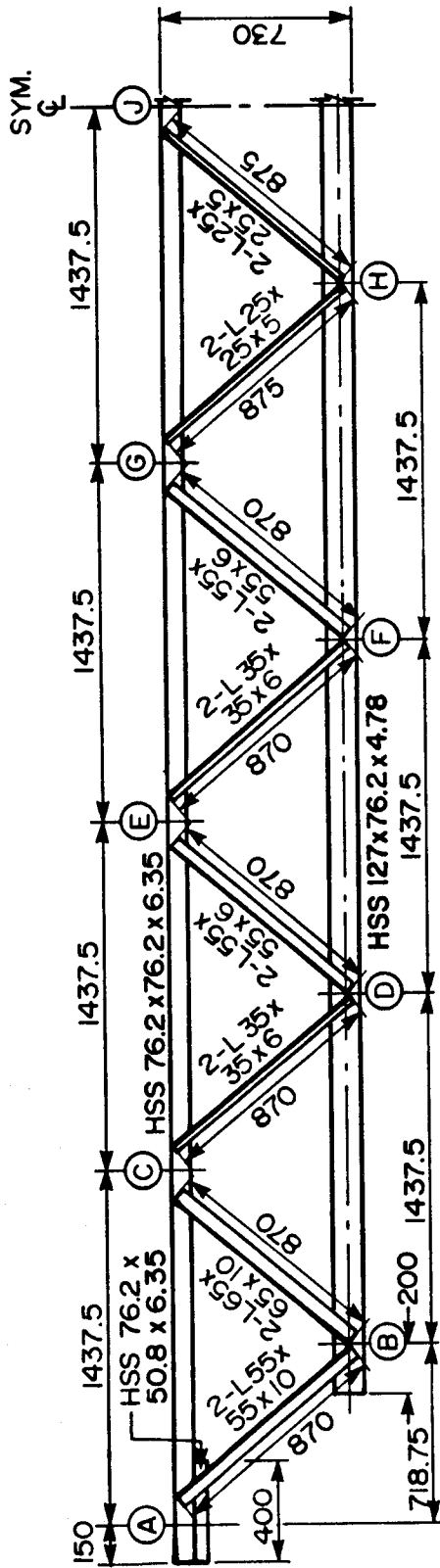


Figure 3.2 Half-elevation of steel truss

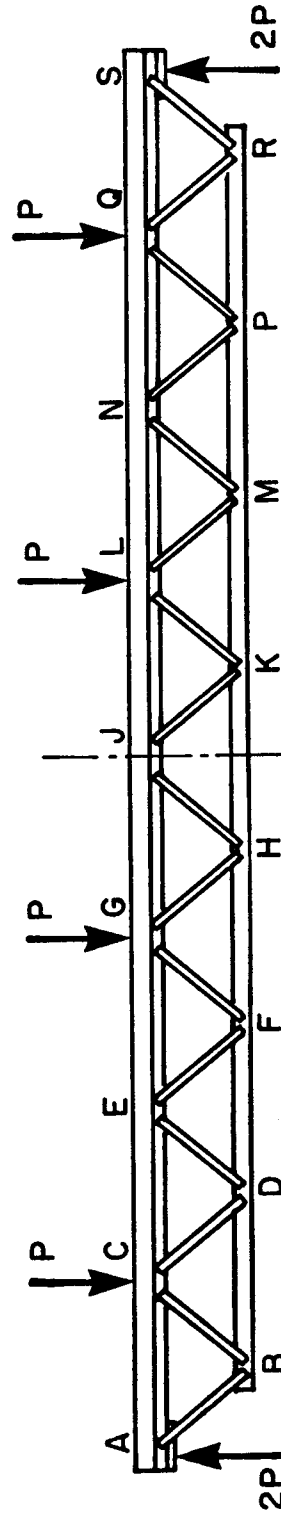


Figure 3.3 Joint designations and loading diagram

3.2.2 Unique Features

3.2.2.1 Bottom Chord

In several previous full-scale tests to failure of composite trusses (Cran, 1972; Bjorhovde, 1981), failure was initiated by buckling of a compression diagonal. Bjorhovde's truss was designed to the requirements of CSA Standard S16.1, with web members proportioned to carry loads consistent with the tensile capacity of the bottom chord, taken to be equal to the yield load. In retrospect, this failure mode could have been predicted. A tension member with welded connections and therefore with a net area equal to the gross area, will not fail at the yield load but only when the ultimate load is reached. Therefore, compression diagonals designed for forces corresponding to yielding of the bottom chord and with little reserve capacity beyond that level are bound to fail before the bottom chord fractures.

The first unique feature of the design of the composite truss test specimens was to base the flexural capacity on the ultimate tensile strength of the bottom chord. Two alternatives were examined. The first was to reduce the size of the bottom chord to provide a resistance just equal to or slightly greater than the factored moment. This could, however, lead to strength and deflection problems during unshored construction and to deflection problems in service. The second alternative, chosen for this design, was to maintain the same bottom chord section, requiring larger web

members and greater shear connection capacity, and resulting, of course, in substantially increased flexural capacity, provided that proper behaviour of the web members and shear connectors is obtained.

3.2.2.2 Triangulation

To avoid the development of in-plane joint eccentricities, it is common practice to position web members so that the centroidal axes of the members meeting at a joint intersect at a common point. In order to accommodate the weldments of the diagonals to the bottom chord of the test specimens, eccentricities of 20 to 30 mm, measured along the centroidal axis of the bottom chord, were needed. These eccentricities range from 1.5 to 2.8 times the distance from the back of an angle web member to its centroidal axis.

Two alternatives exist for positioning the ends of the diagonals on the top chord. The first is to minimize the joint eccentricities of the steel truss so that minimal joint eccentricity moments exist when the unshored steel truss supports the wet concrete and construction loads. The second is to minimize the joint eccentricities of the composite truss resulting in minimal joint eccentricity moments when the composite truss supports the superimposed dead and live loads. The second alternative is likely to provide better ultimate performance by minimizing in-plane joint moments but requires that larger eccentricities be taken into account during the unshored construction stage.

The second alternative, with the centroidal axes of the diagonals intersecting at the mid-depth of the cover slab, was chosen for the test specimen design. This configuration resulted in appreciable spacings of 260 mm between the diagonals at the centroidal axis of the top chord. From a practical point of view, this provided all the space required for welding. In addition, the length over which the top chord bends due to transverse loads (the unbraced length for buckling about the horizontal axis) was reduced to 82% of the panel point spacing. A plane frame analysis of the steel truss supporting the factored construction loads and a stability check of the top chord using the S16.1 interaction equations gave an interaction index for the critical panel of the top chord of 0.96 times that computed by Chien and Ritchie under the same loading but using the other triangulation system. The disadvantage of the diagonals in a Warren truss configuration alternately in tension and compression in introducing appreciable joint moment is recognized; however, the same diagonals, through their axial stiffness, provide much more rotational restraint to the joint and therefore reduce the effective length of the top chord for buckling about its horizontal axis. For this design, the rotational restraint was increased by 54 to 318 times over a configuration using the same web member selections but with their centroidal axes meeting at the centroidal axis of the steel top chord. In addition, the effective depth of the composite member employing

alternate 2 was 1.23 times that of alternate 1.

3.2.2.3 Web Members

All web members were selected to resist axial forces consistent with the development of the ultimate tensile strength of the bottom chord based on the maximum specified ultimate tensile strength of the steel. This would mean that the members should be designed for forces of $620/350 = 1.77$ times those based on yielding of the same size of bottom chord. However, as the probability was small that the bottom chord would have an ultimate strength at the specified upper limit of 620 MPa, the unfactored resistances were used for web member design. Expressed in other words, the factored resistances were selected to correspond to forces obtained when the bottom chord force was 90% of the specified upper limit of the ultimate tensile capacity, or 1.59 times the minimum specified yield force of the bottom chord.

Tension Member Moments

Recognizing that tensile yielding will eventually obliterate the end moments induced by joint rotations or connection eccentricities as discussed subsequently (provided that the eccentric moments can be taken by the chord members), the tension members were designed for tensile forces only.

Compression Member Effective Lengths

Chien and Ritchie use the clear distance between the ends of weldments as the effective length for design of

compression diagonals. For welded connections, where the welds can prevent appreciable relative rotation of the connected parts, this approach appears, if anything, to be conservative. For the test specimen design, an effective length of 0.9 of the distance between the intersections of the centroidal axes, approximately equal to the clear length, was used. This is also likely to be conservative.

Compression Member Connection Eccentricity Moments

The two angles comprising a compression web member are symmetrical about the vertical mid-plane of the truss. The forces in the two members are balanced and do not cause any rotations of the chords. For each angle considered separately, provided that the connection is sufficiently rigid to prevent any relative rotation between the angle web member and the chord, out-of-plane moments arising because the angle is connected on one leg only can be taken out in the joint itself. At each end of the member, a couple is formed in the connection which is equal and opposite to the moment caused by the eccentricity of the connection. The result is that the member is not subject to out-of-plane moments. The same argument applies to in-plane moments which would result when the longitudinal axis of the resisting force of the weld does not coincide with the centroidal axis of the member. In both cases, the connection must resist the eccentric moment with little or no distortion. For out-of-plane moments, the connection moment is formed by a portion of the weld in tension and by compression between

the angle leg and the chord. For in-plane moments, the weld must develop the eccentric moment.

Compression Member Joint Eccentricity Moments

In-plane joint moments arise when the centroidal axes of the members meeting at a joint do not intersect at a point and, as well, when rigid truss joints rotate as the truss deflects. The latter moments are called secondary moments. When the overall behaviour of the truss is elastic, these joint moments are distributed amongst the members at each joint in proportion to their flexural stiffnesses with, of course, the stiffness of compression members decreasing as their axial forces increase. Aziz(1972) and Korol(1982) have shown that the secondary moments tend to dissipate as full plastification, either in tension or compression, develops at the ends of members. Moments due to joint eccentricities will always exist in proportion to the axial forces in the members, but can reduce in web members when tension or compression yielding occurs, provided that the chord moments increase. It appears prudent, however, to design compression web members for a portion of the joint eccentricity moment based on their flexural stiffness. These in-plane moments are then resolved into moments about the principal axes of the angles for use in the interaction equation.

Summary

Although designed for 1.59 times the forces used by Chien and Ritchie, the total mass of the web members of the test specimen design was only 1.11 times that of the Chien and Ritchie design. Part of the reason that the increase in mass is not as much as might be expected is that the web members are, on the average, only 92% of the length of those of Chien and Ritchie because they are positioned with a steeper slope. They therefore also carry shear about 1.07 times as efficiently and the compression members have shorter effective lengths. The same minimum angle size was required (where shears are low) in both trusses.

3.2.2.4 Welded Connections

The out-of-plane moments due to connection eccentricity were neglected in the design of the welds, as proposed by Blodgett (1976). This appears to be justified because the weld only needs to provide the tensile component of the connection eccentricity resisting couple. To ensure that the welds provided the necessary in-plane rigidity and that they were capable of transmitting any connection eccentricity moments as well as the required proportion of joint eccentricity moments, the welds were designed to transfer the axial load of the member and its in-plane yield moment. Even with this simple conservative approach, the throat areas of the welds for members AB and BC of the test truss, when designed for 1.77 times the axial force, were only 1.38 times those of the truss of Chien and Ritchie. More

logically, the welds could have been designed to transfer the axial load plus the maximum in-plane moment that could co-exist.

3.2.2.5 Shear Connection

Shear connectors were selected to transmit 0.9 times the specified upper limit of the ultimate tensile resistance of the bottom chord, that is, 1.59 times the minimum specified yield strength of the bottom chord. A stud diameter of 16 mm was chosen so as not to exceed a value of 2.5 times the thickness of the top chord flange. A stud length prior to welding of 106 mm was chosen to provide a projection above the top surface of the cellular steel deck of two stud diameters. To transfer the horizontal shear force, 19.1 studs were required each side of midspan, and Robertson QL Lock-Rib wide profile steel deck was selected to provide the maximum number of flutes. Thirty-nine studs, one in each flute, were used over the length of the truss. The requirements of Clause 17.4.8 of S16.1 regarding the number of shear connectors between concentrated loads and the nearest point of zero moment means that 19 studs should have been placed between the reactions and the interior loads rather than the 15 that were placed in these lengths. For the test loading configuration used, this requirement appears somewhat severe in view of the fact that, for a uniformly distributed load, when it would be permissible to space the shear connectors uniformly throughout the length, the change in moment corresponding to the zero shear region

for the test truss is only 6%.

3.2.2.6 Longitudinal Shear

Clause 17.3.3 of S16.1 recommends that additional transverse reinforcement be provided, if required, to control longitudinal shear cracking in the concrete slab in the vicinity of the shear connectors. However, no specific guidelines are presented. To avoid a premature failure of this type, the longitudinal shear capacity of the slabs on the test specimens was investigated. Using the equation developed by El-Ghazzi, Robinson, and Elkholy(1976), the minimum amount of transverse reinforcement required to prevent premature shear cracking was determined to be less than the area of welded wire mesh provided for shrinkage and temperature effects. The design method developed by Buckner, Deville, and McKee(1981) confirmed that the shear strength of the slab (with one layer of welded wire mesh) on the critical shear surface adjacent to the row of shear connectors was more than satisfactory.

3.2.2.7 Bearing Detail

An examination showed that the top chord section, in the region between the reaction force and the connection of the first tension diagonal, did not have sufficient shear capacity. Therefore, a short length of HSS 76.2x50.8x6.35 was welded to the top chord at the reactions to increase its shear capacity. This approach was also taken in the Chien and Ritchie design.

4. EXPERIMENTAL PROGRAM

4.1 General

Two essentially identical 11 500 mm span composite trusses, whose design configuration is described in Chapter 3, were tested. The simple span trusses had a T-shaped cross section with a 730 mm deep steel truss supporting a 2350 mm wide concrete slab on wide rib profile steel deck with ribs oriented transverse to the axis of the truss.

These tests were conducted to investigate many aspects of the behaviour of composite trusses, including:

1. deflection of the steel trusses under the weight of the wet concrete to verify camber requirements for unshored construction,
2. deflection of and member stresses in the composite trusses due to slab shrinkage over a minimum time period of 50 days,
3. testing of the composite trusses to failure to determine the load-deflection response, the ratio of the test-to-predicted failure load, and the failure mode,
4. determination of the effective moment of inertia of the composite trusses,
5. distribution of concrete strains across the width of the slab,
6. investigation of interfacial slip and shear transfer between the concrete and steel,
7. determination of the forces in the chords, slab, and web

- members and the behaviour of these components,
8. longitudinal cracking, and
 9. observation of yielding at the connections.

The results and analyses of the shrinkage studies on both trusses are found in Chapters 7 and 8. Chapters 9 and 10 contain results and analyses of the testing of both trusses to failure.

In addition, ancillary tests were conducted to establish material properties. The concrete tests included compressive strength tests of concrete cylinders, split cylinder tests, and flexure tests. The steel tests included tension coupon tests, stub column tests, a full-scale tension test on a bottom chord section including a joint, and push-out tests. The results of the ancillary tests are reported in Chapter 6.

4.2 Test Specimens

4.2.1 Fabrication

Design drawings for the test specimens and a list of the materials required for ancillary tests were supplied to three local fabricators for bids. The successful bidder was Empire Iron Works Ltd., who fabricated the two trusses within a period of three weeks. In general, the next largest Imperial size was substituted for the metric size angles specified for web members. After consultation, even larger size angles were substituted for the four central diagonals

because they were readily available. The web member sections used to fabricate the test specimens are listed in Table 4.1.

Upon delivery, all dimensions of the trusses and the component members and welds were measured to verify that the trusses were manufactured in accordance with the drawings and to establish the dimensions of the cross sections of the members and of the welds. These measurements, along with the results of ancillary tests for material properties, were used to predict the strength of individual components and of each test specimen as a whole. The dimensions of the fabricated trusses agreed closely with those specified on the drawings. Visual inspection of the welds indicated that the workmanship was excellent. The truss measurements as well as the measured cross sectional properties of the chord and web member sections are detailed in Chapter 5.

The weight of steel truss 1, obtained from calibrated load cells located under each end, was 4.35 kN. The weight calculated from the dimensions on the drawing and the nominal member weights was also 4.35 kN. Steel truss 2 was not weighed.

4.2.2 Assembly of Composite Trusses

With each truss in turn, simply supported at either end on pedestals, the wide profile deck, precut to the required width, was placed in position and supported along both edges by wooden shoring consisting of longitudinal 2 x 6's and

Table 4.1 Web member substitutions at fabrication

Web Member Designation	Metric Size Angles Specified in Design	Imperial Size Substitution
AB,RS	2 - L 55x55x10	2 - L 2x2x3/8
BC,QR	2 - L 65x65x10	2 - L 2-1/2x2-1/2x3/8
CD,EF,MN,PQ	2 - L 35x35x6	2 - L 1-1/2x1-1/2x1/4
DE,FG,LM,NP	2 - L 55x55x6	2 - L 2x2x1/4
GH,HJ,JK,KL	2 - L 25x25x5	2 - L 1-1/2x1-1/2x3/16

2 x 6 posts. The sections of deck were crimped together, the cold formed edge angles placed, and the deck and edge angles nailed to the longitudinal runners. Wooden diagonal supports extending from the longitudinal runners to the bottom chord were then placed at intervals of approximately 1450 mm. With these supports, the vertical posts along the edges could be removed during placing and curing of the concrete, allowing deflections to occur unimpeded. Each deck flute was then welded to the top chord at two locations to provide good contact for stud welding. The Nelson Stud Welding Division, TRW Canada Ltd., provided welding equipment and personnel to weld one stud in each flute through the deck to the top chord. By trial and error, the welding parameters established were 575 volts and 200 amperes for 1 second. Both test specimens were assembled to this stage and the second truss was then stored outside for several months while the first truss was tested.

The slab of truss 1 contained one layer of 152 x 152 MW9.1 x MW9.1 welded wire mesh, placed on plastic chairs to locate the mesh 25 mm below the surface of the concrete. Because the mesh tended to curl up during concrete placement, the mesh in the second test (when two layers of mesh were used) was supported on chairs and tied to the deck.

With the welded wire mesh in position, 20 MPa normal weight concrete made with Type 10 cement, supplied by Genstar Building Materials, was cast, vibrated, and

screeded. A batch of 3.5 m^3 was sufficient for each slab plus 20 control cylinders, flexure specimens, shrinkage control specimens, and push-out test specimens.

At various stages of assembly, the weights of both test specimens were measured using Strainert 100 kip (445 kN) capacity load cells under the reactions. In Table 4.2, these measurements are compared with calculated values which are based as much as possible on measured dimensions and densities. The total weight of each test specimen prior to loading to failure (after temporary shoring was removed) was 70.16 kN for truss 1 and 69.85 kN for truss 2, equivalent to uniformly distributed loads of 5.95 kN/m and 5.92 kN/m respectively.

In Fig. 4.1, the concrete slab on truss 1 is shown. Figure 4.2 shows truss 2 completely assembled.

4.3 Shrinkage Tests

4.3.1 Test Set Up

During construction and while the effects of shrinkage were monitored, each truss was supported on 800 mm high concrete pedestals plastered to the laboratory floor. To ensure simply supported conditions at the reactions, a nest of rollers was placed on one pedestal to allow horizontal translation and a puck (a device consisting of 2 cylindrical steel plates with a lubricated convex/concave mating surface) was placed under each reaction to allow rotation.

Table 4.2 Comparison of calculated and measured weights of test specimens

Item	Truss 1		Truss 2	
	Calculated Weight, kN	Measured Weight, kN	Calculated Weight, kN	Measured Weight, kN
Steel Truss	4.35	4.35	4.35	-
Deck	2.60	-	2.60	-
Edge Angles	0.76	-	0.76	0.72**
Shoring	0.88	0.81	0.92	0.85
Mesh	0.28	-	0.57	-
Concrete	61.94	61.98	61.01	61.59
Composite Truss (including shoring)	70.81	71.69*	70.21	71.42
Composite Truss (shoring and longitudinal edge angles removed)	69.80	70.16*	69.16	69.85

* includes calculated weight of mesh

** longitudinal edge angles only

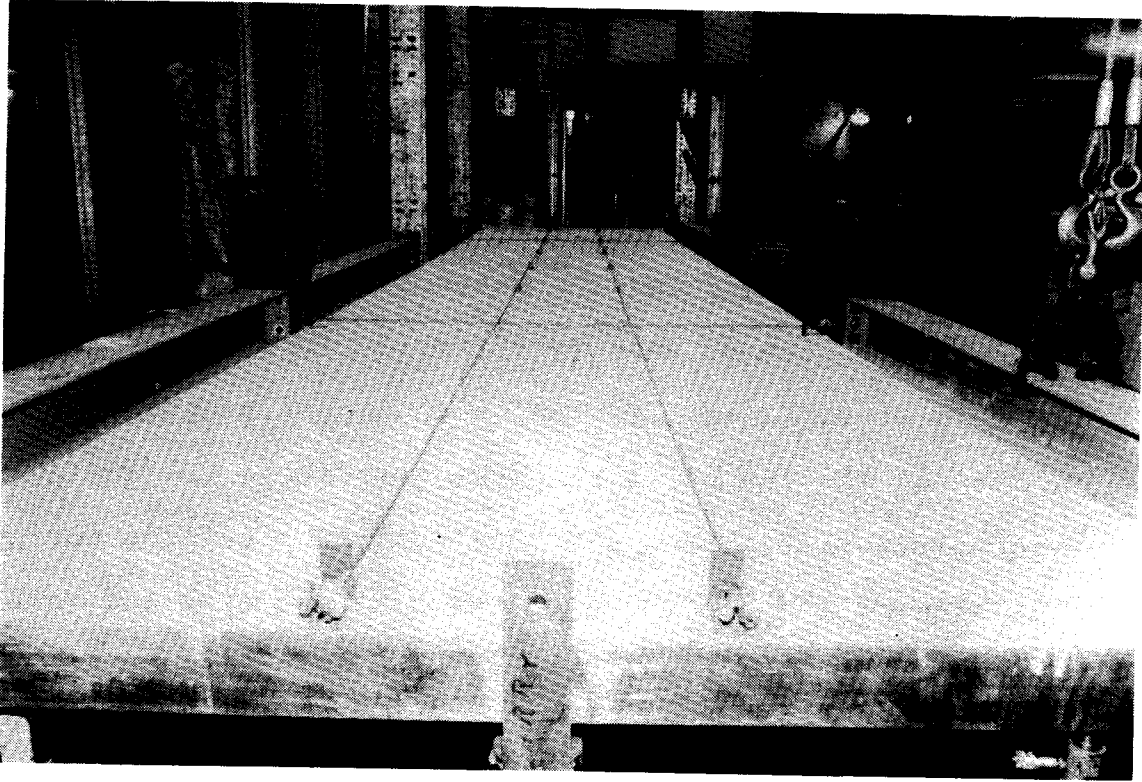


Figure 4.1 Concrete slab on truss 1

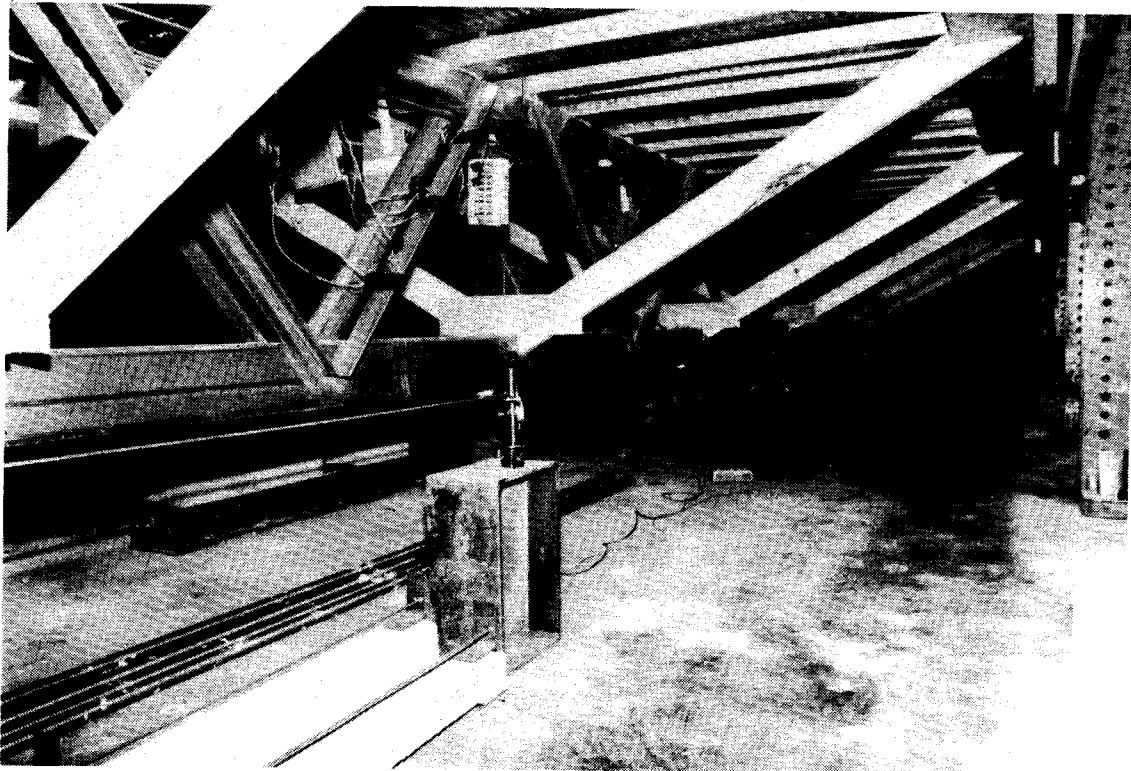


Figure 4.2 Composite truss 2

Calibrated load cells were positioned below the pucks at each end to determine the weight of each composite truss. Lifting plates were welded to the top chord section at the ends of each test specimen to allow substitution of another reaction assembly for the destructive tests.

Small frames were constructed along the longitudinal edges of each test specimen with wooden platforms spanning between the frames at a height just above the surface of the concrete slab. These provided working platforms during placement and finishing of the concrete slab and were also used during the first test to provide access to Demec points on the slab surface without disturbing the truss. Steel pedestals were located at the four corners of the slab with a small clear space between each pedestal and the underside of the slab to limit any rocking motion of the test specimens due to accidental loading.

Along with each test specimen, 4 concrete control specimens 1000 mm long by 100 mm wide were constructed to monitor shrinkage effects. Two thicknesses of 65 mm and 100 mm were used to provide volume-to-surface area ratios consistent with limits considered appropriate for the slab. The 65 mm thickness corresponds to the thickness of the slab above the flutes and the 100 mm thickness corresponds to the mean slab thickness. Two control specimens (one of each thickness), supported on rollers to eliminate any restraint, were situated on the floor near each of the quarter points of the test specimens. The bottom surface and edges of the

control specimens were waxed with paraffin to prevent moisture loss from these surfaces. Possible bowing of the specimens due to uneven shrinkage was not monitored.

4.3.2 Instrumentation

To monitor the effects of slab shrinkage on each composite truss, measurements of truss deflections, steel strains, concrete slab strains, and strains of concrete shrinkage control specimens were made, as well as ambient temperature and humidity readings in the laboratory. The instrumentation to measure truss deflections and steel strains was installed prior to placement of the concrete slab, while that measuring concrete strains was set up one day after the concrete was cast.

Because the atmospheric environment in the structures laboratory was not controlled, temperature and relative humidity measurements were taken at either end of each test specimen with the same frequency as other shrinkage measurements. A sling psychrometer was used to obtain humidity readings.

Deflections were measured at the midspan and quarter points using mechanical dial gauges reading to 0.01 mm.

The overall deformations of the top and bottom chords due to shrinkage of the concrete slab were measured using dial gauges (reading to 0.0001 inches or 0.002 mm) with spindles reacting against light steel rods that extended over the entire length of each chord and were fastened at

the far ends. The rods were suspended at intervals 25 mm below the chords with wire ties. To measure local steel strains, 28 electrical resistance strain gauges were applied on truss 1 and 56 were applied on truss 2. Figures 4.3 and 4.4 show the locations of these gauges and indicate the number of gauges at each location. Gauges on chord members were mounted in pairs at mid-height and mid-panel on the vertical faces of the HSS sections. On truss 1, two gauges each were mounted at mid length on eight web members in an attempt to study the shear transfer between the chords. Only two web members on truss 2 were gauged, but more fully, with 3 gauges per angle leg at 3 levels along the member length for a total of 18 gauges per web member.

Local concrete shrinkage strains on transverse lines on the slab surface were obtained from Demec points fastened to the slab with epoxy at a standard gauge length of 203 mm. A demountable mechanical Demec gauge was used to measure the change in length between the Demec points. Three readings were generally averaged to obtain the final result. More were taken if the repeatability of the readings was poor. Thirteen sets of Demec points were applied on the slab of truss 1 and 21 sets were applied on the slab of truss 2 to measure shrinkage. The overall longitudinal and transverse shrinkage of the slab was measured at two locations each using the dial gauge-steel rod measuring system. The longitudinal and transverse rods were supported at intervals on chairs 54 mm and 45 mm respectively above the slab

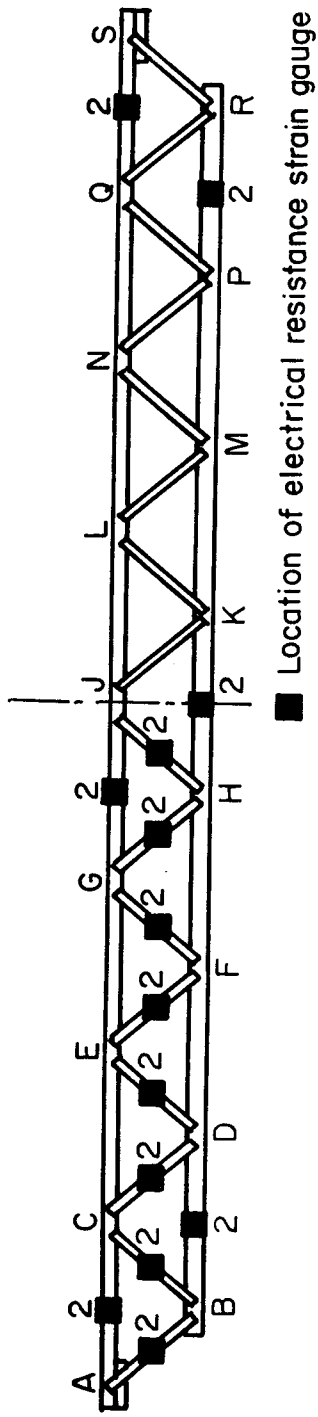


Figure 4.3 Location of strain gauges measuring shrinkage strains on truss 1

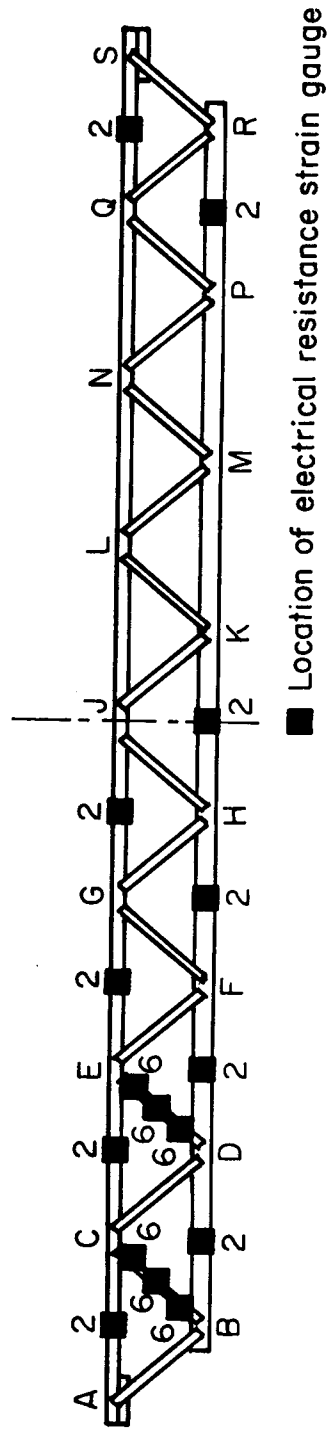


Figure 4.4 Location of strain gauges measuring shrinkage strains on truss 2

surface. Figures 4.5 and 4.6 show the locations of the slab instrumentation. The dial gauge-steel rod system was also used to measure the length change of the concrete shrinkage control specimens.

Shrinkage data was collected manually from dial gauges and Demecs. After ascertaining that the laboratory data acquisition system, a Data General Eclipse S/120, was steady over long time periods, it was used to automatically record the output of electrical resistance strain gauges and load cells. Power supplies for the electrical instrumentation were monitored periodically and adjusted as necessary. All the data was subsequently processed on the University of Alberta's mainframe computer, an Amdahl 5860.

4.3.3 Testing Procedure

Initial readings were obtained on all dial gauges and strain gauges prior to placement of the concrete slab. Readings were also obtained once the wet concrete was screeded and immediately after the concrete had set. The latter set of measurements was the initial point for shrinkage measurements. The slab was covered with polyethylene sheets for an initial curing period of 7 days. The polyethylene was removed briefly to install slab instrumentation one day after casting. Demec points on truss 1 had to be reapplied on day 4 with epoxy because the sealing wax originally used did not bond to the moist concrete surface.

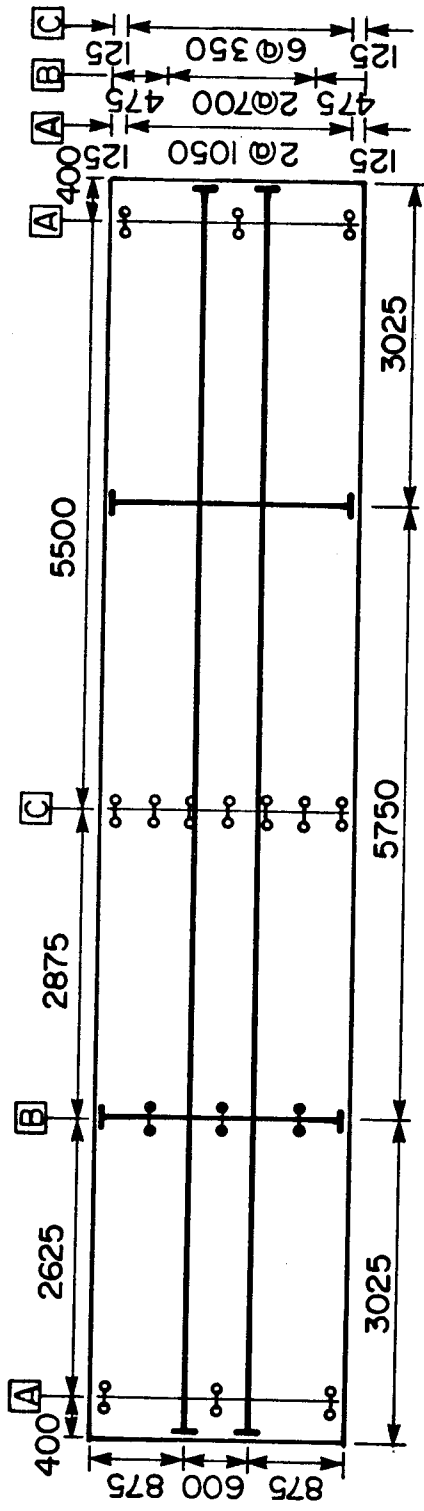

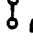



Figure 4.5 Location of slab instrumentation measuring concrete strains on composite truss 1

 Dial gauge - steel rod measuring system
 Demec points (shrinkage and flexural tests)
 Demec points (flexural test only)

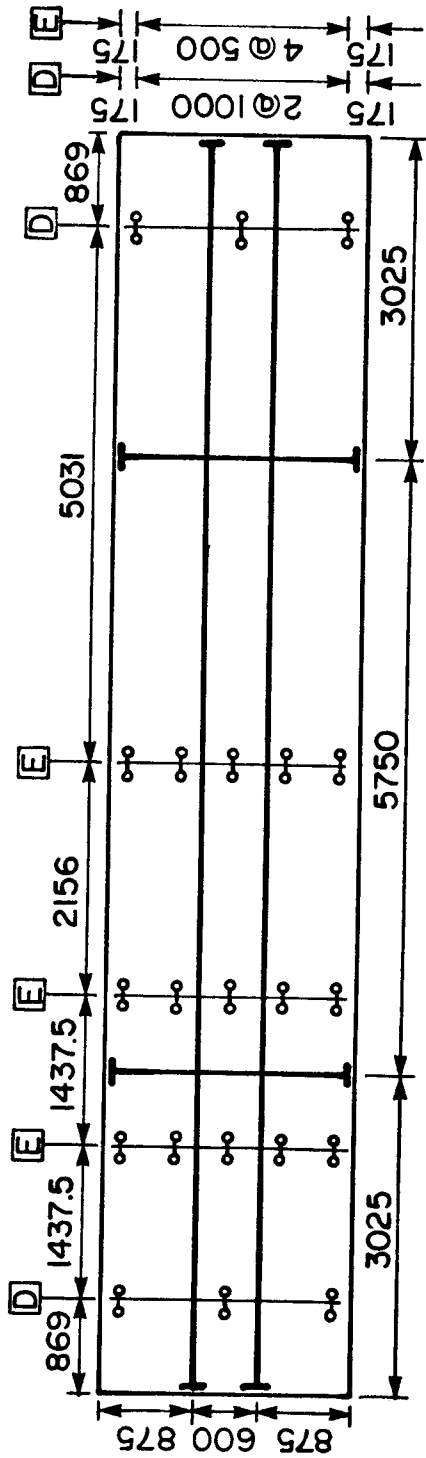


Figure 4.6 Location of slab instrumentation measuring concrete strains on composite truss 2

Shrinkage measurements were taken twice daily on weekdays and once per day on weekends, except for Demec strains, which were obtained only on weekday mornings. Concrete was cast on truss 1 on April 22, 1985 and shrinkage measurements were taken for a period of 65 days to June 26, 1985. Shrinkage measurements on the concrete control specimens were continued for another 20 days while truss 1 was being prepared for destructive testing. The slab on truss 2 was cast on September 25, 1985 and shrinkage was measured for a period of 85 days until December 19, 1985. The temporary wooden shoring system, used to support the deck during concrete placement, remained in place for the duration of both shrinkage tests.

4.4 Flexural Tests

4.4.1 Test Set Up

As a reasonable approximation to the uniformly distributed load used for composite truss design, four hydraulic jacks located at panel points as shown in Fig. 4.7 were used to apply loads to test the specimens to failure. This loading configuration gives a region of constant moment or zero shear over the central two panels of the truss.

Large steel frames bolted to the strong floor provided the reaction system for the jacks loading the test specimens. A pneumatically activated hydraulic system with a reservoir, control console, control valves, and control

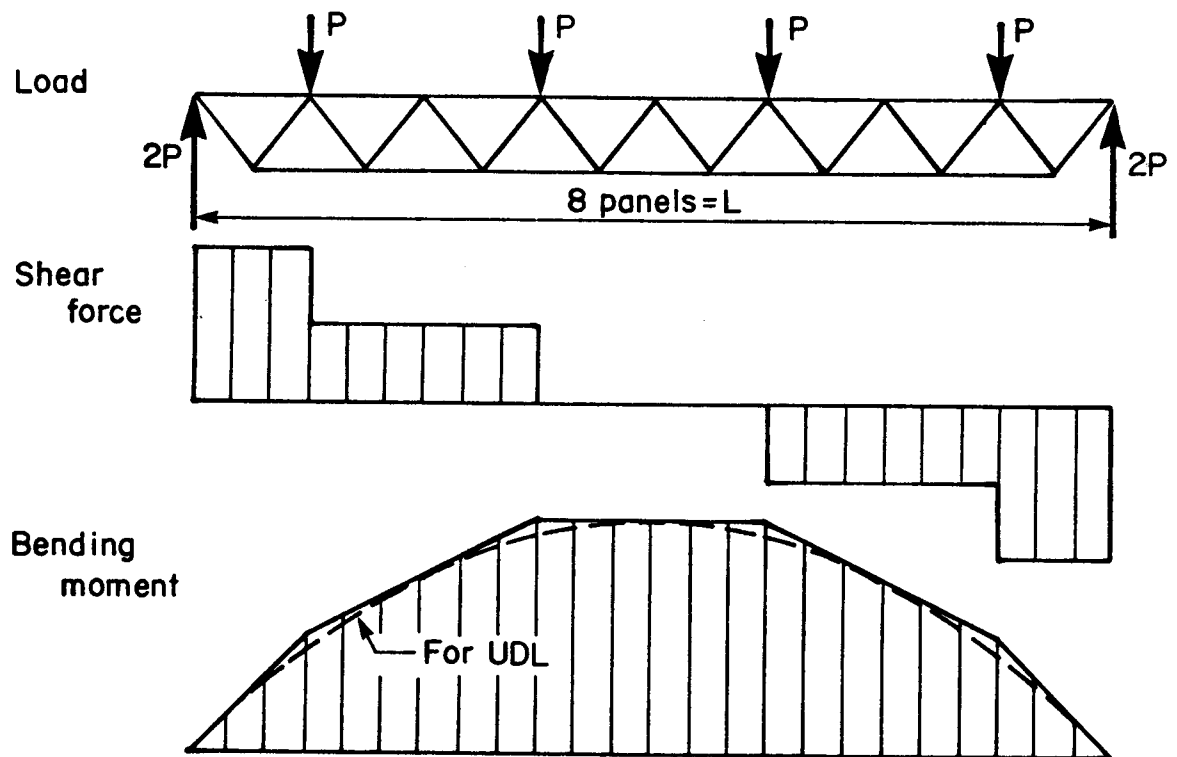


Figure 4.7 Load, shear force, and bending moment diagrams

manifold was used to supply pressure to the jacks. With the valves and manifold, the four jacks could be subject to the same hydraulic pressure and thereby deliver essentially the same load at each location. By closing valves, loads could be maintained on some jacks while the pressure on others was released. Load increments were controlled using the main pressure gauge.

4.4.1.1 Load Apparatus and Reactions

As the truss was designed to reach the ultimate tensile strength of the bottom chord, it was anticipated that the deflections and rotations at load and support points would be very large. The vertical deflections would also cause horizontal movements at reaction points that had to be accommodated. Therefore, at all loads and reactions, knife edges were provided to allow the rotations to occur and rollers were provided to allow the horizontal movements to occur. In addition, the loading jacks had to have sufficient stroke and the pedestals under the reactions had to be high enough to permit large deflections. Figure 4.8 is a schematic diagram of the reaction assembly with the load cell positioned between the rollers resting on the pedestal and the knife edge supporting the truss. Figure 4.9 shows a photograph of the north reaction of truss 2. A schematic diagram and a photograph of a typical jack assembly are shown in Figs. 4.10 and 4.11. The rollers are positioned between the jack and the distributing beam and the jack piston pushes against a load cell and a knife edge at the

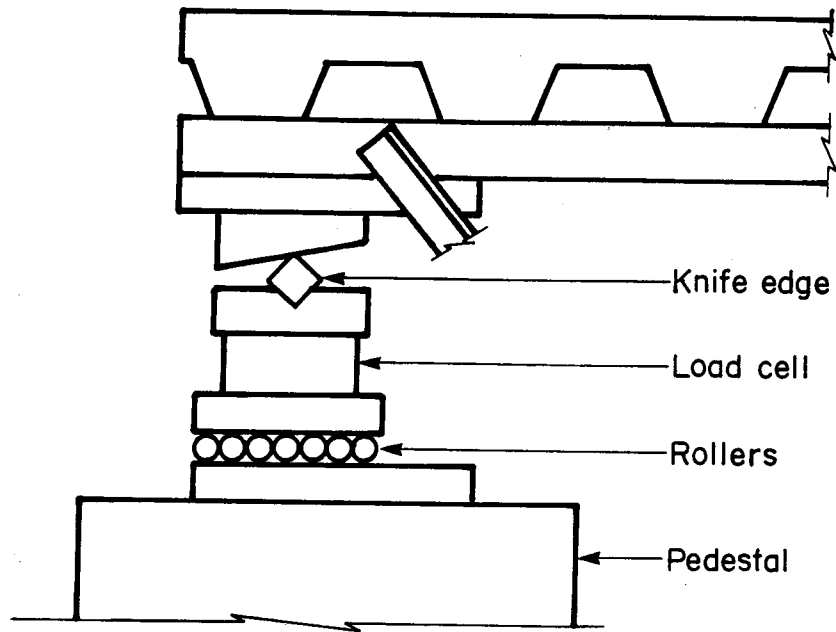


Figure 4.8 Schematic diagram of reaction assembly

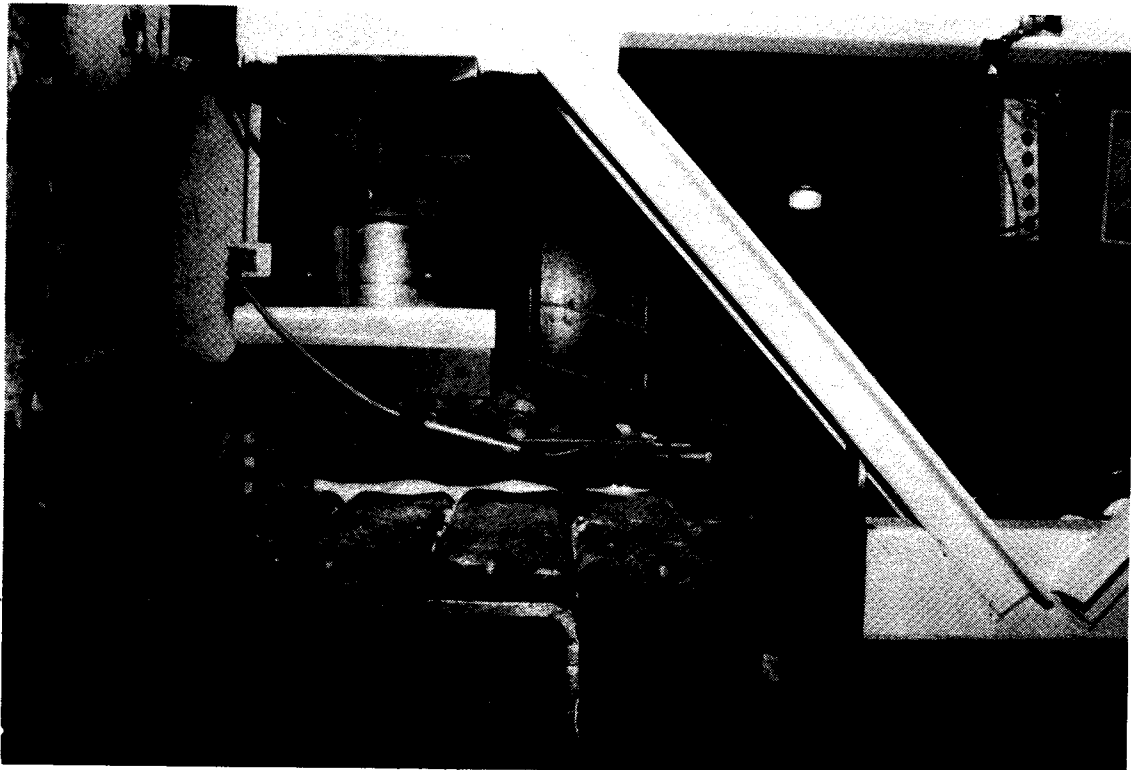


Figure 4.9 Reaction assembly - truss 2

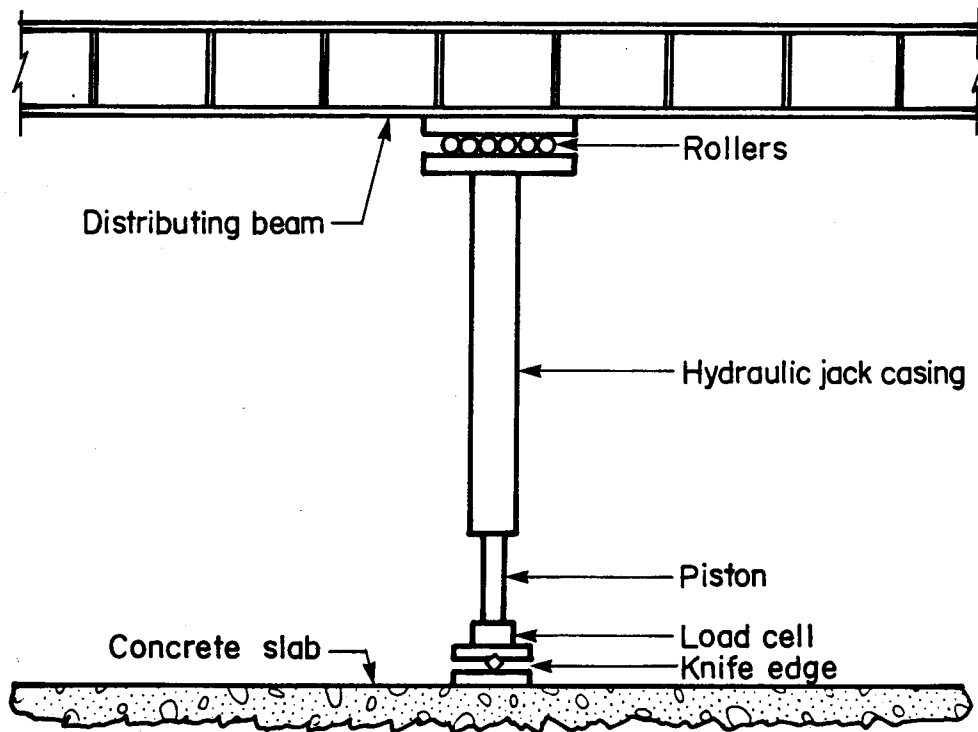


Figure 4.10 Schematic diagram of loading assembly

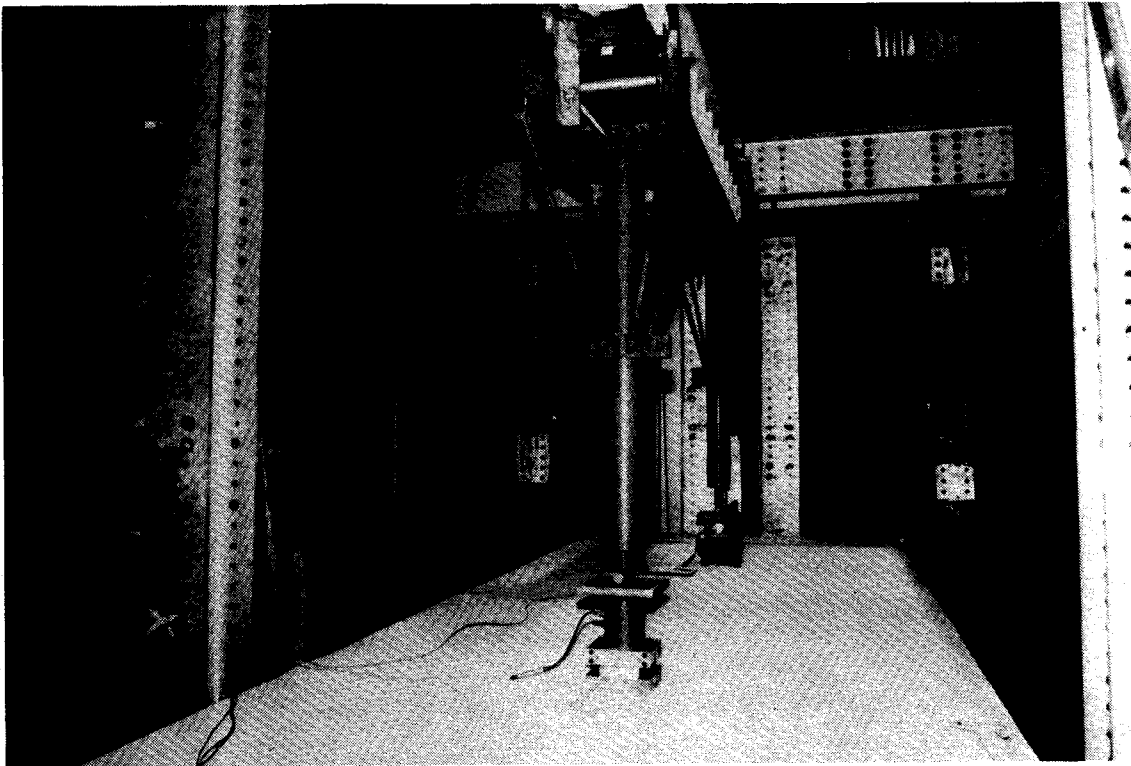


Figure 4.11 Jack assembly - truss 2

lower end, allowing rotations to occur where they originate.

To estimate an upper bound to the deflections, rotations, and horizontal movements that had to be accommodated, a stress-strain curve for the steel bottom chord was assumed based on the upper limit of the specified values, and a failure strain of 0.004 was assumed for the concrete. From the assumed ultimate load in the bottom chord, the forces applied by the jacks, the reactions, and the forces in all the truss members were determined. The strains and member deformations were calculated from the loads in the members. Based on these assumptions, the web members behaved elastically and the deformation in the concrete was very small. The inelastic strains of the bottom chord, giving rise to most of the truss deformation, were determined by assuming a linear strain distribution corresponding to crushing of the concrete at midspan at a strain of 0.004 when the bottom chord reached its ultimate strength. Using the deformed member lengths, the deflected shape of the truss was drawn to scale.

In Table 4.3, the first value for each quantity gives the predicted deflection, movement, or rotation based on the assumed stress-strain curve for the bottom chord steel, and a maximum concrete strain of 0.004. The bracketed value is that based on the actual stress-strain curve for the bottom chord steel and a maximum concrete strain of 0.003, an upper limit of the test results of the concrete.

Table 4.3 Movement at reactions and load points

Movement	Location			
	Reaction	External Load Point	Internal Load Point	Midspan
Vertical Deflection, mm	0 (0)	590 (293)	1610 (808)	1750 (890)
Inward Horizontal Movement, mm	336 (87)	210 (58)	12 (6)	0 (0)
Rotation, degrees	25 (12)	24 (11)	12 (7)	0 (0)

The knife edges at the reactions and external loads were designed to accommodate a rotation of 30° . By using a 15° bevelled plate as seen in Fig. 4.9, the maximum angle between the knife edge plate and the horizontal was reduced to 15° . Even at this angle, the frictional component required between the hardened steel surfaces to provide a vertical reaction would almost be exceeded. Therefore, small teeth were cut into the knife edge and into the mating plate to provide a mechanical interlock.

Because the reaction knife edges lay about 280 mm below the reference point for the reaction movement given in Table 4.3, the inward horizontal movement used for roller design was reduced by this value multiplied by the end rotation, resulting in a design displacement of 250 mm.

Recognizing that the predicted movements were based on extreme values, jacks with a stroke of 1200 mm and a capacity of 218 kN were selected. Pedestals for reactions had a height of 1900 mm to allow adequate clearance for truss deflection.

4.4.1.2 Safety and Stability

With the system of knife edges and rollers provided, the test specimens were partially constrained; that is, constrained against vertical loads but not against horizontal loads. Columns bolted to the laboratory floor at each end of the specimens to support the reaction pedestals prevented the test specimens from moving more than ± 40 mm longitudinally. In addition, for the test of truss 2, a

threaded rod device was mounted to each of the end columns to maintain the midspan of the truss in position.

Stability of each test specimen was ensured by providing lateral support at the four corners of the slab.

4.4.1.3 Calibration of Instrumentation

All electrical instrumentation, including load cells, LVDT's, and strain gauges required calibration prior to use. Load cells were loaded under controlled conditions to define the linear relationship between the change in output voltage of each load cell and the change in load. The output voltage of each LVDT was measured and plotted for the full range of displacement to allow calculation of a calibration factor and to define the limits of the linear range for each LVDT. After the Wheatstone bridge for each strain gauge was balanced, the gauge was calibrated using a 50 000 ohm resistor.

The mechanical Demec gauges also required calibration prior to use. For the 203 mm Demec gauge, the calibration factors were $9.55 \mu\epsilon/\text{dial increment}$ for truss 1 and $9.71 \mu\epsilon/\text{dial increment}$ for truss 2. The calibration factor for the 254 mm Demec gauge, used on truss 1 only, was $7.94 \mu\epsilon/\text{dial increment}$.

4.4.2 Instrumentation

For each flexural test, measurements of loads and reactions, truss deflections, roller movements, separation of compression web members, steel strains, concrete slab

strains, and slip between the concrete slab and top chord were made as the truss was loaded.

Some of the instrumentation used for shrinkage measurements was also monitored during the flexural tests. Demec and dial gauge readings were recorded manually while the output from electrical resistance strain gauges, linear variable differential transformers (LVDT's), and load cells were recorded automatically on the Data General Eclipse S/120 data acquisition system. Power supplies for the electrical instrumentation were monitored throughout each test and adjusted as necessary. The data was subsequently transferred to and processed on an Amdahl 5860, the University of Alberta's mainframe computer.

4.4.2.1 Loads and Reactions

Calibrated load cells were used to measure loads at the 4 load points and at the 2 reactions. This provided a check of statics in the vertical direction and allowed shear force and bending moment diagrams to be drawn at every load step. Table 4.4 describes the specifications of the load cells.

4.4.2.2 Displacements

Mechanical dial gauges reading to 0.01 mm and LVDT's with a stroke of ± 75 mm were used to provide duplicate measurements of truss deflections at midspan and the quarter points. Pointers attached to the bottom chord, moving against a metre scale, were used to obtain gross deflections at midspan on truss 1 and at midspan and the quarter points

Table 4.4 Load cell specifications

Location	Test 1			Test 2		
	Load Cell Type	Capacity, kN	Supply Voltage, volts	Load Cell Type	Capacity, kN	Supply Voltage, volts
North Reaction	StrainInsert	445	15.0	StrainInsert	890	15.0
South Reaction	StrainInsert	445	15.0	StrainInsert	890	15.0
North Exterior Load Point	Sensotec	222	8.0	Sensotec	222	8.0
North Interior Load Point	Kyowa	445	8.0	Kyowa	445	8.0
South Interior Load Point	Kyowa	445	8.0	Kyowa	445	8.0
North Exterior Load Point	1. Sensotec 2. Kyowa	222 178	8.0 8.0	StrainInsert	445	15.0

on truss 2.

At both reactions, dial gauges reading to 0.01 mm and LVDT's with a stroke of ± 75 mm were positioned against the roller plates to measure horizontal movement. On test 2, similar dial gauges also recorded the roller movement at load points. The separation of the two angles of several compression web members was monitored using LVDT's with strokes of ± 25 mm or ± 12 mm. On composite truss 1, compression diagonals BC and QR were instrumented, while diagonals BC, DE, FG, LM, NP, and QR were monitored on composite truss 2.

The slip between the concrete slab and the top chord was measured using LVDT's with a stroke of ± 25 mm at both ends of each truss and an LVDT with a ± 12 mm stroke at the north quarter point.

The LVDT's used were Hewlett Packard models 7DCDT-500, 7DCDT-1000, and 7DCDT-3000, powered with a supply voltage of 6 volts DC. Their maximum non-linearity was $\pm 0.5\%$ of full scale.

4.4.2.3 Steel Strains

One hundred and fifty electrical resistance strain gauges were used on composite truss 1 to measure steel strains. Thirty-two gauges were applied as 16 pairs at the mid-depth and mid-length of each panel of the top and bottom chords. For the three central bottom chord panels, high elongation strain gauges were used, and therefore double gauging was provided on the central panel which had also

been gauged for shrinkage measurements. The 16 gauges on web members applied for shrinkage measurements were monitored during the destructive test. To study the behaviour of the web members, 5 angles were gauged with 6 gauges at each of three levels for a total of 90 gauges. The web members gauged were the west angles of JK, KL, LM, PQ, and QR. Three gauges on the west and east sides of the top chord were applied midway between the diagonals at panel points N and Q in an attempt to determine the effect on the top chord of the centroids of the diagonals intersecting at the mid-depth of the cover slab. The schematic diagram in Fig 4.12 shows the locations of the strain gauges on composite truss 1.

On composite truss 2, 146 strain gauges were used to measure steel strains. Fourteen pairs were applied at mid-depth and mid-length of top and bottom chord panels, with double gauging on panels FH and HK where gauges were applied for shrinkage measurements before high elongation gauges were applied on the three central panels of the bottom chord. In addition, to study local bending moments in the top chord due to the effect of the centroids of the web members intersecting at the mid-depth of the cover slab, 6 gauges (3 per side) were applied at 4 locations on panels GJ, JL, NQ, and QS. To study web member behaviour, 3 angles in addition to those gauged for shrinkage were instrumented in the same fashion, with 18 gauges per web member. The web members gauged were, therefore, the west angles of BC, DE, PQ, QR, and RS. In an attempt to study the mechanism by

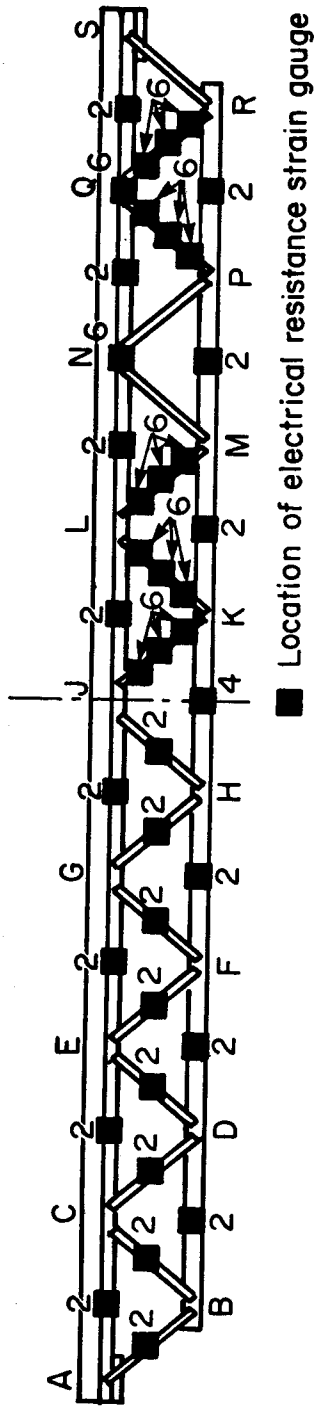


Figure 4.12 Location of strain gauges on composite truss 1

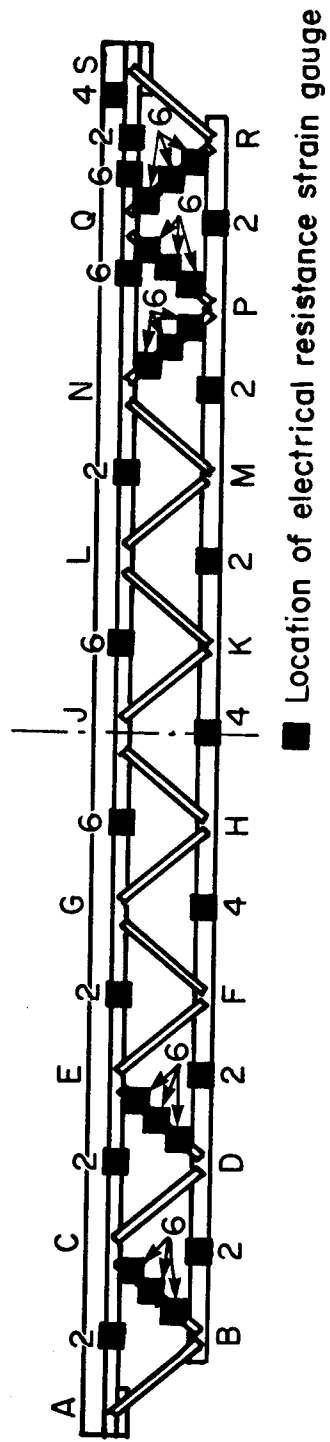


Figure 4.13 Location of strain gauges on composite truss 2

which a stud in a deck flute resists load, two gauges were applied to the stud in flute 37 near the south end of the truss and two gauges were applied on a steel strut extending from the head of the stud to the bottom corner of the flute. The locations of the strain gauges on composite truss 2 are shown schematically in Fig. 4.13.

On both trusses, a pair of Demec points with a 203 mm standard gauge length was applied at mid-depth on either side of the bottom chord at mid-length of the central panel, to duplicate the strain measurement there.

4.4.2.4 Concrete Strains

Demec points set at a 203 mm gauge length, applied on the surface of each concrete slab to measure shrinkage strains, were also used to measure concrete strains during the tests to failure. On truss 1, an additional transverse line of 3 pairs of Demec points was also applied at the north quarter point. Therefore, on composite truss 1, concrete strains were measured using 16 sets of Demec points along 4 transverse lines, as shown in Fig. 4.5, and on composite truss 2, 21 sets of Demec points on 5 transverse lines were used, as shown in Fig. 4.6.

Two pairs of Demec points were also placed at mid-thickness of the cover slab on the west and east sides of the slab at midspan. These Demec points were set at a standard gauge length of 254 mm on truss 1 and 203 mm on truss 2.

4.4.3 Testing Procedure

Anticipating that the behaviour of the composite trusses under load would be essentially elastic up to a load per jack of about 80 kN, load increments of 8 kN per jack were used in the elastic range. When inelastic behaviour became noticeable, each truss was unloaded almost to zero and reloaded to confirm the elastic response, then loaded in smaller increments to failure.

As load was applied, the reactions, loads, and midspan deflection were monitored continuously on the data acquisition screen. When the required load or deflection was reached at any test increment, the hydraulic system valve was closed to maintain the load (as closely as relaxation would allow) while a set of readings was taken. The output from the six load cells (4 under the loading jacks and 2 under the reactions) was used to check the sum of the forces in the vertical direction. The sum of the reactions ranged from 1.015 to 0.991 of the sum of the loads as truss 1 was loaded and from 1.020 to 0.982 as truss 2 was loaded, confirming the calibration of the load cells. The overall behaviour of each truss was monitored during the course of the test by plotting the load versus midspan deflection. When deflections began to increase rapidly in the inelastic range, the load increments were reduced by half to approximately 4 kN per jack. In several previous tests (Cran, 1972; Bjorhovde, 1981), failure was precipitated by buckling of a compression diagonal. Therefore, in these tests, the

separation of the two angles of critical compression web members was closely monitored to ascertain whether or not failure was imminent there. Both steel strains and concrete strains at midspan were monitored to determine when inelastic strains were occurring. The end slip—the relative movement between the top chord and the concrete slab—was also monitored. Roller movements were observed to check that free movement was occurring. The voltage output of the LVDT's was observed at each load step and the LVDT's were reset when the voltages approached the limits of the linear range. Before proceeding to the next load step, the plumbness of the jacks was checked, the concrete slab was inspected and crack progression marked, and the whitewash on the steel truss was examined for signs of yielding.

To ensure proper functioning of all electrical instrumentation, the power supply voltages were monitored periodically during each test. These voltages did not vary by more than 0.8% on test 1 and 1.8% on test 2.

The flexural test on composite truss 1 took place on July 20, 21, and 22, 1985. The truss was unloaded overnight on July 20-21 but the load was maintained overnight on July 21-22. Composite truss 2 was loaded to failure on January 23 and 24, 1986 with the test load maintained overnight.

5. GEOMETRIC PROPERTIES

5.1 Steel Sections

5.1.1 Dimensions

The dimensions of the steel sections from which the trusses were built, were measured with micrometers in order to establish their cross sectional properties. For the most part, these dimensions were within the rolling tolerances prescribed by CSA Standard G40.20-M81 (CSA, 1981a).

The measured dimensions of the HSS top and bottom chord sections are listed in Table 5.1. The table shows that the actual wall thickness of both sections was about 0.94 times the specified wall thickness. The measured outside width and depth "b" and "d" were within 0.4% of the specified values.

Table 5.2 gives the measured dimensions of the five angle sections. Without exception, the actual leg widths and thicknesses are within 0.7% of the specified values.

5.1.2 Section Properties

Cross sectional properties calculated from measured parameters were used rather than nominal values to analyze the test data. Both a geometric and a volumetric method were used to calculate the area of each cross section. The geometric method was based on the measured dimensions of each section, assuming that all rounded corners were circular arcs. In the volumetric method, the area is

Table 5.1 Measured dimensions of HSS sections

Section	Dimension Measured	Number of Measurements	Mean Measured Value, mm	C.O.V.	Measured/Specified Value	Range of Measurements, mm	Tolerance, mm
HSS 127.0x76.2 x4.78	Wall thickness	184	4.478	0.0102	0.937	4.354 to 4.592	4.30 to 5.26
	Width	178	76.276	0.0030	1.001	75.920 to 77.166	75.0 to 77.4
	Depth	147	126.548	0.0040	0.996	125.070 to 127.228	126.0 to 128.0
HSS 76.2x76.2 x6.35	Wall thickness	209	5.984	0.0178	0.942	5.830 to 6.282	5.72 to 6.98
	Width, depth	334	76.368	0.0013	1.002	76.074 to 76.606	75.4 to 77.0

Table 5.2 Measured dimensions of angle sections

Section	Dimension Measured	Number of Measurements	Mean Measured Value,		C.O.V.	Measured/Specified Value	Range of Measurements, mm	Tolerance, mm
			Inches	mm				
L 2-1/2x2-1/2 x3/8	Leg Width	110	2.4845	63.106	0.0031	0.994	62.662 to 63.412	61.5 to 65.5
	Leg Thickness	112	0.3736	9.490	0.0075	0.996	9.324 to 9.626	9.12 to 9.92
L 2x2x3/8	Leg Width	110	2.0123	51.112	0.0031	1.006	50.534 to 51.588	49.8 to 51.8
	Leg Thickness	112	0.3722	9.454	0.0051	0.993	9.320 to 9.578	9.32 to 9.72
L 2x2x1/4	Leg Width	158	2.0065	50.966	0.0100	1.003	49.886 to 51.982	49.8 to 51.8
	Leg Thickness	160	0.2488	6.320	0.0104	0.995	6.198 to 6.528	6.15 to 6.55
L 1-1/2x1-1/2 x1/4	Leg Width	158	1.5174	38.542	0.0088	1.012	37.504 to 39.218	37.1 to 39.1
	Leg Thickness	160	0.2498	6.344	0.0100	0.999	6.196 to 6.478	6.15 to 6.55
L 1-1/2x1-1/2 x3/16	Leg Width	160	1.4956	37.988	0.0016	0.997	37.796 to 38.126	37.1 to 39.1
	Leg Thickness	160	0.1883	4.782	0.0117	1.004	4.648 to 4.902	4.56 to 4.96

calculated from the measured mass and length of specimens of each section and the density of rolled steel. Using the nominal density of 7850 kg/m^3 to calculate areas of the angles gave results that differed from the geometric calculations by 0.5% on the average. The densities of the steel top and bottom chords were found to be 8008 kg/m^3 and 8048 kg/m^3 respectively, up to 2.5% greater than the nominal density. The areas of the chords, calculated by the two methods, were within 0.1% of each other. The geometric areas were selected for further calculations. The location of the centroid and the moment of inertia of each section were determined geometrically.

Table 5.3 gives the nominal and measured values of the cross sectional properties of the steel sections. The actual cross sectional properties were less than the nominal values, particularly for the HSS sections. The overall mean of the measured-to-nominal values for cross sectional area was 0.982 with a coefficient of variation of 0.0249, and for the moment of inertia about the x-axis, the corresponding figures were 0.975 and 0.0247.

The variation of the mass of the sections from the specified values is shown in Table 5.4 and confirms that the actual cross sectional areas of the HSS sections were substantially less than the nominal values.

Table 5.3 Cross sectional properties of steel sections

Section	Nominal Properties			Measured Properties			
	Area, A mm ²	Location of Centroid, mm	Moment of Inertia, I x 4 mm ⁴	Area, A mm ²		Location of Centroid, mm	Moment of Inertia, I x 4 mm ⁴
				Volumetric Method	Geometric Method		
HSS 127.0x76.2x4.78	1790	63.5	3.78x10 ⁶	1685	1686	63.3	3.56x10 ⁶
HSS 76.2x76.2x6.35	1670	38.1	1.31x10 ⁶	1590	1592	38.2	1.29x10 ⁶
L 2-1/2x2-1/2x3/8	1116	19.3	0.408x10 ⁶	1099	1104	19.0	0.390x10 ⁶
L 2x2x3/8	877	16.3	0.200x10 ⁶	858	868	15.9	0.193x10 ⁶
L 2x2x1/4	606	15.0	0.146x10 ⁶	604	606	14.9	0.143x10 ⁶
L 1-1/2x1-1/2x1/4	445	11.9	0.058x10 ⁶	447	447	11.9	0.059x10 ⁶
L 1-1/2x1-1/2x3/16	342	11.2	0.046x10 ⁶	340	341	11.1	0.045x10 ⁶

Table 5.4 Mass variation of sections from specified values

Section	Specified Mass/Unit Length, kg/m	Number of Measurements	Measured Mass/Unit Length,		Tolerance, Percent of Specified
			kg/m	Percent of Specified	
HSS 127.0x76.2x4.78	14.1	3	13.56	-3.8	-3.5 to +1.0
HSS 76.2x76.2x6.35	13.1	2	12.73	-2.8	-3.5 to +1.0
L 2-1/2x2-1/2x3/8	8.77	1	8.624	-1.7	± 2.5
L 2x2x3/8	6.99	1	6.733	-3.7	± 2.5
L 2x2x1/4	4.74	1	4.746	+0.1	± 2.5
L 1-1/2x1-1/2x1/4	3.48	1	3.511	+0.9	± 2.5
L 1-1/2x1-1/2x3/16	2.68	1	2.667	-0.5	± 2.5

5.2 Steel Trusses

5.2.1 Dimensions

The dimensions of the fabricated trusses agreed closely with those specified on the drawings. Both trusses were manufactured to the specified length of 11 800 mm and both had an overall depth of 728 mm, compared to the specified value of 730 mm. The mean measured-to-specified values of the truss measurements are given in Table 5.5 and are indicative of the high quality of fabrication.

5.2.2 Moments of Inertia

Because the moduli of elasticity of the steel chords were not equal, the top chord area was transformed using a modular ratio (the ratio of the moduli of elasticity) of $\frac{208.3}{205.9} = 1.012$ in order to calculate the moment of inertia of the steel trusses. For both trusses, the elastic neutral axis was located 362 mm below the top surface of the top chord, and the moment of inertia was $324.6 \times 10^6 \text{ mm}^4$.

5.3 Composite Trusses

5.3.1 Dimensions

The mean measured values of the width and thickness of the concrete slab on composite trusses 1 and 2 are shown in Table 5.6. The mean thickness of the Robertson QL Lock-Rib steel deck, based on 10 measurements, was 0.87 mm, compared

Table 5.5 Steel truss measurements

Measurement	Truss 1			Truss 2		
	Number of Measurements	Mean Measured/Specified Value	C.O.V.	Number of Measurements	Mean Measured/Specified Value	C.O.V.
Top chord length	2	1.000	0.00000	2	1.000	0.00000
Bottom chord length	2	0.999	0.00003	2	0.999	0.00003
Truss depth	8	0.998	0.00194	8	0.998	0.00229
Web member length	64	0.999	0.00090	64	0.999	0.00080
Inclination of web members from horizontal	64	1.001	0.00493	64	0.998	0.00476
Weld length	64	1.036	0.0346	64	1.051	0.0350
Weld fillet size	-	-	-	25	1.317	0.1305

Table 5.6 Slab dimensions

Dimension	Specified Value, mm	Composite Truss 1			Composite Truss 2		
		Number of Measurements	Mean Measured Value, mm	C.O.V.	Number of Measurements	Mean Measured Value, mm	C.O.V.
Slab width	2350	10	2354	0.0030	10	2350	0.0027
Slab thickness	140.1	78	139.3	0.0138	78	140.2	0.0114
Cover slab thickness	65.0	77	63.2	0.0460	76	64.0	0.0450

to the nominal thickness of 0.91 mm. The out-to-out depth of composite truss 1 was measured to be 868 mm and the out-to-out depth of composite truss 2 was 869 mm.

5.3.2 Moments of Inertia

The transformed moment of inertia of composite truss 1, calculated using the modulus of elasticity of the concrete at the time of the flexural test, was $920.3 \times 10^6 \text{ mm}^4$. When modified to account for the effects of the open web and interfacial slip, as described in Section 3.1.5, the effective moment of inertia became $805.9 \times 10^6 \text{ mm}^4$. The corresponding moments of inertia for composite truss 2 were $895.3 \times 10^6 \text{ mm}^4$ and $784.6 \times 10^6 \text{ mm}^4$. The transformed moments of inertia were calculated using the measured slab widths which were approximately equal to the design effective width. The elastic neutral axis was located 117.7 mm and 134.7 mm below the surface of the concrete slab for composite trusses 1 and 2 respectively.

6. MATERIAL PROPERTIES AND BEHAVIOUR

To establish the stress-strain characteristics of the materials, ancillary tests were carried out on the steel and concrete used to construct the test specimens. These stress-strain relationships enabled the internal forces in the specimens to be evaluated from the strain data collected during the tests, and thus the behaviour of the trusses and their components could be accurately assessed.

6.1 Steel

6.1.1 General

Class C HSS sections and hot rolled angle sections were specified for fabrication of the steel trusses. All components of both trusses with the same section size came from one heat of steel. The chemical composition of each heat, as given in Table 6.1 (based on mill reports supplied by the fabricator), is within the limits specified by CSA Standard CAN3-G40.21-M81 (CSA, 1981b) for each steel grade. The mill certificate for the bottom chord HSS was unavailable.

6.1.2 Ancillary Tests

6.1.2.1 Tension Coupons

A total of 34 tension coupons were tested to determine the material properties of the steel HSS and angle sections.

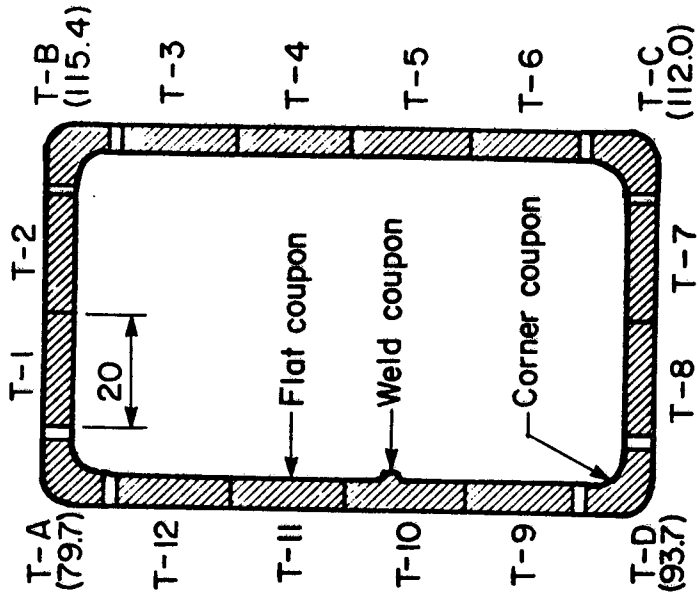
Table 6.1 Chemical composition of steel sections

Section	Grade	Manufacturer	Heat No.	Chemical Composition, %					
				C	Mn	P	S	Si	
HSS 127.0x76.2 x4.78	G40.21 350W	Standard Tube Canada Inc.	-	-	-	-	-	-	
HSS 76.2x76.2 x6.35	G40.21 350W	Standard Tube Canada Inc.	221124	0.21	0.84	0.008	0.020	-	
L 2-1/2x2-1/2x3/8	G40.21 300W	Manitoba Rolling Mills	59185	0.18	1.13	0.025	0.033	0.24	
L 2x2x3/8	G40.21 300W	Manitoba Rolling Mills	51712	0.18	1.06	0.027	0.040	0.25	
L 2x2x1/4	G40.21 300W	Manitoba Rolling Mills	53688	0.12	0.70	0.021	0.035	-	
L 1-1/2x1-1/2x1/4	G40.21 300W	Manitoba Rolling Mills	52156	0.13	0.78	0.028	0.044	-	
L 1-1/2x1-1/2x3/16	G40.21 300W	Manitoba Rolling Mills	65800	0.12	0.69	0.011	0.032	-	

One coupon was sawn from each leg of the 5 different sizes of angles used for web members. Eight coupons were sawn from the flats of the square HSS used for the top chord. A total of 16 coupons, including 4 corner coupons and 1 coupon containing the weld seam, were sawn from the rectangular HSS of the bottom chord. The locations and identity numbers of these coupons are shown schematically in Fig. 6.1.

The flat and weld coupons were cut and milled following ASTM E8-85a recommendations with a gauge length of 50 mm and width of 12.5 mm. The cross sectional areas of the flat and weld coupons were determined prior to testing from measurements of the gauge width and thickness. Each corner coupon had legs of equal size although the leg size and therefore the cross sectional area varied from coupon to coupon. The edges of each corner coupon were milled so that the cross sectional area, determined by the volumetric method, was constant along its length.

The tension coupons were tested in accordance with ASTM E8-85a in a Baldwin testing machine. To grip the corner coupons and distribute the gripping force evenly, short lengths of 12.5 mm diameter steel rod were fitted to the inside radius at the ends of each specimen, and the loading grips for a circular section were used. Strains up to about 2% were measured with a pair of strain gauges mounted on opposite faces of each coupon and wired to a Budd Strain Indicator. Larger strains were measured over the 50 mm gauge length with dividers and a scale.



Number in brackets below corner coupon designation is area of corner coupon in mm²

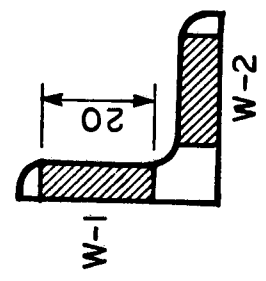
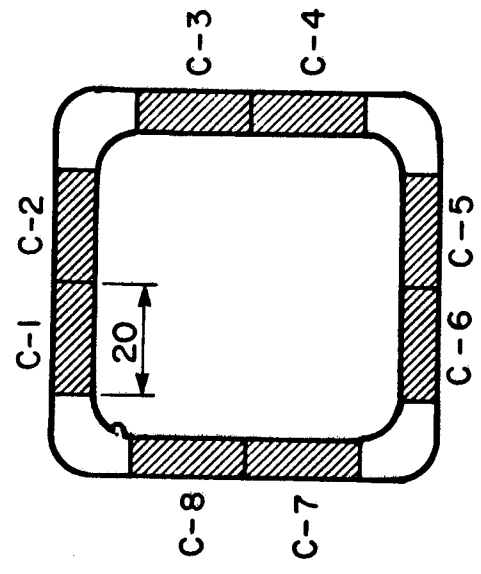


Figure 6.1 Identification and location of tension coupons

The modulus of elasticity was determined using a least squares straight line fit to the data. The proportional limit of the data was selected using a method suggested by Kennedy and MacGregor(1984), based on the trend of a 4 point moving average of the tangent modulus. To calculate the yield strength of the HSS coupons, which had no definite yield plateau due to cold work, a 0.002 strain offset was used.

6.1.2.2 Stub Columns

Two stub columns of each size HSS were tested in compression to obtain the average stress-strain characteristics for the total cross sections of the top and bottom chords (including the corners where the strength is higher due to cold working). Following the guidelines of the SSRC(1976), the HSS 76.2x76.2x6.35 and HSS 127.0x76.2x4.78 stub columns were sawn to lengths of 400 mm and 500 mm respectively, and the ends were milled plane. Four strain gauges were mounted at the centre of the flat faces at mid-height of each column to measure strains. In addition, 2 sets of Demec points with a standard gauge length of 203 mm were mounted at mid-height on opposite faces. Dividers and a scale were used over a 254 mm gauge length to measure large strains. The stub columns were tested according to SSRC(1976) guidelines in an MTS testing machine.

The modulus of elasticity was calculated from the stress-strain data using the method of least squares, after the proportional limit was identified from the trend of a 4

point moving average of the tangent modulus. A 0.002 strain offset was used to calculate the static yield strength.

6.1.2.3 Tension Test on Bottom Chord HSS

Because knowledge of the stress-strain relationship of the bottom chord steel, including the ultimate behaviour, was crucial to the understanding of the composite truss behaviour under load, a full-scale tension test on a section of HSS 127.0x76.2x4.78 was conducted. The test specimen was 1400 mm long and included a web-to-chord joint, as shown in Fig. 6.2, to determine whether the welded connection would initiate the failure.

To grip the test specimen in the MTS testing machine, two snug-fitting steel plugs were inserted into the ends of the tube. Three pairs of 203 mm gauge length Demec points measured strains over the central portion of the specimen on one face. A pair of strain gauges located on opposite faces 305 mm from mid-height of the specimen duplicated one of the Demec strain measurements. Dividers were used in punched holes with a gauge length of 203 mm at the same locations as the Demec points to measure large strains.

The method of least squares was used to determine the modulus of elasticity from each set of stress-strain data, after the proportional limit was chosen based on the trend of a 3 point moving average of the tangent modulus. The static yield strength was determined from a 0.002 strain offset.

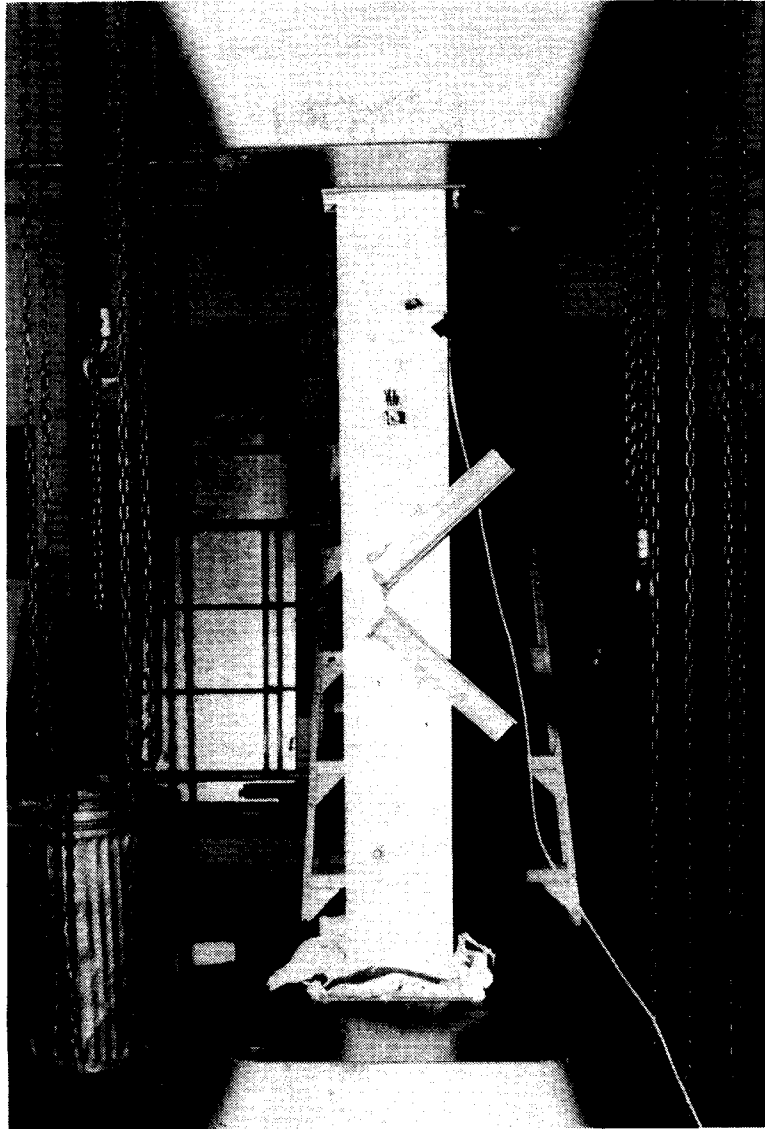


Figure 6.2 HSS 127.0x76.2x4.78 tension test specimen

6.1.3 Test Results

6.1.3.1 Tension Coupons

Angle Sections

The hot rolled angles exhibited stress-strain behaviour typical of a mild steel, with a definite yield plateau at about 300 MPa and significant strain hardening, as shown in Fig. 6.3. Failure strains of about 34% demonstrate the steel ductility. The results of the tension coupon tests from the angle sections are given in Table 6.2. It is suspected that one leg of the L 2x2x1/4 had been bent and straightened prior to testing because of the high yield stress and low strain of coupon W4-2 compared to W4-1.

Square HSS Section

The test results from 8 coupons taken from the flats of the HSS 76.2x76.2x6.35 used for the top chord are given in Table 6.3. These coupons had an average modulus of elasticity of 203 600 MPa, an average static yield strength of 436 MPa, and an average ultimate strength of 491 MPa. It is recognized that the strengths of the corners, where considerable cold working has occurred, would be appreciably higher than those of the flats. The section did not exhibit a yield plateau, as shown in a typical stress-strain curve from one of the flat coupons in Fig. 6.4.

Table 6.2 Mechanical properties of 300W web members

Angle Section	Coupon No.	Modulus of Elasticity, MPa	Static Yield Strength, MPa	Upper Yield Point, MPa	Lower Yield Point, MPa	ϵ_y $\mu\epsilon$	ϵ_{st} $\mu\epsilon$	Ultimate Strength, MPa	ϵ_u $\mu\epsilon$	ϵ_f $\mu\epsilon$
L 2-1/2x2-1/2x3/8	W2 - 1	204 400	293.9	327.5	316.6	1600	15 000	486.7	190 000	365 000
	W2 - 2	209 100	293.8	339.2	317.0	1620	16 000	488.7	210 000	355 000
L 2x2x3/8	W1 - 1	204 700	305.3	340.2	329.0	2440	14 000	508.5	180 000	330 000
	W1 - 2	207 200	303.3	337.7	327.2	1700	13 500	509.4	200 000	340 000
L 2x2x1/4	W4 - 1	204 400	309.2	339.8	329.7	1620	17 000	497.1	200 000	340 000
	W4 - 2	202 700	393.3	431.0	425.0	3330	13 000	494.9	145 600	262 000
L 1-1/2x1-1/2x1/4	W3 - 1	205 400	300.3	325.5	320.0	1590	18 000	487.6	198 000	337 000
	W3 - 2	205 300	302.9	337.9	326.6	1630	17 500	488.8	220 000	350 000
L 1-1/2x1-1/2x3/16	W7 - 1	206 100	315.1	339.1	336.5	1650	18 000	486.2	200 000	340 000
	W7 - 2	207 500	320.8	340.7	338.0	2800	18 000	489.0	210 000	340 000

Table 6.3 Mechanical properties of 350W top chord

Coupon No.	Modulus of Elasticity, MPa	Static Yield Strength, * MPa	ϵ_y $\mu\epsilon$	Ultimate Strength, MPa	ϵ_u $\mu\epsilon$	ϵ_f $\mu\epsilon$
Flats C - 1	209 300	427.5	4040	498.2	30 000	220 000
C - 2	206 400	424.0	4100	493.8	20 500	260 000
C - 3	200 000	428.0	4150	490.9	35 000	300 000
C - 4	201 900	435.0	4150	497.2	20 000	240 000
C - 5	203 100	445.5	4200	494.0	50 000	200 000
C - 6	201 100	457.0	4250	487.5	11 000	220 000
C - 7	203 100	442.0	4150	496.4	16 000	210 000
C - 8	203 500	428.0	4150	472.2	20 000	230 000
Mean	203 600	435.9	4150	491.3	25 300	235 000
C.D.V.	0.015	0.026	0.015	0.017	0.494	0.136

* From 0.2% strain offset

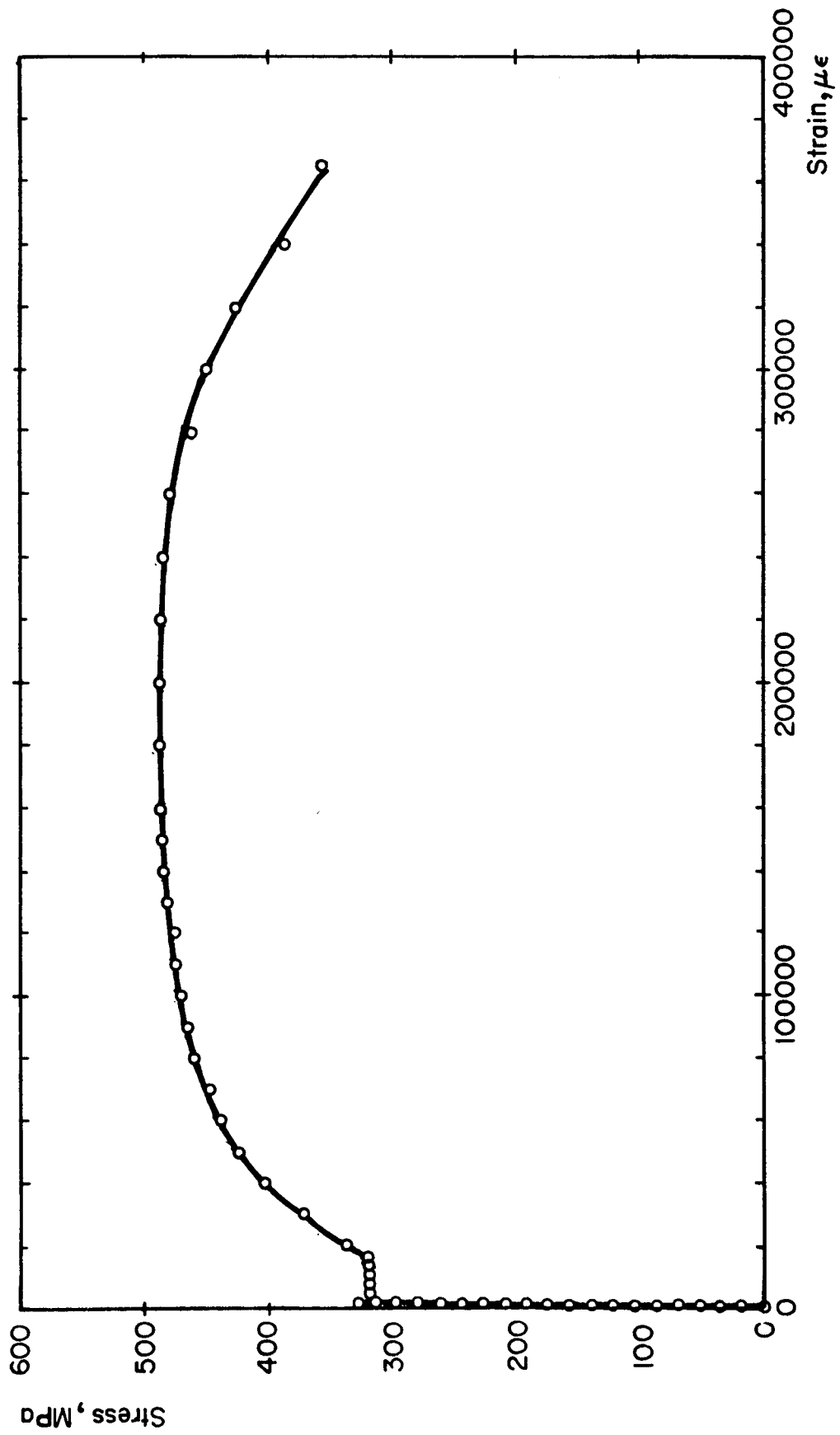


Figure 6.3 Stress-strain curve for angle member BC from tension coupon

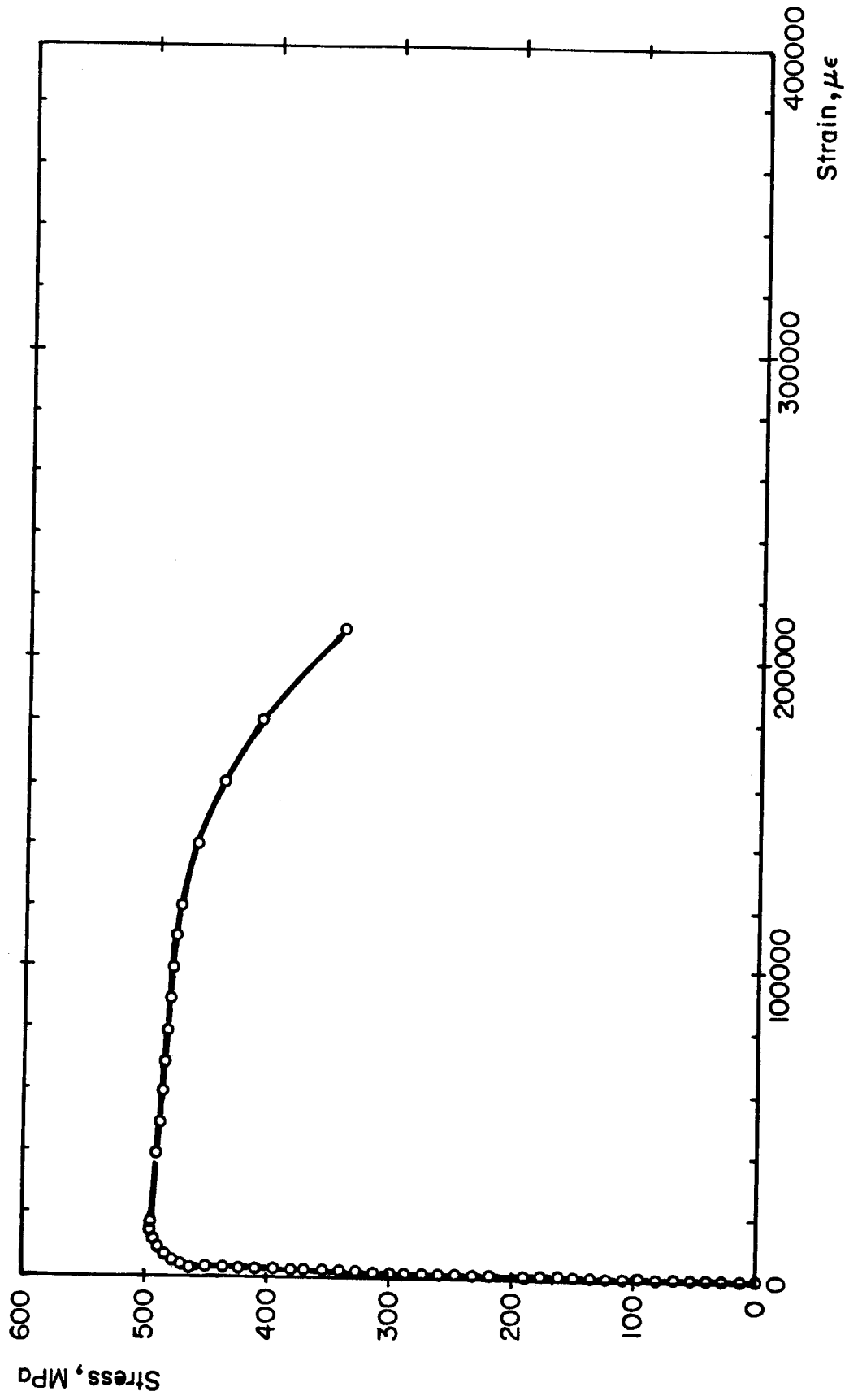


Figure 6.4 Stress-strain curve for HSS 76.2x76.2x6.35 from tension coupon

Rectangular HSS Section

Figure 6.5 shows typical stress-strain curves for the three types of coupons tested from the HSS 127.0x76.2x4.78 used for the bottom chord. As expected, the weld coupon and the corner coupons exhibit much higher strength and considerably less ductility than the coupons taken from the flats. The increased strength of the corners compared to the flats is attributable to cold work during the tube forming process, while the difference in properties of the weld coupon compared to the flats results from the inclusion of weld metal with different mechanical properties. No significant difference in the modulus of elasticity of the corners compared to the flats was observed. The test results for the 11 flat coupons, 1 weld coupon, and 4 corner coupons are given in Table 6.4. A weighted average technique based on the respective areas of the flat, weld, and corner coupons gave a modulus of elasticity of 208 400 MPa, a static yield strength of 451 MPa, and an ultimate strength of 538 MPa for the overall section.

A weighted stress-strain curve based on these data was used to determine loads in the bottom chord beyond the yield level (see also following section).

6.1.3.2 Stub Columns

The stress-strain curves obtained from 2 stub column tests on the HSS 76.2x76.2x6.35 and the HSS 127.0x76.2x4.78, shown in Figures 6.6 and 6.7, were used to reduce strain test data to loads in the top and bottom chords up to the

Table 6.4 Mechanical properties of 350W bottom chord

Coupon No.	Modulus of Elasticity, MPa	Static Yield Strength,* MPa	ϵ_y $\mu\epsilon$	Ultimate Strength, MPa	ϵ_u $\mu\epsilon$	ϵ_f $\mu\epsilon$
Flats T - 1	212 000	429.0	3980	519.8	60 000	220 000
T - 2	206 300	407.5	3980	509.5	65 000	220 000
T - 3	204 000	428.0	3800	506.4	60 600	202 000
T - 4	209 900	417.5	3990	498.9	80 000	240 000
T - 5	204 700	413.5	4250	503.5	70 000	220 000
T - 6	212 300	424.0	4250	508.3	60 000	200 000
T - 7	204 600	401.0	3960	501.5	60 000	230 000
T - 8	208 200	418.0	4000	512.0	65 000	230 000
T - 9	208 900	446.0	4150	517.4	50 000	210 000
T - 11	211 200	435.0	4070	518.8	55 000	220 000
T - 12	206 900	444.0	4125	531.2	45 000	190 000
Mean	208 100	424.0	4050	511.6	61 000	217 000
C.O.V.	0.015	0.034	0.033	0.019	0.155	0.068
Weld T - 10	241 400	589.0	4450	686.7	15 000	70 000
Corners T - A	204 800	520.5	4540	606.0	23 500	**
T - B	202 600	516.5	4550	596.2	28 900	120 000
T - C	206 800	514.5	4490	593.8	28 200	**
T - D	205 000	511.0	4490	588.0	28 700	110 000
Mean	204 800	515.6	4520	596.0	27 300	115 000
C.O.V.	0.008	0.008	0.007	0.013	0.094	0.061

* From 0.2% strain offset

** Failure occurred outside gauge length

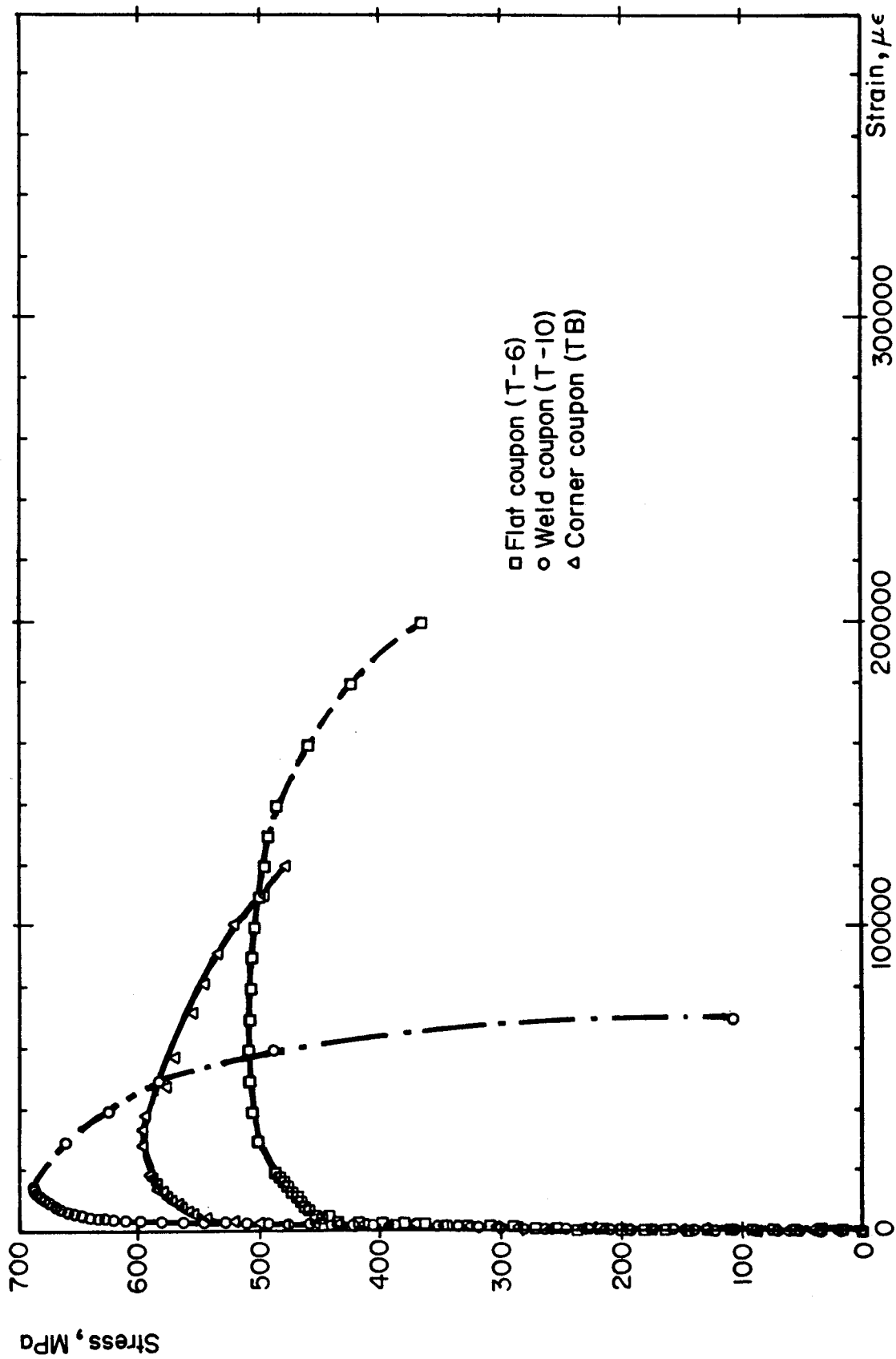


Figure 6.5 Stress-strain curves for HSS 127.0x76.2x4.78 from tension coupons

yield level. The effect of residual stresses is automatically accounted for when the specimens are loaded in compression in the stub column tests. The modulus of elasticity, static yield stress, and 0.2% offset yield strain are given in Table 6.5 for each stub column test, and the average results for the bottom chord HSS are compared to other test results in Table 6.6.

6.1.3.3 Tension Test on Bottom Chord HSS

Failure of the HSS 127.0x76.2x4.78 tension test specimen was initiated in the weld seam of the tube, about 350 mm from one end, and not in the welded web-to-chord connection as expected. This indicates that, in this case at least, discontinuities in the HSS weld manufacturing process were at least as significant as those in the welds of the joints of the web angles to the chord. The failure occurred about 50 mm outside the gauge length of the closest Demec points, and 150 mm from the pair of strain gauges. Averaging the test results from the 2 closest gauges, the modulus of elasticity was found to be 209 600 MPa, the static yield strength was 448 MPa, and the yield strain was 4250 $\mu\epsilon$. The ultimate strength of the specimen was 536 MPa and the failure strain on the face containing the weld seam was estimated to be about 10% while on the opposite face, the strain at failure was about 18%. These results are compared to other test results in Table 6.6. A stress-strain curve for the tension specimen, using strain data from the Demec points closest to the failure section, is given in Fig. 6.8.

Table 6.5 HSS stub column test results

Section Size	Modulus of Elasticity, MPa	Static Yield Strength, MPa	Yield Strain, $\mu\epsilon$
HSS 76.2x76.2x6.35			
Stub Column 1	205 100	446.6	4180
Stub Column 2	206 700	439.0	4140
Mean	205 900	442.8	4160
HSS 127.0x76.2x4.78			
Stub Column 3	211 200	434.8	4050
Stub Column 4	205 400	432.2	4110
Mean	208 300	433.5	4080

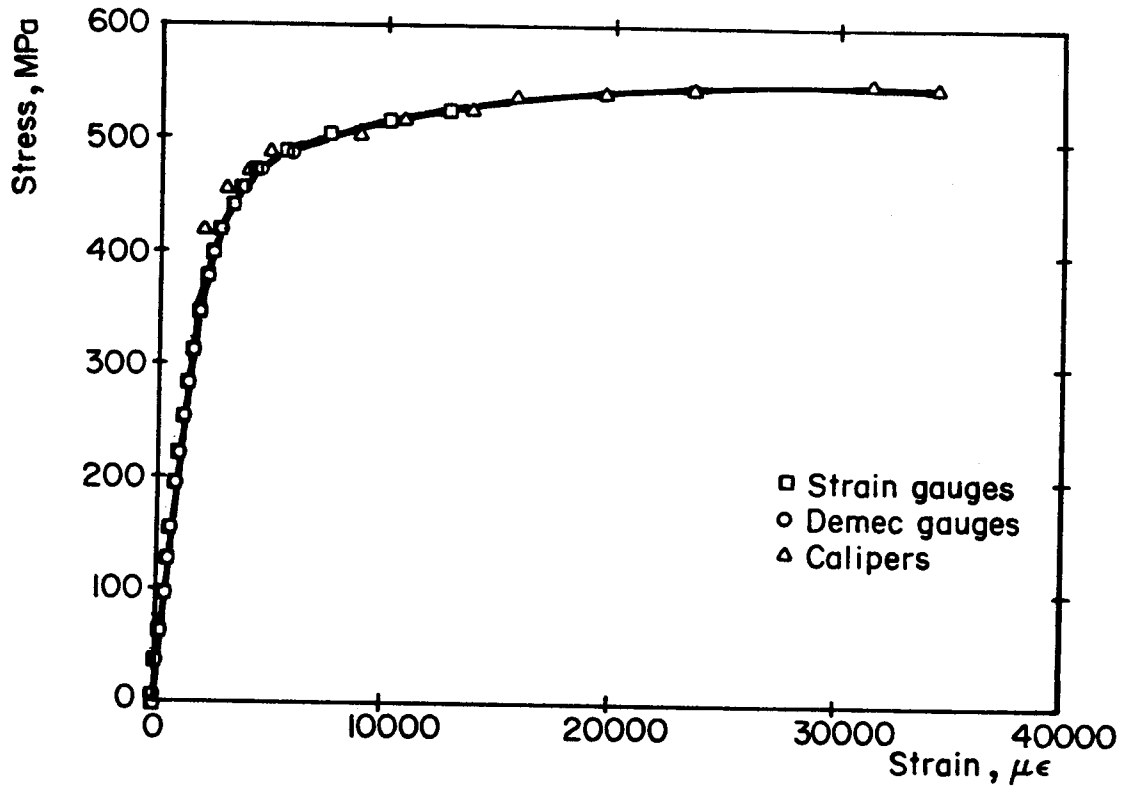


Figure 6.6 Stress-strain curve for HSS 76.2x76.2x6.35 from stub column tests

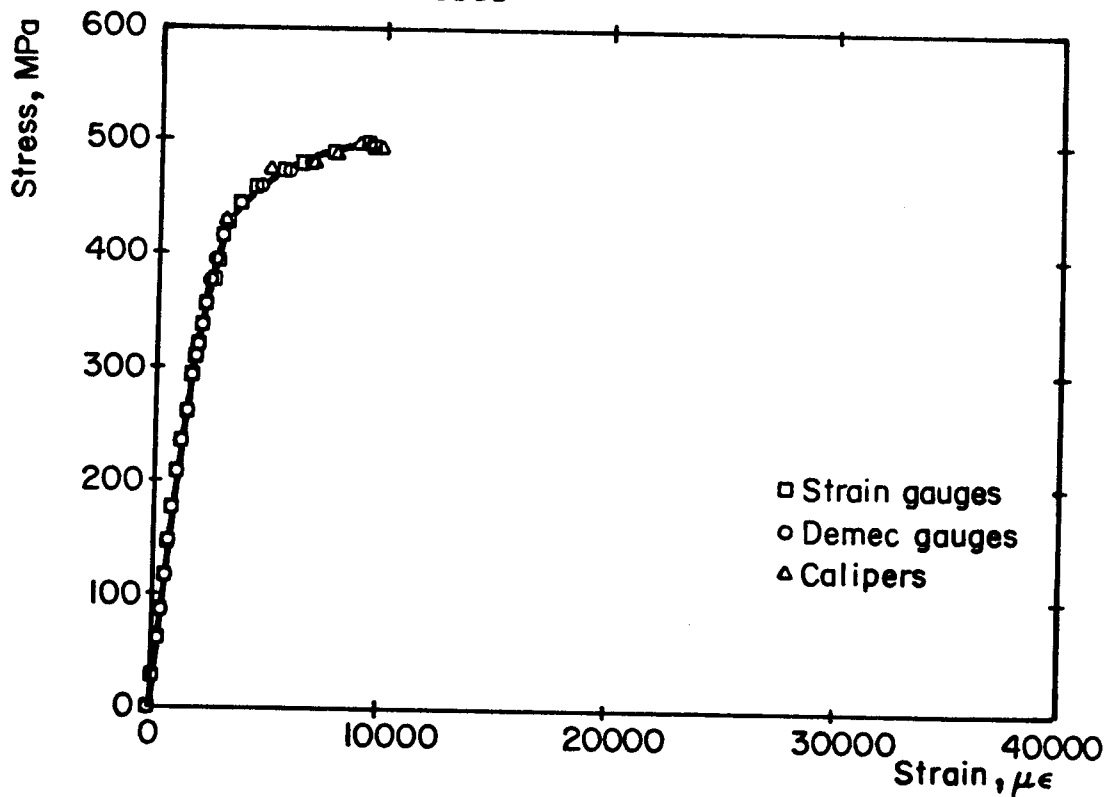


Figure 6.7 Stress-strain curve for HSS 127.0x76.2x4.78 from stub column tests

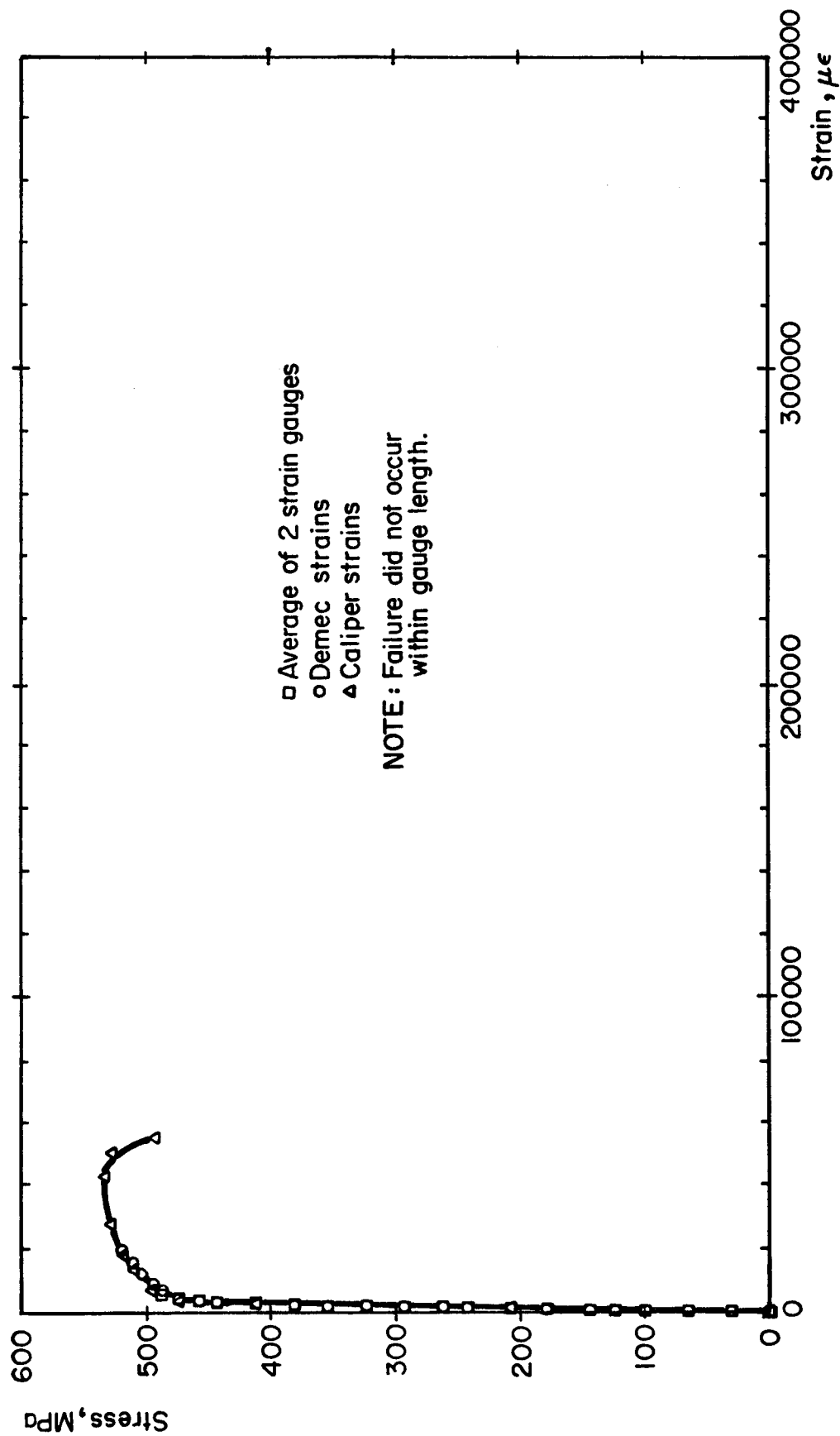


Figure 6.8 Stress-strain curve for HSS 127.0x76.2x4.78 from full-scale tension specimen

6.1.3.4 Summary of Results

The mechanical properties of the HSS 127.0x76.2x4.78 measured from tension coupon tests, stub column tests, and a full-scale tension test are summarized in Table 6.6. For analysis of the test data, a modulus of elasticity of 208 300 MPa was chosen from the average test results of the tension coupons and stub columns, neglecting the value from the full-scale tension test because its correlation coefficient was lower than the others. A static yield strength of 444 MPa and an ultimate strength of 537 MPa were selected, based on average test results.

The somewhat higher test results for modulus of elasticity and static yield strength of the HSS 76.2x76.2x6.35 from stub column tests compared to tension coupons from the flats reflect the influence of cold work at the corners of the tube. The average stub column test results, including the stress-strain curve in Fig. 6.6, were used for subsequent data analysis.

With the exception of the properties of the L 2x2x1/4, based on one test only, the mechanical properties of the angle sections were selected as the average of the results from 2 tension coupon tests.

A summary of the mechanical properties of the steel sections used for analysis of the test data is given in Table 6.7.

Table 6.6 Summary of test results for bottom chord

Test	Modulus of Elasticity, MPa	Static Yield Strength, MPa	ϵ_y $\mu\epsilon$	Ultimate Strength, MPa	ϵ_u $\mu\epsilon$	ϵ_f $\mu\epsilon$
Weighted average of flat, weld & corner tension coupons	208 400	451.3	4170	537.5	51 500	188 000
Average stub column test results	208 300	433.5	4080	-	-	-
Full scale tension test results	209 600	448.0	4250	535.6	-	96 000 to 181 000

Table 6.7 Summary of mechanical properties of steel sections

Section	Modulus of Elasticity, MPa	Static Yield Strength, MPa	ϵ_y $\mu\epsilon$	ϵ_{st} $\mu\epsilon$	Ultimate Strength, MPa	ϵ_u $\mu\epsilon$	ϵ_f $\mu\epsilon$
HSS 127.0x76.2x4.78	208 300	444	4170	-	537	43 000	180 000
HSS 76.2x76.2x6.35	205 900	443	4160	-	499	25 000	235 000
L 2-1/2x2-1/2x3/8	206 800	294	1610	15 500	488	200 000	360 000
L 2x2x3/8	206 000	304	2070	13 800	509	190 000	335 000
L 2x2x1/4	203 600	309	1620	17 000	496	200 000	340 000
L 1-1/2x1-1/2x1/4	205 400	302	1610	17 800	488	209 000	343 000
L 1-1/2x1-1/2x3/16	206 800	318	2220	18 000	488	205 000	340 000

6.2 Concrete

6.2.1 General

Twenty MPa normal weight concrete with a slump of 80 mm and made with Type 10 cement and 20 mm maximum size aggregate, was specified for the slabs on both composite trusses. The 3.5 m³ batch of ready-mix concrete required for each truss was supplied by Genstar Building Materials and had a mix design as shown in Table 6.8.

Slumps of 85 mm and 110 mm were measured from concrete samples taken from the middle portion of batches 1 and 2, respectively. An immersion type vibrator was used to consolidate the concrete in the deck forms. The slabs were screeded and floated, then trowelled to provide a surface where cracking could be easily observed. The concrete obtained its set approximately 4 hours after delivery. The slabs were then covered with polyethylene sheets for a 7 day curing period.

Concrete cylinders and flexural specimens were cast in accordance with CSA test procedure A23.2-3C (CSA, 1977) in order to determine the material properties of each batch of concrete. These ancillary specimens were cured for 7 days under polyethylene sheets and stored under the composite trusses to ensure similar curing conditions. Specimen forms were removed after 3 days for batch 1 and after 2 days for batch 2.

Table 6.8 Concrete mix design

Item	Mass kg/m ³
Cement - Type 10	200
Fly Ash	60
Fine Aggregate*	860
Coarse Aggregate* (5 mm to 20 mm)	1060
Water	150

* Aggregate mass is S.S.D.

Note: Admixture Aquafire used in batch 1.
Admixture WRDA used in batch 2.

6.2.2 Ancillary Tests

Three concrete cylinders were tested at intervals, in accordance with CSA A23.2-9C, to determine the stress-strain behaviour, including the modulus of elasticity, compressive strength, and failure strain of each batch of concrete. A total of 18 cylinders were tested for batch 1 and 15 cylinders were tested for batch 2. The tests were carried out at ages from 2 to 143 days.

Two split cylinder tests were conducted in accordance with CSA A23.2-13C, at 86 days for batch 1 and at 118 days for batch 2, in order to determine the splitting tensile strength of the concrete in each slab at the time of the destructive tests.

To determine the modulus of rupture of the concrete at the time of the destructive tests, two 150 x 150 x 915 mm flexure specimens were tested in accordance with CSA A23.2-8C at 86 days for batch 1 and at 118 days for batch 2.

6.2.3 Properties of Concrete in Compression

The results of compressive strength tests of concrete cylinders from batches 1 and 2, presented in Tables 6.9 and 6.10, are the average of three tests.

At 28 days, the concrete strength of the slab of truss 1 was 1.41 times the specified strength. The modulus of elasticity at 28 days, calculated by dividing the difference between the stress at 40% of the maximum load and the stress at 0.005% strain by the difference in the corresponding

Table 6.9 Concrete properties in compression - truss 1

Age, days	2	7	14	30	88	143
Concrete Strength, MPa	14.9	20.7	26.6	28.5	30.4	29.5
Modulus of Elasticity, MPa	17 400	20 030	19 680	19 680	-	21 070
Strain at Maximum Load, $\mu\epsilon$	1830	1940	2320	2410	-	2370

Table 6.10 Concrete properties in compression - truss 2

Age, days	2	7	14	28	118
Concrete Strength, MPa	6.0	10.4	14.5	17.0	16.8
Modulus of Elasticity, MPa	12 380	14 460	14 980	15 620	16 210
Strain at Maximum Load, $\mu\epsilon$	1240	1240	1820	2010	2000

strains, was only 0.77 of $5000\sqrt{f'_c}$. The strain at maximum load was also considerably less than the commonly accepted value of 0.003. Table 6.9 shows that when truss 1 was tested at 3 months, the average concrete strength was about 30 MPa, the modulus of elasticity was about 20 400 MPa, and the concrete strain at maximum load was about 2400 $\mu\epsilon$. A typical stress-strain plot from a compressive test on a cylinder from truss 1, tested at 143 days, is shown in Fig. 6.9. The curve exhibits an essentially linear response up to about 45% of f'_c .

Table 6.10 shows that the concrete strength of the slab of truss 2 at 28 days was only 85% of the specified strength of 20 MPa. At 28 days, the modulus of elasticity was only 0.76 of $5000\sqrt{f'_c}$ and the concrete strain at maximum load was lower than expected. At 4 months, when truss 2 was tested, the average concrete strength was still about 17 MPa, the modulus of elasticity was about 16 200 MPa, and the concrete strain at maximum load was about 2000 $\mu\epsilon$. Figure 6.10 shows a typical stress-strain curve from a cylinder test at 118 days, which exhibits linear behaviour up to about 40% of f'_c .

6.2.4 Properties of Concrete in Tension

The splitting tensile strength of the concrete of composite truss 1, from 2 split cylinder tests carried out at 86 days, was 2.5 MPa. Two flexural tests carried out at the same time gave moduli of rupture of 3.7 and 3.8 MPa, approximately 1.14 times the value of $0.6\sqrt{f'_c}$ defined in

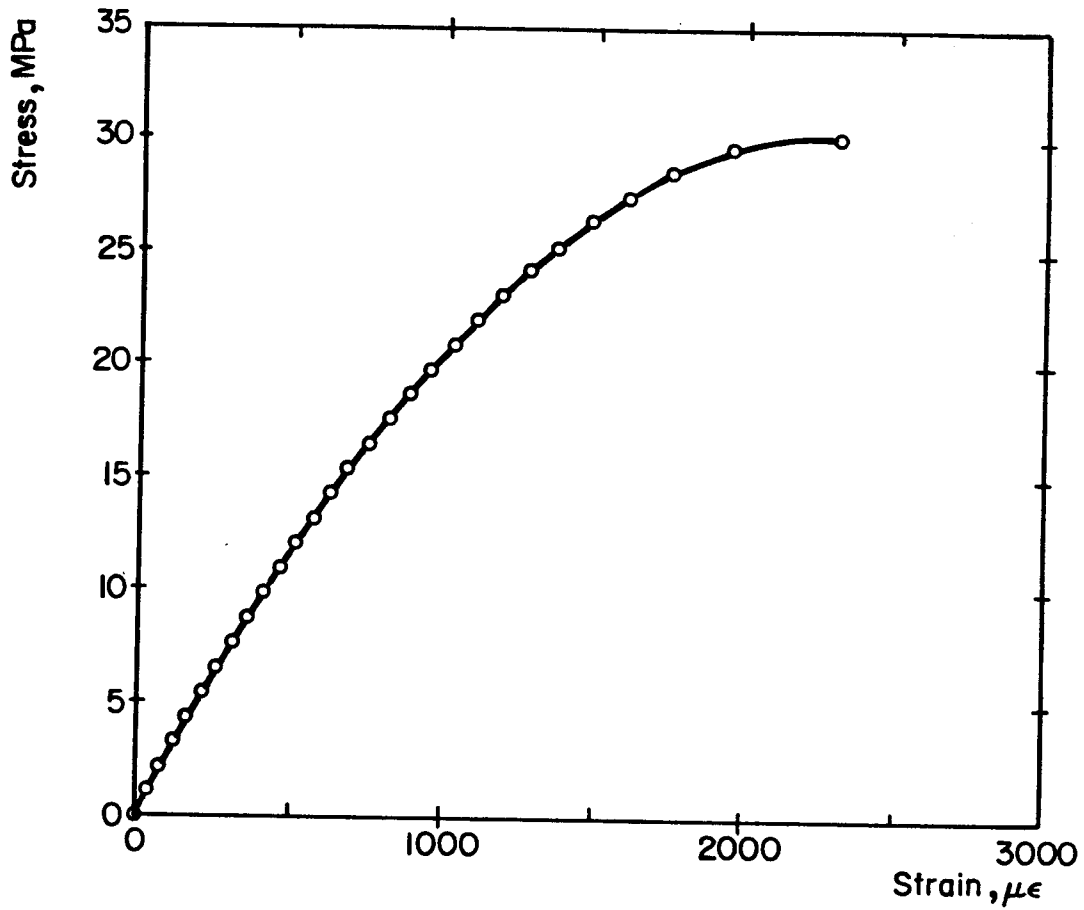


Figure 6.9 Typical stress-strain curve for concrete in compression - truss 1

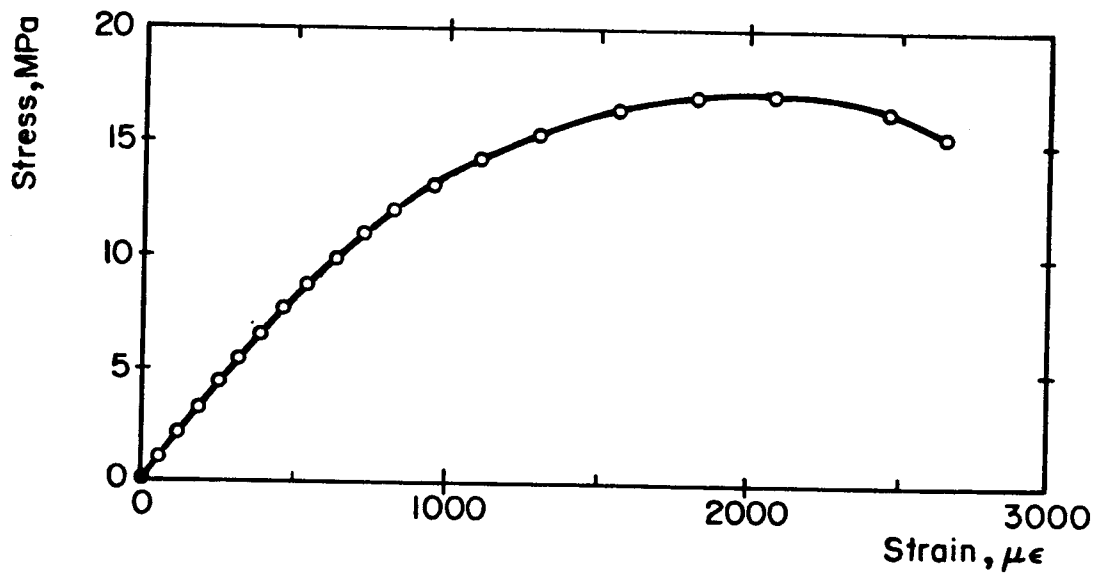


Figure 6.10 Typical stress-strain curve for concrete in compression - truss 2

Clause 9.5.2.3 of CSA Standard CAN3 A23.3-M84 (CSA, 1984b). The splitting tensile strength was 67% of the modulus of rupture, within the range of 50 to 75% observed by Park and Paulay(1975).

Two cylinders representative of the concrete of composite truss 2 had splitting tensile strengths of 1.4 and 1.7 MPa when tested at 118 days. Both flexure tests carried out at the same time had moduli of rupture of 3.5 MPa, about 1.42 times the calculated value of $0.6\sqrt{f'_c}$. The average splitting tensile strength was 43% of the modulus of rupture.

6.3 Nelson Studs

6.3.1 Push-out Tests

Push-out test specimens with a configuration as shown in Fig. 6.11 were constructed to determine the shear capacity of the 16 mm diameter Nelson studs by test. Two specimens without slab reinforcement were cast with truss 1, and one specimen containing a double layer of 152 x 152 MW9.1 x MW9.1 welded wire mesh was cast with truss 2.

To test, each specimen was carefully aligned in an MTS testing machine, with the slabs plastered to the bottom platten of the MTS and the top platten bearing on the milled end of the HSS section. The movement or slip between the concrete and steel during each test was measured at three locations, shown in Fig. 6.11, with dial gauges reading to

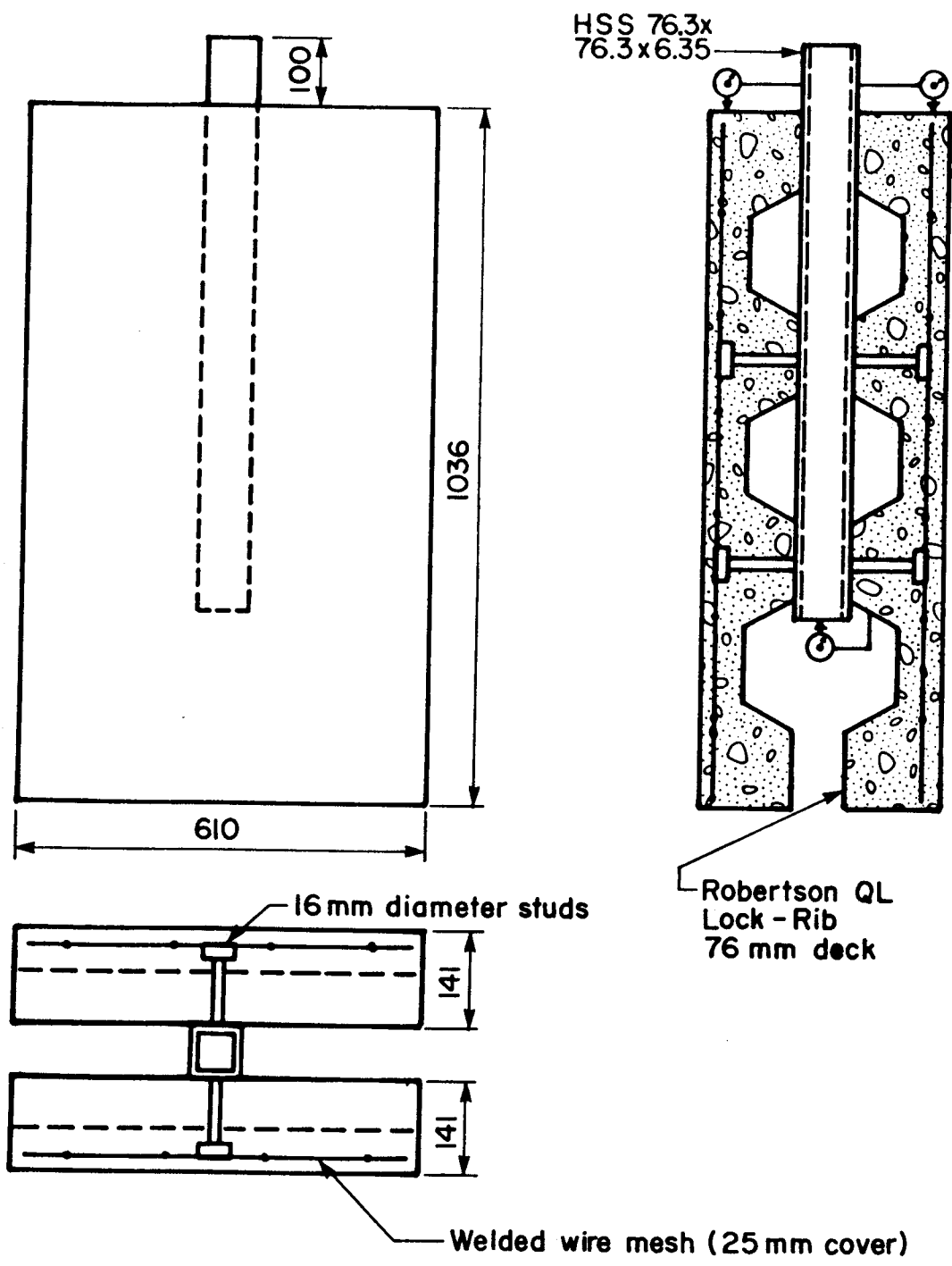


Figure 6.11 Push-out test specimen

0.01 mm. The two specimens associated with truss 1 were tested at 99 days, and the specimen associated with truss 2 was tested at 132 days.

6.3.2 Test Results

The two push-out test specimens cast with truss 1 displayed remarkably similar behaviour, with maximum loads of 270 and 271 kN, corresponding to an average shear per stud of 67.6 kN. This value is lower than the value of 78.6 kN predicted by Equation [3.6] with $\phi_{sc} = 1.0$, probably because the slabs contained no reinforcement. When the maximum load was reached, the deck tended to separate from the HSS at the lower end, where tensile forces are developed as part of the couple counteracting the couple formed in each half of the specimen by the non-colinear vertical loads in the concrete slab and in the HSS. The concrete in the bottom flute failed in tension.

The push-out test specimen cast with truss 2 failed at a maximum load of 258 kN, corresponding to a shear per stud of 64.5 kN, higher than the predicted (unfactored) value of 52.8 kN from Equation [3.6]. Near the maximum load, cracks were observed on the sides of the slab, extending from the top corner of the top flute into the cover slab and from the cover slab in towards the bottom corner of the top flute. After the maximum load was reached, the deck began to separate from the concrete slab. Two of the studs failed in shear, while the other two pulled out of the HSS section.

The load-slip behaviour of this specimen is plotted in Fig. 6.12.

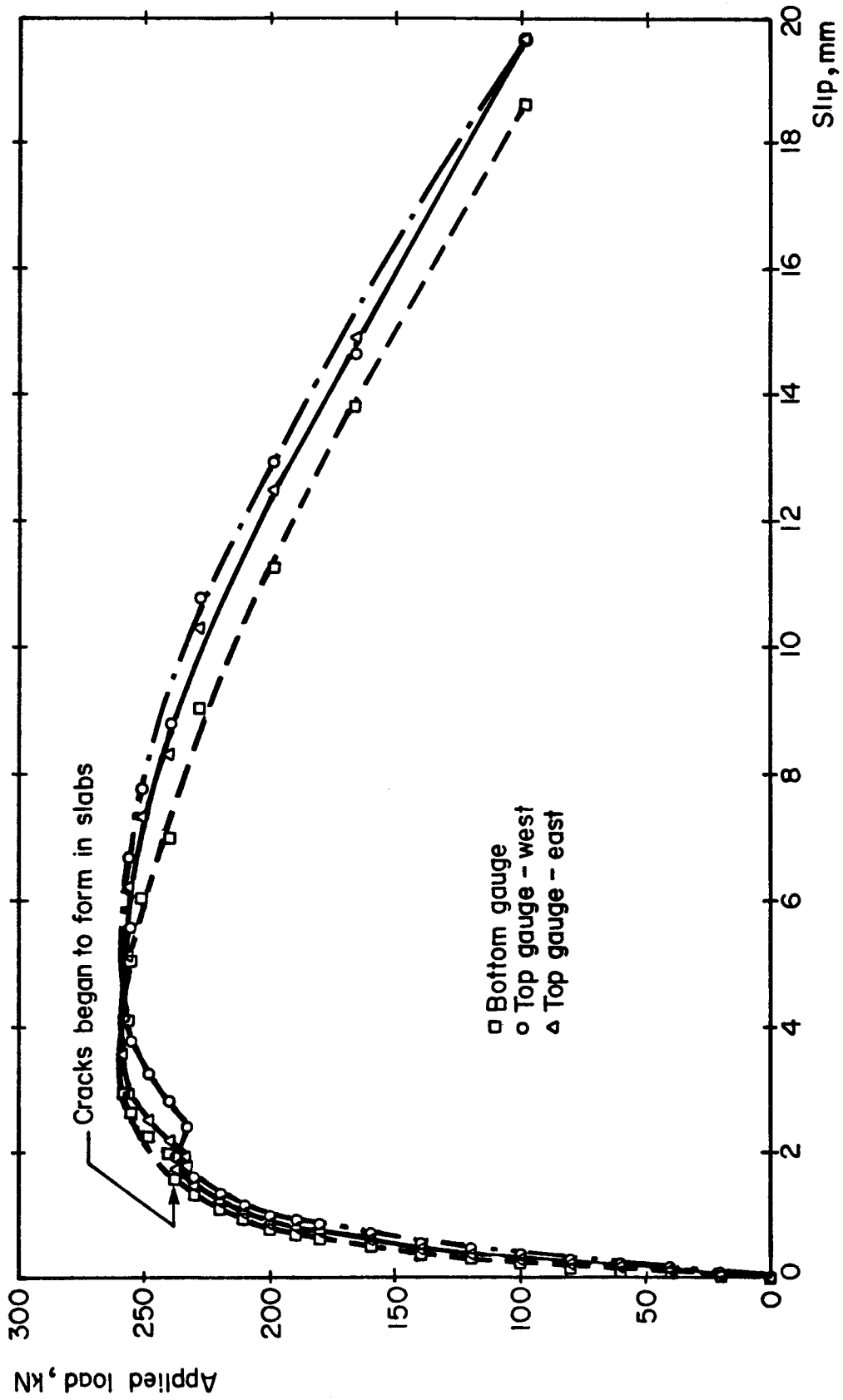


Figure 6.12 Load-slip curve for push-out test - truss 2

7. SHRINKAGE TEST RESULTS

Shrinkage observations on composite truss 1 were made over a period of 65 days from April 22 to June 26, 1985. The shrinkage control specimens associated with this test were monitored for an additional 20 days. Shrinkage measurements were taken on composite truss 2 and its control specimens from September 25 to December 19, 1985, a period of 85 days.

7.1 Deflections

The midspan, north quarter point, and south quarter point deflections of truss 1 due to slab shrinkage are plotted versus time in Fig. 7.1. This figure shows that only 0.8 mm of midspan deflection occurred before the polyethylene sheets that covered the slab during the initial curing period were removed at 6.8 days. The deflections then increased, first rapidly and then at a continuously decreasing rate, until the rate of increase became very small. Seventy-seven percent of the 65 day deflection occurred in the first 30 days or 46% of the shrinkage interval. In the last 15 days, 23% of the shrinkage interval, only 7% of the deflection occurred. At 65 days, the midspan deflection was 8.9 mm or 1/1300 of the span, and the average quarter point deflection was 6.2 mm. The scatter in the observations is attributed to variations of the temperature and relative humidity in the lab during the test period. The temperature, plotted versus time in Fig. 7.2, ranged randomly from 19° to 27° C, while the humidity,

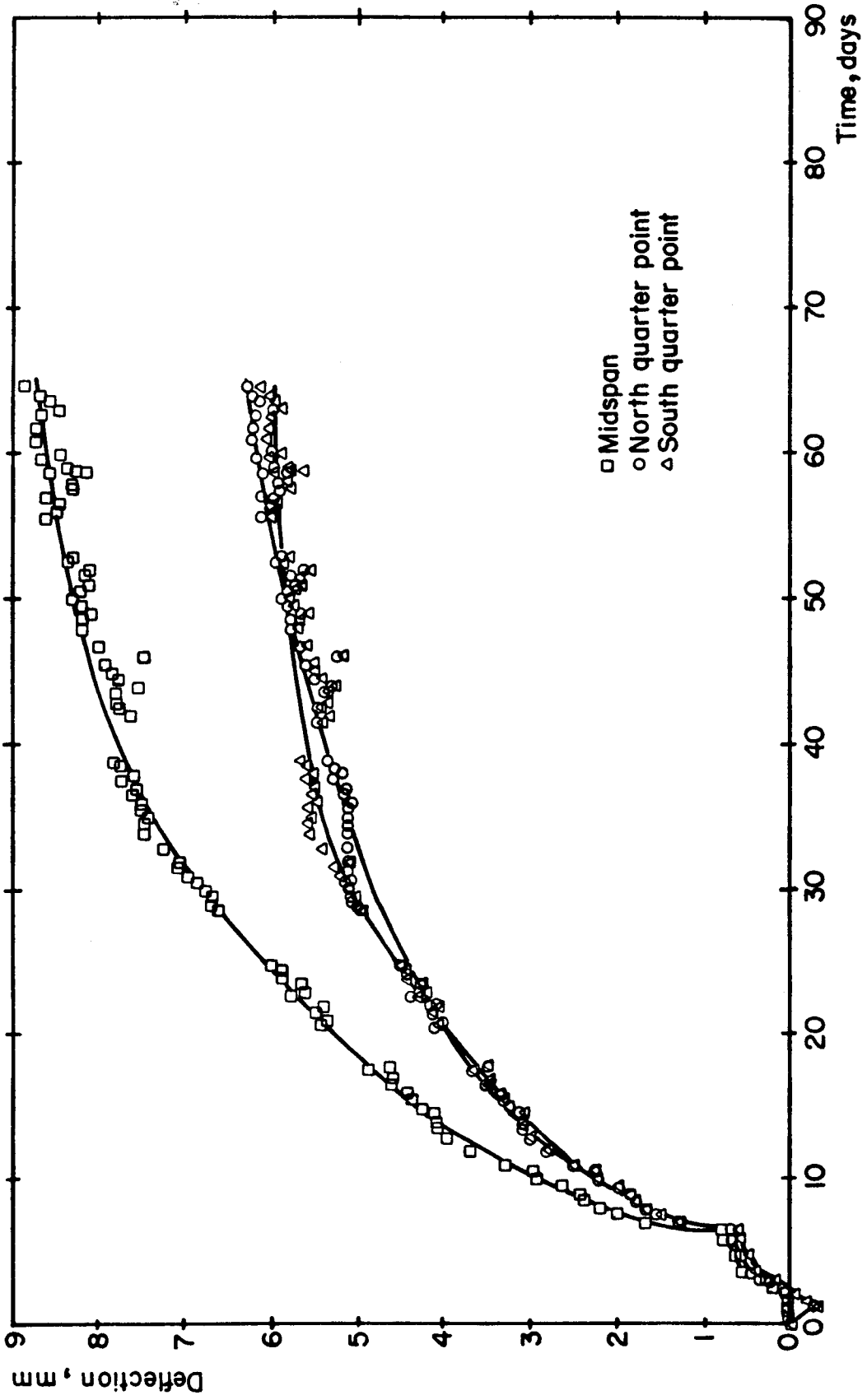


Figure 7.1 Shrinkage deflection of composite truss 1

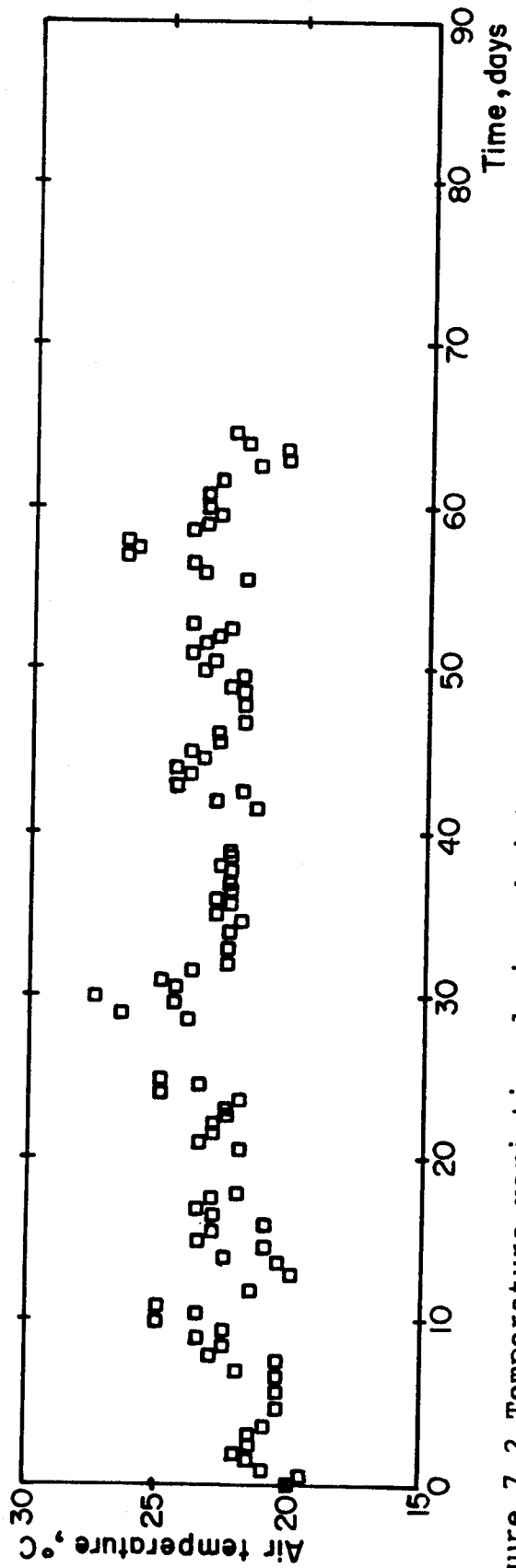


Figure 7.2 Temperature variation during shrinkage interval for truss 1

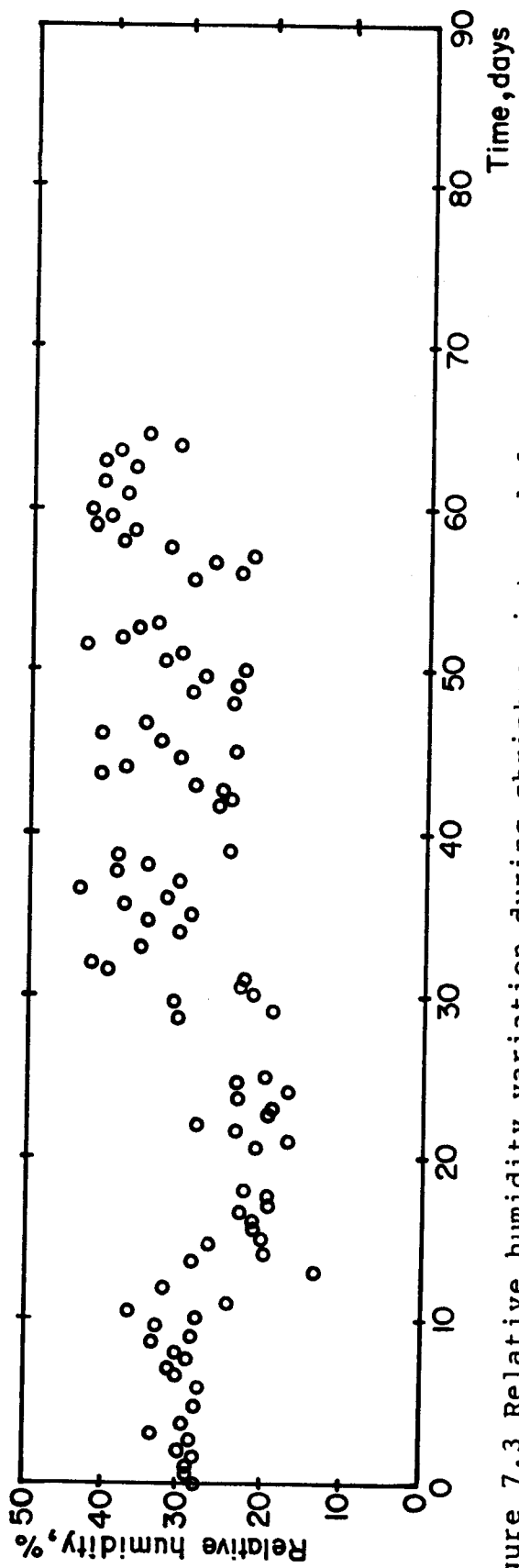


Figure 7.3 Relative humidity variation during shrinkage interval for truss 1

plotted in Fig. 7.3, ranged from 13 to 44%.

Figure 7.4 shows the development of midspan, north quarter point, and south quarter point deflections of truss 2 over time, due to slab shrinkage. Only 0.5 mm of deflection had occurred at midspan when the polyethylene sheets covering the slab were removed at 7.1 days. The initial rate of increase of deflection was not as large as that of truss 1, and did not decrease as quickly. In the first 30 days of the test, 35% of the 85 day shrinkage interval, the deflection reached 67% of the 65 day value or 61% of the total deflection at 85 days. In the period from 50 to 65 days, corresponding to the last 15 days of the truss 1 test, 16% of the deflection to 65 days occurred. Eight percent of the total 85 day deflection occurred in the last 20 days, or 24% of the shrinkage interval. The midspan deflection was 6.6 mm at 65 days and 7.2 mm (or 1/1600 of the span) at 85 days, while the corresponding values for the average quarter point deflection were 4.9 mm and 5.3 mm. During the 85 day test period, the air temperature in the lab ranged from 18° to 24° C, as shown in Fig. 7.5, and the relative humidity, plotted in Fig. 7.6, varied from 8 to 44%.

7.2 Shrinkage Control Specimens

The unrestrained shrinkage of the four shrinkage control specimens cast with truss 1, which are plotted in Fig. 7.7, developed over time in the same manner as the

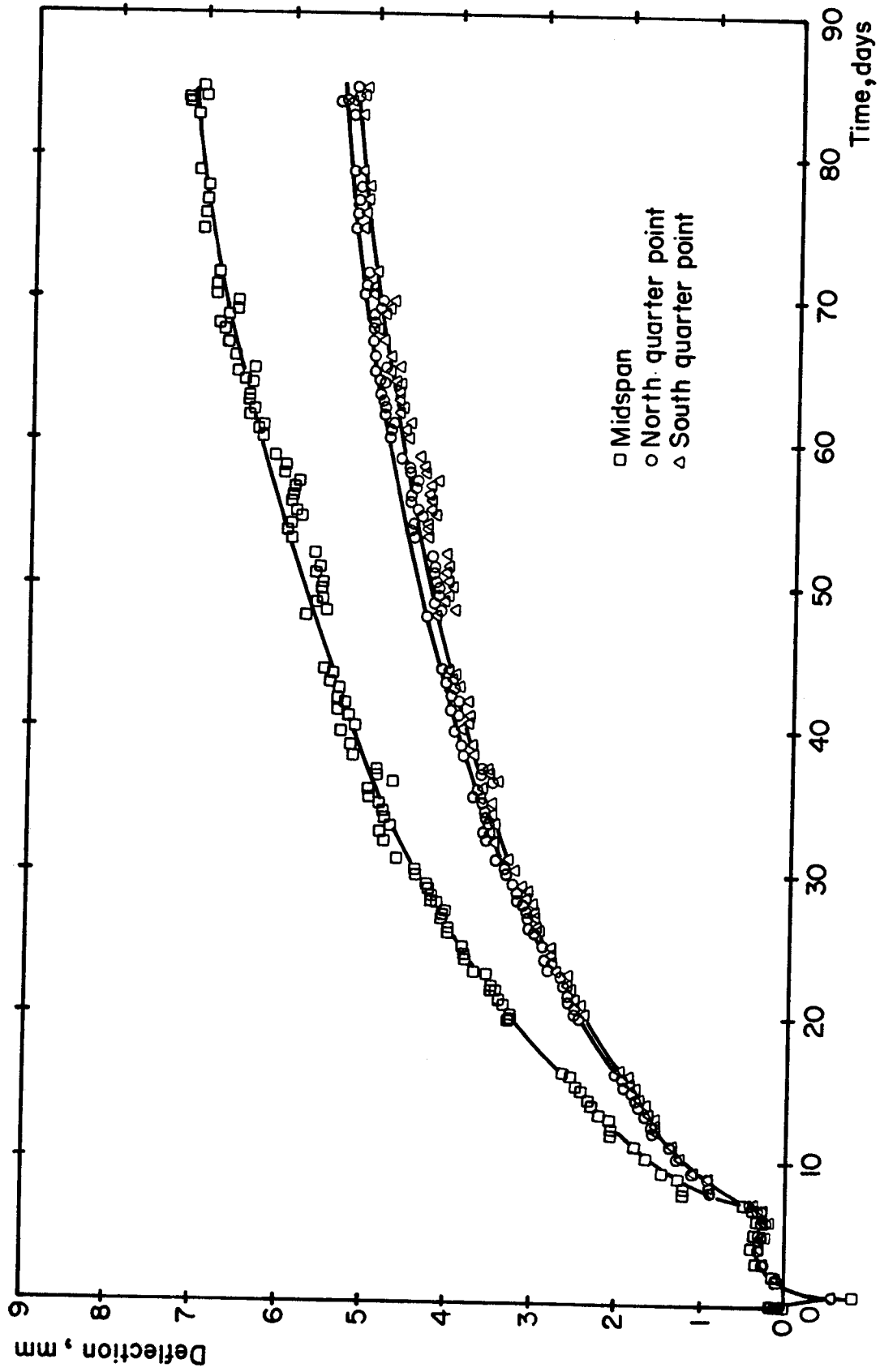


Figure 7.4 Shrinkage deflection of composite truss 2

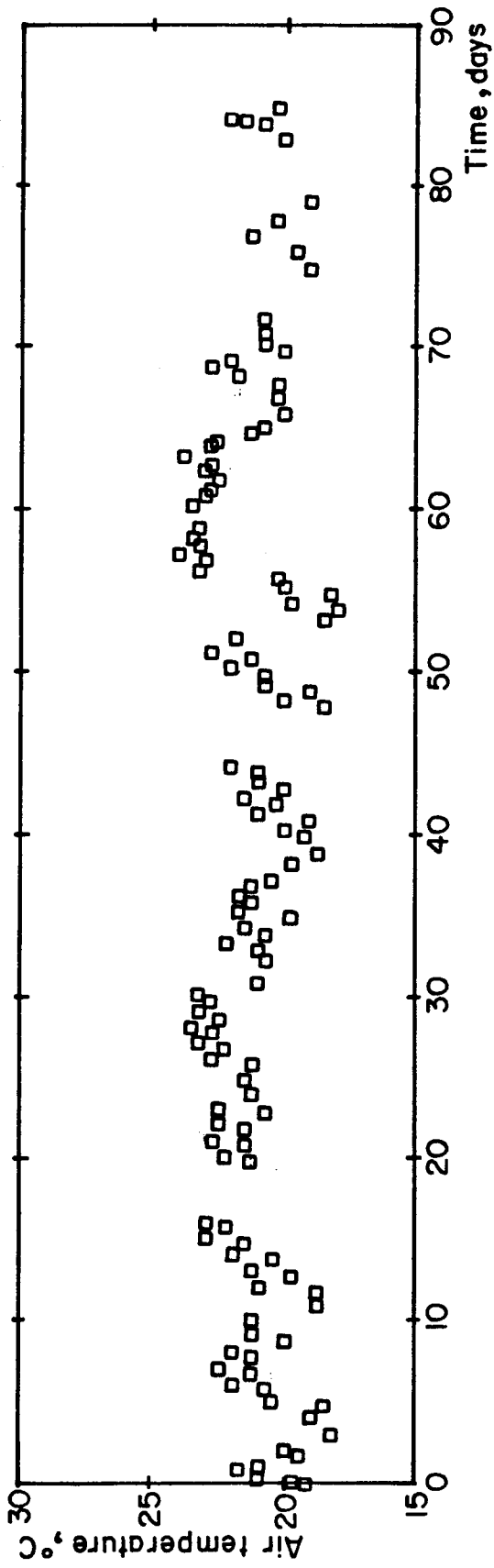


Figure 7.5 Temperature variation during shrinkage interval for truss 2

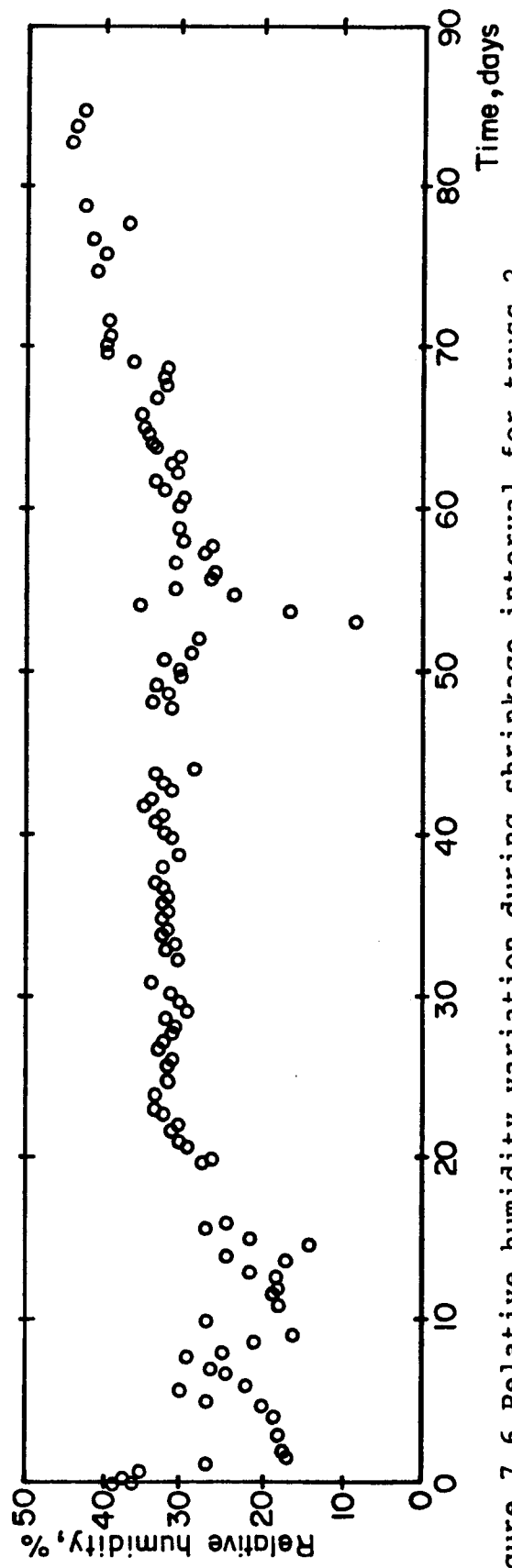


Figure 7.6 Relative humidity variation during shrinkage interval for truss 2

shrinkage deflections—the strains increased rapidly when the polyethylene coverings were removed, then increased at a decreasing rate, gradually approaching a limiting value. At 65 days, the two 65 mm thick specimens had an average free shrinkage strain of $875 \mu\epsilon$, and the two 100 mm thick specimens, with a greater distance for the water to travel to the free surface, had an average free shrinkage strain of $794 \mu\epsilon$. At 85 days, the free shrinkage strain of the 65 mm thick specimens had increased by 1% to $886 \mu\epsilon$, while that for the 100 mm thick specimens had increased by 5% to $834 \mu\epsilon$. At 85 days, the free shrinkage strain of the thicker specimens was 94% of that of the thinner specimens. Eventually, it would be expected that both thicknesses would reach the same limiting free shrinkage strain.

The unrestrained shrinkage of the four shrinkage control specimens cast with truss 2 are plotted versus time in Fig. 7.8. Throughout the 85 day shrinkage period, these strains were lower than those of truss 1. Although the same mix design was specified for both batches of concrete, the concrete for truss 2 was considerably weaker, as discussed in Section 6.2.3. The behaviour of one of the 65 mm thick specimens, whose shrinkage stopped abruptly at about 20 days and increased only minimally over the remaining time interval, was unusual and remains unexplained. The average free shrinkage strain of the 65 mm thick specimens was $692 \mu\epsilon$ at 65 days, while that of the 100 mm thick specimens was $646 \mu\epsilon$, about 93% of the free shrinkage strain of the

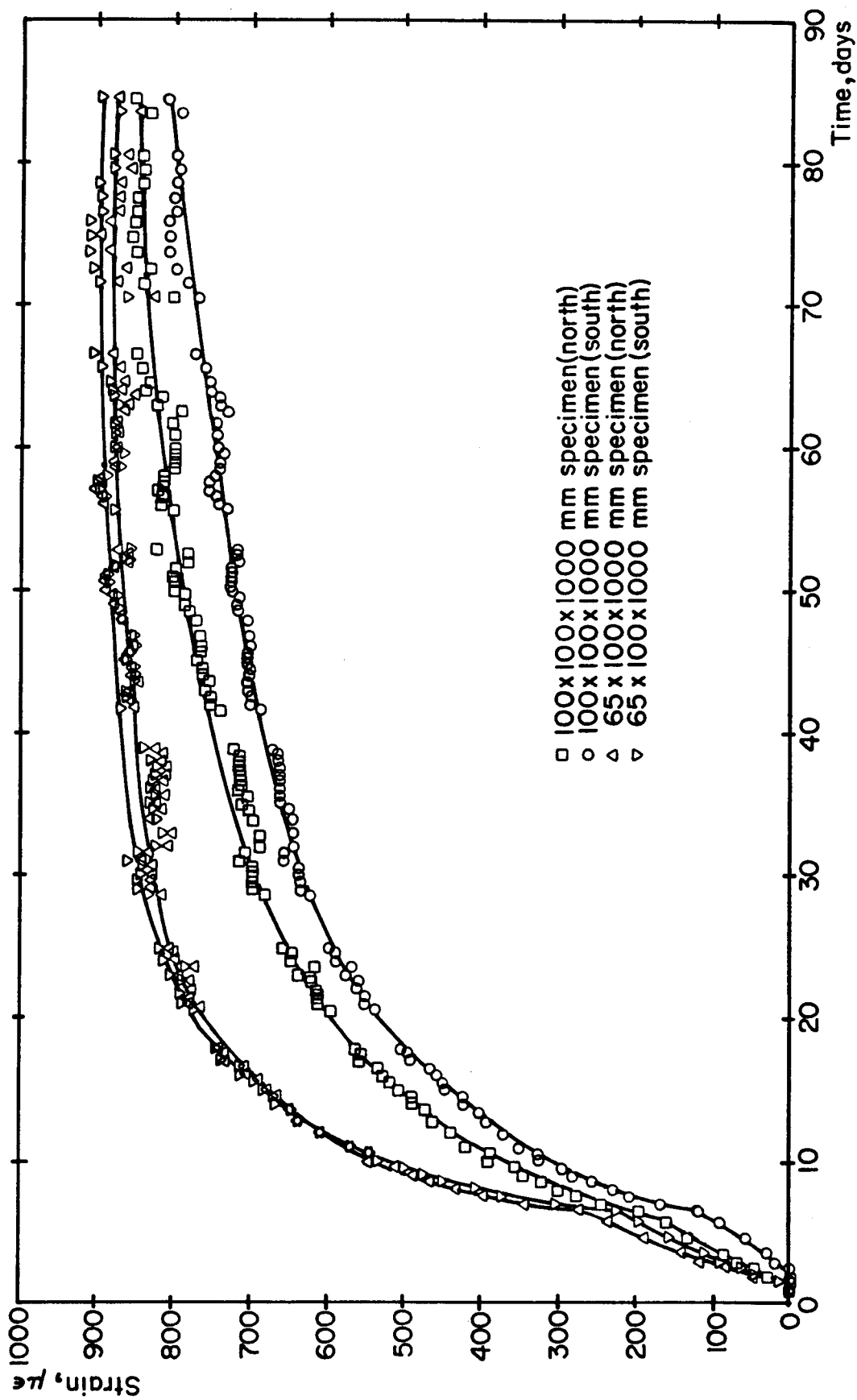


Figure 7.7 Unrestrained shrinkage strain - truss 1

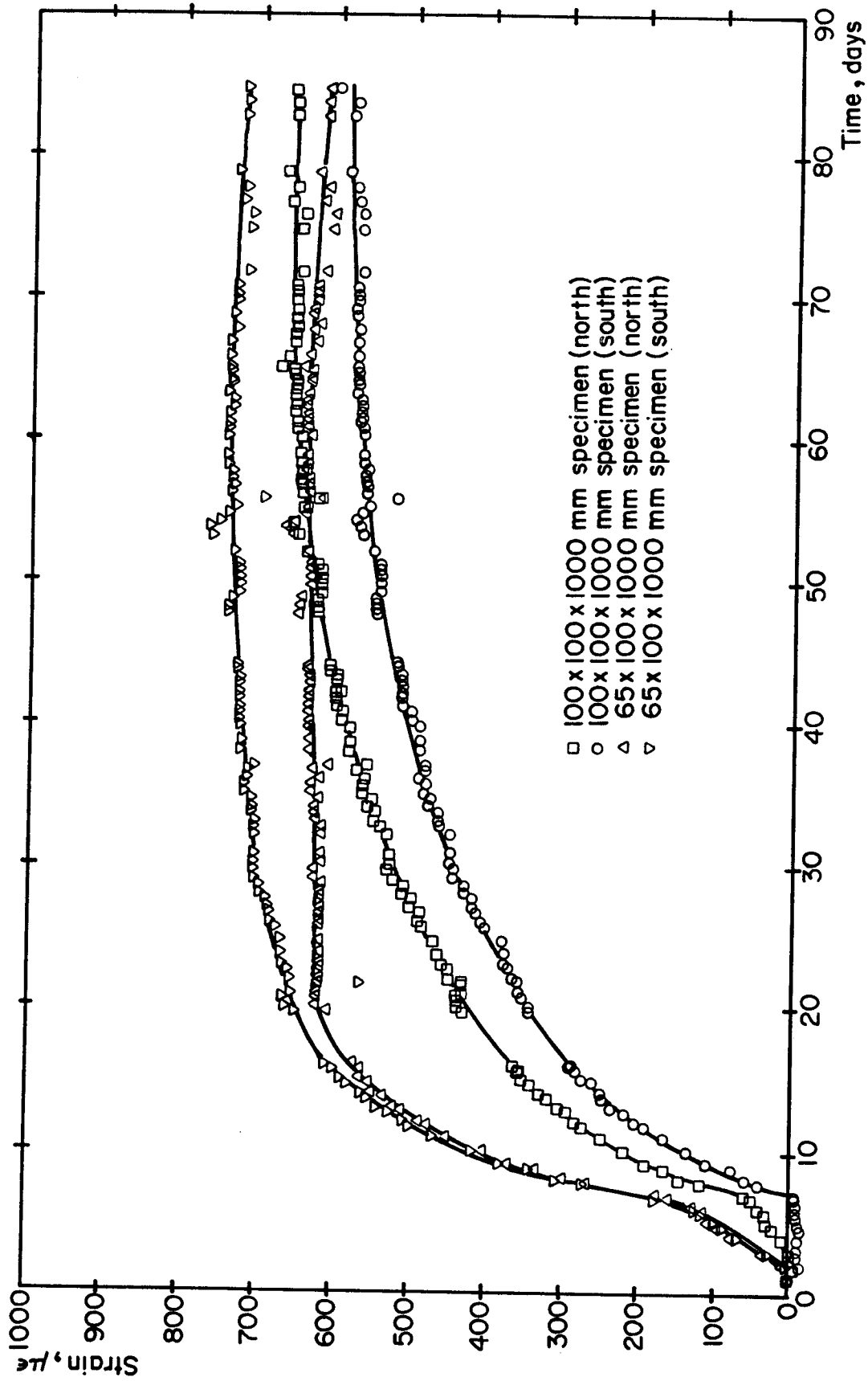


Figure 7.8 Unrestrained shrinkage strain - truss 2

thinner specimens. Between 65 and 85 days, the free shrinkage strain of the 65 mm thick specimens decreased by about $22 \mu\epsilon$ to $670 \mu\epsilon$, probably related to a general increase in the lab humidity. The free shrinkage strain of the 100 mm thick specimens increased by less than 1% in the last 20 days to a value of $650 \mu\epsilon$ at 85 days. It is postulated that this is the net effect of the water loss and the increase in the ambient relative humidity.

7.3 Slab Shrinkage

Figures 7.9 and 7.10 show average and local slab strains plotted versus time for trusses 1 and 2 respectively. The overall average longitudinal and transverse shrinkage of each slab was measured using dial gauge-rod assemblies supported over the slab surface. Local strains were measured on transverse lines from Demec points. All of the curves exhibit the same general time dependent shrinkage behaviour as the concrete control specimens. In the first days after each slab was cast, small increases in length were observed in the overall slab dimensions and locally at Demec point locations. This is attributed to an expansion of the concrete volume caused by the higher temperatures generated during the curing process.

7.3.1 Average Overall Shrinkage

On truss 1, the two measurements of the longitudinal slab shrinkage differed throughout the time interval by

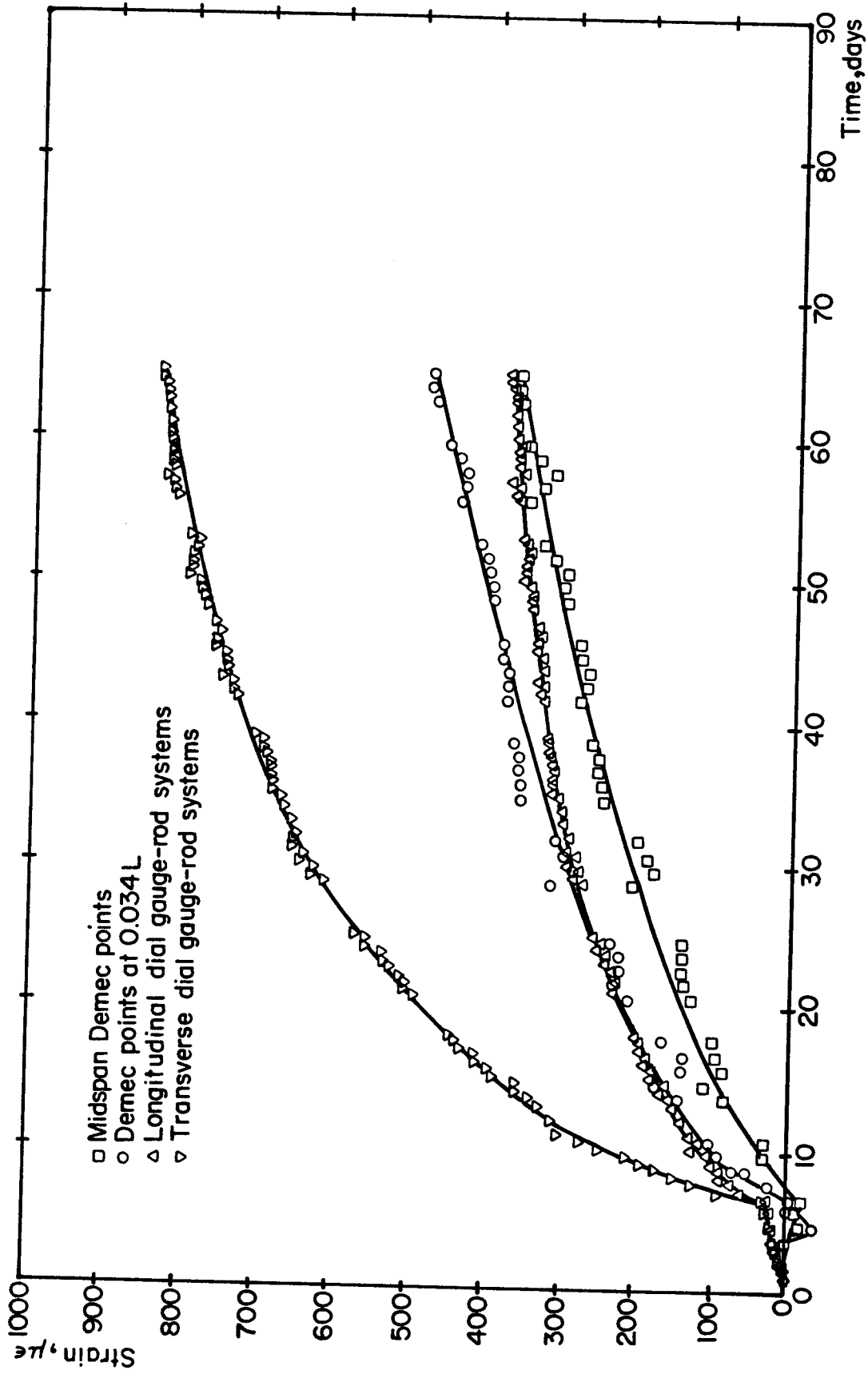


Figure 7.9 Slab shrinkage - truss 1

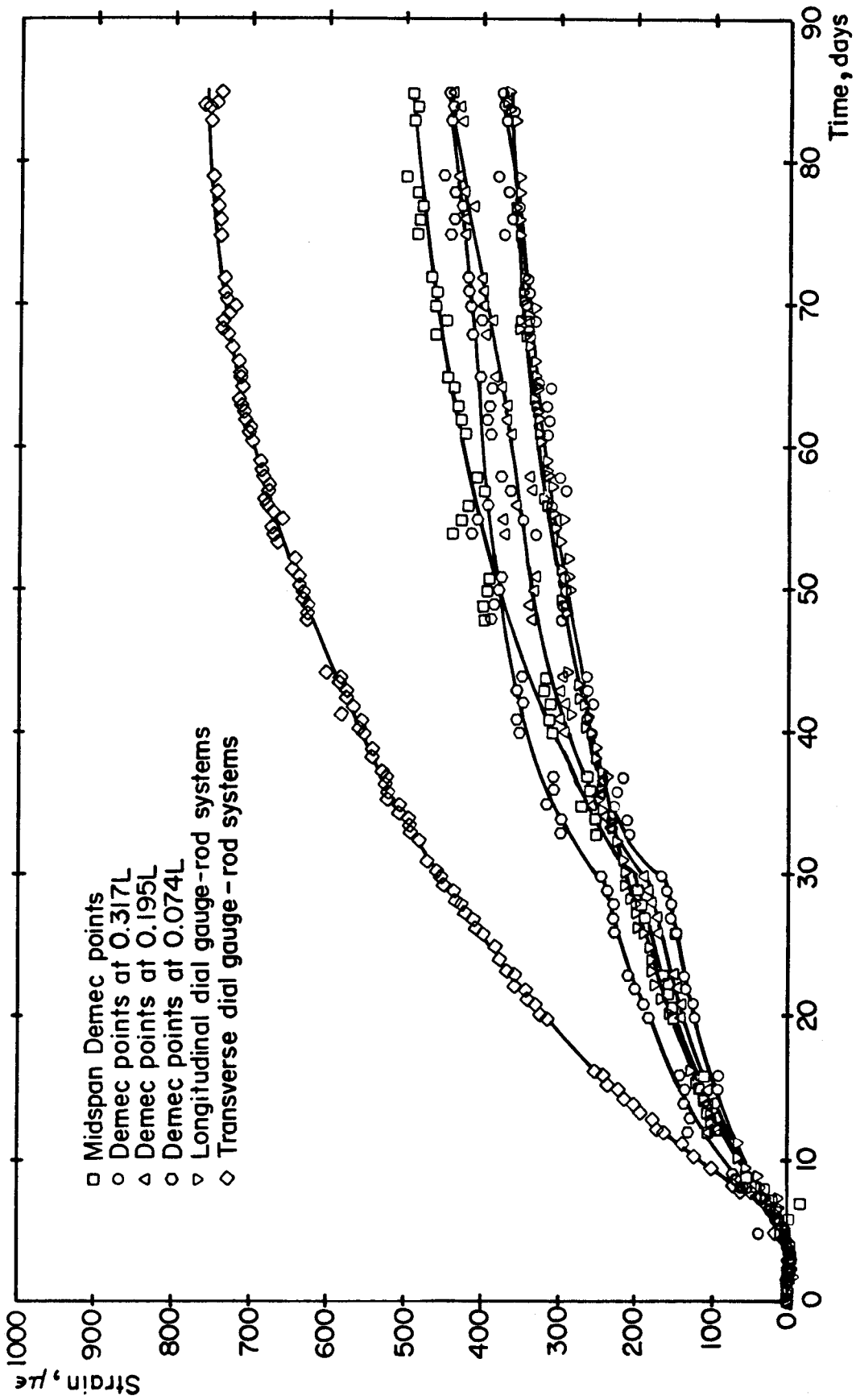


Figure 7.10 Slab shrinkage - truss 2

about 30%, for no apparent reason. At 65 days, the average longitudinal shrinkage measured 54 mm above the slab was 4.43 mm in 11 582 mm, or $382 \mu\epsilon$. Correcting this strain to the surface of the slab, based on a radius of curvature corresponding to the midspan deflection of 8.9 mm, gives an overall average shrinkage strain at the slab surface of $382 - 29 = 353 \mu\epsilon$, 42% of the average free strain of the control specimens. In the transverse direction, where minimal restraint is provided to the slab by the deck, the shrinkage was 1.81 mm in 2166 mm, or $837 \pm 9 \mu\epsilon$, at 65 days. (This might appear to imply that little or no bond exists between the deck and the slab and therefore that the deck could not be considered to provide reinforcement to the slab when the concrete acts flexurally to carry loads to parallel trusses. It should be noted that, because of the very small area-to-bond surface ratio of the deck compared to normal reinforcement, the bond stresses that need to be developed per reinforcement area are also very small. As well, the applied loads acting on the flexural member generate frictional forces between the slab and the deck.)

As for the control specimens, the overall average slab strains of truss 2 were lower than those of truss 1 throughout the time interval. At 65 days, the average longitudinal shrinkage, measured 54 mm above the slab surface, was 3.83 mm in 11 578 mm, or $331 \pm 9 \mu\epsilon$. Using a radius of curvature corresponding to the midspan deflection of 6.6 mm at 65 days, the overall average shrinkage strain

corrected to the slab surface was $331 - 22 = 309 \mu\epsilon$, or 46% of the average free strain of the control specimens. At 85 days, the measured longitudinal shrinkage was 4.30 mm in 11 578 mm or $371 \pm 11 \mu\epsilon$, giving an overall average shrinkage strain corrected to the slab surface of $371 - 24 = 347 \mu\epsilon$, based on a radius of curvature corresponding to the midspan deflection of 7.2 mm at 85 days. This value is 53% of the average free strain of the control specimens. At 65 and 85 days, the shrinkage in the transverse direction was 1.53 and 1.64 mm respectively in a 2148 mm gauge length, corresponding to strains of $714 \pm 4 \mu\epsilon$ and $762 \pm 1 \mu\epsilon$.

7.3.2 Local Slab Strains

The variation of strain across the width of the slab on each transverse line of Demec points did not exhibit any pattern, but rather was random in nature, indicating that shrinkage strain across the width could be considered to be uniform. Therefore, the curves in Figs. 7.9 and 7.10, showing the development of local shrinkage strains at 2 locations on the slab of truss 1 and 4 locations on the slab of truss 2, were obtained by averaging the strains measured on each transverse line of Demec points, after Chauvenet's Criterion had been applied for the rejection of outliers.

Because the Demec points on the slab of truss 1 had to be reapplied at 4 days, an adjustment was made to this strain data to account for strains occurring in the time period from 1 to 4 days. A value of $17 \mu\epsilon$, equal to the

overall average longitudinal shrinkage strain in the slab between 1 and 4 days, was added to the strain at each Demec point location measured from 4 to 65 days. This adjustment is strictly correct only for the midspan strains, where the restrained shrinkage strain is very close to the average strain. Close to the ends of the slab, the strain between 1 and 4 days could be somewhat larger. However, remembering that the Demec gauge sensitivity is about $10 \mu\epsilon$, the value of $17 \mu\epsilon$ was considered satisfactory. At midspan on the slab of truss 1, the shrinkage strain at 65 days, from six of the seven sets of Demec points on that transverse line, was $385 \mu\epsilon$. This local strain is about $32 \mu\epsilon$ more than the overall average shrinkage strain for the same time period, corrected to the slab surface, of $353 \mu\epsilon$. The variation of strain across the width at midspan was random and, with one exception, did not exceed $\pm 6\%$. One set of Demec points indicated shrinkage strains of 80% of the other six, possibly indicative of a local anomaly in the concrete. This data set was rejected as an outlier, based on Chauvenet's Criterion. The shrinkage strain at $0.034L$ on the slab of truss 1 was obtained from Demec points on 2 transverse lines 400 mm from the ends of the slab, excluding one set of Demec points in the north-east corner, which appeared to be an outlier. At 65 days, the measured shrinkage was $502 \mu\epsilon$, less than the free shrinkage strain and about 1.3 times the shrinkage strain at midspan. This indicates that the shrinkage only 400 mm from the ends is approaching the

restrained shrinkage at midspan.

Unlike the comparison of concrete control specimen test results, local shrinkage strains on the slab of truss 2 were as large as or larger than those of truss 1. This is attributed to cracking of the slab of truss 2, which is discussed subsequently. Fluctuations in the strain, measured at each Demec point location on the slab of truss 2, were observed between about 50 and 60 days, as shown in Fig. 7.10. These are directly related to temperature and humidity fluctuations in the lab at that time. Smooth curves have been drawn through the data. At 65 days, the shrinkage strains (measured from 5 Demec points each) at 0.195L, 0.317L, and 0.500L were 328, 381, and 445 $\mu\epsilon$ respectively. The average variation of strain across the width at these locations was 17%. The shrinkage strain at 0.074L, from 6 measurements on 2 transverse lines, was 404 $\mu\epsilon$ over the same time period. The overall average longitudinal shrinkage, corrected to the slab surface, over this time period was 309 $\mu\epsilon$. At 85 days, the shrinkage strains at 0.074L, 0.195L, 0.317L, and 0.500L increased to 445, 373, 439, and 491 $\mu\epsilon$, compared to the overall average longitudinal shrinkage, corrected to the slab surface, of 347 $\mu\epsilon$.

7.3.3 Shrinkage Cracks

Only one shrinkage crack developed in the slab on truss 1 during the 65 day period that shrinkage was monitored. It was observed around day 56 of the test, extending across the

width of the slab approximately 1700 mm south of midspan.

Cracking in the slab of truss 2 during its 85 day shrinkage test was more pronounced, probably due to its lower concrete strength. Transverse shrinkage cracks were first observed in the slab on truss 2 at 34 days. Additional cracks developed at 40 days and at 48 days. The locations of these shrinkage cracks are shown in Fig. 7.11.

7.4 Steel Strains

Strains in the steel top and bottom chords of each truss due to shrinkage of the concrete slab, plotted in Figs. 7.12 to 7.15, developed over time in the same manner as shrinkage deflections and concrete strains—increasing rapidly at first, then increasing at a decreasing rate and gradually approaching a limiting value. The overall compression of the top chord and elongation of the bottom chord were measured by dial gauge-rod assemblies suspended below each chord. Strain gauges positioned in pairs along the length of the chords measured local strains. The steel strains showed considerably greater diurnal variations than did the concrete. This suggests that the variation is chiefly due to temperature fluctuations. Changes in humidity would not affect the length of the steel members but they would respond rapidly to temperature changes because of the high thermal conductivity of the steel. Smooth curves were drawn through the data points to average these diurnal variations.

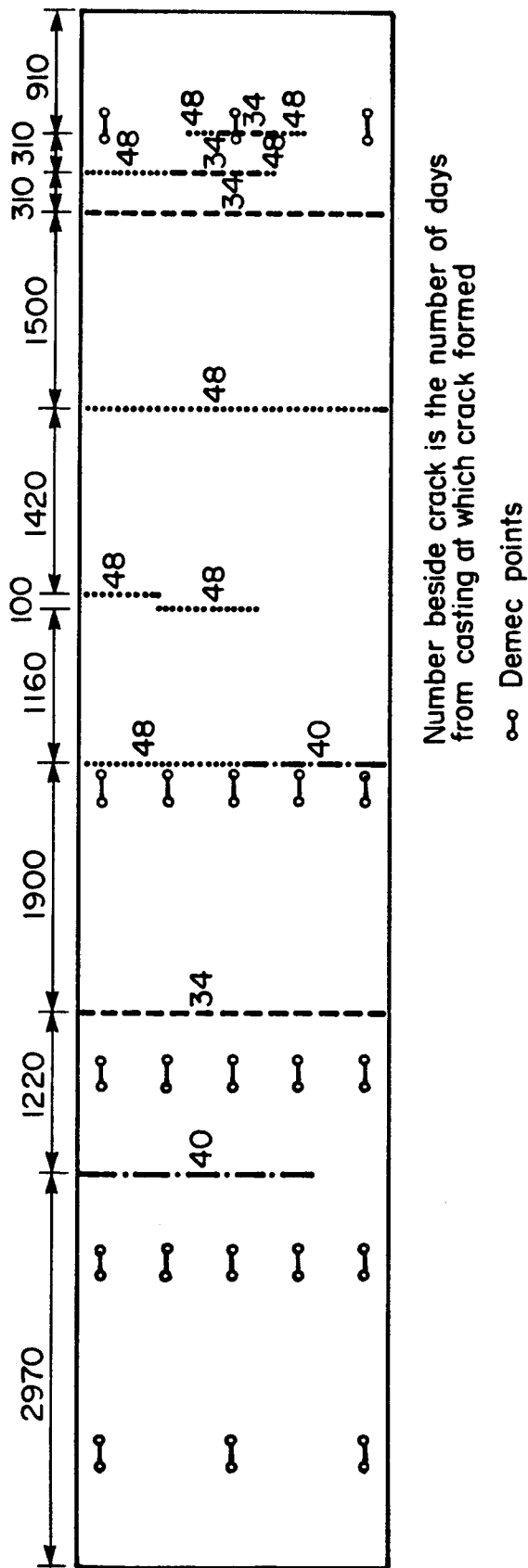


Figure 7.11 Shrinkage cracks in concrete slab - truss 2

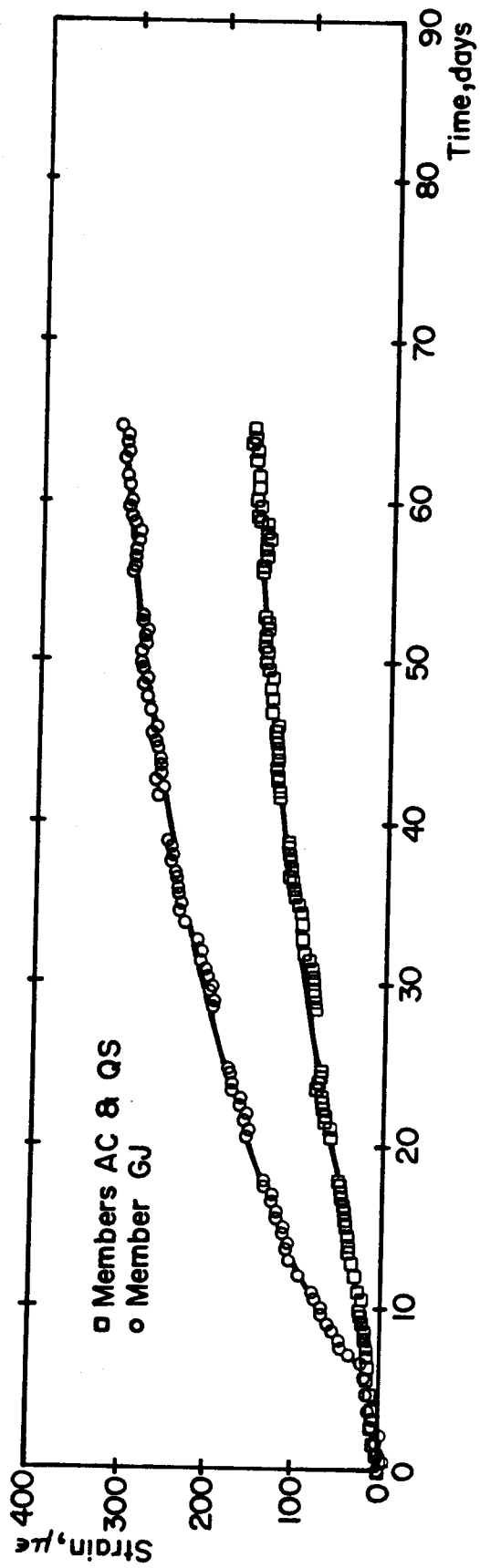


Figure 7.12 Top chord strain due to shrinkage - truss 1

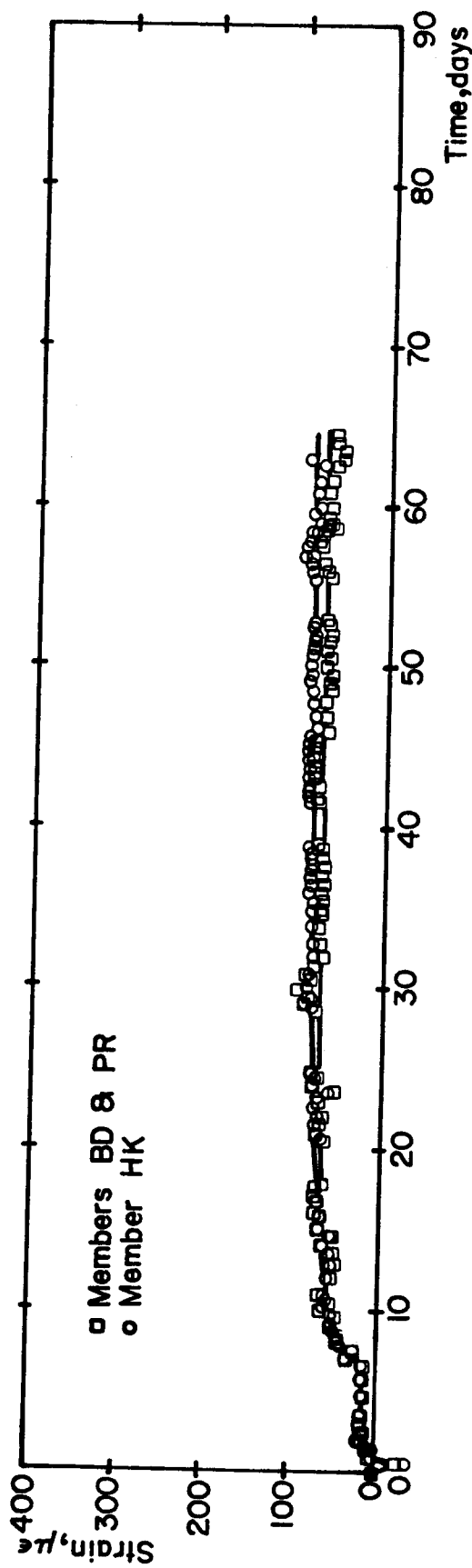


Figure 7.13 Bottom chord strain due to shrinkage - truss 1

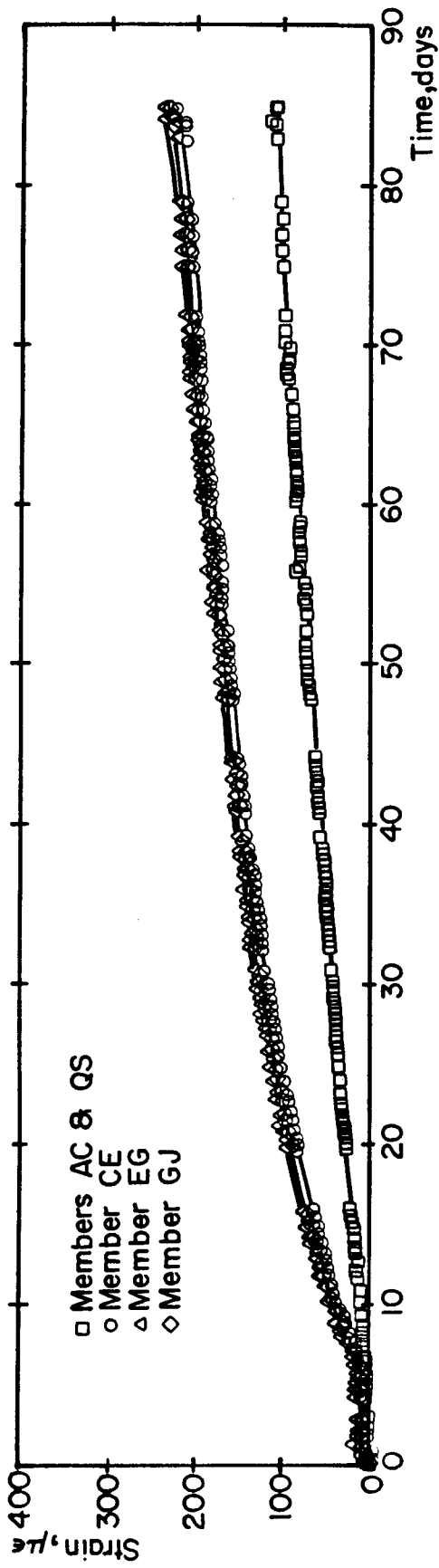


Figure 7.14 Top chord strain due to shrinkage - truss 2

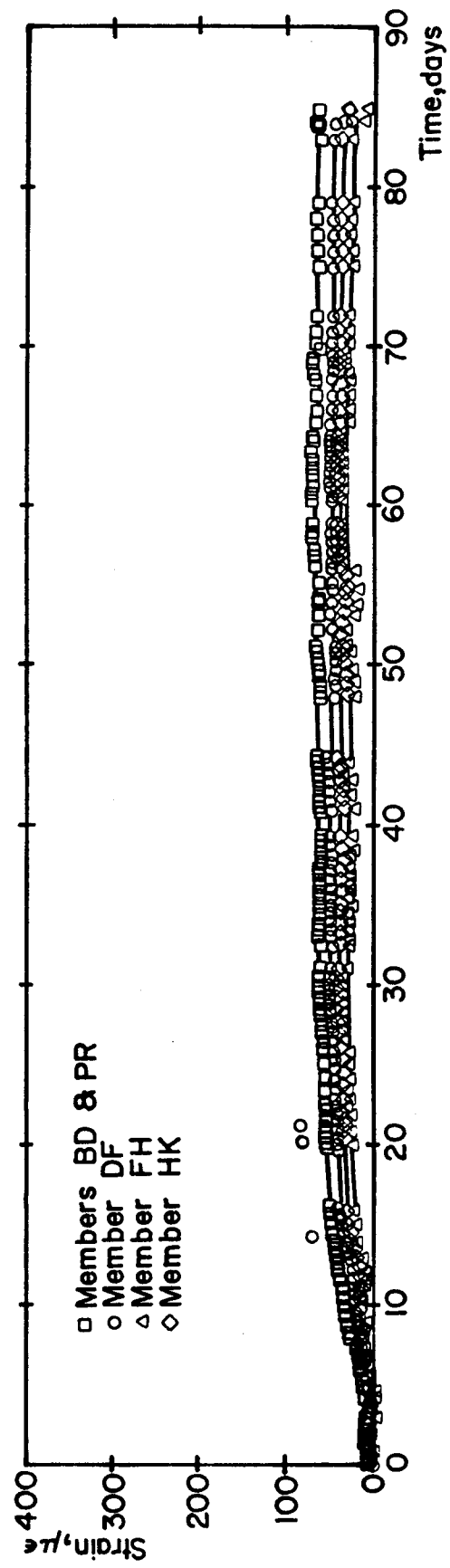


Figure 7.15 Bottom chord strain due to shrinkage - truss 2

7.4.1 Average Chord Strains

The average shortening of the top chord of truss 1 at 65 days, measured 63 mm below its mid-depth, was 2.12 mm in 11 590 mm or 183 $\mu\epsilon$. The bottom chord elongation was 1.13 mm over a length of 10 155 mm at 65 days, resulting in a strain of 111 $\mu\epsilon$ measured 89 mm below the mid-depth of the chord.

The overall average steel strains in the chords of truss 2 were lower than those of truss 1. At 65 and 85 days, the shortening of the top chord of truss 2, measured 63 mm below its mid-depth, was 1.67 mm and 1.91 mm respectively over a length of 11 503 mm, corresponding to strains of 145 and 166 $\mu\epsilon$. The rod positioned 88 mm below the mid-depth of the bottom chord measured elongations of the bottom chord at 65 and 85 days of 0.83 mm and 0.88 mm over a length of 10 152 mm. The corresponding strains are 82 and 87 $\mu\epsilon$, respectively.

7.4.2 Local Steel Chord Strains

For truss 1, local top chord strains due to shrinkage of the concrete slab, measured from 2 gauges near midspan and from 4 gauges on the end panels, are plotted in Fig. 7.12. At 65 days, the average compressive strain was 310 $\mu\epsilon$ near midspan and 160 $\mu\epsilon$ in the end panels. The end panel strain was therefore only 52% of that at midspan. On the bottom chord, local strains were also measured from 2 strain gauges at midspan and 4 gauges on the end panels, and are plotted in Fig. 7.13. The bottom chord strains were

relatively small. The average tensile strain was $84 \mu\epsilon$ at midspan and $73 \mu\epsilon$ in the end panels at 65 days. End panel strain was therefore 87% of the midspan strain.

Shrinkage-induced strains at 4 locations on the top chord of truss 2 are plotted in Fig. 7.14, measured from 4 strain gauges on the end panels and from 2 gauges each on the other top chord panels. The compressive strains in the 4 top chord panels, from the end panel to the one closest to midspan, were 90, 191, 202, and $198 \mu\epsilon$ respectively at 65 days and 109, 216, 225, and $225 \mu\epsilon$ respectively at 85 days. Therefore, the end panel strain was only 45% of the midspan strain at 65 days, and 48% of the midspan strain at 85 days. Fig. 7.15 shows the development of strain over time at 4 locations on the bottom chord of truss 2, measured from 4 strain gauges on the end panels and from 2 gauges each at the other locations. At 65 days, the tensile strains in the 4 bottom chord panels, from the end panel to the midspan panel, were 72, 50, 35, and $50 \mu\epsilon$, respectively. These strains decreased slightly after 65 days, for no apparent reason, so that at the same locations at 85 days, the strains were 68, 46, 30, and $44 \mu\epsilon$. In this test, the strain in the end panels was 1.44 and 1.55 times the midspan strain at 65 and 85 days, respectively.

7.4.3 Web Member Strains

Strains in the web members due to shrinkage of the concrete slab were relatively small.

On truss 1, strains were measured on 8 angle web members with 2 strain gauges at mid-height. The tensile strain in web member AB was significantly larger than the strains in the other web members. At 65 days, the average strains in one angle of web members AB, BC, CD, DE, EF, FG, GH, and HJ were +83, -32, -7, +12, +28, +10, -13, and +10 $\mu\epsilon$ respectively.

Web member strains due to shrinkage of the concrete slab were measured only on members BC and DE of truss 2, with 6 gauges at each of 3 levels along the length of each angle. At 65 days, the average compressive strains at the top, middle, and lower level of gauges on one angle of member BC were 28, 32, and 24 $\mu\epsilon$, respectively. At 85 days, the strains at these locations were 32, 31, and 27 $\mu\epsilon$, respectively. On web member DE, strains were tensile, and very small. At 65 days, the average strains at the top, middle, and lower level of gauges were 13, 12, and 12 $\mu\epsilon$ respectively. As for the bottom chord strains, the strains in member DE dropped off slightly after 65 days so that at 85 days, the strains at the same locations were 9, 8, and 11 $\mu\epsilon$ respectively.

7.5 Variation of Strain Through Truss Depth

Strains at midspan, obtained from Demec points and strain gauges, and average strains, obtained from dial gauge-rod assemblies, are plotted in Figs. 7.16 and 7.17 to show the variation of strain through the depth of trusses 1

and 2 due to slab shrinkage. At any level, the horizontal lines with short vertical bars at the ends indicate the range of measurements. Through each set of points, a best fit straight line has been drawn.

The average and midspan strain distribution with depth is plotted for truss 1 at 65 days in Fig. 7.16. These best fit straight lines have correlation coefficients of 0.995 and 0.998 respectively. The curvatures corresponding to these straight line strain distributions are 0.595×10^{-6} for the midspan strain measurements and 0.509×10^{-6} for the average strains. As full restraint to shrinkage and corresponding reactive strains in the steel chords are not developed for some distance from the ends of the truss, the average curvature would be expected to be less than that at midspan.

Fig. 7.17 shows the average and midspan strain distributions with depth for truss 2 at 85 days. The correlation coefficients for these best fit straight lines are 0.989 and 0.953 respectively. (The correlation coefficient for the midspan strain line has a lower value than that of truss 1 because the value of the concrete strains were affected by the proximity of a shrinkage crack.) The curvatures corresponding to these straight line strain distributions are 0.602×10^{-6} for the midspan strain measurements and 0.463×10^{-6} for the average strains.

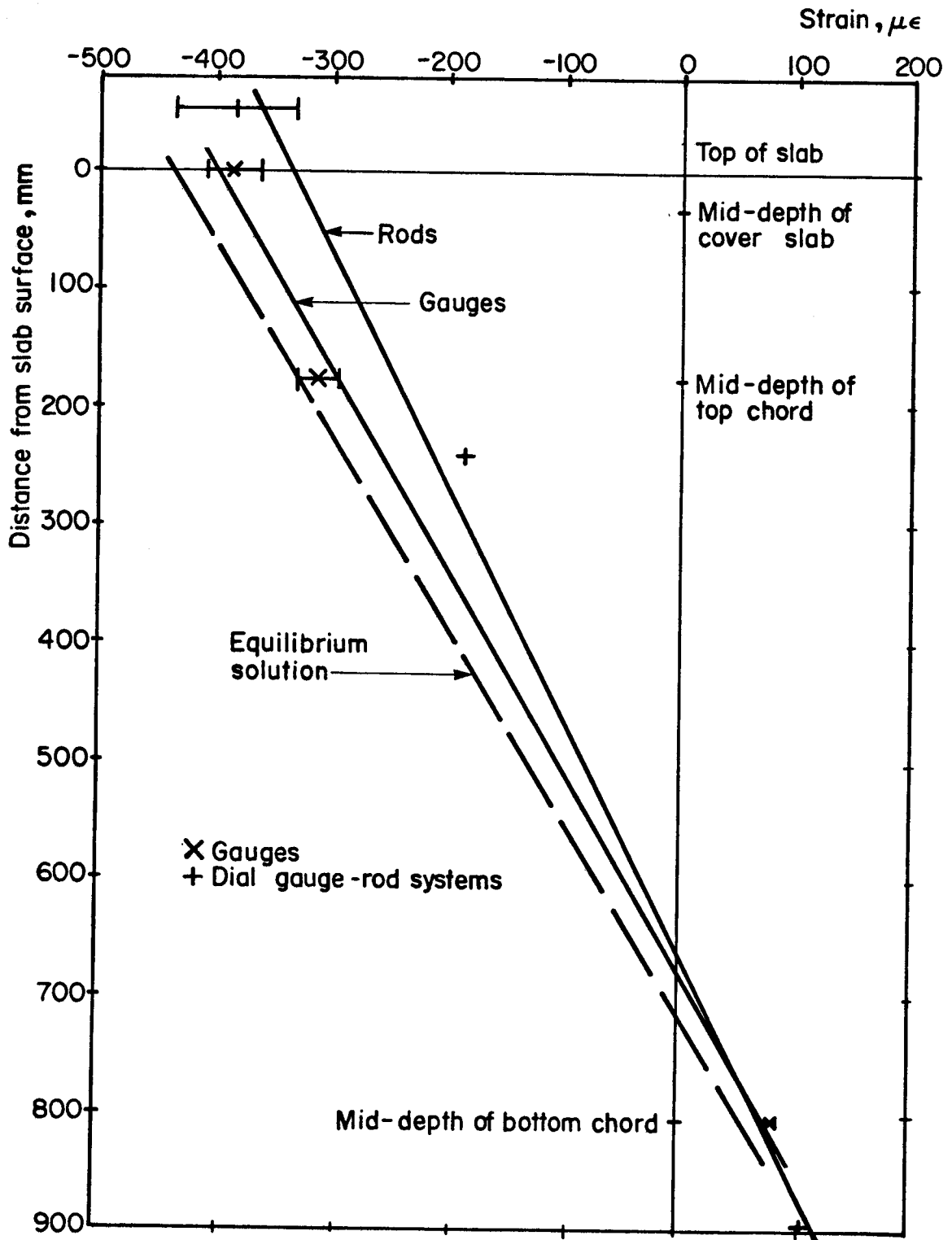


Figure 7.16 Strain variation with depth due to shrinkage - truss 1

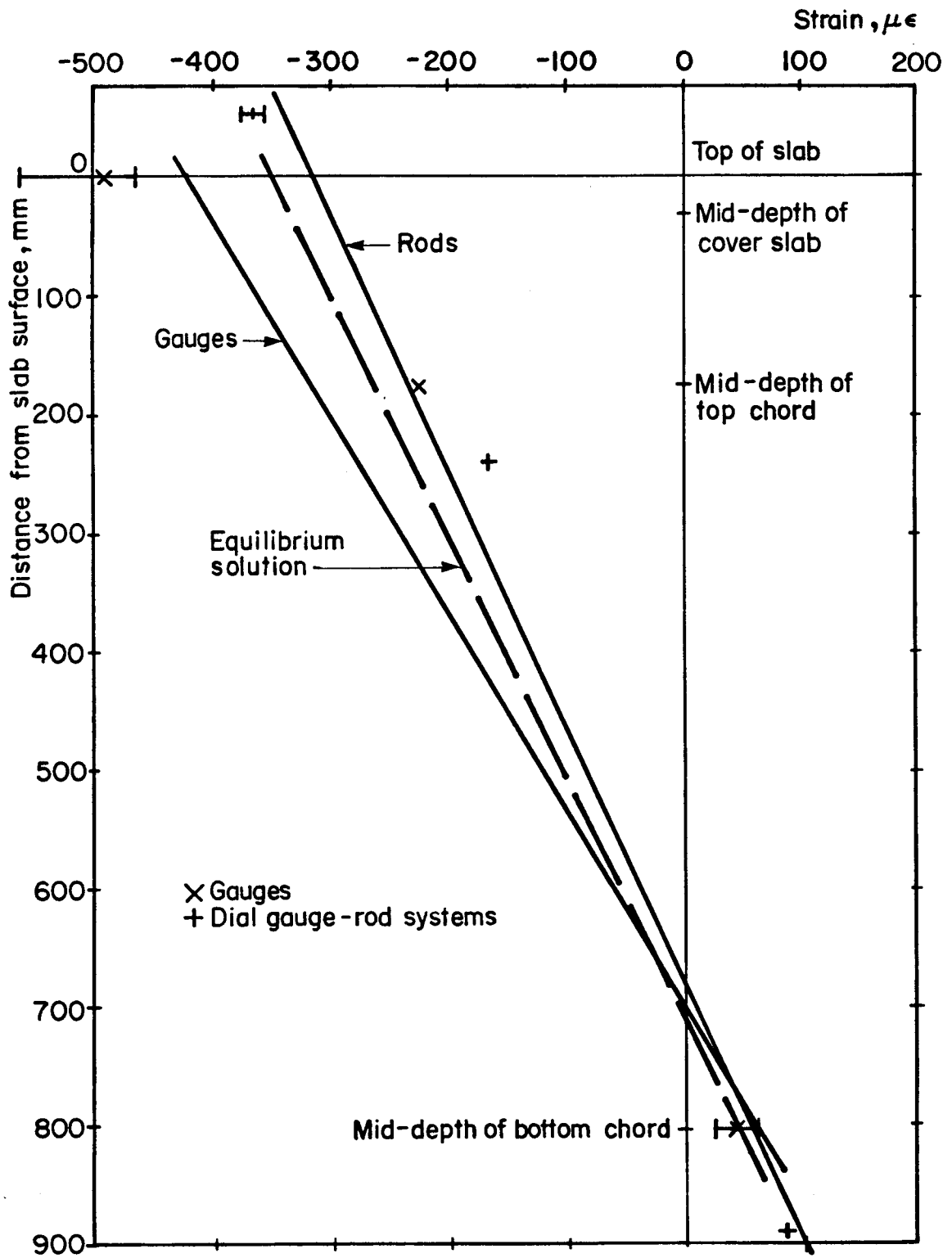


Figure 7.17 Strain variation with depth due to shrinkage - truss 2

8. ANALYSIS OF SHRINKAGE TESTS

8.1 Effective Moment of Inertia of Steel Trusses

As described in Section 3.1.5, it is common practice to estimate the deflection of a steel truss using a moment of inertia for the truss equal to the gross moment of inertia of the steel chords about the truss centroid, and then to multiply the resulting deflection by a factor of 1.10 to account for the flexibility of the open web system. By measuring the weight of concrete placed on each truss during construction of the slab and the resulting truss deflection, the effective moment of inertia of each steel truss can be calculated, allowing the factor which accounts for the effect of the open web in the approximate calculation described above to be determined, as well.

The weight of the concrete slab on truss 1, from Table 4.2, was 61.98 kN, resulting in a midspan deflection of 20.73 mm. The effective moment of inertia of steel truss 1 was therefore $284.2 \times 10^6 \text{ mm}^4$, compared to the value of $324.6 \times 10^6 \text{ mm}^4$ calculated based on the moments of inertia of the steel chords. The ratio of the two moments of inertia, or in other words, the ratio of the actual to the calculated midspan deflection, is 1.14, rather than 1.10.

Truss 2 deflected 19.84 mm under a concrete weight of 61.59 kN. Its effective moment of inertia, based on these values, was $295.1 \times 10^6 \text{ mm}^4$, resulting in a ratio of the moment of inertia calculated from those of the chords over

the effective moment of inertia of 1.10.

These results confirm that the deflection of a steel truss can be estimated, with reasonable accuracy, from a calculation based on a moment of inertia for the truss equal to the gross moment of inertia of the chords about the truss centroid, provided that the resulting deflection is multiplied by a factor of about 1.10 to account for the decreased stiffness of the open web system.

8.2 Distribution of Shrinkage Strains

From measured strains that developed in the members of each composite truss due to shrinkage of the concrete slab, strain distributions on the surface of the concrete slab and in the top and bottom steel chords were plotted along the length of each truss, as shown in Figs. 8.1, 8.3, and 8.4, and studied to ascertain how the shrinkage forces are transferred in a composite truss.

8.2.1 Concrete Slab Strains

Fig. 8.1 shows the distribution of shrinkage strains on the slab surface along the length of each truss from one end to midspan. The strain distributions, as well as the average strains from the dial gauge-rod assemblies (corrected to the slab surface), are plotted at 65 days for truss 1 and at 85 days for truss 2. At the ends of the slab, the shrinkage is unrestrained. The free shrinkage strains plotted at this location correspond to the average transverse slab

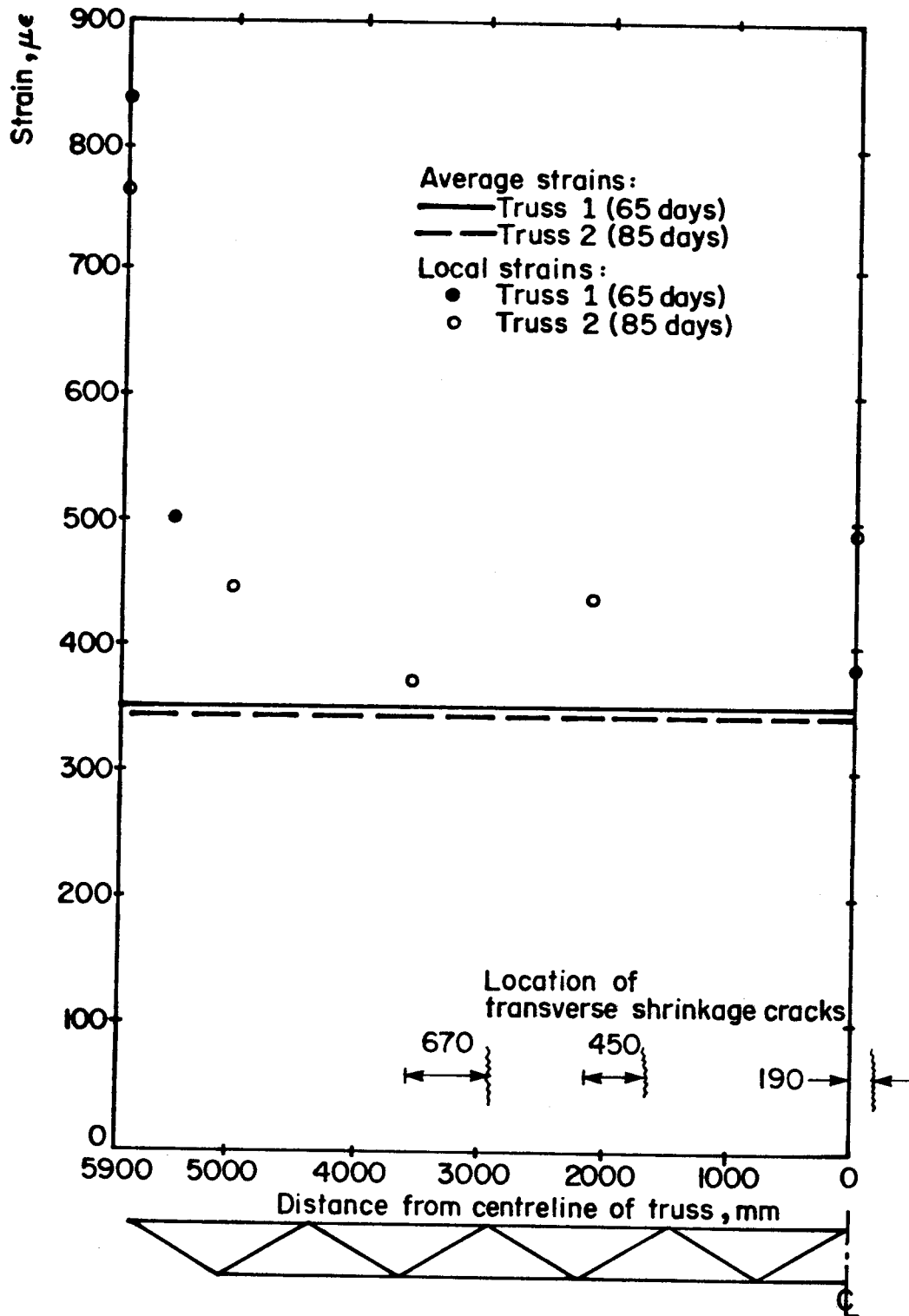


Figure 8.1 Distribution of strains on slab surface due to shrinkage

shrinkage, which is essentially unrestrained (as discussed in Section 7.3.1). Moving in from the ends, the strain decreases rapidly and approaches the restrained shrinkage strain, which is a constant value through the central portion of the length.

The strain only 400 mm from the end of the slab on truss 1 is 60% of the free shrinkage strain and 1.4 times the average longitudinal shrinkage strain. At midspan, the average of the Demec strains is 9% higher than the average longitudinal shrinkage strain. One would expect the restrained shrinkage strain measured at midspan to be lower than the average strain because the area under the strain distribution curve should equal the area under the average curve. The discrepancy is attributed to the $10 \mu\epsilon$ sensitivity of the Demec gauge or to the presence of an unobserved microcrack near midspan which would relieve the restraint to some extent.

On truss 2, the strain measured 869 mm from the ends of the slab is 58% of the free shrinkage strain and 1.3 times the average longitudinal strain at 85 days. The restraint does not appear to have developed in as short a distance on truss 2 as on truss 1. At $0.195L$, $0.317L$, and $0.500L$, the average Demec strains are 7, 27, and 41% higher than the average longitudinal strains at 85 days. These strains are higher than the expected value of the restrained shrinkage strain because of the proximity of shrinkage cracks. Shrinkage cracks developed about 670 mm south of the Demec

points at 0.195L, 450 mm south of the line at 0.317L, and only 190 mm south of the midspan Demec points, as shown in Fig. 8.1. The strain at a shrinkage crack could be expected to equal the free shrinkage strain. The proximity of the crack at each line of Demec points is consistent with the amount each strain varies from the restrained shrinkage value.

A postulated strain distribution for slab shrinkage is shown in Fig. 8.2. The strain decreases parabolically from the free shrinkage value at the ends, giving a total shrinkage deformation equal to that based on the average longitudinal strain. Fitting a parabola to the free shrinkage strain and strain at 0.034L measured on truss 1 at 65 days gives a restrained shrinkage value of $325 \mu\epsilon$, fully developed at 970 mm from the end of the slab. This means that about 84% of the slab undergoes uniform shrinkage. The same technique applied to truss 2 gives a value of $294 \mu\epsilon$ for the restrained shrinkage strain at 85 days, fully developed at a distance about 2000 mm from the end of the slab. In this case, if no shrinkage cracks developed, about 66% of the slab would undergo uniform shrinkage.

Knowles(1973) mentions that the German code DIN 1078 uses a triangular diagram with a length equal to the effective width of the beam to calculate the shrinkage force which must be transferred at the ends of the slab and that the British code simplifies the exact solution from an exponential curve to a straight line.

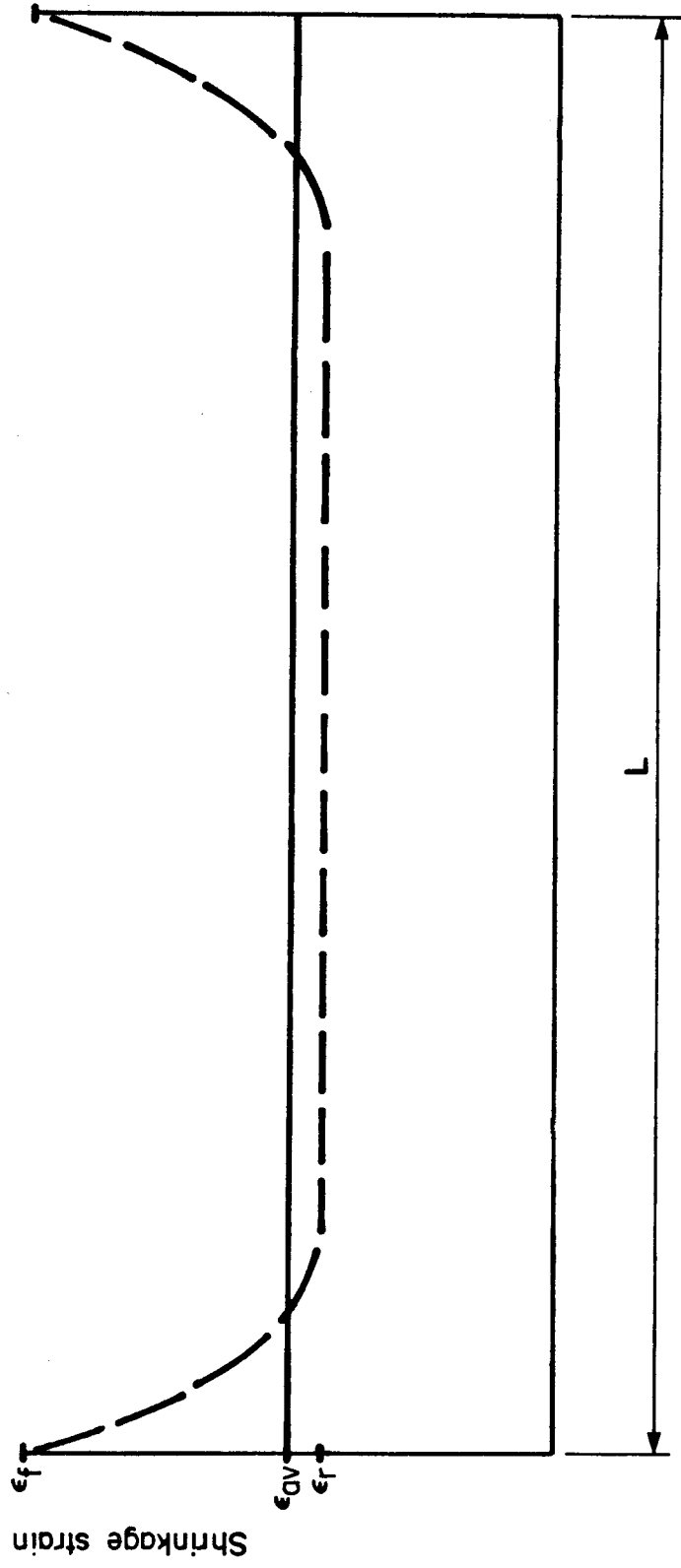


Figure 8.2 Longitudinal shrinkage strain of slab surface

8.2.2 Steel Top Chord Strains

The distribution of strains along the length of the top chord due to shrinkage of the concrete slab is shown in Fig. 8.3 for truss 1 at 65 days and for truss 2 at 85 days. Shrinkage forces are transferred from the concrete to the top chord at shear stud locations. From the concrete strain distribution, it is seen that full restraint to shrinkage develops within about a one or two metre length from each end of the truss. The end shear connectors within this length must therefore be providing this restraint as there is no change in strain in the concrete in the central portion of the length. As would be expected, strains measured in the central panels of the top chord are essentially uniform. The strain in the end panel is 52% of the midspan strain for truss 1 at 65 days and 48% of the midspan strain for truss 2 at 85 days. Assuming that the strain in the end panel of the top chord increases linearly, the average strain in the top chord, calculated from the strain distribution for truss 2, is $194 \mu\epsilon$ at 85 days. The average longitudinal strain in the top chord, measured from a dial gauge-rod assembly and corrected to the mid-depth of the chord, is $193 \mu\epsilon$ at 85 days, as plotted in Fig. 8.3.

8.2.3 Steel Bottom Chord Strains

Fig 8.4 shows the distribution of strains that developed in the bottom chord due to shrinkage of the concrete slab at 65 days for truss 1 and at 85 days for

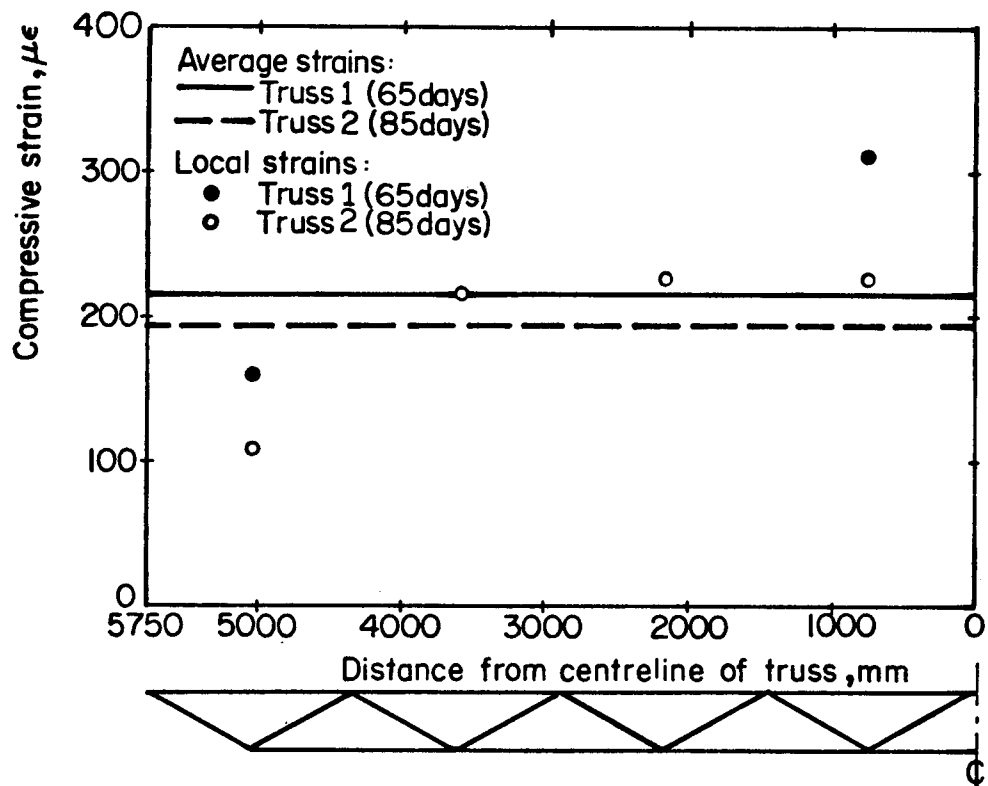


Figure 8.3 Distribution of strains along top chord due to shrinkage

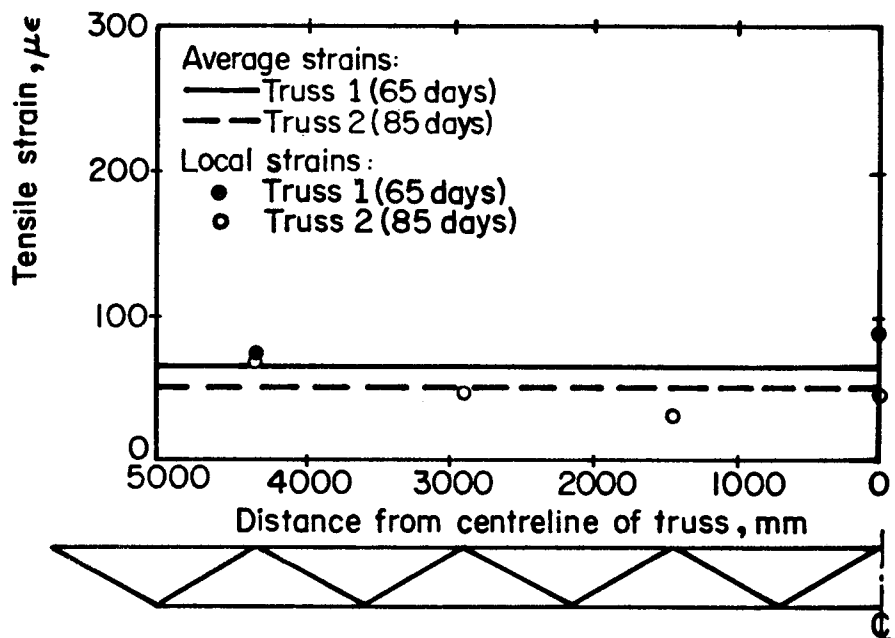
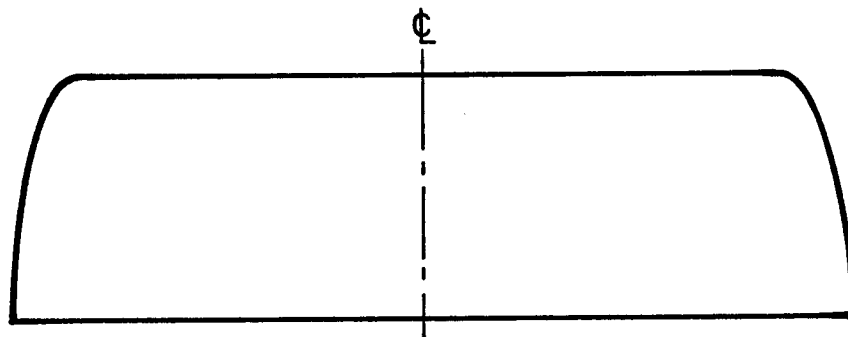


Figure 8.4 Distribution of strains along bottom chord due to shrinkage

truss 2, as well as the average longitudinal strains, corrected to the mid-depth of the chord, as measured by a dial gauge-rod assembly. Strains in the bottom chord are relatively small and are considered to be essentially uniform along the length. Most of the shrinkage force appears to be transferred from the end panels of the top chord to the bottom chord by web members AB and HJ in tension and by BC and GH in compression. This is corroborated by strain measurements of $+83 \mu\epsilon$ and $-32 \mu\epsilon$ in members AB and BC of truss 1 at 65 days. The strains measured in the other web members varied randomly from $+29$ to $-13 \mu\epsilon$ and are considered to be, for all practical purposes, zero. The average strain in the bottom chord at 85 days, calculated from the strain distribution for truss 2, is $47 \mu\epsilon$, almost equal to the average longitudinal strain measured from a dial gauge-rod assembly of $49 \mu\epsilon$.

8.3 Shrinkage Forces in Members

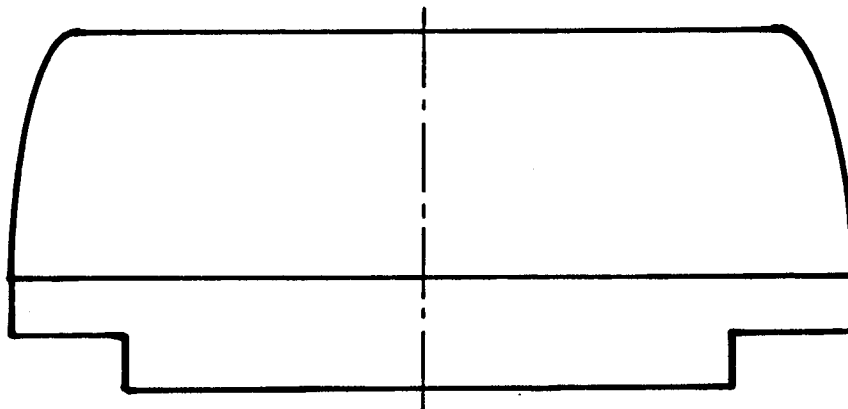
The postulated distribution of longitudinal shrinkage strains in the concrete slab, shown in Fig. 8.2, indicates that full restraint to shrinkage develops in a relatively short distance from the ends and that, for most of its length, the slab undergoes uniform shrinkage. Based on this, the tensile force in the concrete will also be constant over most of the length, as shown in Fig. 8.5(a). From the free body diagram of one half of the truss shown in Fig. 8.6(a), the tensile force developed in the concrete must be resisted



(a) Tensile shrinkage force in concrete slab



(b) Tensile shrinkage force in bottom chord



(c) Compressive shrinkage force in top chord

Figure 8.5 Shrinkage forces

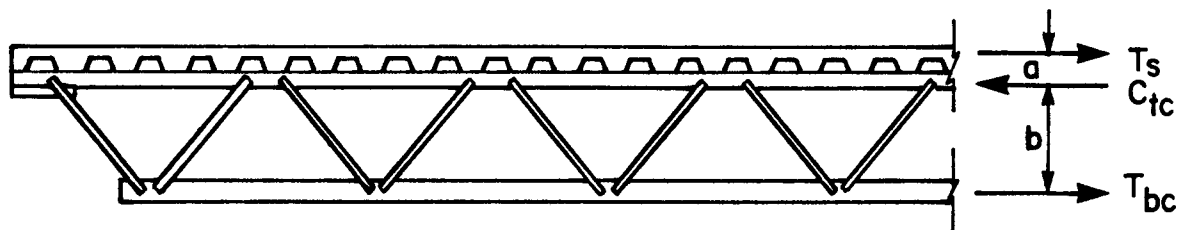
by a set of forces in the steel truss, all of which are in equilibrium. For horizontal equilibrium, the compressive force in the top chord is:

$$[8.1] \quad C_{tc} = T_s + T_{bc}$$

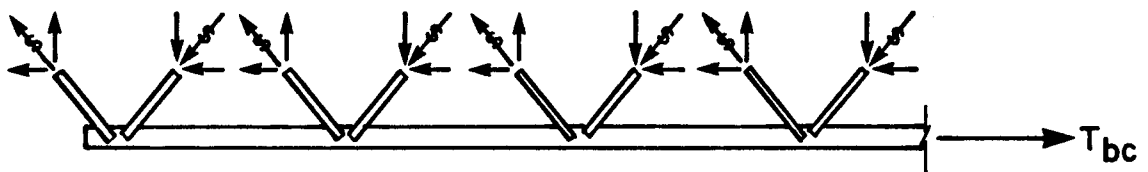
Taking moments about the mid-depth of the steel top chord gives:

$$[8.2] \quad T_{bc} = \frac{a}{b} T_s$$

The free body diagram of the bottom chord in Fig. 8.6(b) shows that the tensile force in the bottom chord can only be introduced at panel points by the horizontal components of the forces in the web members. Because shrinkage restraint develops quickly at the ends of the slab, most of the shrinkage force appears to be transferred to the bottom chord at the ends by web members AB and HJ in tension and by BC and GH in compression. The tensile force in the bottom chord is therefore taken to be constant along its length, as shown in Fig. 8.5(b). At any section, the compressive force in the top chord, from [8.1], must be as shown in Fig. 8.5(c) where the force in each end panel is reduced because of the horizontal component of the forces in the two end diagonals. The force in the top chord is also constant over most of the chord length.



(a) One - half the truss

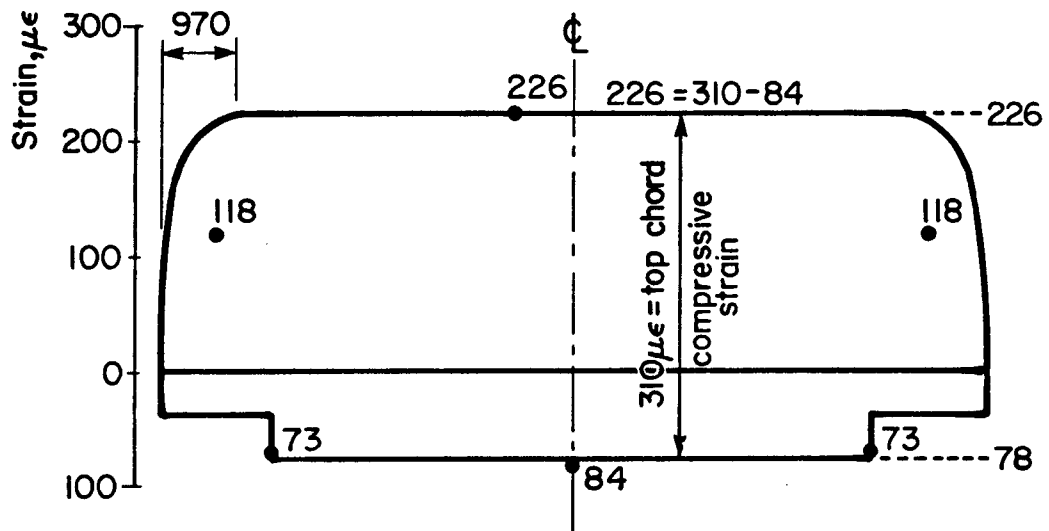


(b) Bottom chord

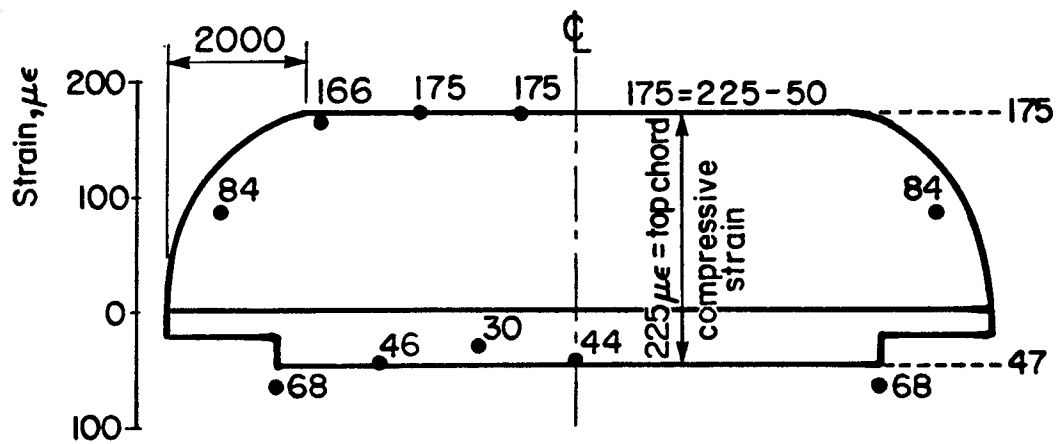
Figure 8.6 Free body diagrams for shrinkage forces

The force distributions in Fig. 8.5 have been confirmed in relative terms by the local strain measurements in the top and bottom chords plotted in Fig. 8.7. The strain gauge measurements on the bottom chord are plotted below the reference axis, and the average tensile strain determined from them is plotted as a constant value. A step is drawn at each end corresponding to the step in the force diagram for the top chord in Fig. 8.5(c). Because the force in the top chord is partly balanced by the force in the bottom chord, the local compressive strain gauge measurements in the top chord are plotted measuring up from the bottom chord strain line. (As well, an adjustment is made in the bottom chord strains to take into account the difference in the axial stiffness (AE) of the top and bottom chords.) The strain distribution for the top chord is completed by drawing a horizontal line through the local strains, and the curve at each end corresponds to the decreasing restraint in the concrete slab, as shown in Fig. 8.5(a). The distribution of strains corresponds reasonably well with the postulated force distribution in Fig. 8.5(c).

In Figs. 7.16 and 7.17, the best fit lines for the distribution of strains obtained from the gauges at midspan should enable the set of forces developed there due to shrinkage to be determined. The compressive and tensile forces in the top and bottom chords can be determined directly from the strains. Combining [8.1] and [8.2] to give



(a) Truss 1 strains at 65 days



(b) Truss 2 strains at 85 days

Figure 8.7 Shrinkage strains in top and bottom chords

$$[8.3] \quad C_{tc} = \frac{a + b}{a} T_{bc}$$

shows that these forces are not independent.

The dashed strain distribution line on Fig 7.16 satisfies the equilibrium conditions and gives a weighted mean to the forces in the chords of truss 1 determined from strain measurements. Based on this strain distribution, the compressive force in the top chord is 107 kN (as compared to a calculated value based on the measured strain of 102 kN) and the tensile force in the bottom chord is 20 kN (as compared to a calculated value based on the measured strain of 30 kN). The tensile force in the slab for equilibrium is therefore $107 - 20 = 87$ kN. From the calculated equilibrium strain diagram, the net strain at the mid-depth of the cover slab is $417 \mu\epsilon$. When this strain is subtracted from the free shrinkage strain of $837 \mu\epsilon$, as shown in Fig. 8.8, the tensile strain in the concrete is found to be $420 \mu\epsilon$. From this, the effective modulus of elasticity of the concrete in tension, as the tension develops during the shrinkage process, is calculated to be 1390 MPa. The curvature of truss 1 obtained from the equilibrium strain diagram at midspan is $0.614 \times 10^{-6} \text{ mm}^{-1}$, which corresponds closely to $0.594 \times 10^{-6} \text{ mm}^{-1}$ determined from the midspan gauges.

Recognizing that the restrained shrinkage measured on the slab surface of truss 2 at midspan was affected by the proximity of a shrinkage crack, a best fit straight line, obtained from the average longitudinal slab shrinkage and

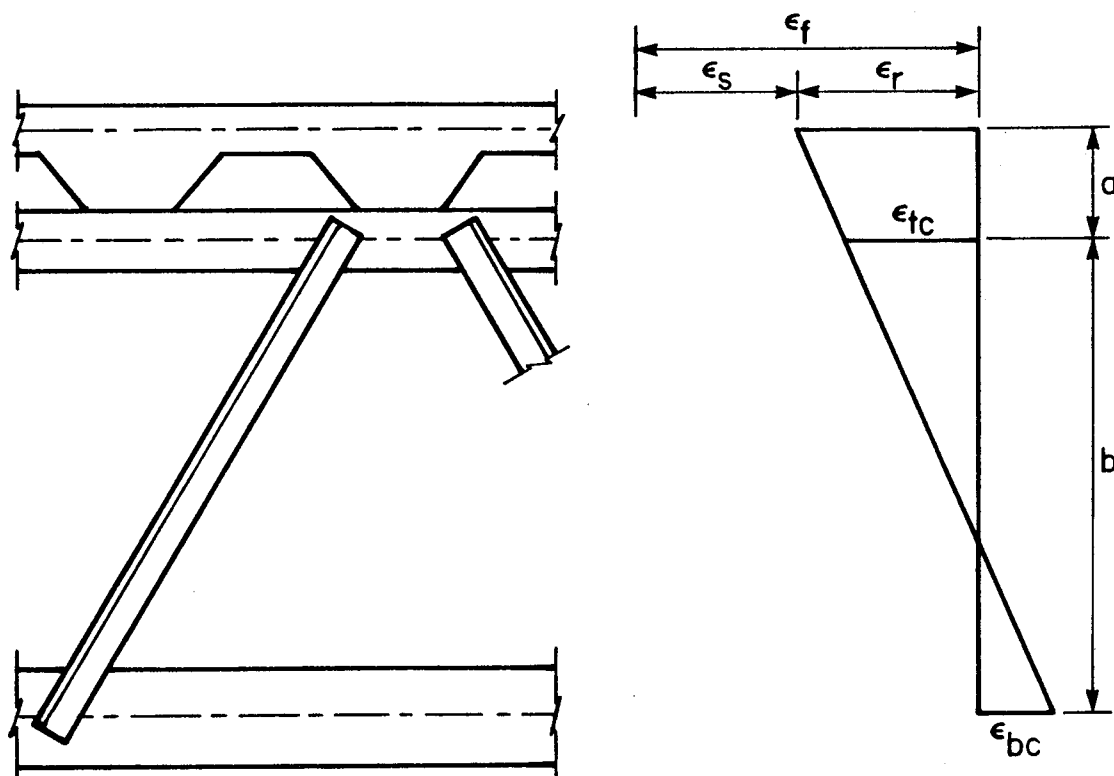


Figure 8.8 Shrinkage strain distribution at midspan

the top and bottom chord strains measured from strain gauges at midspan, was used to calculate the set of forces developed at midspan at 85 days due to shrinkage. The strain distribution that satisfies equilibrium and gives a weighted mean to the forces in the chords calculated from measured strains is shown as a dashed line in Fig. 7.17. The compressive force in the top chord, based on the equilibrium strain distribution, is 85 kN (as compared to a value calculated from the measured strain of 74 kN), while the bottom chord tensile force is 16 kN (as compared to a calculated value from the measured strain of 15 kN). For equilibrium, the tensile force in the concrete slab must be 69 kN. The net strain at the mid-depth of the cover slab, from the equilibrium strain diagram, is $333 \mu\epsilon$, which, when subtracted from the free shrinkage strain of $762 \mu\epsilon$, gives a tensile strain in the concrete of $429 \mu\epsilon$. The effective modulus of elasticity of the concrete in tension is then calculated to be 1070 MPa. The equilibrium strains at midspan give a curvature of $0.490 \times 10^{-6} \text{ mm}^{-1}$, almost equal to $0.488 \times 10^{-6} \text{ mm}^{-1}$ obtained from the best fit line of the midspan gauges, using the average longitudinal slab strain rather than the misleading midspan Demec strain.

8.4 Calculation of Deflection due to Shrinkage

Designers are concerned with the deflection of composite trusses caused by shrinkage of the concrete slab.

Appendix L of CSA S16.1 gives two methods to estimate the deflection of composite beams due to shrinkage. In the method suggested by Montgomery, Kulak, and Shwartsburd (1983), the concrete slab undergoes a shrinkage strain ϵ_{sh} equal to the unrestrained shrinkage strain. To enforce compatibility, a tensile force is then applied to the centroid of the concrete section to pull it back to its original length. Finally, equilibrium is satisfied by applying an equal compressive force to the transformed section at the centroid of the cover slab. The deflection due to shrinkage is then calculated as that produced by equal end moments acting on the composite cross section, using the equation

$$[8.4] \quad \Delta_{sh} = \frac{\epsilon_{sh} E_c A_c L^2}{8 E I_t} y_c$$

In the method proposed by Chien and Ritchie(1984), the composite section is again subject to a constant moment equal in magnitude to a compressive force applied at the centroid of the cover slab, multiplied by the distance from its line of action to the centroid of the transformed section. For this calculation, the magnitude of the compressive force is the force required to shorten the concrete cover slab by an amount equal to the restrained shrinkage strain.

In this section, the measured midspan shrinkage deflections of truss 1, equal to 8.9 mm at 65 days, and

truss 2, equal to 7.2 mm at 85 days, are compared to those calculated using average truss curvatures, the method of Chien and Ritchie (based on restrained shrinkage), the method of Montgomery, Kulak, and Shwartsburd (based on unrestrained shrinkage), and a proposed new method.

8.4.1 Curvatures

The average curvature of truss 1 at 65 days, obtained from the dial gauge-rod assemblies as shown in Fig. 7.16, was $0.509 \times 10^{-6} \text{ mm}^{-1}$, corresponding to a radius of curvature of $1.97 \times 10^6 \text{ mm}$. This radius of curvature on a span of 11.5 m gives a midspan deflection of 8.4 mm, in excellent agreement with the measured deflection of 8.9 mm. An upper bound to the midspan deflection of 9.8 mm is obtained by using the maximum curvature of $0.595 \times 10^{-6} \text{ mm}^{-1}$ found from the strain measurements at midspan.

Truss 2 had an average curvature at 85 days of $0.463 \times 10^{-6} \text{ mm}^{-1}$ as shown in Fig. 7.17, corresponding to a radius of curvature of $2.16 \times 10^6 \text{ mm}$ and a midspan deflection of 7.7 mm in an 11.5 m span, compared to the measured value of 7.2 mm. The maximum curvature at midspan of $0.602 \times 10^{-6} \text{ mm}^{-1}$ gives an upper bound of 10.0 mm to the midspan deflection.

8.4.2 Restrained Shrinkage Method

The method proposed by Chien and Ritchie to calculate the deflection of a composite beam due to shrinkage uses the

restrained shrinkage strain in [8.4], as well as the modulus of elasticity of concrete at 28 days and a transformed moment of inertia of the section based on the 28 day modulus of the concrete. Chien and Ritchie suggest that a restrained shrinkage strain in the range of 200 to 350 $\mu\epsilon$ is appropriate.

For truss 1, the restrained shrinkage at the mid-depth of the cover slab, from the best fit line of average strains in Fig. 7.16, is 319 $\mu\epsilon$ at 65 days. Using the values for the other quantities in [8.4] shown in Table 8.1, the calculated midspan deflection is 7.2 mm. When the moment of inertia of the section is adjusted, as described in Section 10.1, by multiplying by 1/1.10 to account for the flexibility of the open web system, the deflection calculated is 7.9 mm. A further modification of the moment of inertia using [3.7] to account for interfacial slip gives an effective moment of inertia of $757 \times 10^6 \text{ mm}^4$, resulting in a deflection of 8.7 mm, which agrees well with the measured deflection of 8.9 mm.

From the average strains for Truss 2 in Fig. 7.17, the restrained shrinkage at mid-depth of the cover slab is 301 $\mu\epsilon$ at 85 days. The midspan deflection calculated from [8.4], using the values found in Table 8.2, is 6.7 mm. The moment of inertia, adjusted to account for the flexibility of the open web, of $810 \times 10^6 \text{ mm}^4$ gives a calculated deflection of 7.3 mm. The effective moment of inertia, taking into account the increased flexibility due to interfacial slip is $737 \times 10^6 \text{ mm}^4$. This increases the

Table 8.1 Shrinkage deflection parameter values for truss 1

Parameter	Restrained Shrinkage Method	Unrestrained Shrinkage Method
$\epsilon_{sh}, \mu\epsilon$	319	837
E_C, MPa	19 680	11 660
A_C, mm	148 800	148 800
L, mm	11 500	11 500
E_S, MPa	208 300	208 300
I_t, mm	916×10^6	847×10^6
y_C, mm	88.7	132.5

Table 8.2 Shrinkage deflection parameter values for truss 2

Parameter	Restrained Shrinkage Method	Unrestrained Shrinkage Method
$\epsilon_{sh}, \mu\epsilon$	301	762
E_C, MPa	15 620	8020
A_C, mm	150 400	150 400
L, mm	11 500	11 500
E_S, MPa	208 300	208 300
I_t, mm	891×10^6	790×10^6
y_C, mm	105.7	169.8

calculated deflection to 8.0 mm, again in good agreement with the measured value of 7.2 mm.

8.4.3 Unrestrained Shrinkage Method

In the unrestrained shrinkage method (Montgomery et al., 1983) the shrinkage deflection is calculated from [8.4] as well, but the free shrinkage strain, an age-adjusted modulus of elasticity for the concrete, and a transformed moment of inertia of the cross section calculated from the age-adjusted concrete modulus are used. For design purposes, the free shrinkage strain can be calculated using an approach suggested by the American Concrete Institute Committee 209 (1971), which takes into account the time interval over which shrinkage occurs, the relative humidity, the volume-to-surface area ratio of the slab, as well as the slump, percent fines, air content, and cement content of the concrete. Using the age-adjusted modulus for the concrete in [8.4] takes into account that shrinkage develops slowly as the concrete ages, producing tensile stresses that are reduced by creep, and that the concrete properties f'_c and E_c increase as the concrete ages. The expression

$$[8.5] \quad E_c^*(t) = \frac{E_c(t_0)}{1 + \chi(t, t_0) \phi(t, t_0)}$$

(Bazant, 1972) is used to calculate the age-adjusted modulus of elasticity of the concrete, where $\phi(t, t_0)$ is the creep coefficient (the ratio of creep strain to initial elastic

strain) of the concrete for the time interval considered, and α is the aging coefficient, which is defined for a specific creep function and varies with age at loading, time under load, and member dimensions. In the following calculations, the creep coefficient was evaluated by the procedure suggested by the American Concrete Institute Committee 209 (1971), taking into account curing and loading conditions, as well as the concrete mix proportions. The aging coefficient was obtained from Bazant(1972), whose calculations used the ACI creep function for structural concrete. A trial calculation using a different creep coefficient calculated from the CEB-FIP Model Code(1978) and an aging coefficient based on the CEB-FIP creep function (Dilger, 1982) did not have a significant effect on the calculated shrinkage deflection.

The transverse slab strain for truss 1 at 65 days of $837 \mu\epsilon$, almost equal to the average free strain of the two sizes of concrete control specimens, was chosen as a representative value for the unrestrained shrinkage strain. Other values used in [8.4] are shown in Table 8.1, and a shrinkage deflection of 18.0 mm is calculated. Adjusting the modulus of elasticity to account for the flexibility of the open web system gives a reduced value of $770 \times 10^6 \text{ mm}^4$, and a corresponding deflection of 19.8 mm. An adjustment to account for interfacial slip reduces the moment of inertia further to $703 \times 10^6 \text{ mm}^4$, resulting in a calculated midspan deflection of 21.7 mm, significantly greater than the

measured value of 8.9 mm.

The shrinkage test results from truss 1 indicate that the transverse slab strain is essentially a free shrinkage strain. Therefore, for truss 2 at 85 days, the transverse slab strain of $762 \mu\epsilon$ was chosen as a representative value for the unrestrained shrinkage, although its value is greater than either of the free shrinkage strains measured from the control specimens, because the properties of the concrete in the control specimens may have been slightly different from the average properties of the concrete placed in the slab. Using [8.4], the calculated midspan deflection due to shrinkage is 15.7 mm. The calculated deflection increases to 17.2 mm when the modulus of elasticity is reduced to $718 \times 10^6 \text{ mm}^4$ to account for the effect of the open web system. A further adjustment to the moment of inertia to account for increased flexibility due to interfacial slip results in an effective moment of inertia of $659 \times 10^6 \text{ mm}^4$ and a calculated midspan deflection of 18.8 mm. Once again, this is considerably greater than the measured value of 7.2 mm at 85 days.

Park and Paulay(1975) suggest an approach to calculate the shrinkage stresses in a reinforced concrete beam in which the concrete is allowed to shrink unrestrained. A compressive force is then applied to the steel area at its centroid to shorten the steel by the same amount. To satisfy external equilibrium, an equal tensile force is applied to the transformed section at the location of the centroid of

the steel. The shrinkage stresses are then found by the principle of superposition. The deflection due to shrinkage can again be calculated as that produced by a constant moment acting on the transformed section equal to the tensile force with a lever arm from the centroid of the transformed section to the centroid of the steel. Using this approach for a composite member, the end moments would be identical to those produced by a compressive force applied to the composite section at the centroid of the cover slab (as used in both the restrained and the unrestrained shrinkage methods) provided that the elastic neutral axis of the composite member does not lie in the cover slab.

8.4.4 Equilibrium Method

Based on the development of shrinkage forces in the truss members discussed in Section 8.3, an equilibrium method for computing the midspan shrinkage deflection of a composite truss is proposed. Recognizing that curvature is proportional to the sum of the top surface strain and the bottom chord tensile strain, the strain diagrams in Fig 8.7 represent curvature diagrams. The average height of these diagrams is about 90% of the maximum value. As shown in Section 8.4.1, an excellent estimate of the midspan deflection due to shrinkage can be calculated using the average curvature. Thus, midspan deflections can be computed using an average curvature equal to 90% of the midspan curvature. The midspan curvature itself is calculated based

on equilibrium conditions, strain compatibility, and the stress-strain characteristics of the materials.

The steps in the equilibrium method are:

1. Estimate the free shrinkage strain of the concrete. (The calculation procedure suggested by the American Concrete Institute Committee 209, as summarized by Park and Paulay(1975), could be used.)
2. Determine the effective modulus of elasticity of the concrete in tension over the time interval during which shrinkage occurs.
3. From the strain diagram in Fig. 8.8, it is seen that

$$[8.6] \quad \epsilon_r = \epsilon_f - \epsilon_s$$

where ϵ_s , the tensile strain in the concrete, is

$$[8.7] \quad \epsilon_s = \frac{T_s}{A_c E'_c}$$

Substituting [8.7] in [8.6] gives

$$[8.8] \quad T_s = (\epsilon_f - \epsilon_r) A_c E'_c$$

The equation expressing the linear distribution of strain through the member depth is

$$[8.9] \quad \frac{\epsilon_r + \epsilon_{bc}}{\epsilon_{tc} + \epsilon_{bc}} = \frac{a + b}{b}$$

The compressive and tensile forces in the top and bottom chords, respectively, expressed in terms of their respective strains are

$$[8.10] \quad C_{tc} = \epsilon_{tc} E A_{tc}$$

$$[8.11] \quad T_{bc} = \epsilon_{bc} E A_{bc}$$

From [8.1] and [8.2] expressing the equilibrium conditions, [8.9] expressing the strain distribution, and [8.8], [8.10], and [8.11] relating strains with forces, the three equations giving the equilibrium strain distribution are:

$$[8.12] \quad \epsilon_{tc} E A_{tc} - \epsilon_{bc} E A_{bc} = (\epsilon_f - \epsilon_r) A_C E'_C$$

$$[8.13] \quad \epsilon_{bc} E A_{bc} = \left[\frac{a}{b} \right] (\epsilon_f - \epsilon_r) A_C E'_C$$

$$[8.14] \quad \left[\frac{a+b}{b} \right] \epsilon_{tc} + \left[\frac{a}{b} \right] \epsilon_{bc} = \epsilon_r$$

These 3 equations can be solved simultaneously to find a unique value for ϵ_r , ϵ_{tc} , and ϵ_{bc} .

4. The midspan curvature calculated from these strains is

$$[8.15] \quad \frac{1}{\rho} = \frac{\epsilon_{bc} + \epsilon_r}{a + b} = \frac{\epsilon_{bc} + \epsilon_{tc}}{b}$$

5. Taking the average curvature $1/\rho_{av}$ to be 90% of the

midspan curvature, the shrinkage deflection is calculated from

$$[8.16] \quad \Delta_{sh} = 0.90 \rho \left[1 - \cos\left(\sin^{-1} \frac{L}{2\rho}\right) \right]$$

Using the measured cross sectional properties of composite truss 1, a free shrinkage strain of $837 \mu\epsilon$, and an effective tensile modulus of elasticity for the concrete of 1390 MPa at 65 days, as calculated in Section 8.3, the equilibrium method gives equilibrium strains as shown in Fig. 7.16 and an estimated midspan shrinkage deflection of 9.1 mm, in excellent agreement with the measured value of 8.9 mm.

For truss 2, using the measured cross sectional properties, a free shrinkage strain of $762 \mu\epsilon$, and an effective tensile modulus of elasticity for the concrete of 1070 MPa in [8.12] to [8.16] gives the equilibrium strains shown in Fig 7.17 and an estimated shrinkage deflection of 7.3 mm at 85 days, in excellent agreement with the measured midspan deflection of 7.2 mm.

The modulus of elasticity of the concrete in tension over the interval during which shrinkage occurred was calculated to be 1390 MPa for truss 1 and 1070 MPa for truss 2. This modulus is considered to be a time-dependent property of the concrete, unrelated to the amount of restraint. The calculated values bear no resemblance to the measured moduli of elasticity of the concrete in compression

(19 700 MPa for truss 1 and 15 600 MPa for truss 2) at 28 days. As a matter of fact, they do not even correspond to commonly accepted values when taking creep into account. Age-adjusted moduli for the concrete on the two trusses, calculated using Bazant's method for loading at 7 days when moist curing was stopped, are 11 700 and 8300 MPa respectively. The effective moduli of elasticity of the concrete in tension are only about 7% of the moduli of elasticity of the concrete in compression and about 12% of the age-adjusted moduli. It therefore seems inappropriate to calculate shrinkage deflections based on the modulus of elasticity of concrete in compression as the modulus of elasticity in tension under these circumstances is only a fraction of that in compression.

8.4.5 Summary

The estimated and measured midspan shrinkage deflections for both composite trusses are summarized in Table 8.3. Most of the calculated deflections are in reasonable agreement with the measured values.

Based on these results, either the restrained shrinkage method or the equilibrium method are recommended to estimate the deflection of a composite truss due to slab shrinkage. Although in the restrained shrinkage method the modulus of elasticity of concrete in compression at 28 days, which has no relation to the actual shrinkage behaviour, is used, the estimated deflection is within 11% of the measured value for

Table 8.3 Midspan shrinkage deflection calculations

Calculations based on:	Truss 1 deflection at 65 days, mm			Truss 2 deflection at 85 days, mm		
	I_t	Open Web	Interfacial Slip	I_t	Open Web	Interfacial Slip
Average Curvature	-	-	8.4	-	-	7.7
Restrained Shrinkage	7.2	7.9	8.7	6.7	7.3	8.0
Unrestrained Shrinkage	18.0	19.8	21.7	15.7	17.2	18.8
Equilibrium Method	-	-	9.1	-	-	7.3
Measured	-	-	8.9	-	-	7.2

both test trusses. For general use, however, the restrained shrinkage strain would have to be estimated as a measured value would not be available. It appears that the increased flexibility due to the open web and to interfacial slip should be taken into account. The equilibrium method gives results that are within 2% of the measured deflection for both trusses, when using measured values of the unrestrained shrinkage strain of the concrete and the effective modulus of elasticity of the concrete in tension over the time interval during which shrinkage occurs. For general use, these quantities would have to be estimated. There appears to be little information available about the development of the modulus of elasticity of concrete in tension.

The unrestrained shrinkage method gives the least accurate prediction of the shrinkage deflection of the trusses. The age-adjusted modulus of elasticity of the concrete is approximate only because the creep coefficient was developed for concrete under a constant compressive stress, while shrinkage stresses are tensile and increase with time. However, the prediction does not appear to be overly sensitive to the variables reflecting the influence of the age-adjusted modulus of elasticity in [8.4]. Using the unrestrained shrinkage strain in this calculation does not appear to reflect the true behaviour of the trusses due to shrinkage.

The midspan deflection of truss 2 was less than that of truss 1 because of its lower concrete strength and resultant

shrinkage cracks in the slab, relieving the tensile stresses. The development of such shrinkage cracks should be avoided in practise. The tests were not significantly affected by creep because the steel trusses alone carried the dead load of the concrete, and no external loads were applied to the composite trusses during each shrinkage interval.

9. FLEXURAL TEST RESULTS

The two full-scale composite trusses were tested to failure as described in Section 4.4. The specimens were intended to be essentially identical, with only a small variation in the amount of slab reinforcement. However, because the failure of the first truss resulted from concrete tensile cone failures above the shear connectors, the length of the shear studs on the second specimen was modified, and, in addition, the strength of the concrete placed on truss 2 was only 57% of that of truss 1 at the time of each flexural test.

Composite truss 1 was tested to failure over a period of 3 days, from July 20 (90 days after the concrete slab was cast) to July 22, 1985. The test to failure of composite truss 2 took place over 2 consecutive days, beginning on January 23, 1986 (120 days after the slab was cast).

In the following discussion and figures, the test load refers to the load applied to the specimen at each of the 4 jack locations, obtained by averaging the individual measured values.

9.1 Deflections and Overall Behaviour

The behaviour of composite truss 1 under load can best be described by examining Fig. 9.1, where test load is plotted versus midspan and north and south quarter point deflections of the truss. The load-deflection relationship is linear up to a load of about 38 kN per jack. Small

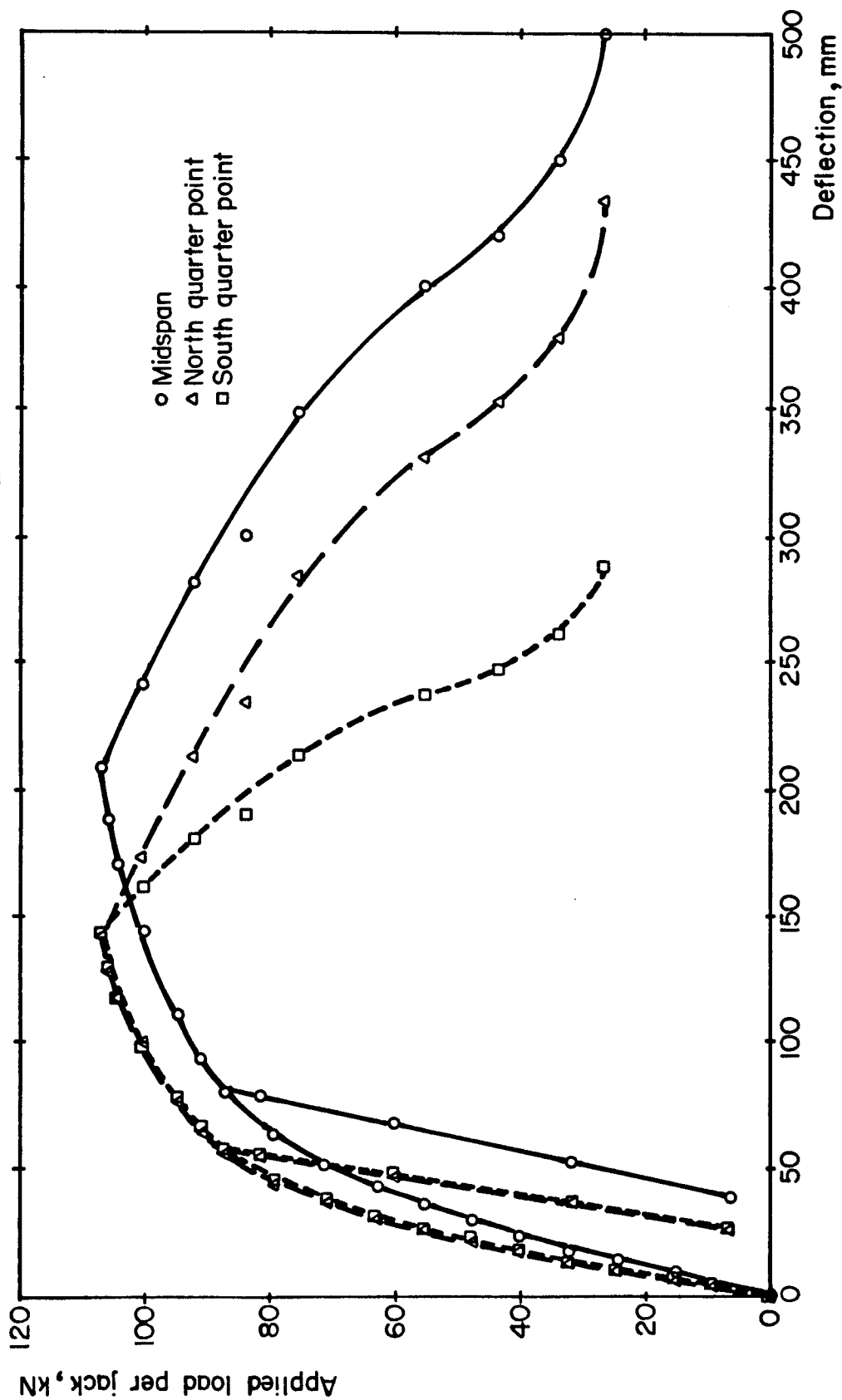


Figure 9.1 Load deflection diagrams - composite truss 1

non-linearities gradually increase until, at a load of 87 kN, the non-linear midspan deflection comprises 36 mm of the total of 87 mm. On unloading from this load, the truss responded elastically to a projected permanent deflection of 36 mm. The reloading was also linearly elastic up to the previously attained load of 87 kN. At this load, very limited yielding of web members was noted, as indicated by flaking of the whitewash at the upper ends of the diagonals at panel points C and Q. With further load application, inelastic deflections became more pronounced and the load increments were reduced to 4 kN per jack. At a load of 100 kN and corresponding midspan deflection of 143 mm, Leuder's bands were clearly evident just below the ends of the welds at the top ends of the web members at panel points C and Q. Limited yielding was also evident on some of the adjacent diagonals. At this stage, a small increase in load was producing a very large deflection. While attempting to load beyond 100 kN, some difficulty was encountered in keeping the jacks plumb. In the extended position, the rod and piston seals provided little lateral restraint and the pistons tended to rotate within the cylinders about a transverse axis. The potential for forming a mechanism existed at each jack location due to this rotation, coupled with the knife edges provided to accommodate rotation between the lower end of each jack and the concrete slab. It therefore became necessary to plumb the jacks continually as the test progressed. At a load of 106 kN, a cracking noise

was heard. The metal deck had lifted slightly from the top chord just above panel point N, indicating that a shear connector at that location had failed. At this load, longitudinal cracking in the concrete slab was noticed along the centreline above the top chord, extending almost continuously from each end of the slab to the interior load points. Cracking also existed in the slab around the exterior load plates. Figure 9.2 shows the deflected truss at a load of 106 kN with a midspan deflection of 190 mm. In attempting to deflect the truss an additional 20 mm, the maximum instantaneous load of 107 kN was reached at a midspan deflection of 212 mm. Simultaneous cracking noises were heard and the longitudinal crack progressed along the entire length of the slab. Figures 9.3 to 9.5 show components of the deformed truss at the maximum applied load. With further deflections, the load dropped off. Separation between the deck and the slab increased considerably, particularly between the north load points. Yielding of the bottom chord near midspan was evident from flaking of the whitewash. Cracking noises indicated that shear connection was failing. At a midspan deflection of 300 mm, the load had dropped to 92 kN and the slab had separated from the deck to the extent that one could see through to the other side. There was very significant in-plane distortion of the top chord and the web members. Compression diagonals were undergoing significant out-of-plane distortions as well. In Fig. 9.6, when the load

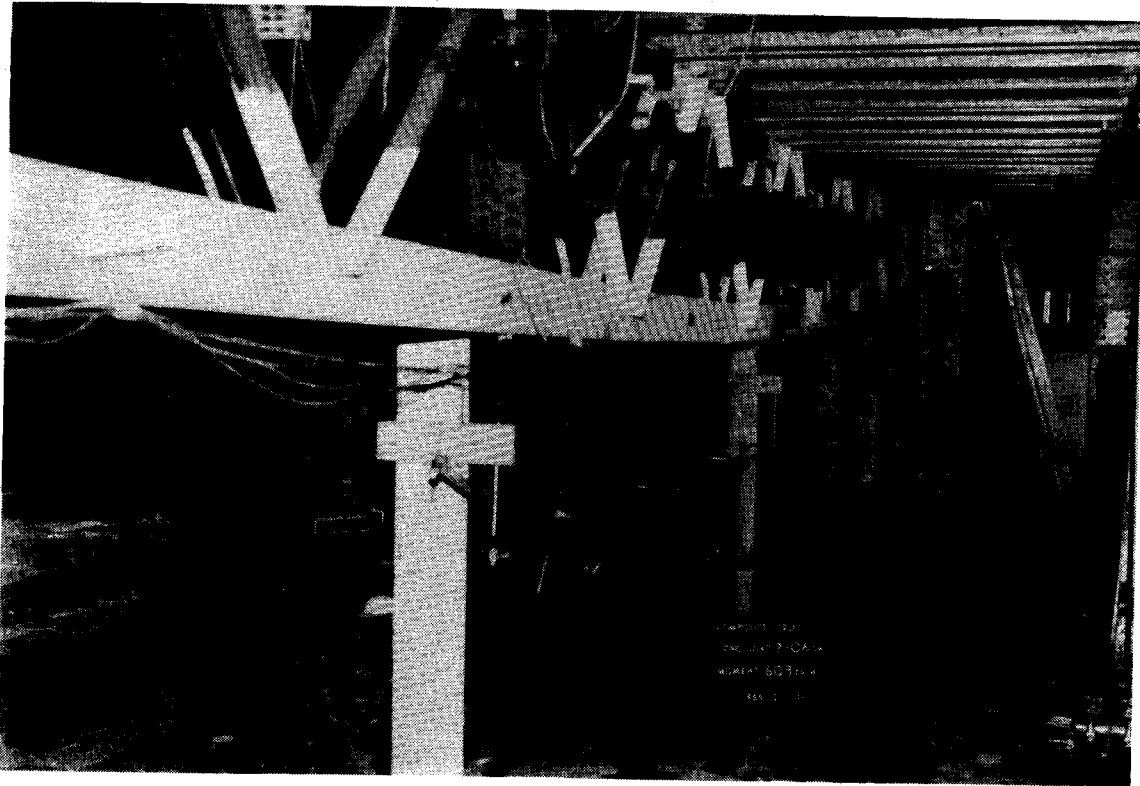


Figure 9.2 Deformed truss at 0.99 of maximum load - truss 1

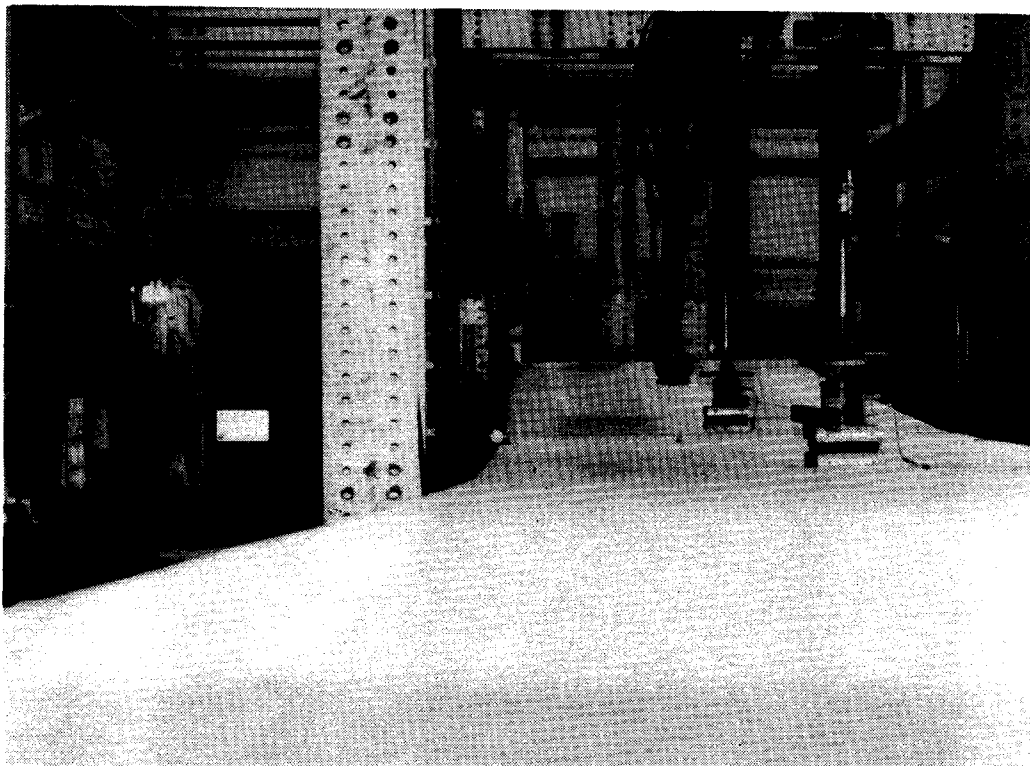


Figure 9.3 Deformed slab at maximum load - truss 1

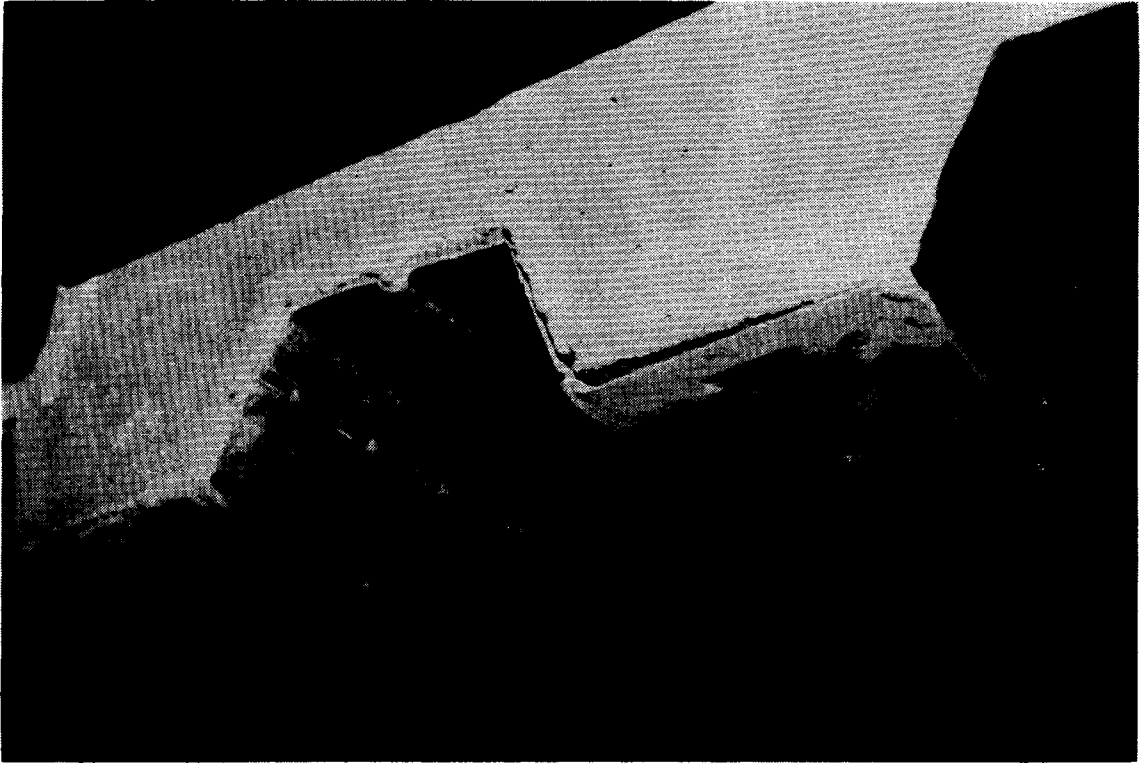


Figure 9.4 Separation of concrete from deck at maximum load
- truss 1

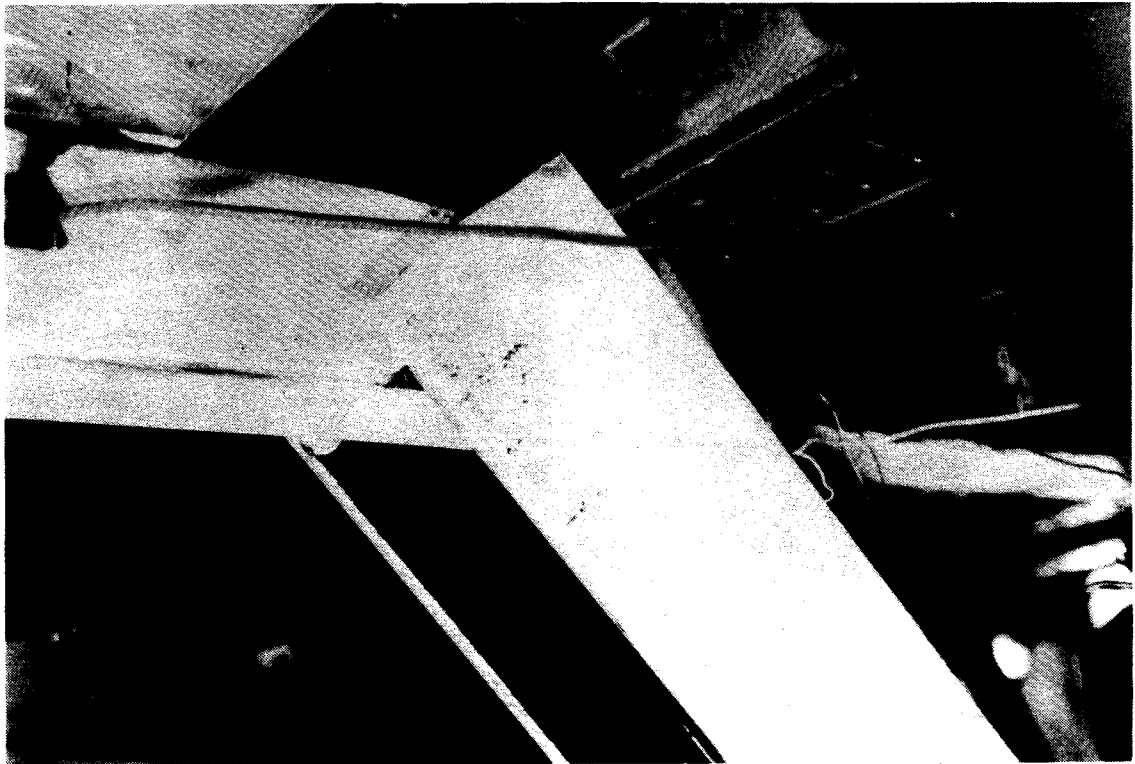


Figure 9.5 Yield lines in compression diagonal BC at maximum
load - truss 1

had dropped to 75 kN, the distortion of the web members is evident and a distinct bulge in the side of the deck flute is a further sign of the distress in the shear connection. Figure 9.7 shows the truss when a midspan deflection of 500 mm was reached. The separation of the slab from the deck is clearly visible. In Fig. 9.8 is shown the buckle that developed in the top chord long after the maximum load was reached and after the slab had separated from the deck. The significant in-plane deformations of the web members are evident. While some of the welds cracked when these large deformations were reached, no welds fractured. Figure 9.9 shows tensile failure cones in the concrete around the tops of the studs upon removal of the concrete slab.

Test load versus midspan and north and south quarter point deflections are plotted for truss 2 in Fig. 9.10. The load-deflection response at midspan follows almost exactly the same path as that of truss 1, shown in Fig. 9.1, up to a load of about 104 kN. The initial relationship is linear to about 40 kN, when the first minor cracking noises were heard. These noises became more frequent as the load increased and the response became more non-linear. At a load of 81 kN, limited yielding was first observed as indicated by flaking of the whitewash at the upper ends of web members BC and QR near the welds. At 88 kN, web members CD and PQ also showed signs of yielding at their upper ends, and, as well, cracks were visible in the concrete slab along the outside edges of the exterior load plates. The midspan

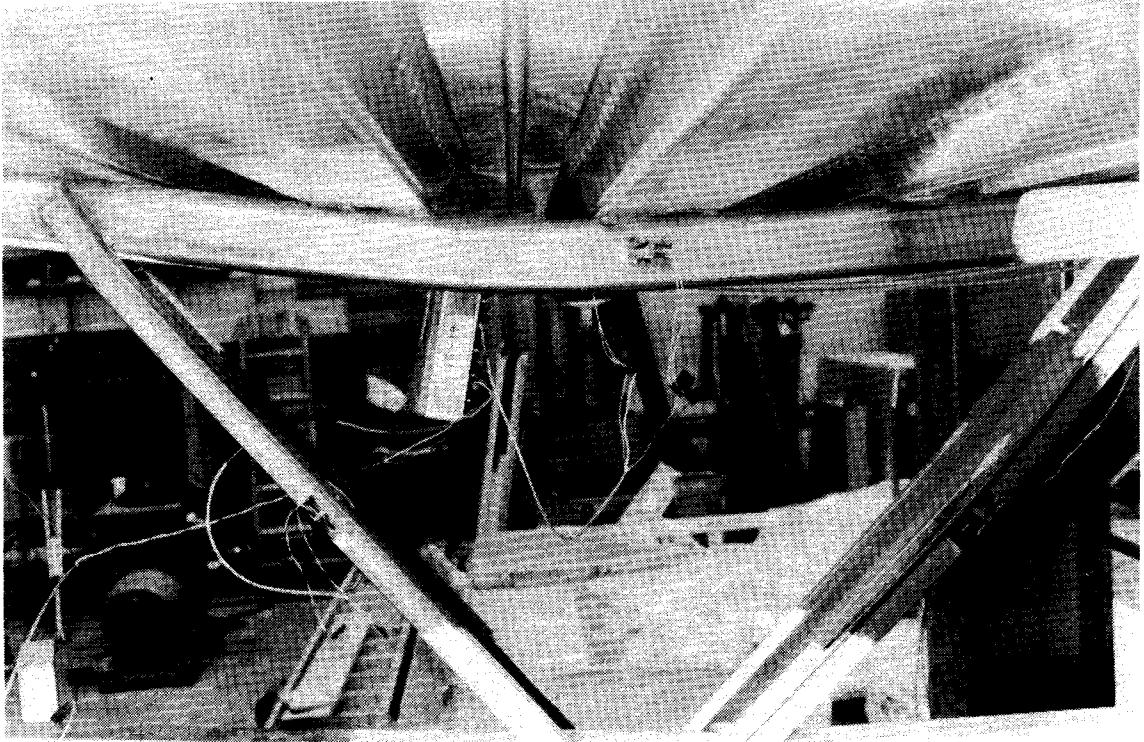


Figure 9.6 Distortion of truss components beyond maximum load - truss 1



Figure 9.7 Truss 1 at midspan deflection of 500 mm

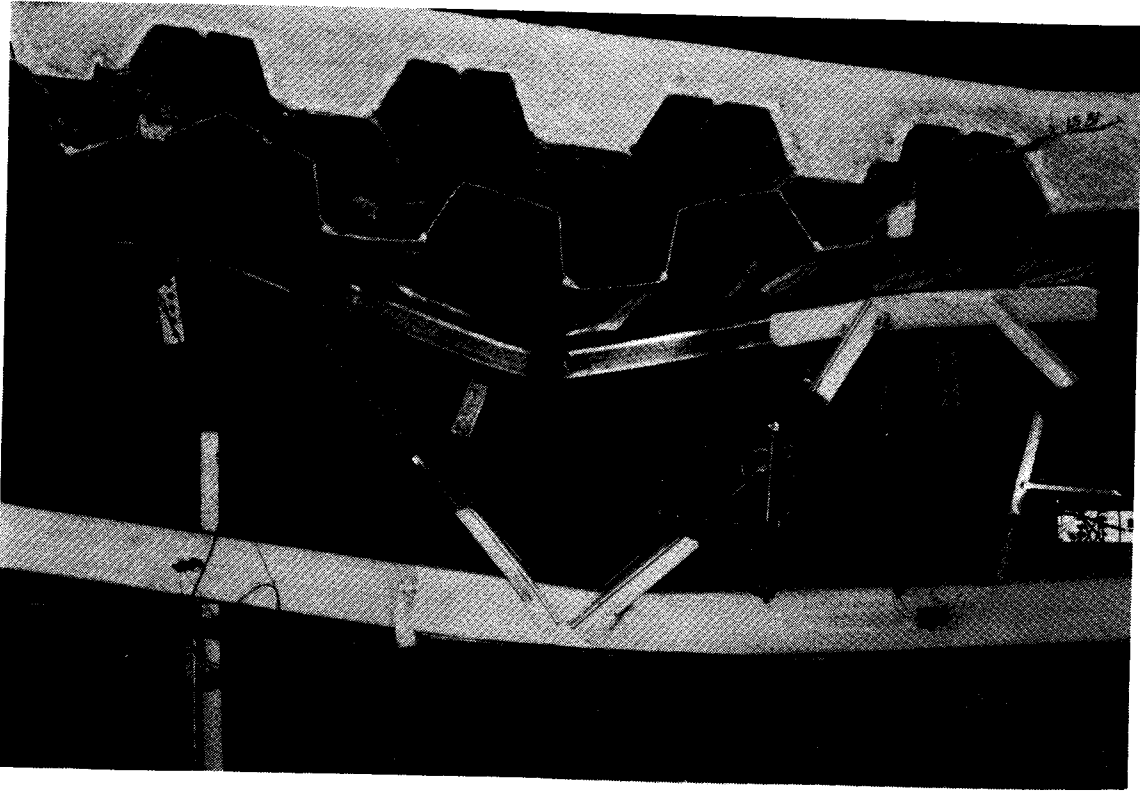


Figure 9.8 Buckled top chord and slab separation at failure
- truss 1

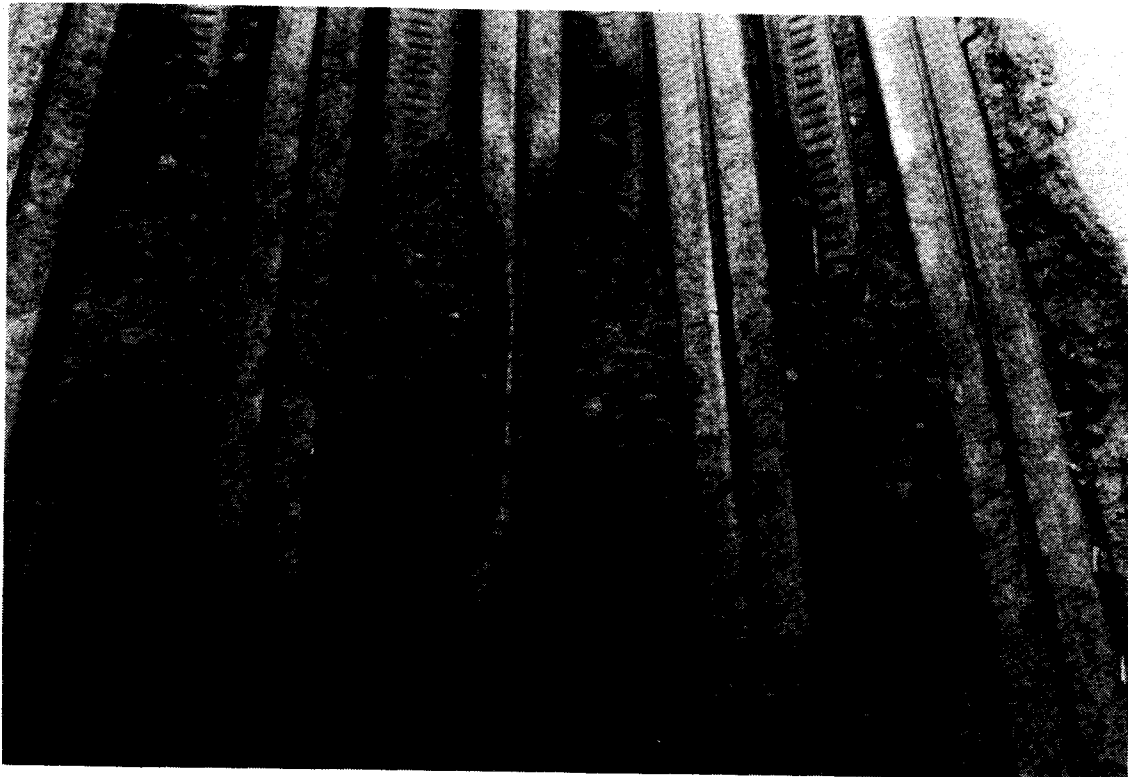


Figure 9.9 Concrete tensile cone failures around studs
- truss 1

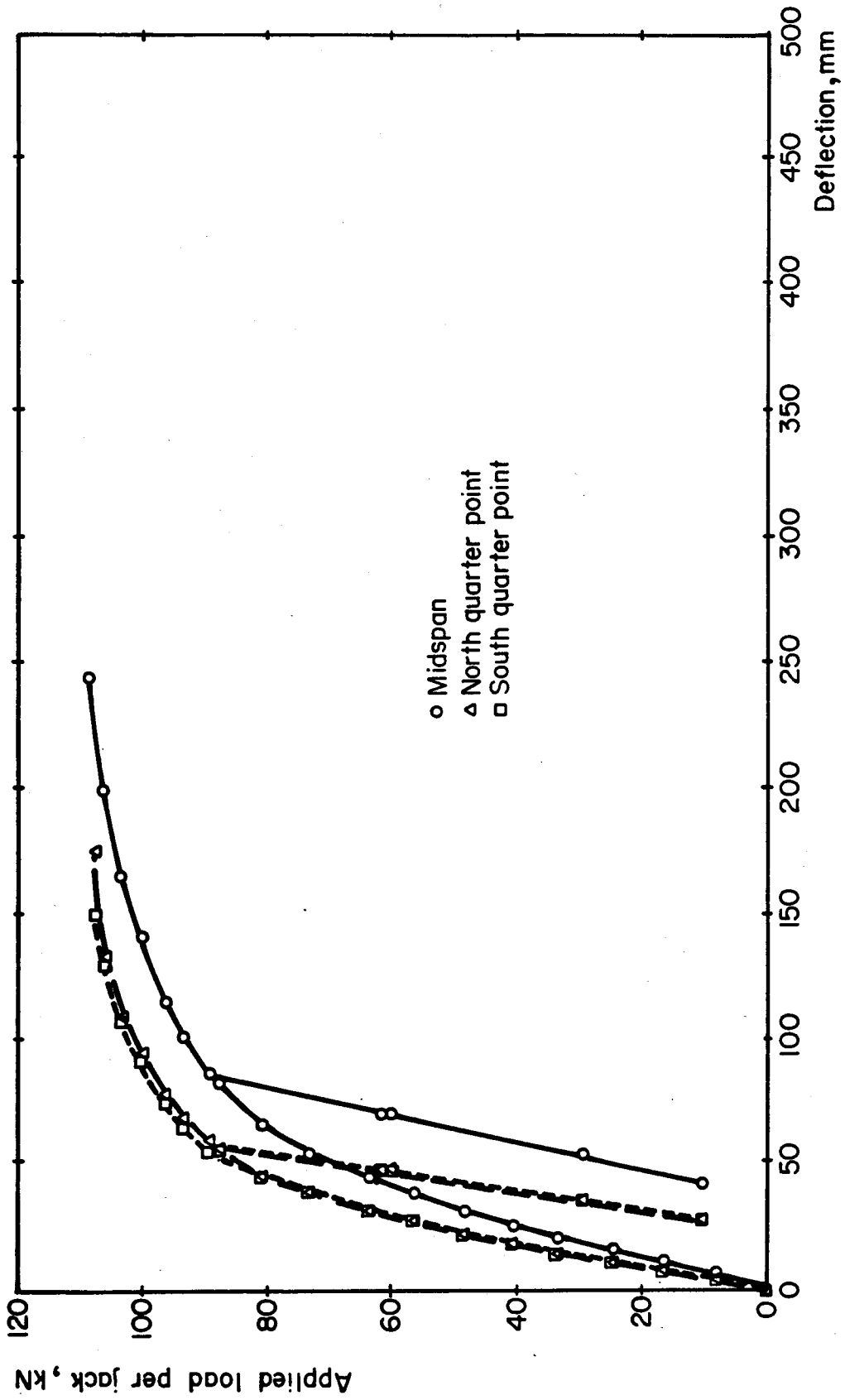


Figure 9.10 Load-deflection diagrams - composite truss 2

deflection at this load was 83 mm. The truss responded elastically to unloading and reloading, with a projected permanent midspan deflection of 36 mm. With the application of another load increment to 93 kN, distinct Leuder's bands became visible in the whitewash at the top ends of the web members at panel points C and Q. At 96 kN, short longitudinal cracks had developed at the exterior load points near the ends of the concrete slab, running along the centreline over the top chord. Figure 9.11 shows composite truss 2 with a midspan deflection of 141 mm at a load of 100 kN per jack. During the loading increment from 103 to 106 kN, a cracking noise followed by a loud tinny bang was heard from the north end of the truss when the midspan deflection was about 190 mm, and the north end slip between the concrete slab and the top chord increased from 2 to 7 mm, indicating that the shear connection was beginning to fail. At a load of 106 kN and corresponding midspan deflection of 200 mm (10 mm more than that of truss 1 at the same load), a longitudinal crack was observed along the centreline of the concrete slab extending a distance of 700 mm from the north end. Several additional loud cracking noises were recorded during the next load increment before the concrete slab began to separate from the deck over the first flute from the north end when the midspan deflection was 218 mm. A loud cracking noise emanating from the south end of the truss was heard at a midspan deflection of 237 mm, just prior to reaching a maximum load of 108 kN at a

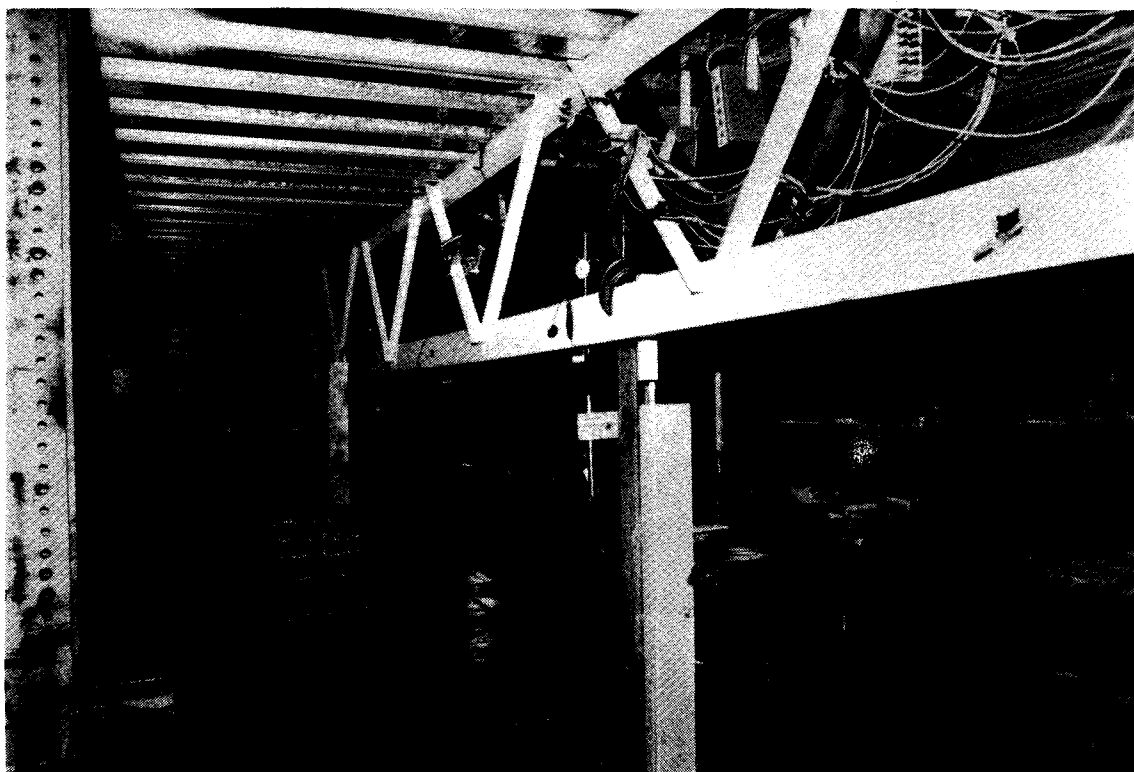


Figure 9.11 Composite truss 2 at load of 100 kN per jack

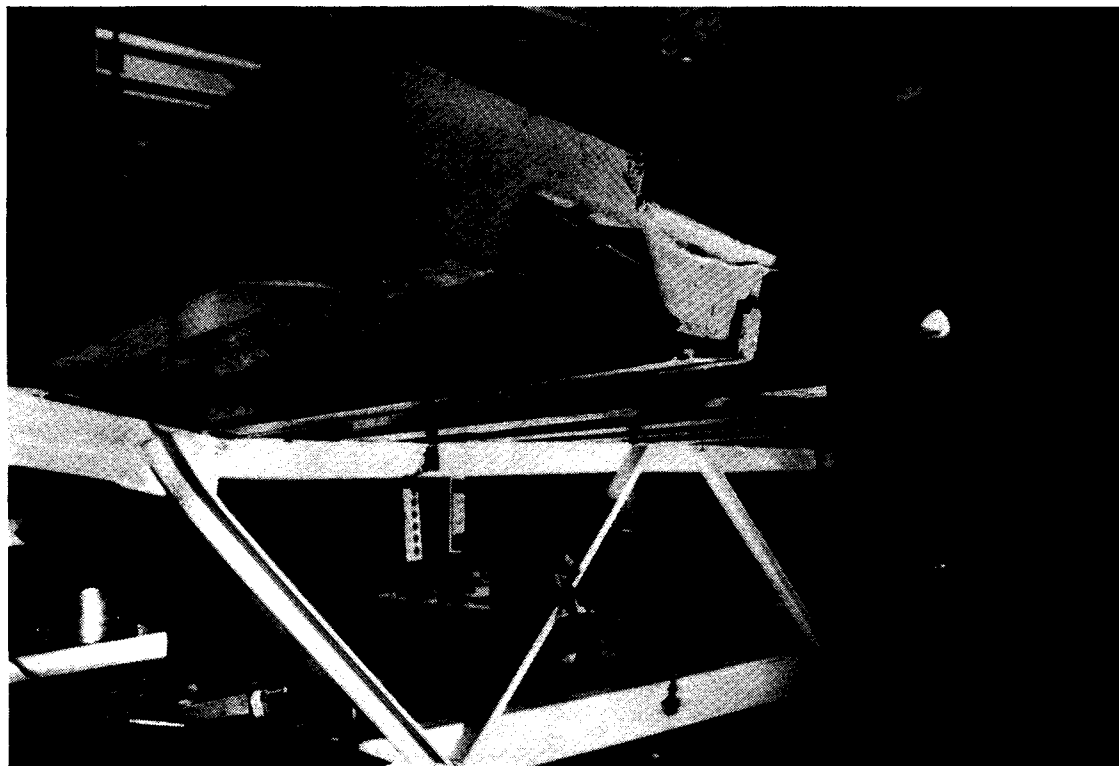


Figure 9.12 Separation of concrete from deck at north end of truss 2

midspan deflection of 245 mm. At this load, the longitudinal centreline crack in the concrete slab had progressed almost the full length of the truss. Figures 9.12 to 9.14 show the damage to the integrity of the composite truss at a load of 108 kN, caused by the loss of shear connection. The separation between the concrete slab and the metal deck is evident in Fig. 9.12. The end section of the concrete slab behaved as though it were hinged, resulting from a transverse crack at the north end of the slab, shown in Fig. 9.13. Due to the loss of composite action, the top chord was failing locally in bending at the location where the top chord shear reinforcement at the reaction terminated, as shown in Fig. 9.14. An attempt was made to increase the moment capacity of the top chord, hoping to reinforce the local weakness and allow the test to proceed further, by welding a 6 mm by 40 mm steel bar between the underside of the shear reinforcement and the underside of the top chord at panel point C. Fig. 9.15 shows that this modification had a limited effect, and enabled a maximum instantaneous load of 109 kN to be reached at a deflection of 262 mm before the load began to drop off. During this load increment, a second parallel crack line developed along the centreline of the concrete slab between the interior jacks. A further attempt to reinforce the buckle in the walls of the top chord by welding plates to the sides failed, and as the load dropped off to 102 kN at a midspan deflection of 287 mm, another shear connector at the north

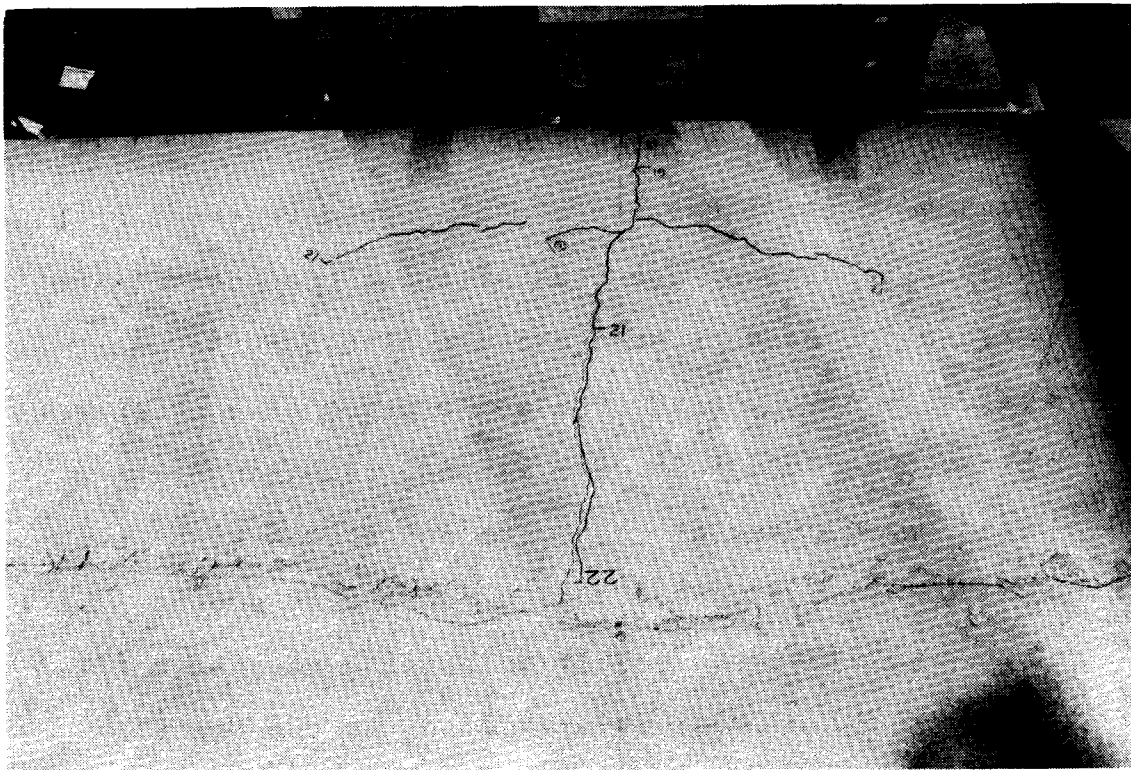


Figure 9.13 Transverse crack at north end of slab - truss 2

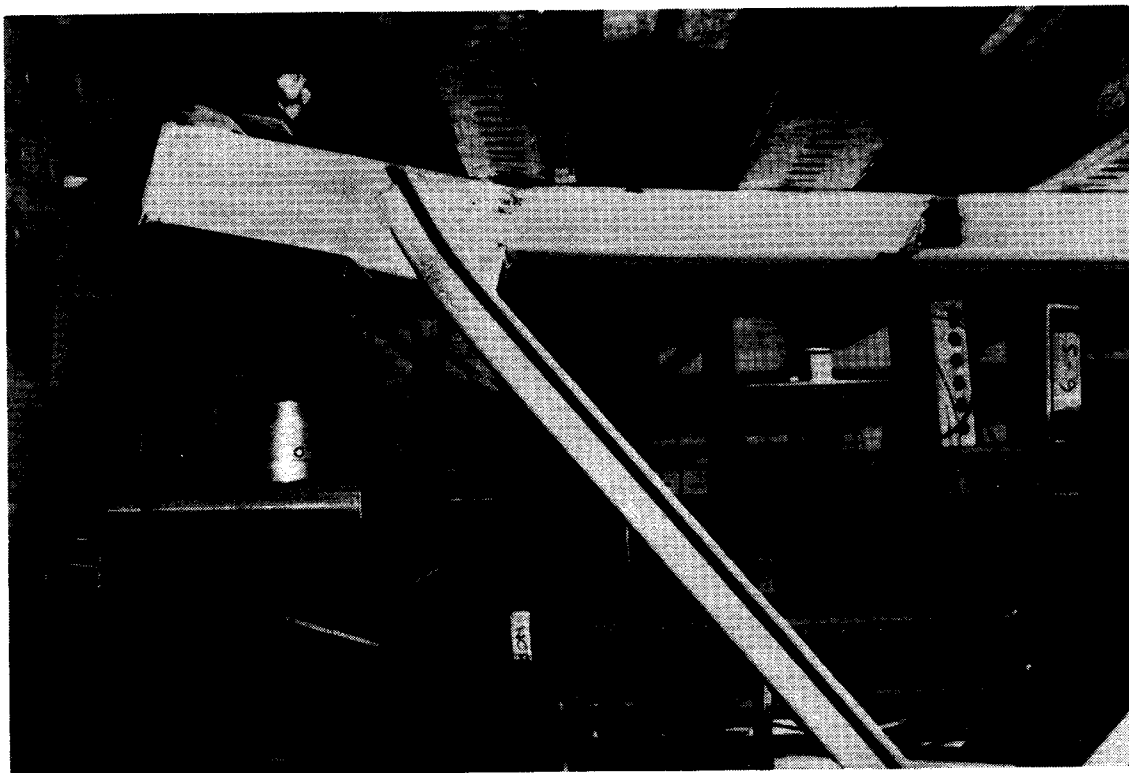


Figure 9.14 Local failure of top chord of truss 2

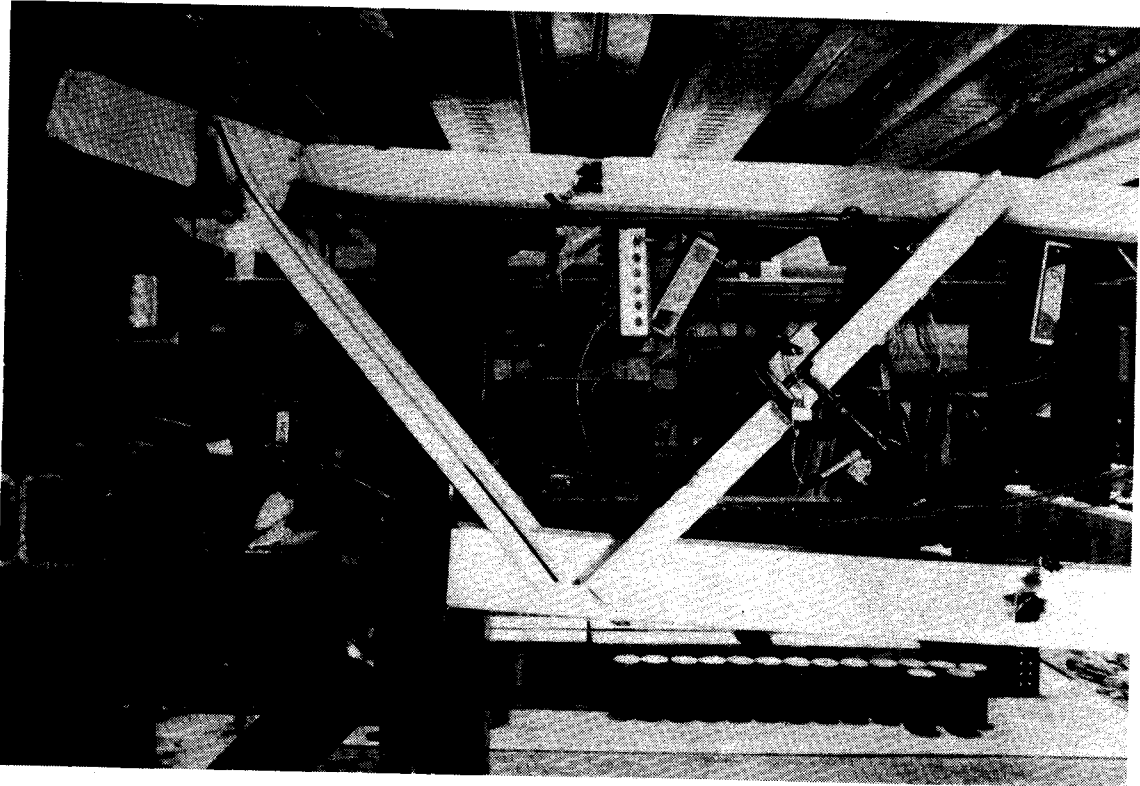


Figure 9.15 Reinforcement of top chord of truss 2 at maximum load

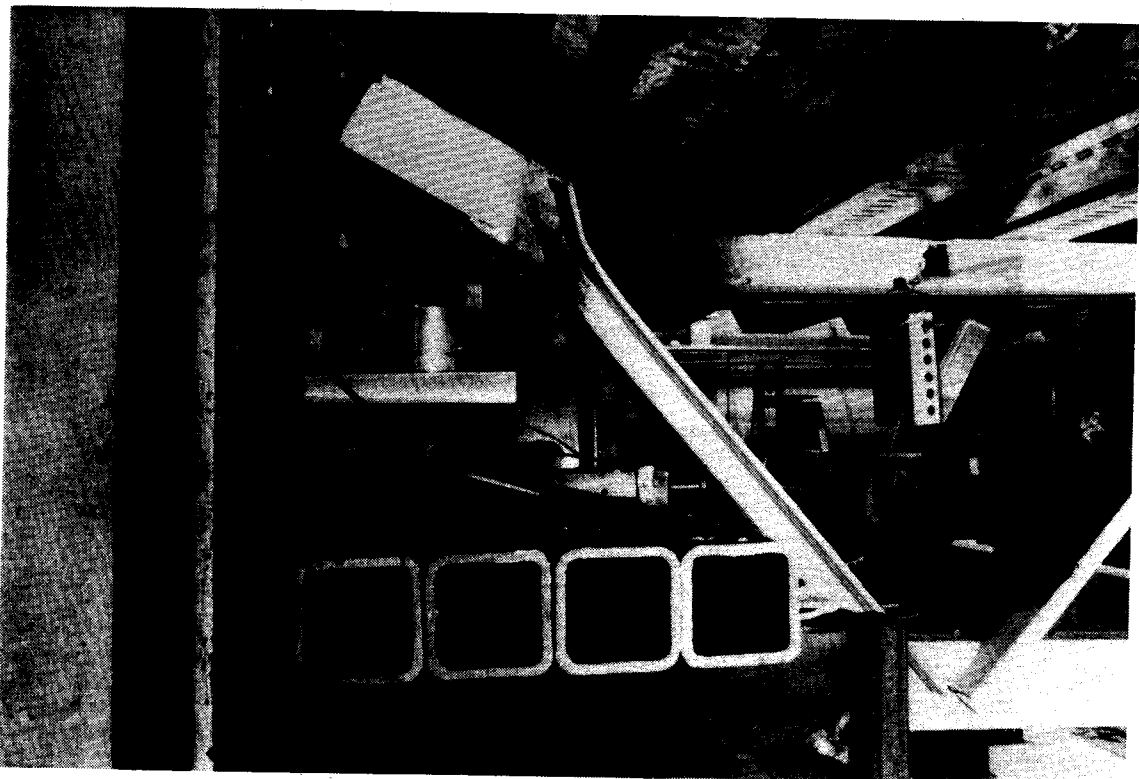


Figure 9.16 North end of truss 2 at failure

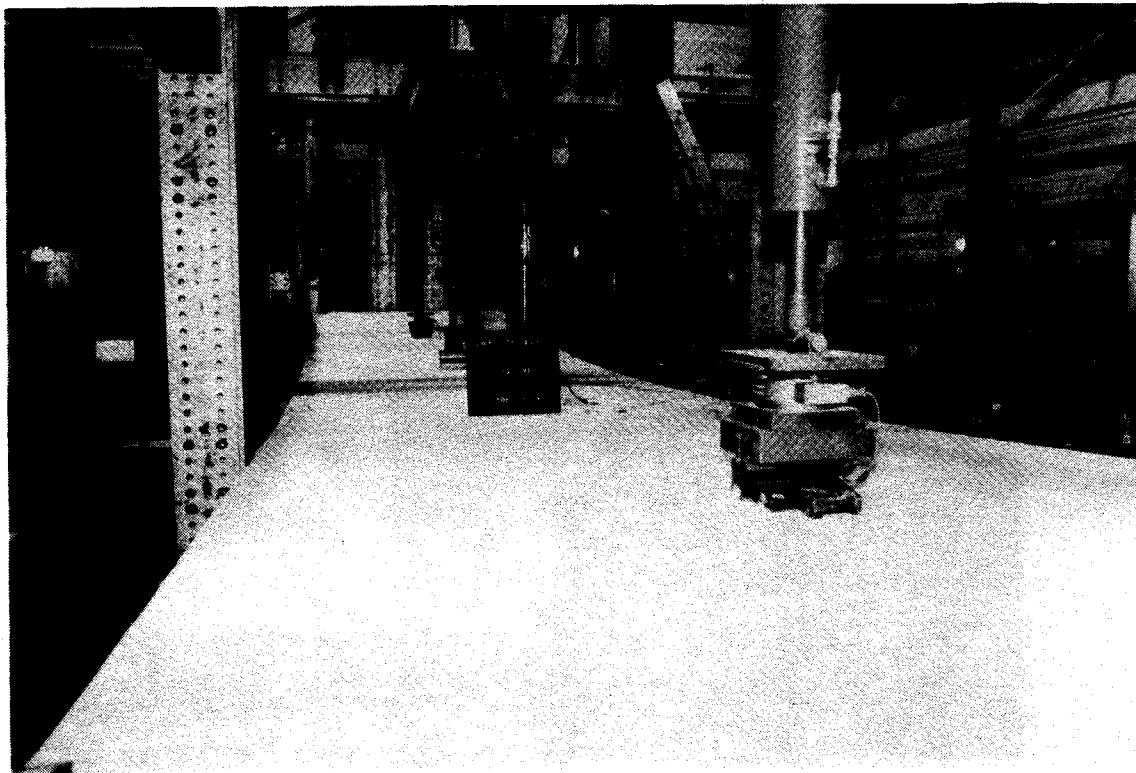


Figure 9.17 Deformed slab at failure - truss 2

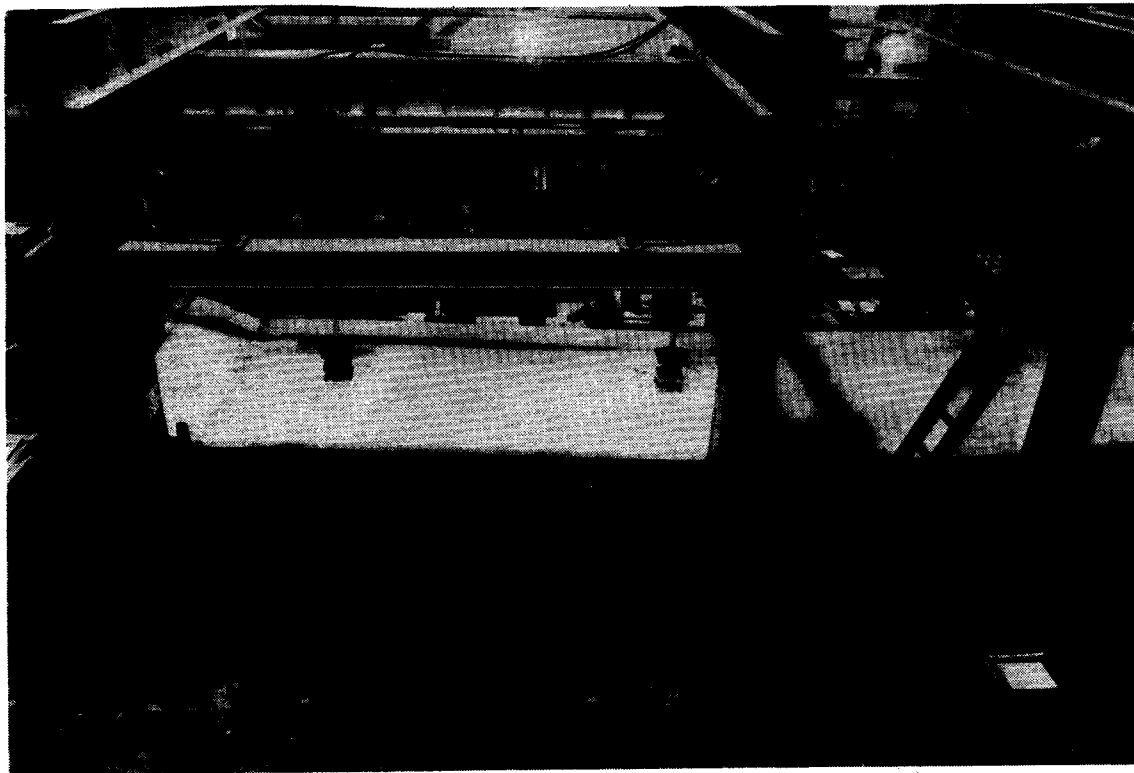


Figure 9.18 Truss 2 at failure

end failed, resulting in complete failure of the truss, as shown in Figs. 9.16, 9.17, and 9.18. After the test, the broken section of the concrete slab at the north end of the truss was removed, and revealed that the shear stud in the first concrete rib from the north end had been only superficially fused to the top chord, and that the shear stud in the second rib had sheared off, causing complete failure of the composite truss.

9.2 Bottom Chord Strains

In Figs. 9.19 and 9.20 are plotted test load versus midspan bottom chord strains for truss 1 and truss 2 respectively, obtained as the average of 4 strain gauges and, as well, from 2 Demec gauges. The plots are almost identical. The bottom chords of trusses 1 and 2 had initial tensile strains of $465 \mu\epsilon$ and $413 \mu\epsilon$ respectively due to the dead load of the steel deck and concrete and due to shrinkage, which are not shown in the figures.

For truss 1, the 0.2% offset yield strain of the bottom chord steel, equal to $4170 \mu\epsilon$, corresponds to a load per jack of 88 kN. The maximum strain reached was 1.21%, or 2.9 times the yield strain. This strain corresponds to a stress which is approximately 110% of the yield strength of the bottom chord and 91% of the ultimate strength. As the load on the truss fell off, the bottom chord strains decreased elastically.

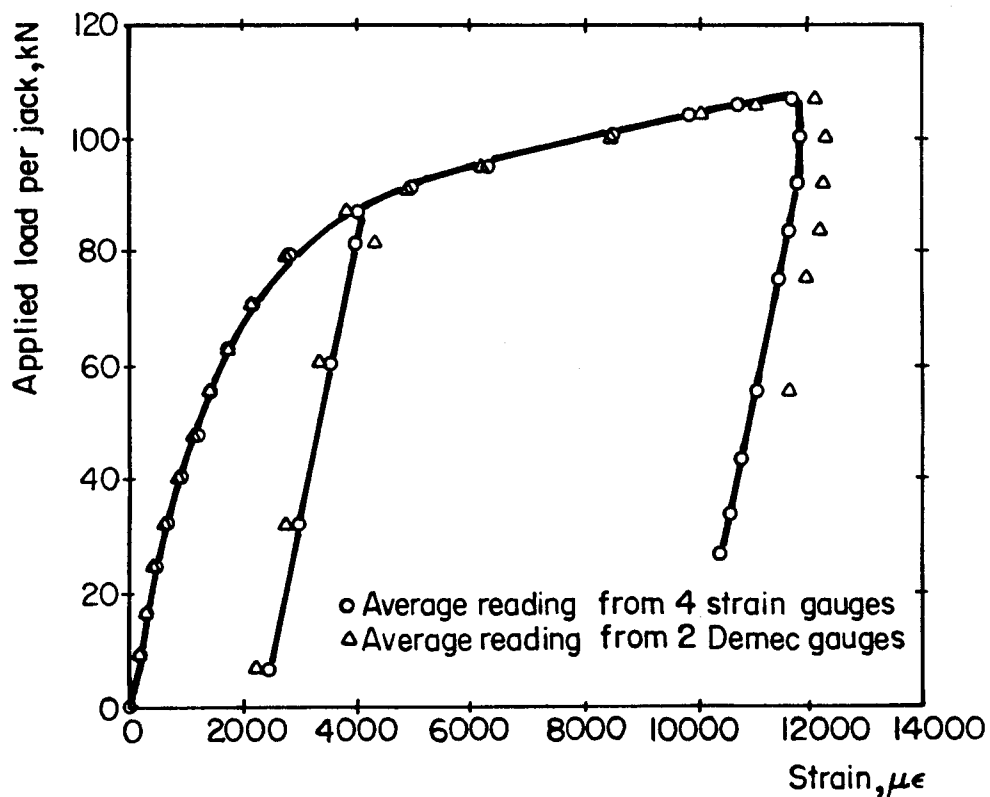


Figure 9.19 Bottom chord strains at midspan - composite truss 1

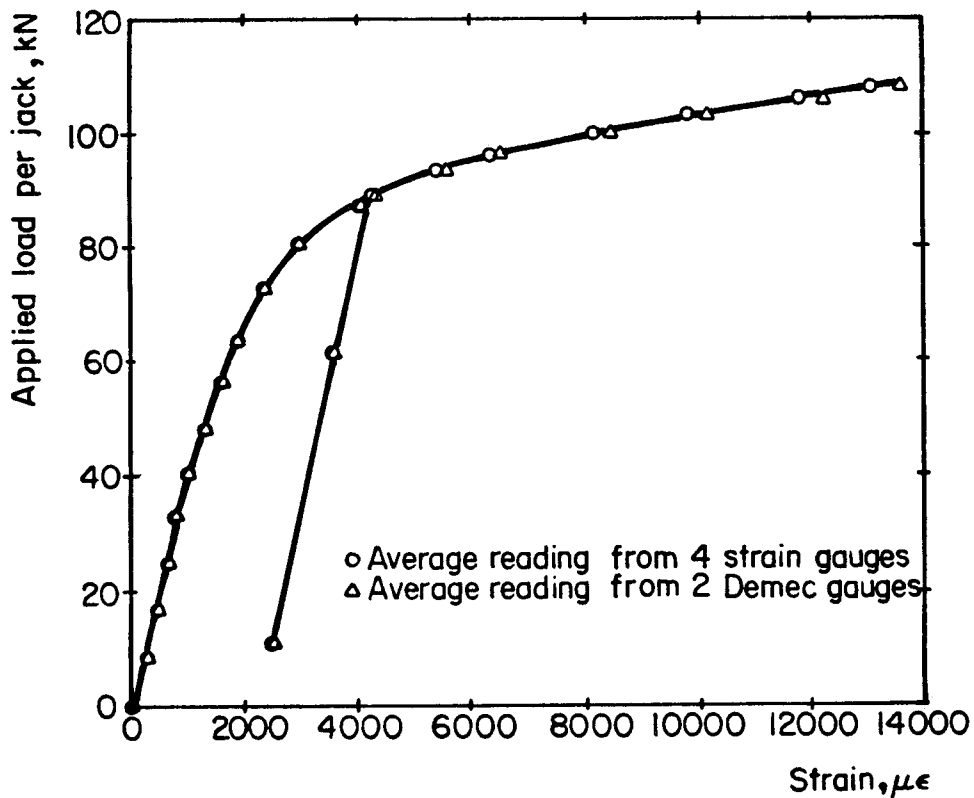


Figure 9.20 Bottom chord strains at midspan - composite truss 2

From Fig. 9.20, using the yield strain of $4170 \mu\epsilon$, the bottom chord of truss 2 began to yield at a load of 88.5 kN per jack. The bottom chord reached a maximum strain of 1.36%, equal to 3.3 times the yield strain, at a stress equal to 111% of the yield strength and 92% of the ultimate strength of the bottom chord steel.

9.3 Top Chord Strains

The test load versus top chord strains at midspan, averaged from 4 strain gauges, are plotted in Figs. 9.21 and 9.22 for trusses 1 and 2 respectively. The plots show similar behaviour.

Both top chords had initial compressive strains due to the dead load of the steel deck and concrete and due to shrinkage. As test loads were applied, these compressive strains diminished, eventually becoming tensile near the load at which the bottom chord began to yield. At maximum load, the top chord is strained appreciably in tension, to approximately one quarter of the yield strain, showing that the top chord contributes to the flexural strength of the composite truss.

9.4 Concrete Strains

Figures 9.23 and 9.24 are plots of test load versus average strain at midspan on the top surface of the concrete slab of trusses 1 and 2 respectively. The average strains were obtained from 7 sets of Demec points on truss 1 and

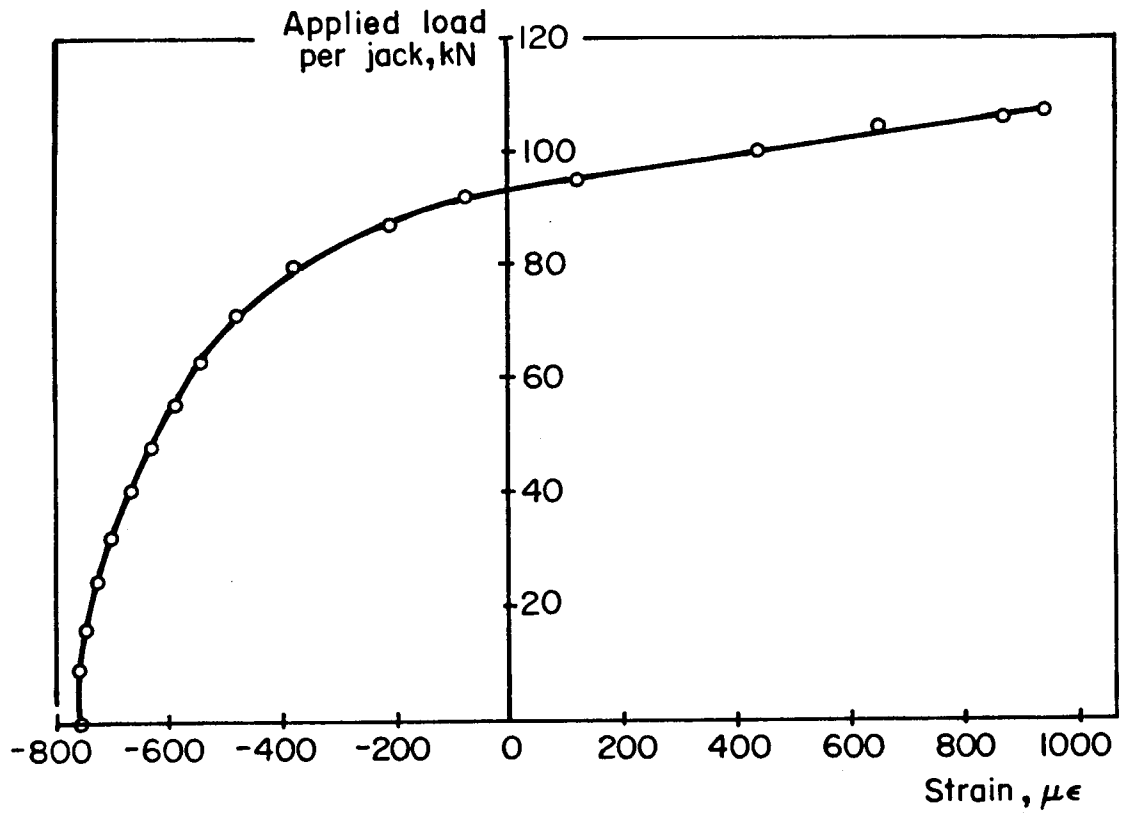


Figure 9.21 Top chord strains at midspan - composite truss 1

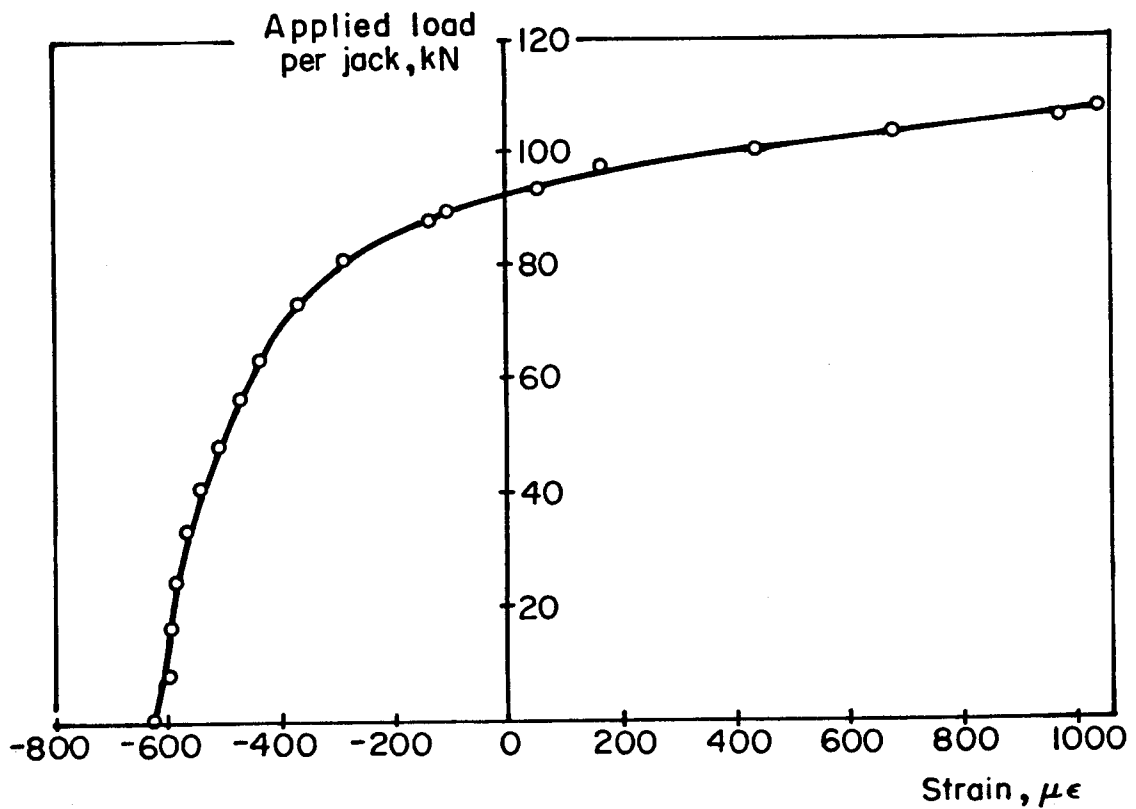


Figure 9.22 Top chord strains at midspan - composite truss 2

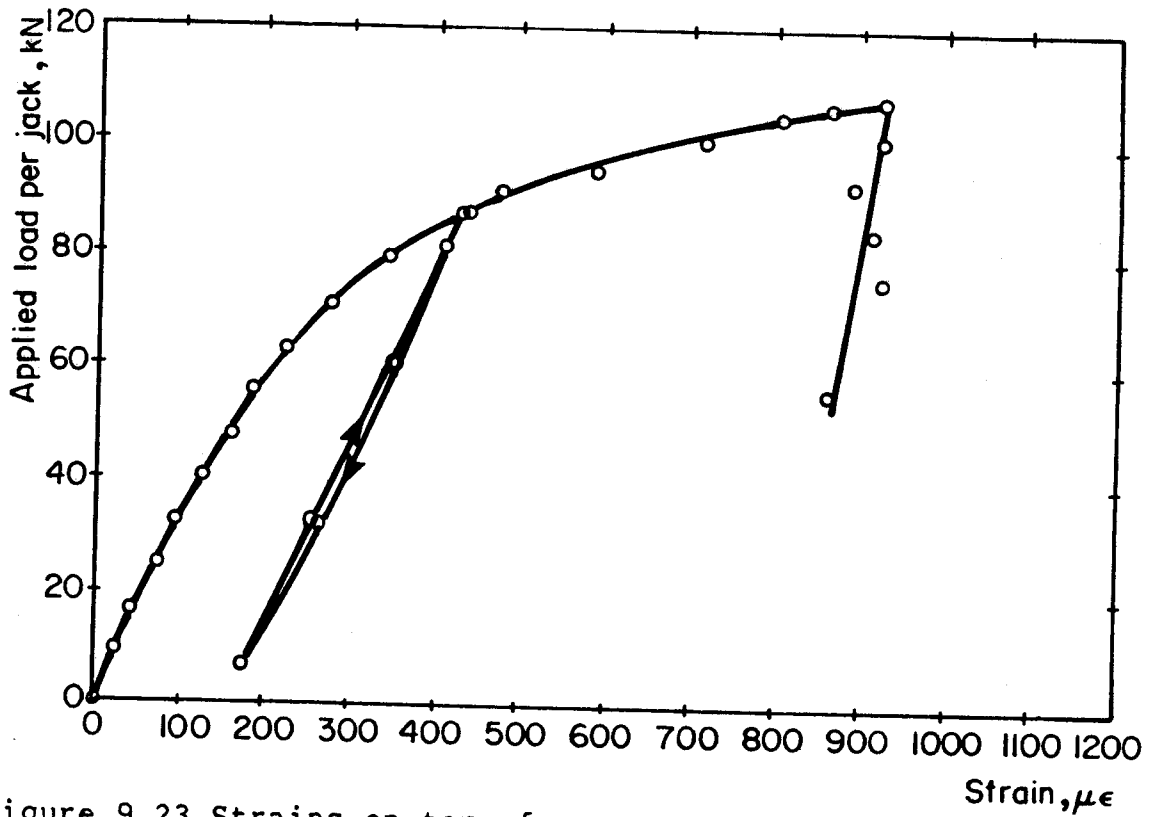


Figure 9.23 Strains on top of concrete slab at midspan - truss 1

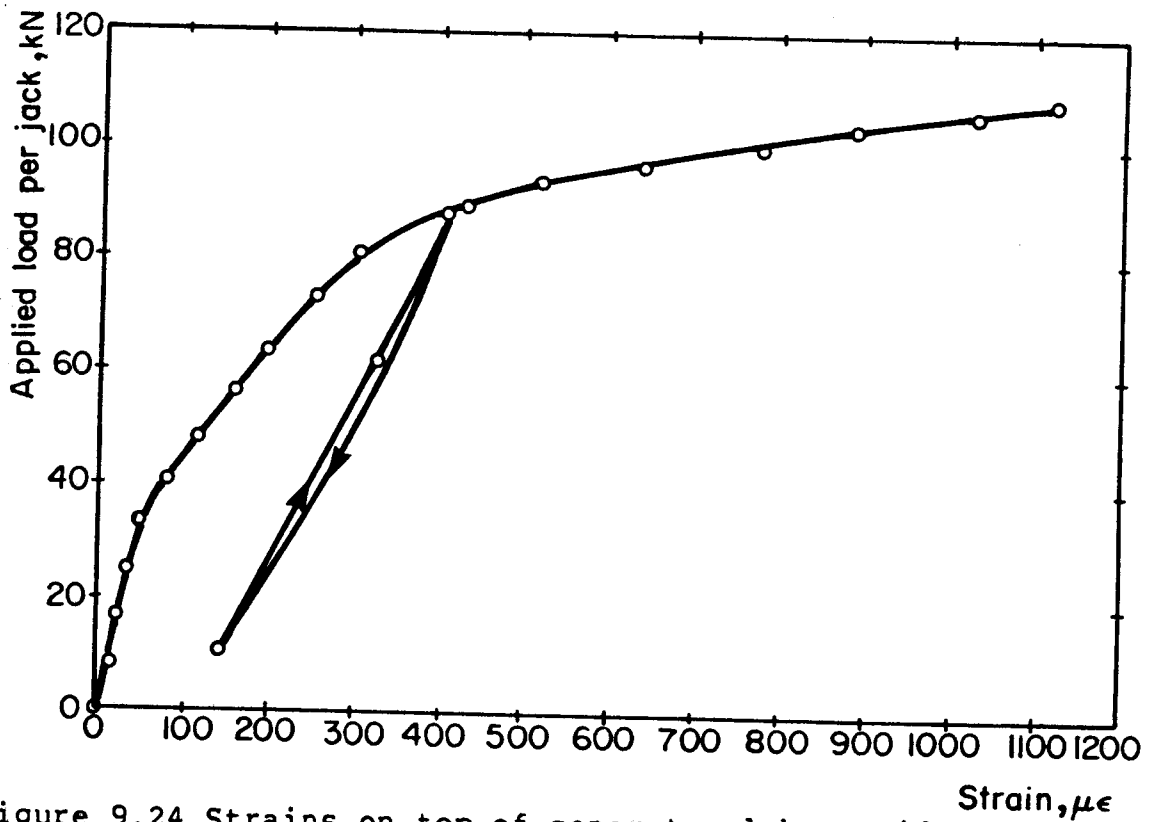


Figure 9.24 Strains on top of concrete slab at midspan - truss 2

from 5 sets of Demec points on truss 2. The initial compressive strains of $360 \mu\epsilon$ for truss 1 and $491 \mu\epsilon$ for truss 2 due to shrinkage of the concrete slab are not plotted in the figures. In both plots, the strains vary non-linearly with load and increase more rapidly beyond the load corresponding to yielding of the bottom chord. On truss 1, the maximum average concrete strain reached of $925 \mu\epsilon$ is about 39% of the strain at maximum load obtained from cylinder tests between 30 and 143 days. With unloading from the maximum strain, little elastic recovery took place. The maximum average concrete strain on truss 2 at midspan was $1118 \mu\epsilon$, 56% of the strain at maximum load measured from cylinder tests at 118 days.

The distribution of concrete strains across the width of the slab on truss 1 is shown at 2 locations along the length, in Figs. 9.25 and 9.26, for several load levels. At midspan, the distribution of strains across the width, plotted in Fig. 9.25, is relatively uniform, especially at low load levels, and indicates that there is no evidence of shear lag. At the higher load levels, gauge 6 (numbered from the left) in particular and gauge 7 to a lesser extent, exhibit somewhat higher strains than the remainder. The shrinkage strain measured at gauge 6 was the reverse, suggesting that the concrete in this area had a lower modulus of elasticity. Figure 9.26 shows the transverse distribution of concrete strains 400 mm from the north end of the slab for six of the same loads as shown at midspan in

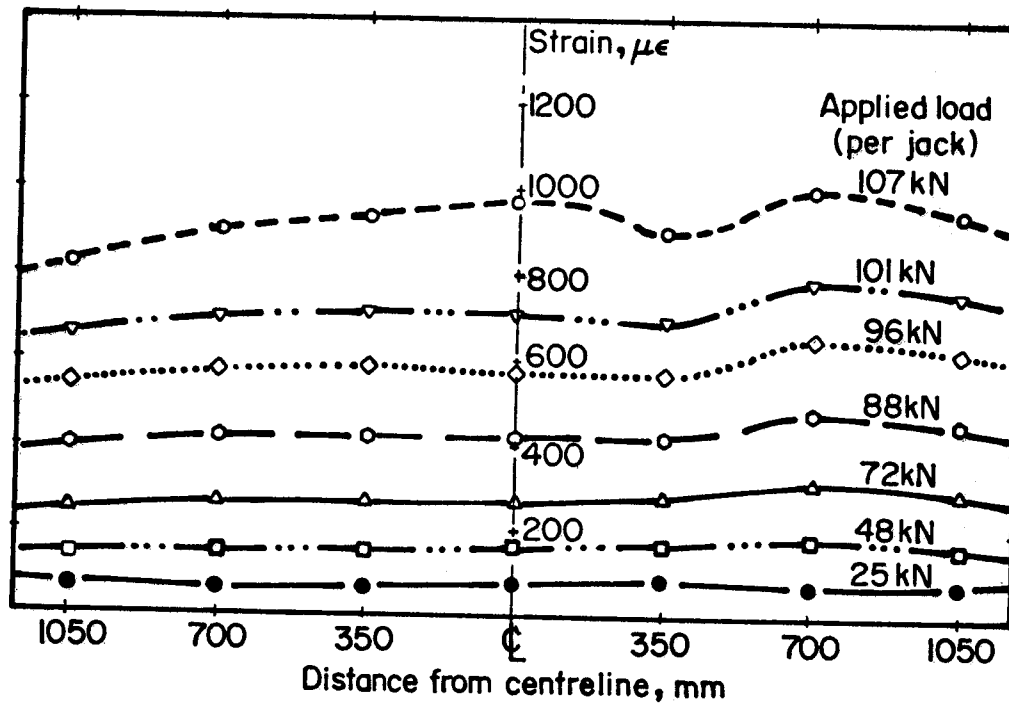


Figure 9.25 Midspan concrete surface strains across the slab - truss 1

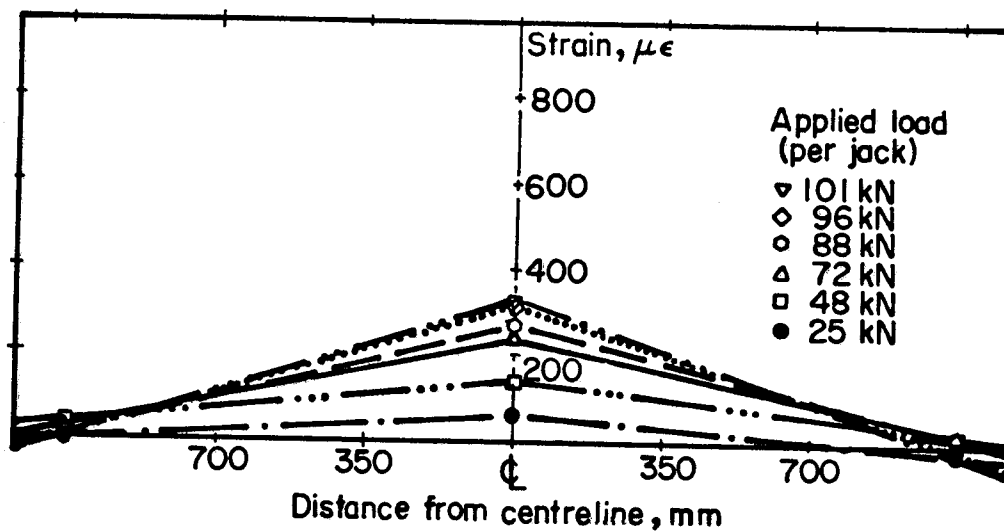


Figure 9.26 North end concrete surface strains across the slab - truss 1

Fig. 9.25. It is apparent that the strains are much less here, as would be expected, and that significant shear lag exists, with the strains near the west and east edges being essentially zero.

Figures 9.27 to 9.30 show the distribution of concrete strains across the width of the slab at 4 locations along the length of truss 2 at various load levels. At midspan, the strain distribution is relatively uniform, as shown in Fig. 9.27, and there is very little evidence of shear lag, even at the higher loads. Plots of the transverse strain distribution at $0.074L$, $0.195L$, and $0.317L$ in Figs. 9.28 to 9.30 respectively indicate that, at each location, the strains are uniform at low load levels and only minimal shear lag exists at the higher load levels. This is contrary to the results from truss 1, where significant shear lag was observed close to the ends of the slab. This may be because the truss 1 measurements are closer to the ends of the slab than those of truss 2. As expected, the magnitudes of the strains increase moving towards the midspan.

9.5 Variation of Strain Through Truss Depth

The strain variation through the depth of each truss in the constant moment region at or near midspan is plotted in Figs. 9.31 and 9.32 for selected loads. Straight lines have been fitted to the measured strains, neglecting any discontinuity at the interface between the top chord and the concrete slab due to slip. The straight lines fit the data

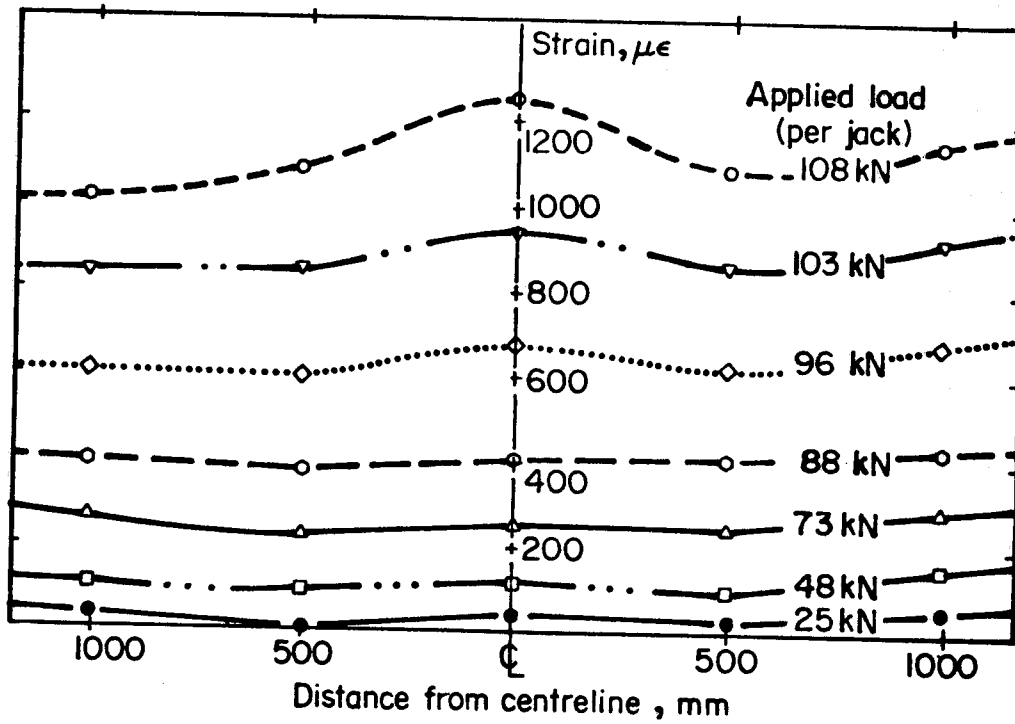


Figure 9.27 Midspan concrete surface strains across the slab - truss 2

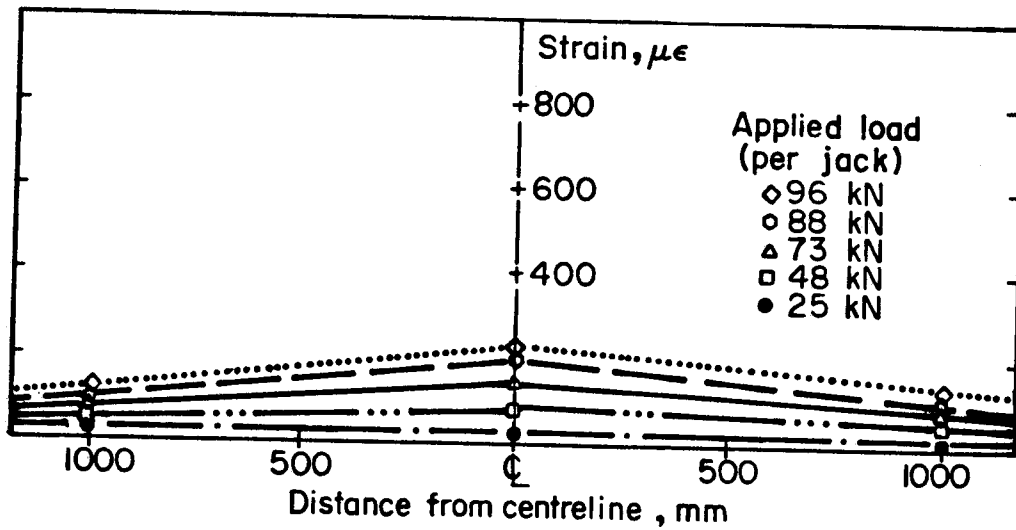


Figure 9.28 North end concrete surface strains across the slab - truss 2

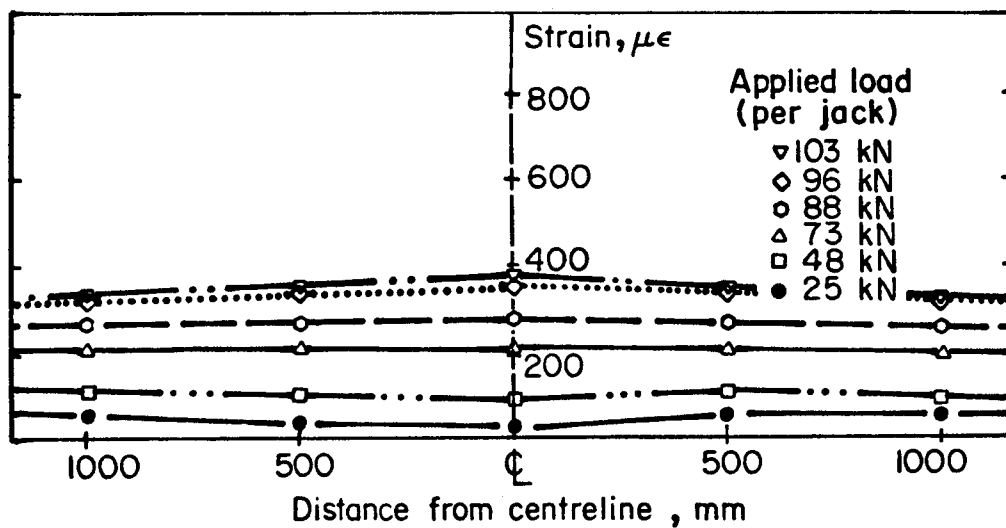


Figure 9.29 Concrete surface strains across the slab at 0.195L - truss 2

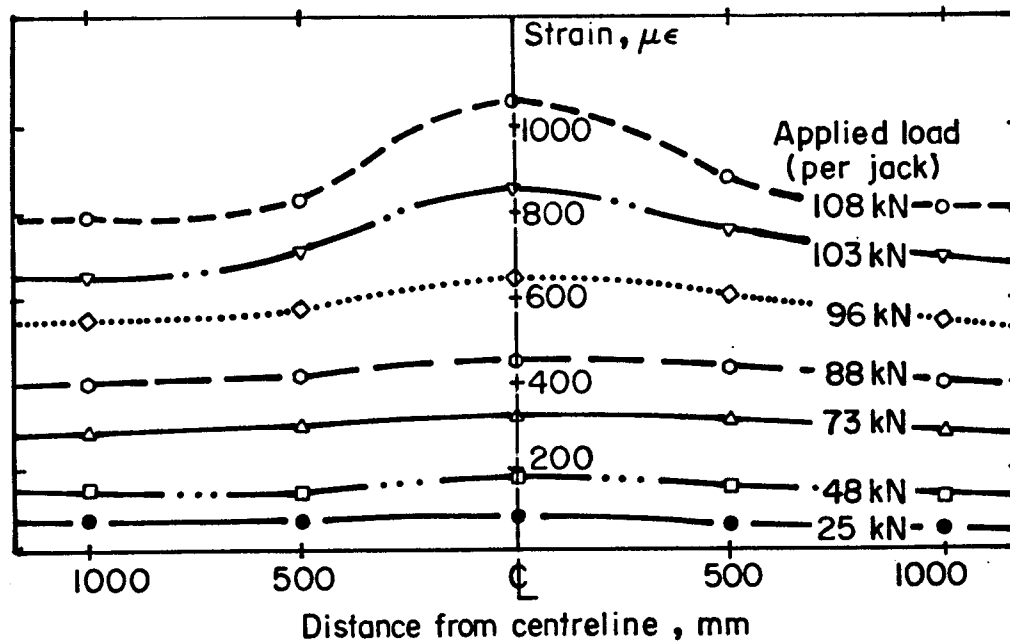


Figure 9.30 Concrete surface strains across the slab at 0.317L - truss 2

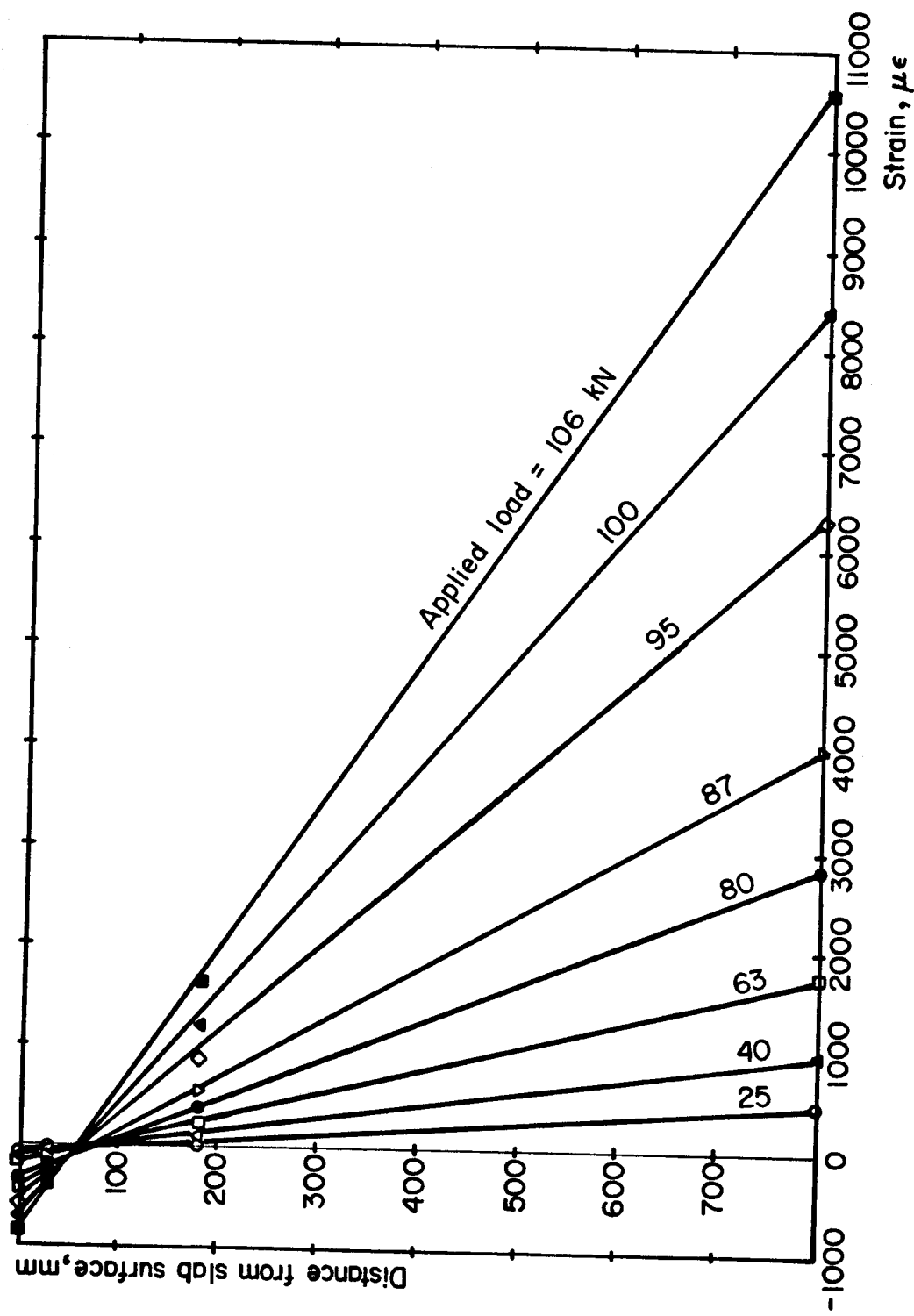


Figure 9.31 Strain variation with depth - truss 1

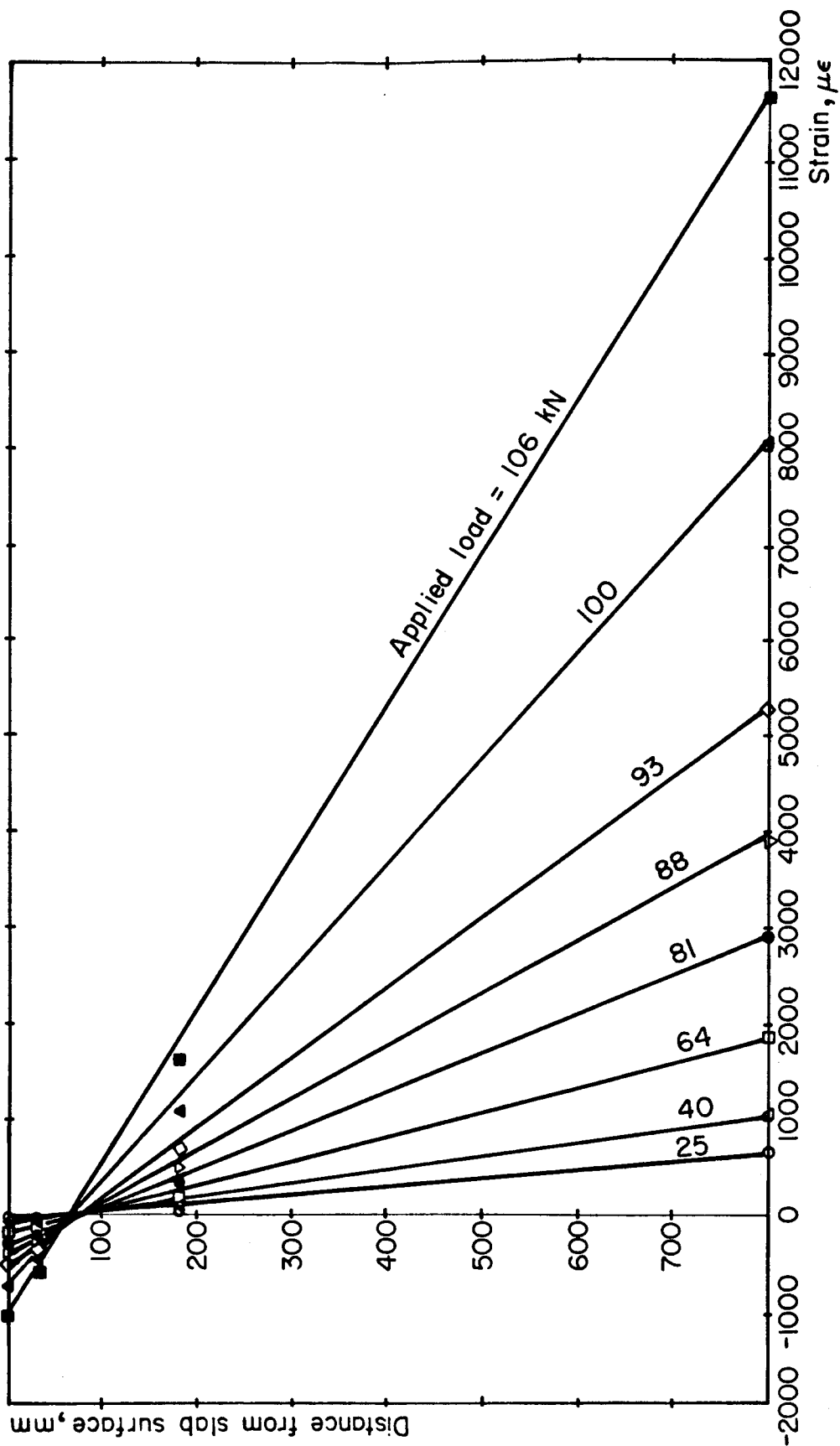


Figure 9.32 Strain variation with depth - truss 2

well and show that the position of the neutral axis rises for the higher loads, indicating that the bottom chord is yielding. It is also noted that the top chord is strained appreciably in tension, as discussed in Section 9.3, and must be contributing to the flexural strength of the composite truss.

9.6 Separation of Compression Angle Web Members

The out-of-plane separation at mid-height of the two angles comprising web members BC and QR of truss 1 are plotted versus load in Fig. 9.33. Assuming the two angles of each web member behave in the same fashion, the movement of one angle would be half of that shown. The behaviour of web members BC and QR are very similar. The slope of the load-separation curves changes from an initial value (parallel to the unloading curves) to a considerably smaller value at a load on the truss of about 38 kN. The maximum displacement of one angle of 1.95 mm at maximum load is $1/445$ of the out-to-out length of the angle. At the maximum load, both load-separation curves have a positive slope.

On truss 2, the out-of-plane separation at mid-height of 6 web members was monitored. To compare the behaviour of the web members of truss 2 with those of truss 1, the mid-height separation of the two angles comprising web members BC and QR of truss 2 are plotted versus load in Fig. 9.34. These plots have a shape very similar to those in Fig. 9.33, with a distinct change in slope at a load of about

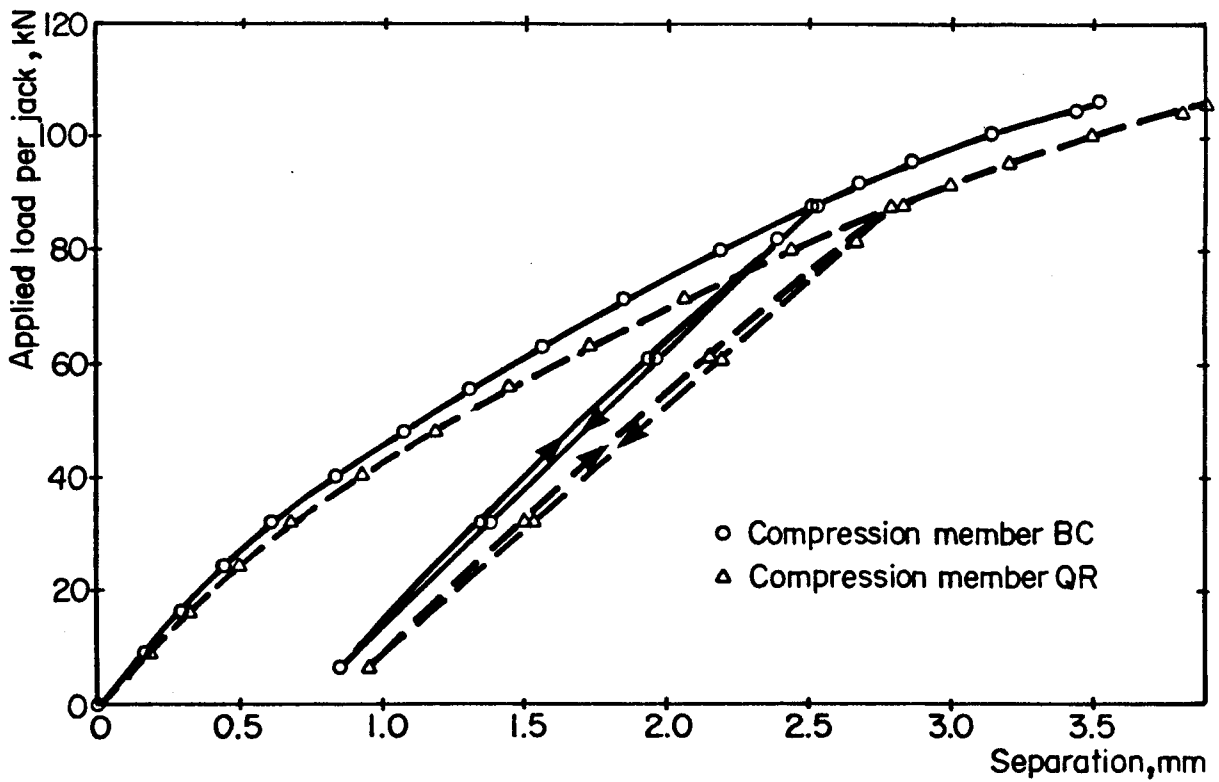


Figure 9.33 Separation of angle web members at mid-height - truss 1

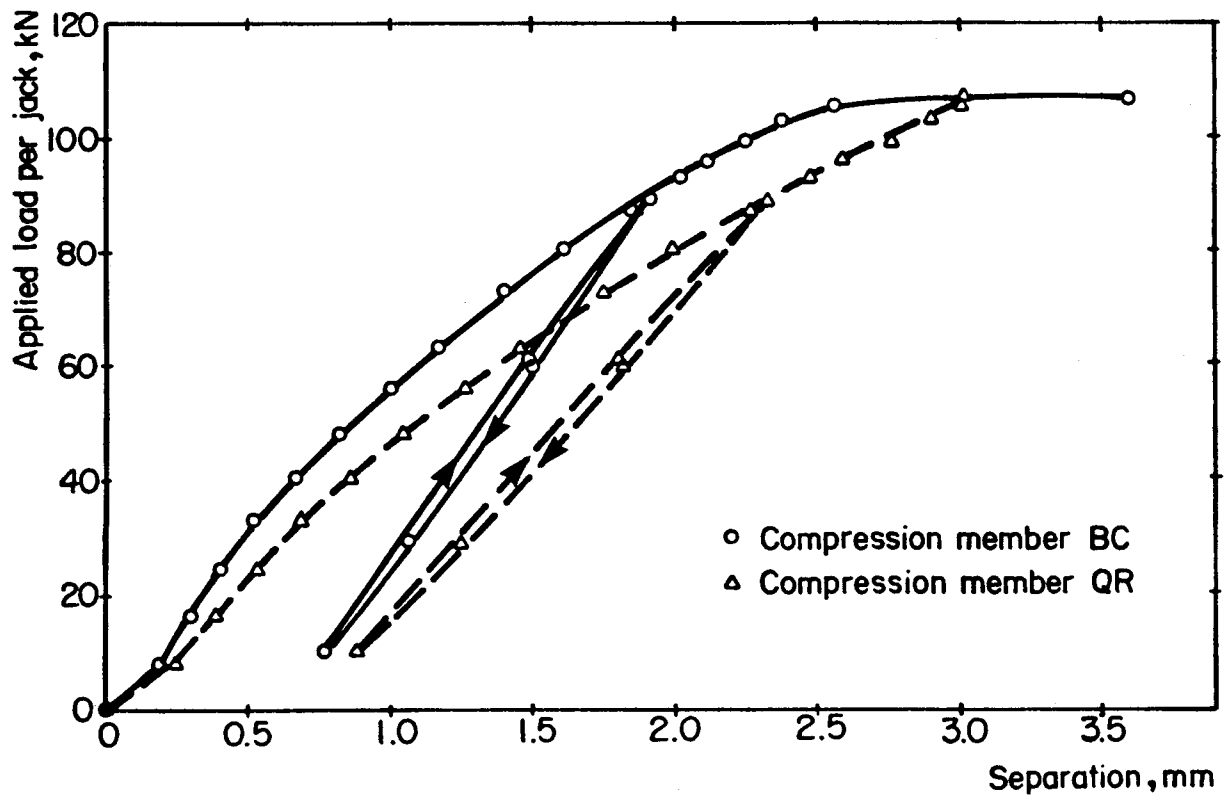


Figure 9.34 Separation of angle web members at mid-height - truss 2

40 kN. However, the maximum displacement of one angle of 1.79 mm, or 1/485 of the out-to-out length of the angle, is less than the maximum value recorded during the test of truss 1, although the second test reached a higher load. This improved performance may be attributable to more effective load transfer as a result of the improved performance of the extended stud shear connection. Web members BC and QR exhibit similar behaviour and their load-separation curves have a positive slope up to the failure load.

9.7 Interface Slip Between Slab and Top Chord

Figure 9.35 plots the test load versus slip measured between the slab and top chord of truss 1 at the north and south ends and at the north quarter point. Even though the first shear connector failure occurred at panel point N, the south end slip was less than that at the north end. The quarter point slip, as expected, was less than the end slips. All slips were initially linear, then deviated from a straight line at something less than one half the maximum load attained—at about the same load where the truss behaviour as a whole became non-linear. When the maximum load was reached, the north end slip increased very rapidly and was followed by a large increase in the north quarter point slip. A modest but limited increase in slip occurred at the south end at maximum load. The very large slips of the north one quarter of the truss indicate that shear

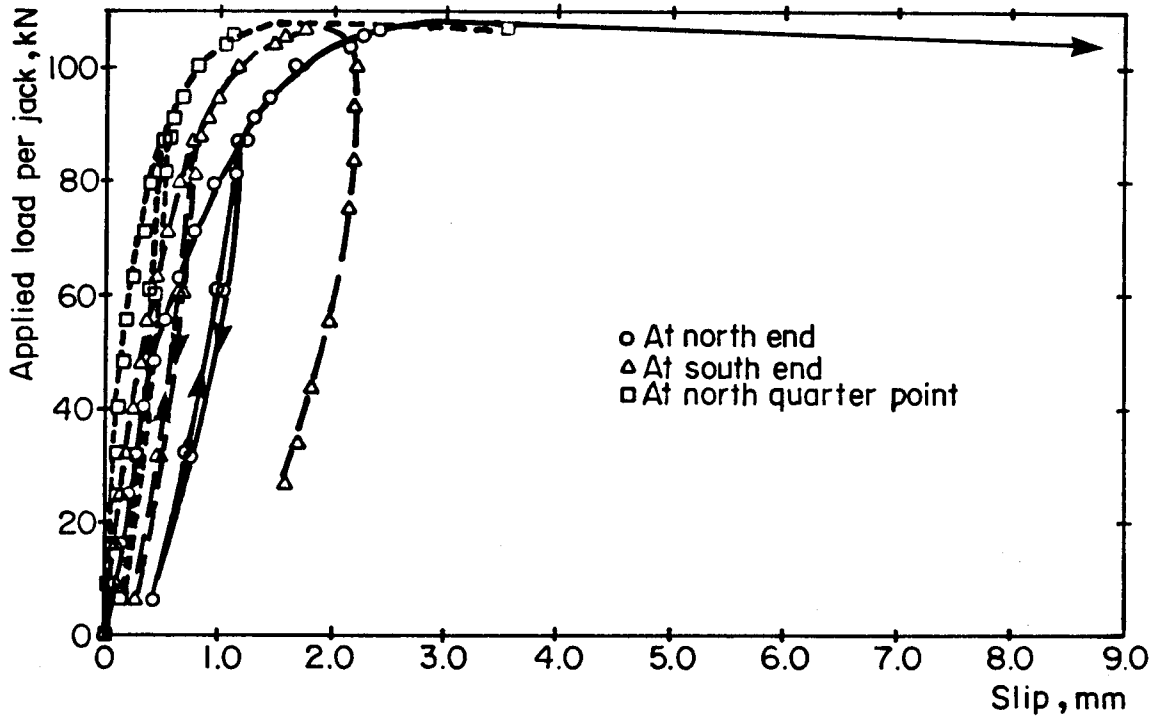


Figure 9.35 Interface slip - truss 1

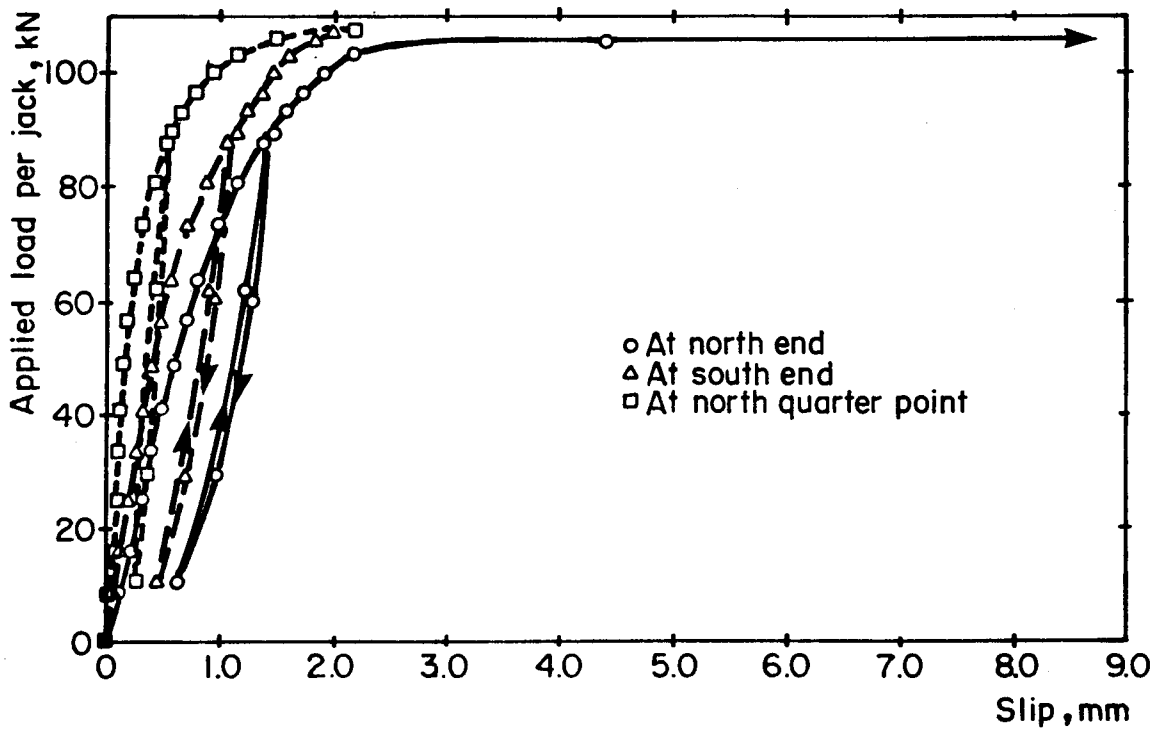


Figure 9.36 Interface slip - truss 2

connector failure had occurred.

The load-slip curves for truss 2, plotted in Fig. 9.36, have shapes similar to those of truss 1. The diagrams become non-linear at a load of about 40 kN when the truss behaviour as a whole becomes non-linear. Similar to the first test, the north end slip was somewhat larger than the south end slip, and was a good indication that eventually, failure would occur in the north half of the span. Between a load of 103 and 106 kN, the dramatic increase in the magnitude of the north end slip indicates that a shear connector had failed. Approaching the maximum load, another large increase in the north end slip and only a modest increase in the north quarter point slip indicate the local nature of the shear connection failure.

9.8 Failure Modes

Failure of truss 1 occurred at a maximum load of 107 kN per jack and a midspan deflection of 212 mm. At this load, the midspan steel strain was 1.21% corresponding to 91% of the ultimate strength of the bottom chord. Cracking noises and a lifting of the slab from the deck beyond a load of 105.8 kN indicated that rupture was occurring between the deck and the slab. The significant increase in end slip at maximum load also shows that the shear connection was failing. Failure was precipitated by shear connection failure progressing inward from the north end toward the centre. Between load points, the slab lifted away from the

truss. With continued deflection, the very pronounced distortions of the top chord and the lack of shear connection resulted in a significant decrease in the load carried. The truss, however, exhibited considerable ductility. Subsequent examination of the zones around the studs at the north end showed that, in eleven of the fourteen cases where failure occurred, a cone of concrete around the stud had apparently failed in tension (designated as a shear cone failure by Iyengar and Zils, 1973). The top of each cone was level with the top of the stud and extended downward at an angle of about 45° to intersect the walls of the flute. Transversely, the cones were between 200 and 770 mm wide. Two studs were pulled off the top chord, and in one case, the stud pulled out of the top chord. Several studs were severely distorted, the deck was torn at many stud locations, and the seams between deck panels were ripped.

Although the stud length of 106 mm before welding just met the minimum requirements given in CSA Standard S16.1 for projection of the stud above the top of the flute, the failure surfaces through the concrete suggest that the studs should have been longer. Indeed, it could be argued that they should extend into the flexural compression zone of the concrete. Grant et al. (1977) recommend a minimum projection of the stud above the top of the flute of:

$$[9.1] \quad H - h_d = \frac{1}{0.85} \left[\frac{h_d^2}{w_d} \right]$$

to ensure that the stud has the same shear capacity as one in a solid slab. This equation indicates that a stud length of 121 mm is required. For truss 2, the studs were extended by 25 mm to within 10 mm of the concrete surface to meet this requirement. A short length of 16 mm diameter A307 bolt, with a washer of the same diameter as the stud head welded to it, was welded to each stud.

Truss 2 failed at a maximum load of 109 kN per jack and a midspan deflection of 262 mm. The midspan steel strain at maximum load reached a higher value than that of truss 1, equal to 1.36% or 92% of the ultimate strength of the bottom chord, indicating that the extended stud shear connectors did improve the performance of the composite truss. Except for a local shear connection failure at the north end, the truss would undoubtedly have continued to take further load, and the bottom chord steel at midspan might have reached its ultimate strength (assuming that the web members and shear connectors continued to perform satisfactorily). A tinny sounding bang during the load increment from 103 to 106 kN, accompanied by the formation of a 700 mm long centreline crack at the north end of the slab and a large increase in the north end slip, were the first indications that the shear connection was beginning to fail. During the next loading increment, the concrete slab began to separate from the deck over the first flute from the north end and the top chord began to fail in bending at the location where the reaction shear reinforcement was terminated. Attempts to

reinforce the top chord to resist the additional moment that it was forced to carry because of the shear connection failure had a limited effect. Another shear connector failed at the north end as the load dropped off from the maximum load of 109 kN, terminating the load-carrying ability of the composite truss. Upon removal of the broken concrete slab at the north end of the truss, it was found that a faulty weld of the stud in the first concrete rib from the north end (the one which, in theory, resists the largest force) led to the failure. The stud was only superficially fused to the top chord and therefore was unable to transfer the required interface shear or provide the tensile restraint to prevent the slab from lifting off the top chord. The overloaded stud in the second concrete rib from the north end sheared, resulting in failure of the composite truss. That stud exhibited no distortion.

Calculations show that, had the two end studs reached their shear capacity, the axial load and moment coexisting in the top chord at the end of the reaction shear reinforcement would have resulted in an interaction value of 0.7 in the axial load-moment interaction equation. With only one stud participating, the interaction value at a test load of about 104 kN reaches 1, consistent with the failure mode.

10. ANALYSIS OF FLEXURAL TESTS

10.1 Effective Moment of Inertia of Composite Trusses

To calculate the deflection of composite members, Clause 17.3.1.1 of S16.1 requires that the effects of creep and shrinkage of the concrete and increased flexibility due to partial shear connection and interfacial slip be taken into account. For composite trusses, which must be designed with full shear connection, increased flexibility results both from the open web system and from interfacial slip. This increased flexibility can be calculated as described in Section 3.1.5. Using this procedure, a value of $805.9 \times 10^6 \text{ mm}^4$ was obtained for the effective moment of inertia of composite truss 1 and a value of $784.6 \times 10^6 \text{ mm}^4$ was calculated for composite truss 2. These values do not include the effects of creep and shrinkage.

To verify this calculation procedure, the value of the effective moment of inertia for each composite truss was determined from the results of the short term load tests. Given that the deflection at midspan of a simply supported beam with 4 concentrated loads, located as shown in Fig. 4.7 (the test loading configuration), is

$$[10.1] \quad \Delta = \frac{41}{768} \left[\frac{P L^3}{E I} \right]$$

the effective moment of inertia can be computed from the slope of the initial linear portion of the applied

load-midspan deflection curves in Figs. 9.1 and 9.10. The method of least squares was used to fit a straight line to the data, after the limits of the linear portion of the curve were determined from the trend of a 3 point moving average of the tangent modulus. The effective moment of inertia of composite truss 1 was found to be $692.7 \times 10^6 \text{ mm}^4$, only 86% of the calculated value. Similarly, the effective moment of inertia of composite truss 2 was $700.1 \times 10^6 \text{ mm}^4$, or 89% of the calculated value. These results indicate that the trusses were more flexible than the calculations would predict. The smaller effective moment of inertia of composite truss 1 compared to composite truss 2 can be attributed to the greater flexibility of steel truss 1 compared to steel truss 2, as discussed in Section 8.1.

Based on this, a modification to the procedure used to calculate the effective moment of inertia of composite trusses is recommended (as originally proposed by Cran, 1972), which agrees more closely with the measured values of the effective moments of inertia of the test trusses. The effect of an open web on member deflection for a composite truss should be similar to that of a steel truss. Therefore, the transformed moment of inertia of the composite truss should be decreased by the ratio $1/1.10$, the same factor used to reduce the moment of inertia of a steel truss to account for the flexibility of the open web system. Using the measured values reflecting the decreased stiffness due to the open web, found in Section 8.1, this results in

effective moments of inertia of $733.7 \times 10^6 \text{ mm}^4$ for composite truss 1 and $740.5 \times 10^6 \text{ mm}^4$ for composite truss 2. These are 94% of the calculated values. From this, it is deduced that the effective moment of inertia in [3.7] should be calculated based on a fraction equal to 0.77, so that equation [3.7] becomes

$$[10.2] \quad I_e = I_s + 0.77 (p)^{0.25} (I_t - I_s)$$

10.2 Moment-Deflection Response

Non-dimensionalized moment-deflection curves for composite trusses 1 and 2 are shown in Figs. 10.1 and 10.2 respectively. The moments were non-dimensionalized by dividing by the yield moment of each composite truss calculated from the measured cross-sectional properties and the measured material properties of the steel chords and concrete slab. The moments plotted include the dead load moment of each truss (98.3 kNm for truss 1 and 97.9 kNm for truss 2). The deflections were normalized by dividing by the midspan deflection at yield, calculated by assuming that the behaviour is elastic until attainment of the yield moment. To draw each curve through zero, the test deflections, due to applied concentrated loads only, were increased by an amount equal to the elastic deflection that would have occurred due to the dead weight of each truss acting on the composite truss.

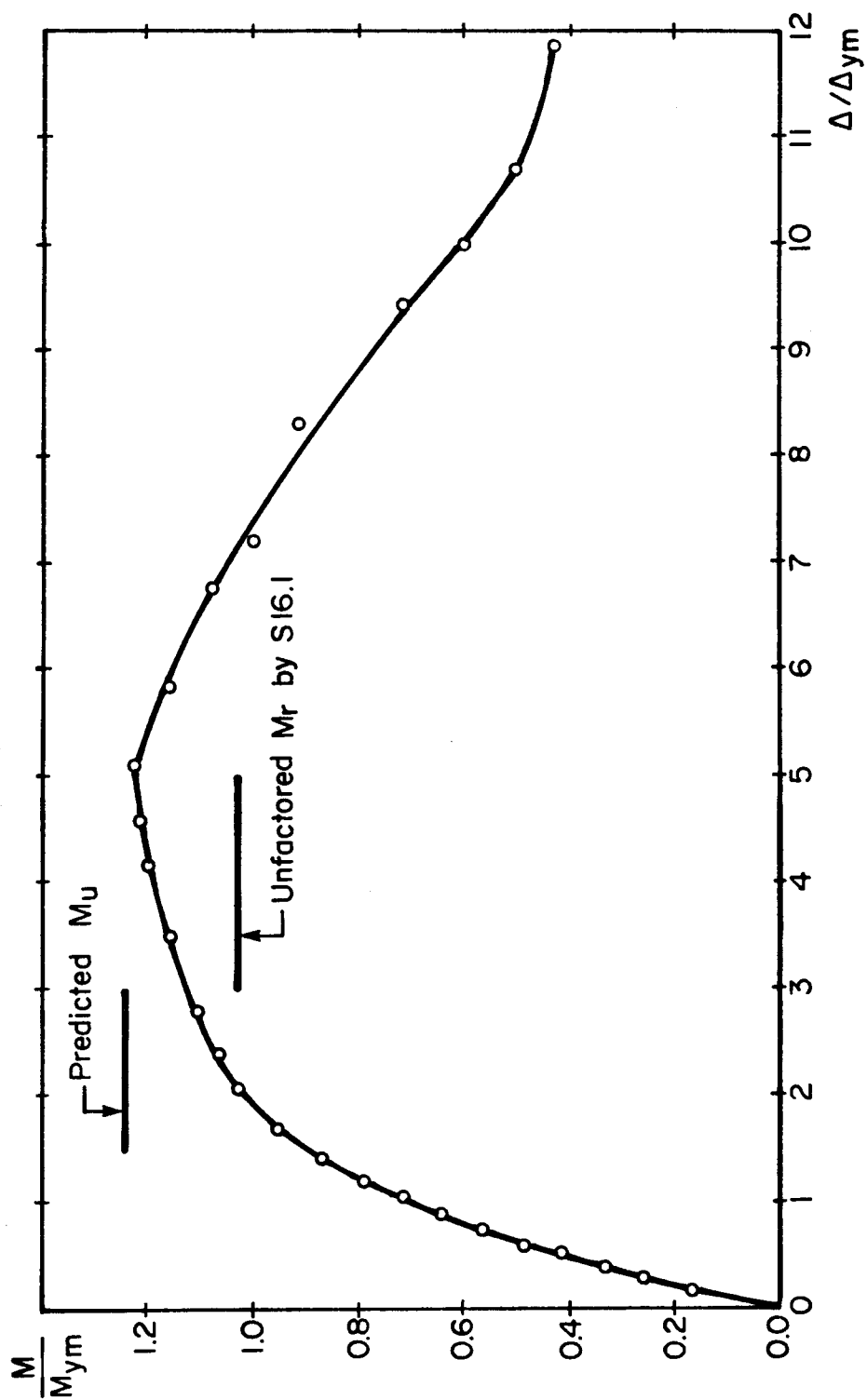


Figure 10.1 Moment-deflection response of composite truss 1

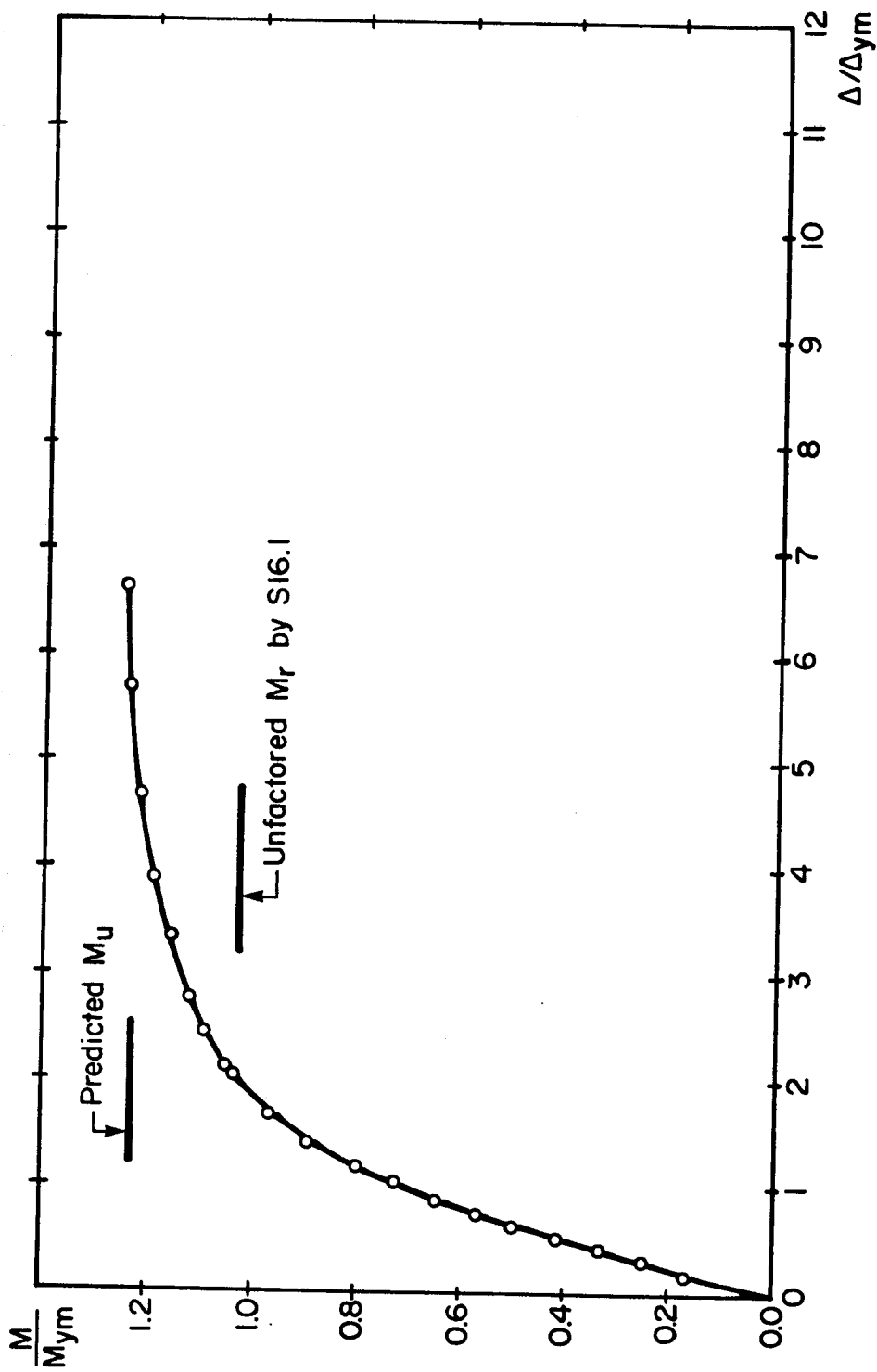


Figure 10.2 Moment-deflection response of composite truss 2

Both trusses exhibited good strength and ductility even though premature failure of the shear connection occurred. Truss 1 reached a maximum moment of 1.23 times the yield moment, or 1.19 times the unfactored resistance as given in CSA Standard S16.1 based on the yield strength of the bottom chord (The unfactored moment resistance by S16.1 corresponding to complete yielding of the bottom chord is itself 1.03 times the moment at first yield). This indicates that the bottom chord was strained considerably beyond yield, as confirmed by a measured maximum strain of 1.21%, shown in Fig. 9.19. Similarly, for truss 2, the maximum moment obtained was 1.24 times the yield moment and 1.21 times the unfactored moment resistance by S16.1, with a measured maximum strain in the bottom chord of 1.36%, equal to 3.3 times the yield strain, as shown in Fig. 9.20.

For trusses 1 and 2 respectively, the maximum moments attained were 98.8% and 100.7% of the predicted ultimate moments based on the ultimate strength of the bottom chord, but not taking into account any contribution of the top chord to moment resistance. Had the shear connection not failed, it is anticipated that both trusses would have reached a somewhat larger maximum moment corresponding to the ultimate strength of the bottom chord and with some contribution from the top chord, as both were exhibiting considerable ductility and no other distress was apparent. It is noted that the predicted ultimate moment for each truss is 1.21 times the unfactored moment given by S16.1.

Deflections at maximum moment of 5.1 and 6.7 times the deflection at the attainment of the yield moment for trusses 1 and 2 respectively demonstrate their ductility. At a test-to-yield moment ratio of 1, the deflection of both trusses is almost double the predicted elastic deflection. Several factors contribute to this behaviour. The cold worked steel does not possess a sharply defined yield point so that, at the yield moment, small inelastic strains have already occurred. The presence of residual stresses results in additional softening. As well, the open web system and interfacial slip increase the flexibility of the trusses. When these latter two factors are considered, using the methods discussed in Section 10.1, the deflection of the trusses at a test-to-yield moment ratio of 1 reduces to about 1.6 times the predicted elastic deflection.

Figure 10.3 illustrates the difference in the moment-deflection response between the composite trusses reported here and another previously tested (Bjorhovde, 1981). The moments plotted include the moments due to the self-weight of each truss. The only common data available for normalizing the curves were the nominal values of the cross-sectional properties and material strengths.

The truss of the previous test was designed assuming that the flexural capacity would be reached when the bottom chord yielded. Consequently, the web members were designed for the concomitant forces. A premature failure occurred when a compression diagonal buckled. After repair, a

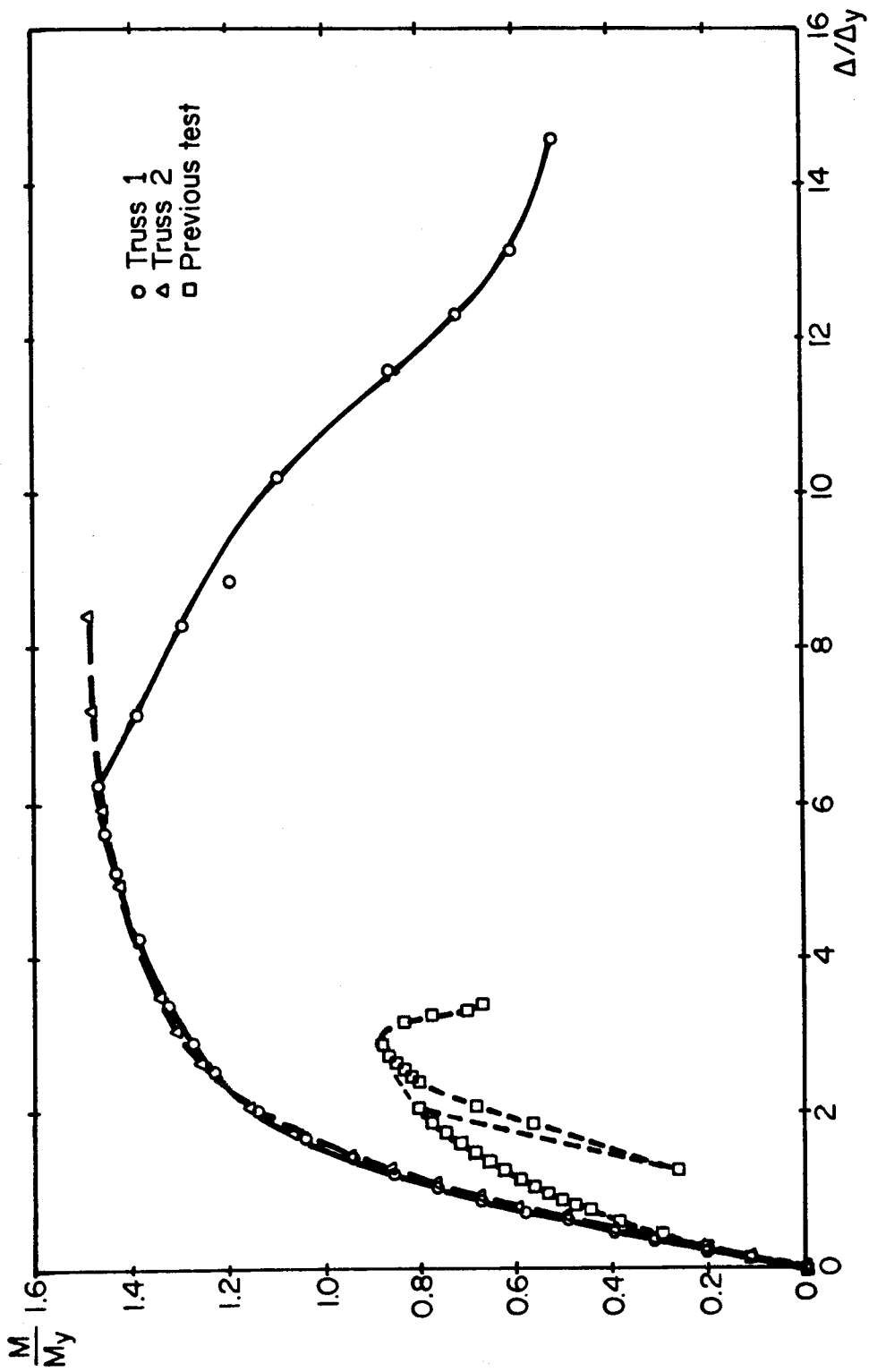


Figure 10.3 A comparison of moment-deflection diagrams

slightly higher moment was reached.

The trusses for the tests reported here were designed on the basis that the bottom chord could reach the ultimate tensile strength of the steel. Figure 10.3 shows that their behaviour is superior to that of the truss designed based on the yield strength of the bottom chord. The strengths obtained (based on nominal properties) were about 1.7 times and the ductility, as measured by the deflection at maximum load, was over 2 times that of the earlier design. As well, the web members, designed for forces consistent with the attainment of the ultimate strength of the bottom chord, did not fail and were able to sustain appreciable rotations in the plane of the truss.

10.3 Strain-Force-Moment Relationships

From the strain distributions through the depth at midspan, shown in Figs. 9.31 and 9.32 for trusses 1 and 2 respectively, it is possible to calculate the forces in the concrete slab and in the steel top and bottom chords, and from these, the internal bending moment, provided that load-strain or stress-strain relationships are known for these components. Alternatively, knowing the bending moment at midspan and the stress-strain relationships, the strains through the depth can be calculated. Measured strains through the depth were selected at 4 load levels for further study. Calculated strains corresponding to the applied moment at each load level are compared to the measured

strains in Figs. 10.4 and 10.5 for trusses 1 and 2 respectively. The figures show that the calculated strains (dashed lines) are in reasonable agreement with the measured values (solid lines) at loads less than that causing yielding of the bottom chord. Differences do occur (up to 2.9 times in the case of truss 2) when the bottom chord has strained substantially so that a small load increment corresponds to a large strain increment. The differences are also relatively large when the strains are very low and the sensitivity of the measurements becomes crucial, as is the case for strains on the top surface of the concrete at low loads. Slip between the top chord and the slab would also contribute to differences between the measured and calculated strains. Because the slip increases with increasing load, this effect would be greatest for the higher loads. In most cases, the calculated position of the neutral axis agrees closely with that measured.

Having determined a best-fit line for the measured strains through the depth, the compressive force in the slab and the tensile forces in the top and bottom chords were determined from the appropriate stress-strain curves. Due to the dead load of the steel deck and concrete and due to shrinkage, the top chords of trusses 1 and 2, respectively, had been strained to $-755 \mu\epsilon$ and $-625 \mu\epsilon$ and, similarly, the bottom chords had been strained to $+565 \mu\epsilon$ and $+465 \mu\epsilon$ before the test loads were applied. Therefore, the strains due to the applied loads were added to these values when

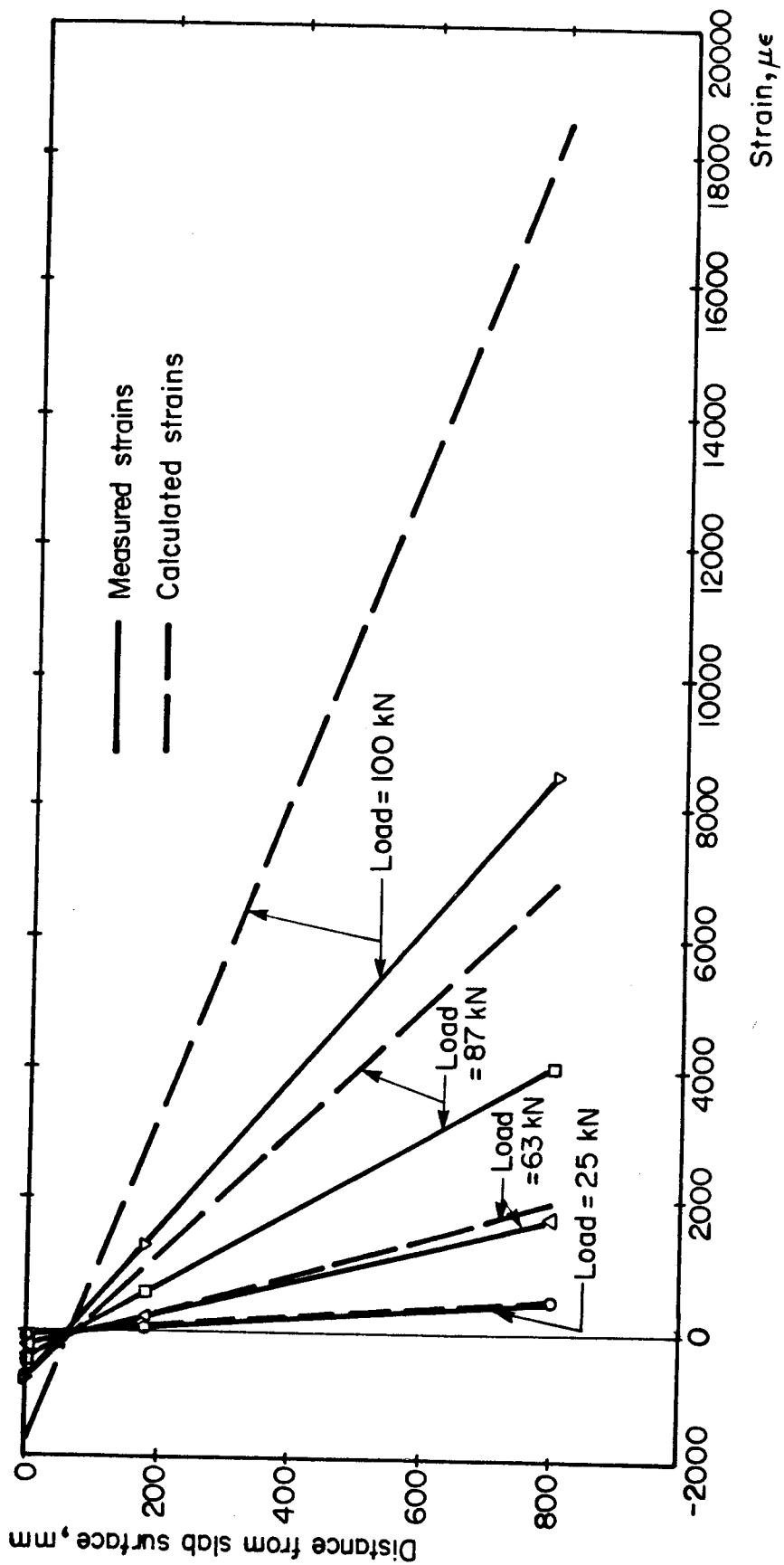


Figure 10.4 Calculated strain variation with depth - truss 1

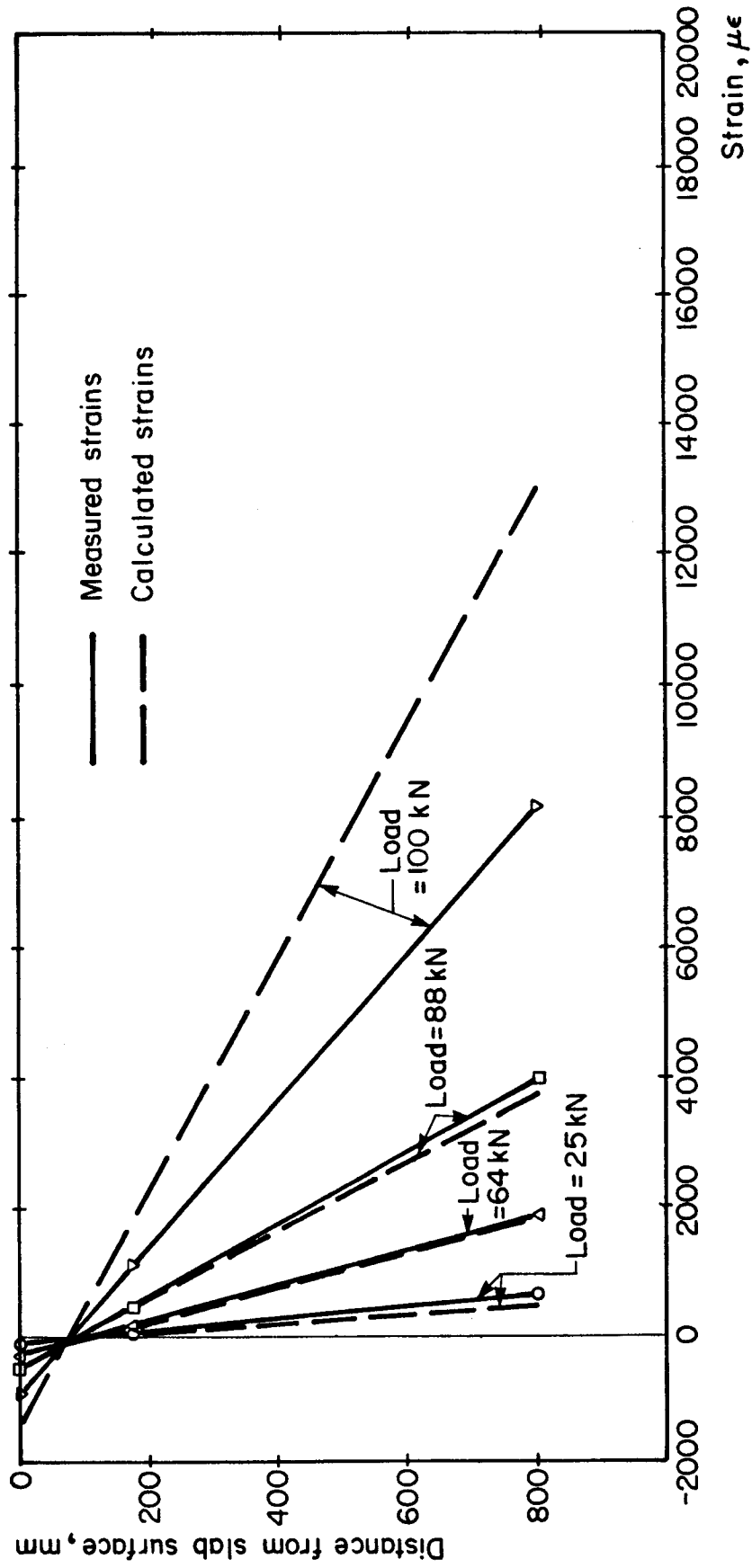


Figure 10.5 Calculated strain variation with depth - truss 2

computing force increments in these members (that is, the appropriate portion of the stress-strain curve was used to calculate the stress and therefore the force increment). On truss 1, for the 4 load levels studied, the tensile forces calculated from the observed strains ranged from 0.86 to 1.10 times the compressive forces, and the computed moment, based on horizontal equilibrium, ranged from 0.86 to 1.02 times the applied moment. Similarly, the tensile forces in truss 2 ranged from 0.84 to 1.94 times the compressive forces for the 4 load levels studied, and the computed moment was between 0.89 and 1.06 times the applied moment. The calculated member forces that maintained horizontal equilibrium and provided an internal moment equal to the applied moment ranged from 0.91 to 1.17 times the forces calculated from measured strains in the concrete and from 1.03 to 1.16 times the forces calculated from measured strains in the steel for truss 1. For truss 2, the respective ranges are 0.87 to 1.60 for the concrete forces and 0.83 to 1.03 for the steel forces. In spite of the fact that extreme care was taken during application of the instrumentation, these results indicate that it is quite difficult to calculate forces from strains, even when full stress-strain curves have been accurately derived and even for a statically determinate system when the applied loads and moments are known. This suggests that, in structural testing, every effort should be made to determine the applied and reactive forces directly to avoid inferring

values from strain measurements.

10.4 Top Chord Behaviour

One of the unique design features of the composite trusses was that the triangulation system for the web members intersected at the mid-depth of the cover slab. The web members were up to 260 mm apart at "panel points" on the top chord. The alternating compressive and tensile forces in the web members, in the Warren truss configuration, would therefore induce bending moments in the top chord. No distress attributed to this web member configuration was noted within the panel point areas even when buckling of the top chord occurred subsequent to the loss of shear connection.

10.5 Web Member Behaviour

For each composite truss, the strain data from web member QR were analyzed to determine the variation in bending moments along the member length. Three different load levels were studied. At each load level and at 3 instrumented locations along the member length, best-fit linear strain distributions were found from the 3 strain measurements on each leg of the angle. These strain distributions, adjusted to the mid-thickness of the legs, were used to calculate the axial force in the member, assuming that the behaviour was elastic, as was appropriate at the load levels studied. For truss 1, the mean value of

the nine measurements of the axial force was 0.97 times the equilibrium value determined by the method of sections, with a coefficient of variation of 0.052. For truss 2, the mean value was 0.99 times the calculated force with a coefficient of variation of 0.035. Having established the strains corresponding to the axial forces, the bending strains about the strong and weak axes were determined from the strain distributions and thus, bending moments about these axes were determined. These bending moments were then resolved to give the in-plane and out-of-plane bending moments, and from these, the eccentricities of the compressive axial forces were determined.

Figures 10.6 and 10.7 show the in-plane and out-of-plane eccentricities of the force in member QR of trusses 1 and 2, respectively, at 3 load levels. The behaviour was similar in the two tests. For members subjected to end moments and axial forces, the eccentricity will not vary linearly. The axial force acting on the shape, deformed due to the end moments, causes an additional deformation and hence eccentricity.

For truss 2, for the intermediate load level (73 kN), the in-plane eccentricity and, in particular, the out-of-plane eccentricity calculated at the lower third point do not appear to be consistent with the other data. This may be because the out-of-plane moment is the difference of components of moments about the principal axes. In drawing the out-of-plane curves at this load level,

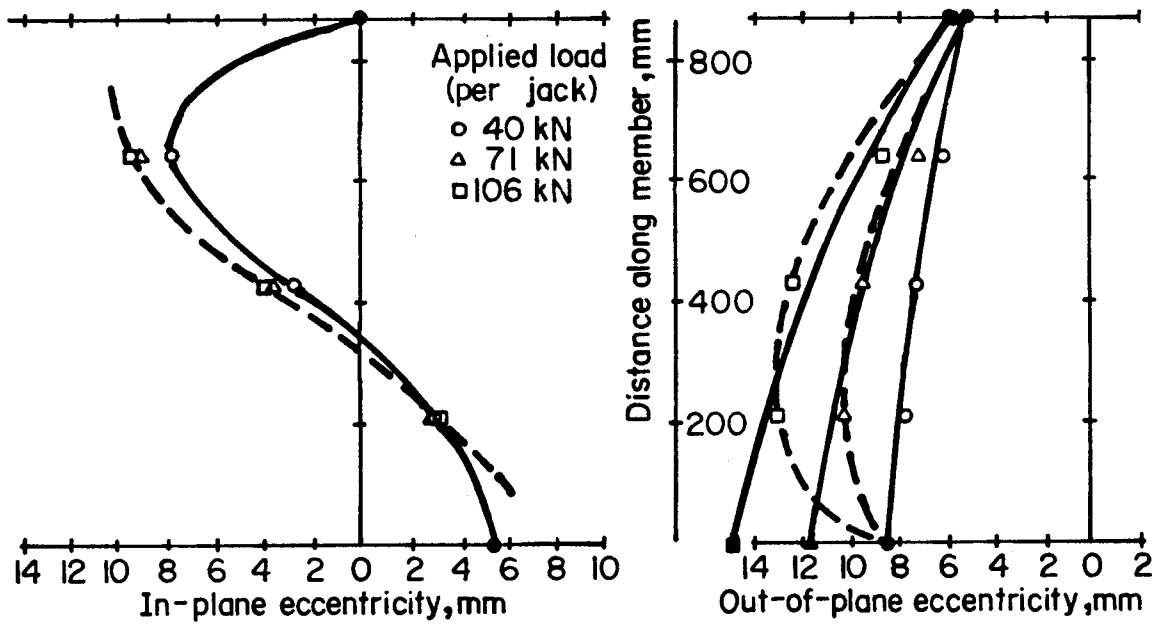


Figure 10.6 Eccentricities of axial load in member QR - truss 1

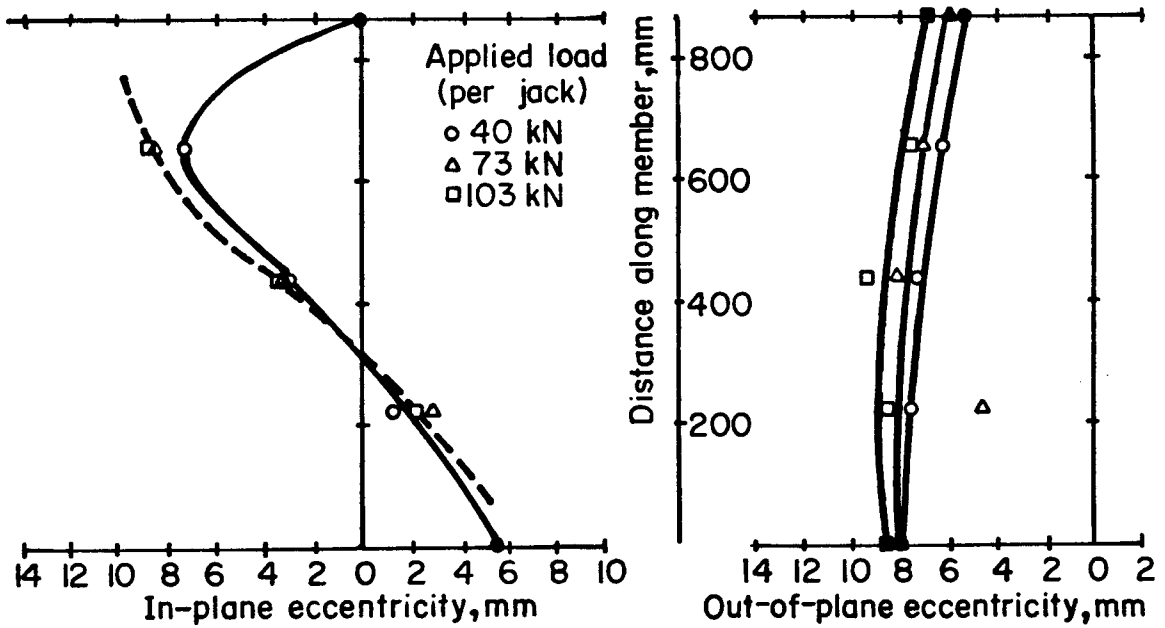


Figure 10.7 Eccentricities of axial load in member QR - truss 2

only the upper two points have been used.

On the diagrams for in-plane eccentricity, unique end eccentricities due to the eccentricity of the members meeting at the joint (as discussed in Section 3.2.2.3) were calculated and plotted as solid points. These calculated end eccentricities do not include any eccentricity resulting from joint rotations. For the lowest load, where the joint rotations are small, S-shaped curves have been drawn through the data points. In general, the data indicate that the joint rotations are causing double curvature and that the curvature of the member becomes more pronounced with increasing loads. It would be expected that the end eccentricities would increase with increasing loads, as indicated by the incomplete curves sketched for the largest load. The moments due to joint rotation are greater at the upper end.

For drawing the curves for out-of-plane eccentricity, the measured out-of-plane movements ($1/2$ the separations) of the angles at mid-height were also used. With these data, the deflected shape of the members can be extracted and used to estimate the eccentricities at the top and bottom ends, as shown by solid symbols on Figs. 10.6 and 10.7, thus defining the eccentricity curves at 5 points. The out-of-straightness increases as the load increases, as would be expected, but did not exceed 1.95 mm for truss 1 and 1.79 mm for truss 2. (These eccentricities correspond to only about 0.10 of the radius of gyration of the angle about

this axis.) The out-of-straightness develops due to the initial out-of-plane end eccentricity and due to the out-of-plane movement that results from joint rotations. As the joint rotations cause double curvature in-plane, the latter contribution would be relatively small.

Of greater significance are the eccentricities at the top and bottom ends. All of the data, with the exception of the calculated end eccentricities at the lower end for truss 1 for the two higher load levels, indicate that these eccentricities are close to the average of about 6.7 mm. This value is only 35% of the distance from the back of the angle to the centroid and suggests that the design procedure used in Section 3.2.2.3, where the moments due to out-of-plane eccentricity were considered to be accommodated in the connection, is reasonably accurate but that the angles should be designed for a portion (say 1/3) of the out-of-plane moment. In Fig. 10.6, for out-of-plane eccentricity, a second set of dashed eccentricity curves has also been drawn for the 2 higher loads. These curves are consistent with all of the data except that they would require the out-of-plane movement of the angle to amount to about 5 mm at the largest load rather than the 2 mm determined on the basis of the separation of the angles. A possible hypothesis is that the out-of-plane moments were affected by initial out-of-straightness of the angles, with one of the pair having a substantially greater out-of-straightness (and therefore movement) than the other.

11. SUMMARY, CONCLUSIONS, AND RECOMMENDATIONS

11.1 Summary

1. Two essentially identical full-scale composite trusses, designed and constructed for shrinkage and flexural tests, had the following features:
 - a. the flexural capacity was based on the ultimate tensile strength rather than the yield strength of the bottom chord,
 - b. the centroidal axes of the web members at each top chord joint intersected at the mid-depth of the concrete cover slab,
 - c. web members were selected to withstand axial forces that would develop when the bottom chord reached its ultimate strength,
 - d. tension diagonals were designed for axial forces only,
 - e. compression diagonals were designed for the combination of axial force and the proportion of in-plane joint eccentricity moments that they carry based on their relative flexural stiffness and resolved about the principal axes. No out-of-plane moments were considered.
 - f. the welds were conservatively designed, using the CISC Handbook design tables for eccentrically loaded welds, to withstand the axial forces described and

in-plane moments equal to the yield moments of the web members, and

- g. shear connectors were selected based on the maximum force developed in the bottom chord.
2. The measured geometric properties of the steel sections and of the composite trusses were used for all analyses of test data.
3. Material properties were determined from ancillary tests on steel tension coupons, stub columns, a tension specimen consisting of a section of bottom chord (including a joint), push-out specimens, concrete cylinders, and concrete prisms.
4. The effect of concrete slab shrinkage on each composite truss was monitored over a period of up to 85 days, and included measurements of truss deflections, concrete strains, steel strains, and ambient temperature and relative humidity. The free shrinkage strains of two 100 x 100 x 1000 mm and two 65 x 100 x 1000 mm plain concrete control specimens were also monitored during each test.
5. The restrained shrinkage strains measured on the concrete slabs were compared to the free shrinkage strains of the control specimens. Steel and concrete shrinkage strains were studied to develop a theory of force transfer, and measured shrinkage deflections were compared to predicted results from calculations suggested in S16.1 and from a proposed new method.

6. Special knife edges and rollers were designed and manufactured to accommodate, without restraint, the large movements (horizontal movement, rotation, deflection) anticipated at load points and reactions of the simply supported flexural test specimens.
7. Each test specimen was loaded in flexure up to failure using 4 concentrated loads at panel points. Loads and reactions, deflections, concrete strains, steel strains, interface slip, and web member deformations were measured at intervals during the tests. Premature failure of both test specimens occurred in the shear connection, but only after the strains in the bottom chord had exceeded the yield strain considerably.
8. The flexural test data was analysed to obtain the moment-deflection response of each composite truss and to study the behaviour of individual components.
9. The effective moments of inertia of the steel and composite trusses were determined from load and deflection measurements.

11.2 Conclusions and Recommendations

1. The measured densities of the steels comprising the HSS sections (used as top and bottom chords of the trusses) had an average value of 8028 kg/m^3 , significantly higher than the commonly accepted value of 7850 kg/m^3 .
2. Deflections and strains due to shrinkage increased at a

decreasing rate over the 65 and 85 day test periods for trusses 1 and 2 respectively.

3. Seventy-seven percent of the 65 day midspan deflection of truss 1 of 8.9 mm occurred within the first 30 days of the test, while 61% of the 85 day midspan deflection of truss 2 of 7.2 mm occurred in the same interval. The deflections of truss 2 were lower than those of truss 1 due to stress relief as a result of the formation of shrinkage cracks.
4. The free shrinkage strains of the concrete control specimens ranged from 800 to 900 $\mu\epsilon$ for truss 1 and from 600 to 700 $\mu\epsilon$ for truss 2 at 65 to 85 days. The restrained longitudinal shrinkage of the slab was 353 $\mu\epsilon$ (42% of the free shrinkage strain) on truss 1 and 347 $\mu\epsilon$ (53% of the free shrinkage strain) on truss 2.
5. Strain distributions along the length of each truss show that restraint to shrinkage of the slab developed within a short distance from each end. The constant tensile force in the concrete slab over the remainder of the truss length is in equilibrium with a compressive force developed in the top chord and a much smaller tensile force developed in the bottom chord. Most of the shrinkage force is transferred to the bottom chord by the 2 web members closest to each end of the truss.
6. At midspan, shrinkage strains varied linearly through the depth of each truss.
7. Computed midspan shrinkage deflections based on

curvature measurements, the restrained shrinkage method of Chien and Ritchie, and the unrestrained shrinkage method of Montgomery, Kulak, and Shwartsburd were 8.4 mm, 8.7 mm, and 21.7 mm respectively for truss 1 at 65 days and 7.7 mm, 8.0 mm, and 18.8 mm respectively for truss 2 at 85 days, compared to measured deflections of 8.9 and 7.2 mm for trusses 1 and 2 respectively. Of the two methods suggested in Appendix L of S16.1 for calculating the shrinkage deflection of a composite flexural member, the method of Chien and Ritchie appears to be the most accurate.

8. An equilibrium method is proposed for calculating shrinkage deflections, based on the equilibrium of the shrinkage-induced forces at midspan, a linear strain distribution through the depth, the free shrinkage strain of the concrete, the stress-strain characteristics of the concrete in tension over the period that shrinkage occurs, and the stress-strain characteristics of the steel.
9. To estimate the elastic deflection of a steel truss, an effective moment of inertia equal to the gross moment of inertia of the chords about the truss centroid, divided by a factor of 1.10 to 1.14 to account for the decreased stiffness of the open web system, can be used, confirming the present design recommendation in Clause 16.5.14.2 of S16.1.
10. To estimate the elastic deflection of a composite truss,

the transformed moment of inertia should be divided by 1.10 (as originally suggested by Cran, 1972), the same factor used to account for the decreased stiffness of the open web system of a steel truss, and the effective moment of inertia (accounting for interfacial slip) can be calculated as recommended in Clause 17.3.1.1 of S16.1, possibly using an interfacial slip factor of 0.77 rather than 0.85.

11. At low loads, the moment-deflection response of the composite trusses is essentially linearly elastic. At the yield moment, the measured deflections are about 1.6 times the calculated values based on the transformed moment of inertia. The maximum moments attained were about 1.2 times the unfactored ultimate moments predicted by S16.1. The respective deflections at maximum moment of 5.1 and 6.7 times the yield value demonstrate the ductility of the trusses.
12. The maximum moments attained were 98.8% and 100.7% of the predicted ultimate moment based on rupture of the bottom chord. The prediction does not take into account that the top chord was strained appreciably in tension and therefore was contributing to the flexural strength of the composite truss.
13. The maximum strains in the bottom chord, for trusses 1 and 2 respectively, were 2.9 and 3.3 times the yield strain. These strains correspond to stresses equal to 110% and 111% of the yield stress or 91% and 92% of the

- ultimate strength of the bottom chord.
14. A comparison with previous test results in which failure was precipitated by buckling of a compression diagonal shows that increased strength and ductility are obtained when the various components are designed for the forces consistent with the ultimate strength of the bottom chord.
 15. The flexural capacity of a composite truss should be based on the ultimate tensile strength of the bottom chord and the other truss components (web members and shear connection) should be designed accordingly to ensure that the desired ductile flexural mode of failure is obtained.
 16. Premature failure of truss 1 occurred when the concrete cover slab in the northern part of the span broke away above the shear connectors. This failure suggests that additional rules for establishing the length of stud shear connectors for use in deck-slabs should be provided in S16.1. Grant, Slutter, and Fisher's equations to calculate the reduced strength of stud shear connectors in deck-slabs could be used to calculate a minimum stud length. It appears that the shear connectors should project into the compression zone of the concrete at ultimate load (above the plastic neutral axis) to ensure good shear transfer and prevent separation between the concrete and steel.
 17. Failure of truss 2 occurred when the shear failure of an

improperly welded stud near the north end caused overloading of the top chord in combined bending and axial load. To guard against this type of failure, either the end diagonal could be positioned so that its line of action intersects the centroid of the steel top chord directly over the reaction or the reaction shear reinforcement could be extended to the first interior panel point.

18. A linear variation of bending strains through the depth, neglecting any discontinuity at the interface between the top chord and the concrete slab due to slip, fits the data well and is in reasonable agreement with calculated strains. At higher loads, the neutral axis rose as the bottom chord strained beyond yield.
19. Compressive strains across the width of the concrete slabs were essentially uniform. Significant shear lag was observed only in close proximity to the ends of the truss.
20. No distress of the top chord was noted due to the web member configuration in which the centroidal axes of the diagonals meet at the mid-depth of the cover slab.
21. Failure of the web members did not occur, in spite of significant joint rotations near maximum load. The maximum out-of-plane displacement of the first compression diagonal was less than 2 mm for both trusses at maximum load.
22. An adequate design procedure for web members, based on

test observations, appears to be to design them for the axial loads consistent with the bottom chord reaching its ultimate strength together with their portion of the in-plane joint eccentricity moment plus one-third of the out-of-plane connection eccentricity moment.

11.3 Areas of Further Research

Several areas needing further research have been identified as a result of this investigation:

1. Further testing of long span composite trusses with full shear connection, designed based on the ultimate strength of the bottom chord, is required to verify their ultimate behaviour.
2. An analytical study may be needed to determine if the deflection at service load levels (a serviceability limit state) will govern for design purposes, because of the reserve strength of the composite truss between yield and ultimate. If, for a given flexural capacity, the size of the bottom chord cannot be reduced due to serviceability limitations, the web members and shear connection must still be designed for forces consistent with reaching the ultimate strength of the bottom chord to ensure a ductile failure mode.
3. Experimental studies should be conducted to determine how shear is transferred from the concrete to the steel by a shear stud. The strut model proposed by Leonhardt and Andrä should be investigated.

4. The work of Goble on stud failure by pull-out from the steel flange should be expanded to include steels with higher strengths.
5. A study of longitudinal shear in composite flexural members with slabs on deck (with ribs running perpendicular to the axis of the members) should be undertaken to confirm whether or not the present design provisions are adequate to prevent failure due to longitudinal shear.
6. A more detailed study of the behaviour of the web members should be undertaken to confirm the design procedures proposed in this study.
7. Further experimental studies on the effect of interfacial slip on composite truss stiffness would allow the slip factor in the equation to calculate the effective moment of inertia to be determined on a statistical basis.
8. Additional experimental studies to measure shrinkage deflections of a wide array of composite flexural members are needed to develop a proven, simple procedure for estimating shrinkage deflections.
9. The value of the modulus of elasticity of concrete in tension as it develops over time should be investigated.

REFERENCES

- Adekola, A.O. 1968. Effective Widths of Composite Beams of Steel and Concrete. *The Structural Engineer*, Vol. 46, No. 9, September, pp. 285-289.
- American Concrete Institute (ACI) Committee 209. 1971. Prediction of Creep, Shrinkage, and Temperature Effects in Concrete Structures. *Designing for the Effects of Creep, Shrinkage, and Temperature in Concrete Structures*, SP 27, American Concrete Institute, Detroit, Michigan, pp. 51-93.
- American Concrete Institute (ACI) Committee 209. 1982. Prediction of Creep, Shrinkage, and Temperature Effects in Concrete Structures. *Designing for Creep and Shrinkage in Concrete Structures*, SP-76, American Concrete Institute, Detroit, Michigan, pp. 193-300.
- American Institute of Steel Construction (AISC). 1948. *Steel Construction Manual*, 5th ed. American Institute of Steel Construction, New York, 432 p.
- American Institute of Steel Construction (AISC). 1983. Proposed Load and Resistance Factor Design Specifications for Structural Steel Buildings. American Institute of Steel Construction, Chicago, September, 166 p.
- American Society for Testing and Material (ASTM). 1977. Standard Methods and Definitions for Mechanical Testing of Steel Products. ASTM A370-77, Philadelphia, Pennsylvania.
- American Society for Testing and Material (ASTM). 1982. Standard Test Method for Young's Modulus, Tangent Modulus, and Chord Modulus. ASTM E111-82, Philadelphia, Pennsylvania.
- American Society for Testing and Material (ASTM). 1985. Standard Methods of Tension Testing of Metallic Materials. ASTM E8-85a, Philadelphia, Pennsylvania.

- American Society of Civil Engineers (ASCE). 1974. Composite Steel-Concrete Construction. Report of the Subcommittee on the State-of-the-Art Survey of the Task Committee on Composite Construction of the Committee on Metals of the Structural Division, Journal of the Structural Division, American Society of Civil Engineers, Vol. 100, No. ST5, May, pp. 1085-1139.
- Atkinson, A.H. and Cran, J.A. 1972. The Design and Economics of Composite Open Web Steel Joists. Presented at the March 6-7, 1972 Canadian Steel Construction Council, Canadian Structural Engineering Conference, held at Montréal, Québec, 55 p.
- Aziz, T.S.A. 1972. Inelastic Non-Linear Behaviour of Steel Triangulated Planar Frames. Master of Engineering thesis, Department of Solid Mechanics and Structural Engineering, Carleton University, Ottawa, Ontario, 187 p.
- Azmi, M.H. 1972. Composite Open-Web Trusses with Metal Cellular Floor. Master of Engineering thesis, McMaster University, Hamilton, Ontario, April, 95 p.
- Barnard, P.R. and Johnson, R.P. 1965. Ultimate Strength of Composite Beams. Proceedings, Institution of Civil Engineers, London, Vol. 32, October, pp. 161-179.
- Bazant, Z.P. 1972. Prediction of Concrete Creep Effects Using Age-Adjusted Effective Modulus Method. Proceedings, Journal of the American Concrete Institute, Vol. 69, April, pp. 212-217.
- Bjorhovde, R. 1981. Full-Scale Test of a Composite Truss. Structural Engineering Report No. 97, Department of Civil Engineering, The University of Alberta, Edmonton, Alberta, June, 40 p.
- Blodgett, O.W. 1966. Design of Welded Structures. The James F. Lincoln Arc Welding Foundation, Cleveland, Ohio.
- Branson, D.E. 1964. Time-Dependent Effects in Composite Concrete Beams. Proceedings, Journal of the American Concrete Institute, Vol. 61, February, pp. 213-229.

- Branson, D.E. and Christiason, M.L. 1971. Time Dependent Concrete Properties Related to Design-Strength and Elastic Properties, Creep, and Shrinkage. Designing for the Effects of Creep, Shrinkage, and Temperature in Concrete Structures, SP 27, American Concrete Institute, Detroit, Michigan, pp. 257-277.
- Brendel, G. 1964. Strength of the Compression Slab of T-Beams Subject to Simple Bending. Proceedings, Journal of the American Concrete Institute, Vol. 61, January, pp. 57-75.
- Buckner, C.D., Deville, D.J., and McKee, D.C. 1981. Shear Strength of Slabs in Stub Girders. Journal of the Structural Division, American Society of Civil Engineers, Vol. 107, No. ST2, February, pp. 273-280.
- Canadian Institute of Steel Construction (CISC), M.I. Gilmor, editor. 1985. Handbook of Steel Construction, 4th ed. Canadian Institute of Steel Construction, Willowdale, Ontario.
- Canadian Portland Cement Association (CPCA). 1978. Design and Control of Concrete Mixtures-Metric Edition. Canadian Portland Cement Association, Toronto, Ontario, 131 p.
- Canadian Standards Association (CSA). 1974. Steel Structures for Buildings-Limit States Design. National Standard of Canada CAN3-S16.1-1974, Canadian Standards Association, Rexdale, Ontario.
- Canadian Standards Association (CSA). 1977. Methods of Test for Concrete. National Standard of Canada CAN3-A23.2-M77, Canadian Standards Association, Rexdale, Ontario.
- Canadian Standards Association (CSA). 1981a. General Requirements for Rolled or Welded Structural Quality Steel. National Standard of Canada CAN3-G40.20-M81, Canadian Standards Association, Rexdale, Ontario.

- Canadian Standards Association (CSA). 1981b. Structural Quality Steels. National Standard of Canada CAN3-G40.21-M81, Canadian Standards Association, Rexdale, Ontario.
- Canadian Standards Association (CSA). 1984a. Steel Structures for Buildings (Limit States Design). National Standard of Canada CAN3-S16.1-M84, Canadian Standards Association, Rexdale, Ontario.
- Canadian Standards Association (CSA). 1984b. Design of Concrete Structures for Buildings. National Standard of Canada CAN3-A23.3-M84, Canadian Standards Association, Rexdale, Ontario.
- Chapman, J.C. 1964. Composite Construction in Steel and Concrete—The Behaviour of Composite Beams. The Structural Engineer, Vol. 42, No. 4, April, pp. 115-125.
- Chien, E.Y.L. and Ritchie, J.K. 1984. Design and Construction of Composite Floor Systems. Canadian Institute of Steel Construction, Willowdale, Ontario, 323 p.
- Cook, J.P. 1977. Composite Construction Methods. John Wiley and Sons, New York, 330 p.
- Comité Euro-International du Béton—Fédération Internationale de la Précontrainte (CEB-FIP). 1978. International System of Unified Standard Codes of Practice for Structures, Vol. 2: CEB-FIP Model Code for Concrete Structures (English translation). Comité Euro-International du Béton, April.
- Cran, J.A. 1972. Design and Testing Composite Open Web Steel Joists. Technical Bulletin 11, Stelco, January, 28 p.
- Culver, C. and Coston, R. 1961. Tests of Composite Beams with Stud Shear Connectors. Journal of the Structural Division, American Society of Civil Engineers, Vol. 87, No. ST2, February, pp. 1-17.

- Dallaire, E.E. 1971. Cellular Steel Floors Mature. Civil Engineering, American Society of Civil Engineers, Vol. 41, No. 7, July, pp. 70-74.
- Davies, C. 1969. Tests on Half-Scale Steel-Concrete Composite Beams with Welded Stud Connectors. The Structural Engineer, Vol. 47, No. 1, January, pp. 29-40.
- Davies, C. 1975. Steel-Concrete Composite Beams for Buildings. George Godwin Limited, London, 125 p.
- Dilger, W.H. 1982. Creep Analysis of Prestressed Concrete Structures Using Creep-Transformed Section Properties. Journal, Prestressed Concrete Institute, Vol. 27, No. 1, January-February, pp. 98-118.
- El-Ghazzi, M.N., Robinson, H. and Elkholy, I.A.S. 1976. Longitudinal Shear Capacity of Slabs of Composite Beams. Canadian Journal of Civil Engineering, Vol. 3, No. 4, December, pp. 514-522.
- Fahmy, E.H.A. 1974. Inelastic Analysis of Composite Open-Web Steel Joists. Master of Engineering thesis, McMaster University, Hamilton, Ontario, December, 141 p.
- Fisher, J.W. 1970. Design of Composite Beams with Formed Metal Deck. Engineering Journal, American Institute of Steel Construction, Vol. 7, No. 3, July, pp. 88-96.
- Glanville, W.H. 1930. Studies in Reinforced Concrete, Part II-Shrinkage Stresses. Department of Scientific and Industrial Research, Building Research Technical Paper No. 11, London, 49 p.
- Goble, G.G. 1968. Shear Strength of Thin Flange Composite Specimens. Engineering Journal, American Institute of Steel Construction, Vol. 5, No. 2, April, pp. 62-65.
- Grant, J.A. Jr., Fisher, J.W., and Slutter, R.G. 1977. Composite Beams with Formed Steel Deck. Engineering Journal, American Institute of Steel Construction, Vol. 14, First Quarter, pp. 24-43.

- Hagood, T.A. Jr., Guthrie, L., and Hoadley, P.G. 1968. An Investigation of the Effective Concrete Slab Width for Composite Construction. Engineering Journal, American Institute of Steel Construction, Vol. 5, No. 1, January, pp. 20-25.
- Hansell, W.C., Galambos, T.V., Ravindra, M.K., and Viest, I.M. 1978. Composite Beam Criteria in LRFD. Journal of the Structural Division, American Society of Civil Engineers, Vol. 104, No. ST9, September, pp. 1409-1426.
- Heins, C.P. and Fan, H.M. 1976. Effective Composite Beam Width at Ultimate Load. Journal of the Structural Division, American Society of Civil Engineers, Vol. 102, No. ST11, November, pp. 2163-2179.
- Hobbs, D.W. 1982. Drying Shrinkage of Symmetrically Reinforced Concrete and Some Estimates of the Creep of Concrete in Tension. Fundamental Research on Creep and Shrinkage of Concrete. Martinus Nijhoff Publishers, The Hague, Netherlands, pp. 213-225.
- Iyengar, S.H. and Zils, J.J. 1973. Composite Floor System for Sears Tower. Engineering Journal, American Institute of Steel Construction, Vol. 10, Third Quarter, pp. 74-81.
- Iyengar, H.S. 1977. State-of-the-Art Report on Composite or Mixed Steel-Concrete Construction for Buildings. American Society of Civil Engineers, New York, 153 p.
- Johns, A.B. 1978. Discussion of Robinson, H., Fahmy, E.H., and Azmi, M.H. 1978. Composite Open-Web Joists with Formed Metal Floor. Canadian Journal of Civil Engineering, Vol. 5, No. 4, December, pp. 615-618.
- Johnson, R.P. 1970. Longitudinal Shear Strength of Composite Beams. Proceedings, Journal of the American Concrete Intitute, Vol. 67, June, pp. 464-466.
- Johnson, R.P. 1975. Composite Structures of Steel and Concrete, Volume 1: Beams, Columns, Frames and Applications in Building. Crosby Lockwood Staples, London, 210 p.

- Johnson, R.P. and Oehlers, D.J. 1981. Analysis and Design for Longitudinal Shear in Composite T-Beams. Proceedings, Institution of Civil Engineers, London, Vol. 71, December, pp. 989-1021.
- Joint ASCE-ACI Committee on Composite Construction. 1960. Tentative Recommendations for the Design and Construction of Composite Beams and Girders for Buildings. Progress Report of the Joint ASCE-ACI Committee on Composite Construction, Phillip P. Page, Chmn., Journal of the Structural Division, American Society of Civil Engineers, Vol. 86, No. ST12, December, pp. 73-92.
- Kennedy, J.B. and Neville, A.M. 1976. Basic Statistical Methods for Engineers and Scientists, 2nd ed. Harper and Row, Publishers, New York, 490 p.
- Kennedy, S.J. and MacGregor, J.G. 1984. End Connection Effects on the Strength of Concrete Filled HSS Beam Columns. Structural Engineering Report No. 115, Department of Civil Engineering, The University of Alberta, Edmonton, Alberta, 251 p.
- Knowles, P.R. 1973. Composite Steel and Concrete Construction. Butterworth and Co. (Publishers) Ltd., London, 200 p.
- Korol, R.M. 1982. An Investigation of the Behaviour of HSS Double Chord Trusses and Implications for Design. Presented at the February 22-23, 1982 Canadian Steel Construction Council, Canadian Structural Engineering Conference, held at Vancouver, B.C., 34 p.
- Lay, M.G. 1982. Structural Steel Fundamentals—An Engineering and Metallurgical Primer. Australian Road Research Board, Victoria, Australia, 241 p.
- Leonhardt, F. and Andrä, H.P. 1982. Discussion of Johnson, R.P. 1981. Loss of Interaction in Short-span Composite Beams and Plates. Journal of Constructional Steel Research, Vol. 2, No. 1, January, pp. 43-44.

- Mackey, S. and Wong, F.K.C. 1961. The Effective Width of a Composite Tee-Beam Flange, *The Structural Engineer*, September, pp. 277-285.
- Mattock, A.H., Li, W.K., and Wang, T.C. 1976. Shear Transfer in Lightweight Reinforced Concrete. *Journal, Prestressed Concrete Institute*, Vol. 21, No. 1, January-February, pp. 20-39.
- Mindess, S. and Young, J.F. 1981. *Concrete*. Prentice-Hall, Inc., Englewood Cliffs, N.J., 671 p.
- Montgomery, C.J., Kulak, G.L., and Shwartsburd, G. 1983. Deflection of a Composite Floor System. *Canadian Journal of Civil Engineering*, Vol. 10, No. 2, June, pp. 192-204.
- National Research Council of Canada (NRCC). 1942. *National Building Code*. NRC No. 1068, National Research Council, Ottawa, 422 p.
- Nixon, D. 1982. Effective Widths at Ultimate Load Level. Report to CSA S16 Technical Committee, May, 7 p.
- Ollgaard, J.G., Slutter, R.G., and Fisher, J.W. 1971. Shear Strength of Stud Connectors in Lightweight and Normal Weight Concrete. *Engineering Journal, American Institute of Steel Construction*, Vol. 8, No. 2, April, pp. 55-64.
- Park, R. and Paulay, T. 1975. *Reinforced Concrete Structures*. John Wiley and Sons, New York, 769 p.
- Reddy, V.M. and Hendry, A.W. 1970. Ultimate Strength of a Composite Beam Allowing for Strain Hardening. *Indian Concrete Journal*, Vol. 44, No. 9, September, pp. 388-396.
- Robinson, H. 1967. Tests on Composite Beams with Cellular Deck. *Journal of the Structural Division, American Society of Civil Engineers*, Vol. 93, No. ST4, August, pp. 139-164.

- Robinson, H. 1969. Composite Beam Incorporating Cellular Steel Decking. Journal of the Structural Division, American Society of Civil Engineers, Vol. 95, No. ST3, March, pp. 355-380.
- Robinson, H. and Wallace, I.W. 1973. Composite Beams with 1/2 inch Metal Deck and Partial and Full Shear Connection. Transactions, Canadian Society for Civil Engineering, Vol. 16, No. A-8, published in The Engineering Journal, EIC, September, pp. I-VII
- Robinson, H. 1978. Composite Open-Web Joists with Formed Steel Deck. Presented at the March 13-14, 1978 Canadian Steel Construction Council, Canadian Structural Engineering Conference, held at Toronto, Ontario, 25 p.
- Robinson, H., Fahmy, E.H., and Azmi, M.H. 1978. Composite Open-Web Joists with Formed Metal Floor. Canadian Journal of Civil Engineering, Vol. 5, No. 1, March, pp. 1-10.
- Roll, F. 1971. Effects of Differential Shrinkage and Creep on a Composite Steel-Concrete Structure. Designing for the Effects of Creep, Shrinkage, and Temperature in Concrete Structures, SP 27, American Concrete Institute, Detroit, Michigan, pp. 187-214.
- Sabnis, G.M. 1979. Handbook of Composite Construction Engineering. Van Nostrand Reinhold Company, New York, 380 p.
- Schuster, R.M. 1976. Composite Steel-Deck Concrete Floor Systems. Journal of the Structural Division, American Society of Civil Engineers, Vol. 102, No. ST5, May, pp. 899-917.
- Slutter, R.G. and Driscoll, G.C. Jr. 1965. Flexural Strength of Steel-Concrete Composite Beams. Journal of the Structural Division, American Society of Civil Engineers, Vol. 91, No. ST2, April, pp. 71-98.

- Structural Stability Research Council (SSRC), B.G. Johnston, editor. 1976. Guide to Stability Design Criteria for Metal Structures, 3rd ed. John Wiley and Sons, New York, N.Y., 616 p.
- Tide, R.H.R. and Galambos, T.V. 1970. Composite Open Web Steel Joists. Engineering Journal, American Institute of Steel Construction, Vol. 7, No. 1, January, pp. 27-36.
- Viest, I.M. 1956. Investigation of Stud Shear Connectors for Composite Concrete and Steel T-Beams. Proceedings, Journal of the American Concrete Institute, Vol. 27, April, pp. 875-891.
- Viest, I.M. 1960. Review of Research on Composite Steel-Concrete Beams. Journal of the Structural Division, American Society of Civil Engineers, Vol. 86, No. ST6, Proc. Paper 2496, June, pp. 1-21.
- Wang, P.C. and Kaley, D.J. 1967. Composite Action of Concrete Slab and Open Web Joist (Without the Use of Shear Connectors). Engineering Journal, American Institute of Steel Construction, Vol. 4, No. 1, January, pp. 10-16.
- Winter, G. 1971. Discussion of Fisher, J.W. 1970. Design of Composite Beams with Formed Steel Deck. Engineering Journal, American Institute of Steel Construction, Vol. 8, No. 1, January, pp. 32-35.
- Yam, L.C.P. and Chapman, J.C. 1968. The Inelastic Behavior of Simply Supported Composite Beams of Steel and Concrete. Proceedings, Institution of Civil Engineers, London, Vol. 41, December, pp. 651-683.